SYNTHESIS, CHARACTERIZATION, AND ANTIBACTERIAL EVALUATION OF METAL COMPLEXES OF SURFACTANT BASED SCHIFF BASES

A THESIS SUBMITTED TO THE

CENTRAL DEPARTMENT OF CHEMISTRY

INSTITUTE OF SCIENCE AND TECHNOLOGY

TRIBHUVAN UNIVERSITY

NEPAL

FOR THE AWARD OF

DOCTOR OF PHILOSOPHY

IN CHEMISTRY

BY

JANAK ADHIKARI

MARCH 2024

SYNTHESIS, CHARACTERIZATION, AND ANTIBACTERIAL EVALUATION OF METAL COMPLEXES OF SURFACTANT BASED SCHIFF BASES

A THESIS SUBMITTED TO THE

CENTRAL DEPARTMENT OF CHEMISTRY

INSTITUTE OF SCIENCE AND TECHNOLOGY

TRIBHUVAN UNIVERSITY

NEPAL

FOR THE AWARD OF

DOCTOR OF PHILOSOPHY

IN CHEMISTRY

BY

JANAK ADHIKARI

MARCH 2024

EXTERNAL EXAMINERS

The Title of Ph.D. Thesis: "Synthesis Characterization, and Antibacterial Evaluation of Metal Complexes of Surfactant Based Schiff Bases "

Name of Candidate: Janak Adhikari

External Examiners:

(1)   Prof. Dr. Amar Prasad Yadav
       Vice-Chancellor
       Rajarshi Janak University
       Janakpur, NEPAL

(2)   Prof. Dr. Har Lal Singh
       Mody University of Science and Technology
       Rajasthan, INDIA

(3)   Dr. Hanna Wilczura-Wachnik
       University of Warsaw
       Warsaw, POLAND

March 22, 2024

(Dr. Surendra Kumar Gautam)
Asst. Dean

DECLARATION

Thesis entitled **"Synthesis, characterization, and antibacterial evaluation of metal complexes of surfactant based Schiff bases"** which is being submitted to the Central Department of Chemistry, Institute of Science and Technology (IOST), Tribhuvan University, Nepal, for the award of the degree of Doctor of Philosophy (Ph.D.), is a research work carried out by me under the supervision of Asst. Prof. Dr. Narendra Kumar Chaudhary of Department of Chemistry, Mahendra Morang Adarsh Multiple Campus, Biratnagar, Tribhuvan University, Nepal and co-supervised by Prof. Dr. Ajaya Bhattarai of Department of Chemistry, Mahendra Morang Adarsh Multiple Campus, Biratnagar, Tribhuvan University, Nepal.

This research is original and has not been submitted earlier in part or full in this or any other form to any university or institute, here or elsewhere, for the award of any degree.

Janak Adhikari

RECOMMENDATION

This is to recommend that **Mr. Janak Adhikari** has carried out research entitled **"Synthesis, characterization, and antibacterial evaluation of metal complexes of surfactant based Schiff bases"** for the award of Doctor of Philosophy (Ph.D.) in **Chemistry** under our supervision. To our knowledge, this work has not been submitted for any other degree.

He has fulfilled all the requirements laid down by the Institute of Science and Technology (IOST), Tribhuvan University, Kirtipur, for the submission of the thesis for the award of Ph.D. degree.
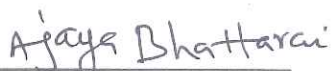
Dr. Narendra Kumar Chaudhary
(Assistant Professor)
Supervisor
Department of Chemistry
Mahendra Morang Adarsh Multiple Campus, Biratnagar
Tribhuvan University, Nepal

Dr. Ajaya Bhattarai
(Professor)
Co-Supervisor
Department of Chemistry
Mahendra Morang Adarsh Multiple Campus, Biratnagar
Tribhuvan University, Nepal

March 2024

त्रिभुवन विश्वविद्यालय
TRIBHUVAN UNIVERSITY
विज्ञान तथा प्रविधि अध्ययन संस्थान
Institute of Science and Technology
रसायन शास्त्र केन्द्रीय विभाग
CENTRAL DEPARTMENT OF CHEMISTRY
कीर्तिपुर, काठमाडौं, नेपाल
Kirtipur, Kathmandu, NEPAL

पत्र संख्या:
Ref. No.:

LETTER OF APPROVAL

Date: 22/03/2024

On the recommendation of Asst. Prof. Dr. **Narendra Kumar Chaudhary** and Prof. Dr. **Ajaya Bhattarai,** this Ph.D. thesis submitted by **Mr. Janak Adhikari**, entitled **"Synthesis, characterization, and antibacterial evaluation of metal complexes of surfactant based Schiff bases"** is forwarded by Central Department Research Committee (CDRC) to the Dean, IOST, T. U..

Dr. Jagadeesh Bhattarai
Professor,
Head,
Central Department of Chemistry,
Tribhuvan University
Kirtipur, Kathmandu,
Nepal

ACKNOWLEDGEMENTS

Janak Adhikari

March 2024

ABSTRACT

Modern pharmaceutical science needs more efficient drug delivery systems (DDSs) that permit poorly aqueous soluble drugs to work effectively. Consequently, medications function effectively. Pharmacological science has found Surfactants to be an invaluable alternative for enhancing the potential of conventional drugs and improving the efficacy of drugs with poor water solubility. Solid drugs can be solubilized more easily when surfactant molecules are added and membrane permeability can be increased in lipid layers as a result.

In the last few years, the synthesis of transition metal complexes of Schiff bases has drawn a lot of interest as an alternative to coordination compounds for the creation of chelating agents. Metal chelates have suitable biological activities.

This research aims to design and develop surfactant-containing Schiff bases and their metal complexes, which can serve as a drug to solve the problems with antibiotic resistance and drug delivery. The study has focused on the structural modification of compounds under study (Pyrrole-2-carboxaldehyde, Pyrrole-3-carboxaldehyde, and Dodecylamine) by forming the Schiff bases and metal complexes and their correlation with bio-functional activities. Given this, two new Schiff bases [DDAP2C and HL (DDAP3C)] have been prepared and further complexed with four transition metal ions, Co^{2+}, Ni^{2+}, Cu^{2+}, and Zn^{2+}. The newly prepared metal complexes and Schiff bases were fully characterized by elemental microanalysis, conductivity measurement, melting point measurement, $^{1}HNMR$, $^{13}CNMR$, FT-IR, UV/Vis, ESI-mass, MALDI-TOF-mass spectrometry, and magnetic susceptibility, studies.

The conductivity data were used to calculate the synthesized compounds' critical micelle concentration (CMC), which was further utilized to derive the Gibbs free energy of micellization (ΔG°_{m}). Thermal stability and kinetic properties of the complexes were determined using thermogravimetric and differential thermal analysis (TGA/DTA). The Coats-Redfern method was used to extract thermodynamic parameters that describe the kinetic activity of the complexes. Most complexes showed high thermal stability and non-spontaneous decomposition steps.

The powder X-ray diffraction study was conducted to verify the crystalline nature of the complexes. The Origin and X'pert high score software were used to analyze PXRD data, and the diffractograms were carefully analyzed to get information about the nature of complexes. Most of the complexes were found to crystalline with nanocrystalline size.

Scanning electron microscopy (SEM) studies enabled the characterization of the surface morphology of Schiff bases and complexes and revealed their different surface textures. Molecular modeling has provided additional support for the geometry of the complexes determined by spectroscopic methods. The structure optimization was achieved by running the proposed molecular structures in CsChemOffice Ultra 16 and Argus Lab 4.0.1 software with MM force field calculation.

The standard Kirby-Bauer paper disk diffusion technique demonstrated the antibacterial potency of the Schiff bases and metal complexes. Several clinical strains of both gram-positive and gram-negative bacteria have been isolated and cultured in laboratories to achieve this objective. They have interacted with synthesized complexes solution prepared in DMSO at variable concentrations. These were further quantified more precisely by performing a minimum inhibitory concentration (MIC) test. In most biological studies, the free Schiff bases and compounds under study were found to have lower antibacterial efficacy than the Schiff base metal complexes. The copper complexes of both the Schiff bases showed excellent antibacterial activity.

शोध सार

आधुनिक औषधि विज्ञानलाई अझ प्रभावकारी औषधि वितरण प्रणालीको आवश्यकता छ, जसको उपलब्धताले खराब जलीय घुलनशील औषधिलाई पनि प्रभावकारी रुपमा कार्य गर्ने बाटो खुल्न जान्छ। परिणामस्वरुप औषधिहरूले अझ प्रभावकारी ढंगले आफ्नो कार्य सम्पादन गर्दछन्। फार्माकोलोजिकल विज्ञानले परम्परागत औषधिहरूको प्रभावकारीता बढाउन, खराब जलीय घुलनशिलता एवम् औषधिहरूको प्रभावकारीतामा सुधार गर्न सर्फेक्टेन्टहरूलाई अमूल्य विकल्प को रुपमा पहिचान गरेको छ। जब औषधिहरूमा सर्फेक्टेन्ट अणुहरु थपिन्छ, ठोस औषधिहरूको घुलनशिलतामा बृध्दि हुन जान्छ फलस्वरुप लिपिड तहहरुमा झिल्ली पारगम्यता बढ्न गई औषधिहरूको प्रभावकारीता बढ्न जान्छ। पछिल्ला केही वर्षहरुमा शिफ बेशहरुबाट धातु कम्प्लेक्सहरूको सश्लेसिंग हुने तथ्यले चेलेटिंग एजेन्टहरूको सिर्जनाको लागि समन्वय यौगिकहरूको विकल्पको रुपमा अधिक ध्यान आकर्षण गरेको छ। धातु चेलेटहरुमा उपयुक्त जैविक गतिविधिहरु विद्यमान हुन्छन्। यस अनुसन्धानले सर्फेक्टेन्ट्युक्त शिफ बेशहरु र तिनीहरुका धातु कम्प्लेक्सहरुका डिजाइन र विकाश गर्ने लक्ष्य राखेको छ, जसले एन्टिवायोटिक प्रतिरोध र औषधि वितरणको समस्याहरु समाधान हेतु औषधिको रुपमा कार्य सम्पादन गर्न सक्छन्। यो अध्ययनले शिफ बेशहरु र धातु कम्प्लेक्सहरु निर्माण पश्चात, अध्ययनमा लिइएका यौगिकहरूको संरचनात्मक परिमार्जन र जैविक-कार्यात्मक गतिविधिहरुसँग तिनीहरुको अन्तर सम्बन्धका बारेमा ध्यान केन्द्रित गरेको छ। यस तथ्यलाई हृदयङ्गम गर्दै, दुई नयाँ शिफ बेशहरु तयार गरी, तिनीहरुको चार धातु आयनहरुसँग (Co^{2+}, Ni^{2+}, Cu^{2+}, & Zn^{2+}) थप धातु कम्प्लेक्सहरु बनाइएको छ। नयाँ तयार गरिएका शिफ बेशहरु र धातु कम्प्लेक्सहरुलाई सम्पूर्ण रुपमा Elemental microanalysis, चालकता मापन, पग्लने बिन्दु मापन, ^{1}HNMR, ^{13}CNMR, FT-IR, UV-Vis, ESI-mass, MALDI-TOF-mass Spectrometry र चुम्बकीय संवेदनशीलता अध्ययनहरु द्वारा चरित्र चित्रण गरिएको थियो। चालकता तथ्याङ्क सश्लेसित यौगिकहरूको महत्वपूर्ण मिसेलि एकाग्रता (CMC) को गणनाको लागि प्रयोग गरिएको थियो, जुन गिब्स फ्री एनर्जी अफ माइसलाइजेशन ($\Delta G°_m$) प्राप्त गर्न पुन: प्रयोग गरिएको थियो। थर्मोग्राभीमेट्रिक र विभेदक थर्मल विश्लेषण प्रयोग गरेर तापीय स्थिरता र कम्प्लेक्सहरुको गति सम्बन्धित गुणहरु निर्धारण गरिएको थियो। कोट्स-रेडफर्न (Coats-Redfern) विधि प्रयोग गरी

थर्मोडायानामिक प्यारामिटरहरु निकालिएको थियो, जसले कमप्लेक्सहरुको काइनेटिक गतिविधि वर्णन गर्दछन् । धातु कमप्लेक्सहरुले उच्च तापीय स्थिरता र गैर-स्वस्फूर्त विघटन चरणहरु देखाएका थिए।

पाउडर एक्सरे विवर्तन (PXRD) अध्ययन, कमप्लेक्सहरुको क्रिस्टलीय प्रकृति प्रमाणित गर्न प्रयोग गरिएको थियो। Origin र X' Pert High Score Software हरु प्रयोग गरी PXRD तथ्याङ्कहरुको विश्लेषण गरिएको थियो र कमप्लेक्सहरुको प्रकृतिबारे जानकारी प्राप्त गर्न तिनीहरुको Diffractograms हरुलाई सावधानीपूर्वक विश्लेषण गरिएको थियो। कमप्लेक्सहरु नैनोक्रिस्टलाइन प्रकृतिका थिए।

स्क्यानिङ्ग इलेक्ट्रोन माइक्रोस्कोपी (SEM) अध्ययनद्वारा शिफ बेशहरु र कमप्लेक्सहरुको सतह उजागर गरिएको थियो र तिनीहरुको विभिन्न सतहगत बनावट पाइएको थियो।

आणविक मोडेलिंगले, स्पेक्ट्रोस्कोपिक विधिद्वारा निर्धारित कमप्लेक्सहरुको ज्यामितीको लागि अतिरिक्त समर्थन प्रदान गरेको छ। CsChem Office Ultra 16 र Argus Lab 4.0.1 Software मा MM Force field गणनाको साथै प्रस्तावित आणविक संरचनाहरुलाई चलाएर, संरचना अनुकूलन हासिल गरिएको थियो।

मानक किर्बी-बाउर पेपर डिस्क प्रसारण प्रविधिले शिफ बेश र धातु कमप्लेक्सहरुको जीवाणुरोधी शक्ति प्रदर्शन गरिएको थियो। यो उदेश्य हासिल गर्न प्रयोगशालामा ग्राम-पजिटिभ र ग्राम-नेगेटिभ व्याक्टेरियाका धेरै क्लिनिकल स्ट्रेनहरुलाई पृथकीकरण एवम् संवर्धन गरिएको थियो। तिनीहरुले विभिन्न एकाग्रता का DMSO मा तयार गरिएको सश्लेषित यौगिकहरुको घोलसँग अन्तरक्रिया गरेका थिए। सश्लेषित यौगिकहरु को जीवाणुरोधी सक्रियता थप सटिक रुपमा न्यूनतम अवरोध एकाग्रता (MIC) परीक्षण गरेर प्रमाणित गरिएको थियो। जैविक अध्ययनहरुमा, अध्ययन अन्तर्गतका यौगिकहरु र शिफ बेशहरु, तिनीहरुका धातु कमप्लेक्सहरुभन्दा कम जीवाणुरोधी क्षमताका पाइएका थिए।

LIST OF ACRONYMS AND ABBREVIATIONS

BHPP : 1,4-Bis[(2-hydroxybenzaldehyde)propyl]piperazine

BM : Bohr Magneton

Co-DDAP2C : Cobalt Complex of Dodecylamine-Pyrrole-2-Carboxaldehyde Ligand

Co-DDAP3C : Cobalt Complex of Dodecylamine-Pyrrole-3-Carboxaldehyde Ligand

Cu-DDAP2C : Copper Complex of Dodecylamine-Pyrrole-2-Carboxaldehyde Ligand

Cu-DDAP3C : Copper Complex of Dodecylamine-Pyrrole-3-Carboxaldehyde Ligand

DDA : Dodecylamine

DDAP2C : Dodecylamine-Pyrrole-2-Carboxaldehyde Ligand

DDAP3C : Dodecylamine-Pyrrole-3-Carboxaldehyde Ligand (HL)

DMF : Dimethyl Formamide

DMSO : Dimethyl Sulphoxide

DTA : Differential Thermal Analysis

DTG : Differential Thermogravimetric

E. coli : *Escherichia coli*

EAS : Electronic Absorption Spectroscopy

EDX : Energy Dispersive X-Ray Analysis

ESI-MS : Electrospray Ionization Mass Spectrometry

FT-IR : Fourier Transform – Infra Red

FWHM : Full Width Half Maximum

ILCT : Intra Ligand Charge Transfer

IR : Infra Red

K. pneumonia : *Klebsiella pneumonia*

LA : Laurylamine

LMCT : Ligand-Metal Charge Transfer

MALDI-TOF-MS : Matrix-Assisted Laser Desorption Ionization Time-of-Flight Mass Spectrometry

M. P. : Melting Point

MM2	:	Molecular Mechanics 2
MS	:	Mass Spectrum
Ni-DDAP2C	:	Nickel Complex of Dodecylamine-Pyrrole-2-Carboxaldehyde Ligand
Ni-DDAP3C	:	Nickel Complex of Dodecylamine-Pyrrole-3-Carboxaldehyde Ligand
nm	:	Nanometer
NMR	:	Nuclear Magnetic Resonance
P. aureginosa	:	*Pseudomonas aureginosa*
P2C	:	Pyrrole-2-Carboxaldehyde
P3C	:	Pyrrole-3-Carboxaldehyde
ppm	:	Parts Per Million
RMS	:	Root Mean Square
S. aureus	:	*Staphylococcus aureus*
SEM	:	Scanning Electron Microscopy
TOF	:	Time of Flight
TG	:	Thermogravimetric
TGA	:	Thermogravimetric Analysis
UV/Visible	:	Ultraviolet/ Visible
XRPD	:	X-ray Powder Diffraction
Zn-DDAP2C	:	Zinc Complex of Dodecylamine-Pyrrole-2-Carboxaldehyde Ligand
Zn-DDAP3C	:	Zinc Complex of Dodecylamine-Pyrrole-3-Carboxaldehyde Ligand

LIST OF SYMBOLS

A	: Absorbance
$Å$	: Angstrom
A	: Arrhenius Pre-Exponential Factor
a	: Crystallite Size
c	: Concentration of Solution in mole/L
d	: Interplanar Distance
E*	: Activation Energy
h	: Plank's Constant
I	: Intensity of Transmitted Light
I_0	: Intensity of Incident Light
k_B	: Boltzmann Constant
r	: Correlation Coefficient
R	: Gas Constant
T	: Absolute Temperature
T	: Transmittance
α	: Fraction Decomposed
β	: Conversion Constant Called Bohr Magneton
β	: Full Width Half Maximum
$β$	: Linear Heating Rate
$ΔG*$	: Free Energy of Activation
$ΔH*$	: Enthalpy of Activation
$ΔS*$	: Entropy of Activation
$ε$	: Molar Absorptivity
θ	: Scattering Angle
λ	: Wavelength
$Λ_M$	: Molar Conductivity
ν	: Frequency of Absorption
$μ$	: Micro
μg/μL	: Microgram per Microliter
$μS\ cm^{-1}$	: Micro Siemens per centimeter

LIST OF TABLES

LIST OF FIGURES

LIST OF SCHEMES

TABLE OF CONTENTS

CHAPTER 1

CHAPTER 2

CHAPTER 3

CHAPTER 4

CHAPTER 5

CHAPTER 6

APPENDIX

List of Publications and Scientific Paper Presentations

CHAPTER 1

1. INTRODUCTION

1.1 Introduction

A wide range of applications in chemical and medical fields has led to a recent surge in interest in coordination chemistry of transition metal complexes. They comprise a large body of research in bio-inorganic chemistry. Chemists worldwide have been inspired by it to design and fabricate new metal complexes. Due to metal ions' ability to build bridges between drug compounds and pathogenic organisms, the study of metal-drug interaction chemistry has grown significantly in both the chemical and medical sciences. Based on the physical and chemical nature of the metal ions, interactions between microbes and metal ions in different oxidation states may be beneficial or detrimental (El-Sonbati *et al.,* 2019). From ancient times, humanity has sought to treat diseases with pure herbal medicines derived from nature's chest. As a result of their complex chemical extraction processes and slow interaction with diseases, pure herbal medicines are currently used less frequently (Sen & Chakraborty, 2016). The discovery of penicillin inspired pharmaceutical research to expand to the extensive screening of microorganisms for new antibiotics after the Second World War. It would be a vital pharmaceutical discovery effort to identify new metabolites from living organisms with a successful synthetic, medicinal chemistry record. Pharmaceutical research today is driven by the desire to discover synthetic drugs that address the current problem of drug resistance. Despite the fact that numerous medications made from natural products are currently in clinical trials, more research is still required (Hutchings *et al.,* 2019; Mukherjee *et al.*, 2015).

Metal-based drugs were first discovered in the late 19th century with Cisplatin, which opened the door to an unexplored world of metal-based chemotherapeutics. In terms of anticancer efficacy, it was the best (Ghosh, 2019; Makovec, 2019). In the past few decades, Cisplatin and its analogs have resoundingly proven to be effective therapeutic drugs, leading to a tremendous amount of research on alternative metal-based chemotherapeutic agents. Since then, Coordination chemistry has focused on metal-drug interactions well and is considered an active research area (Fan *et al.,*

2021). Medical science currently needs help with antibiotic research and increasing antibacterial resistance, which provides ample opportunity for generating new antibiotics with high-grade biological effects. For treating current diseases, drugs with improved activity, selectivity, bioavailability, and fewer side effects than traditional medications must be quickly identified and characterized.

In this research, we are interested in the Schiff bases of biologically active pyrrole carboxaldehyde and the fabrication of these compounds using selected 3d metal ions. The incorporation of metallo-elements into the cage of a new Schiff base ligand having different donor atoms alters such molecules' physiological and biological characteristics (Pervaiz *et al.*, 2018). In our research, the azomethine linkage of the Schiff base is a vital component of its structure, providing multifunctional actions in various scientific domains. The ligands play a crucial role in regulating the interactions involved in identifying biological target sites and controlling the reactivity of the metal in the complexes. Numerous biologically active, naturally occurring compounds with structures very similar to Schiff bases have a wide range of bio-functional properties, including antibiotic, antimicrobial, antitumor, analgesics, anti-inflammatory, and many others (Alaghaz *et al.*, 2014). The relationship between the Schiff base metal complexes and several interdisciplinary research fields, such as material science, catalysis, corrosion science, magnetochemistry, and electronics, is the prime factor in the prospective interest in this study. In recent years, its application in electronics has grown significantly.

1.1.1 Chemistry of Schiff Bases

One of the most common families of organic compounds, Schiff bases, is produced by the condensation reaction between an active primary amine and a carbonyl group. The discovery and chemistry of these substances resulted from the pioneering work of German chemist Hugo Schiff in 1864. Coordination chemistry gained much attention in chemistry research in the late 19th century due to this discovery (Fabbrizzi, 2020; Turtoi *et al.*, 2021). During his research on aniline chemistry, he studied the reactions between aniline and a wide range of aldehydes, leading him to discover the imine-based chemical molecule Schiff base. They can also be referred to as azomethines, imines, or Anils. Compounds in this class usually contain an active imine group (-

CH=N-), which carries potential metal ion binding sites via the free electrons on the nitrogen atom (Ghanghas *et al.*, 2021). In the current research, we have also found that the Schiff bases contain many hetero-elements, such as oxygen and sulfur, which are essential for chelate formation with metals. The bonding ability of the ligands is primarily determined by the nature, electronegativity, and steric factors of the donor atoms that act as coordination sites. Since the N-atom has lone pair electrons, the double bond is electron-donating, and nitrogen has a low electronegativity, the N-atom of the azomethine group (>C=N) acts as a good donor site, and hence Schiff bases are regarded as an excellent ligand (Mahmoud *et al.*, 2016).

Recently, Schiff bases have become one of the most attractive leads in metal coordination chemistry for creating novel lead compounds because they are simple to prepare, vary in properties, and have applications in many biomedical, biochemical, and industrial fields (Kashyap *et al.*, 2018). The library of organic chemistry contains numerous amines and carbonyl compounds that can synthesize Schiff bases with various structural characteristics. An aldehyde (aliphatic or aromatic) or a ketone can be used as the primary carbonyl group for synthesizing a Schiff base. The substituent groups attached to (>C=N) linkages control the stability of imine groups. **Scheme 1** illustrates the general reaction for forming Schiff bases.

Azomethine group

$$R-NH_2 \; + \; R-\overset{\overset{\displaystyle O}{\|}}{C}-R^1 \; \longrightarrow \; \underset{R^1}{\overset{R}{C}}=N-R \; + \; H_2O$$

Primary amine   Aldehyde or Ketone   Schiff base
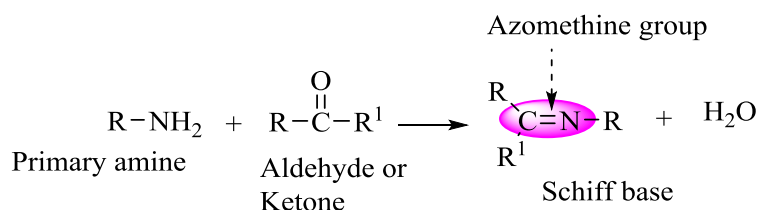
Scheme 1: Reaction scheme for Schiff base formation

R denotes a substitutable heterocyclic, cycloalkyl, alkyl, or aryl group, and R^1 represents an alkyl, aryl, or hydrogen atom. A Schiff base formation is a reversible process; it is usually formed by refluxing the mixture with an acid or base catalyst or under neutral conditions. In general, the formation of the product is completed by separating the product or removing water.

1.1.2   Transition Metal Complexes of Schiff Bases

Schiff bases metal complexes and pharmacology has been the subject of many research papers published over the last few decades. Schiff bases are adaptable pharmacophores that incorporate metal ions into their structural unit because of their diverse donor atoms (Calu *et al.*, 2014; Shabbir *et al.*, 2016). In general, Schiff base ligands are chelated with metal ions at various oxidation states to create transition metal complexes. The nonbonding electrons of ligand donor atoms can coordinate effectively with metal ions that have unoccupied d-orbitals, and even in some cases, this ligation takes place after deprotonation. According to the general rule in coordination chemistry, chelation increases the stability of the complexes by circulating electrons inside the ring and changes their physiological profiles (Abdel-Rahman *et al.*, 2016; Arunadevi *et al.*, 2019). In fact, when the chelate ring contains five or six members, they become more stable. As far as azomethine chains are concerned, aryl groups bonded to nitrogen or carbon prevent their polymerization and rapid decomposition.

The sp^2 hybrid orbital of azomethine nitrogen has a lone pair electron, which makes it easy to coordinate with metals; therefore, this electron is of considerable chemical and biological significance. The stereochemistry of metal complexes is governed by the denticity of Schiff bases, which has an impact on their physiological profiles. In addition to their many applications in catalytic chemistry, clinical, analytical, and biochemical fields, these complexes display many physiological activities (El-Gammal *et al.*, 2021; Kareem *et al.*, 2016; Yaşar *et al.*, 2021). Metal-based research in chemical science relies heavily on such multifunctional metal complexes. Many drug substances' metal ions make them biologically more effective (Frei *et al.*, 2020). Numerous research papers have reported that metal complexes have enhanced activities than free ligands. Several recent studies have highlighted Schiff bases as potential antibiotics that can enhance their potency by chelating metals. Chelation drastically alters the biological properties of ligands and metal moieties (Savić *et al.*, 2020). Several diseases, including cancer, have been reported to be caused and cured by chelation. The present study involves the synthesis of a number of Schiff base ligands from various seed compounds, and their metal complexes with 3d-metal ions.

Human intestinal cells readily absorb these Schiff bases chelated complexes and are more effective at fighting bacteria.

1.1.3 Schiff Bases and Their Metal Complexes: Biological Applications

Several advances in coordination chemistry have led to the emergence of Schiff bases as privileged ligands because many biomolecules that exist in living systems are structurally similar to these compounds. The successful clinical application of Cisplatin as a potential anticancer drug has sparked the interest of scientists in the bioactivities of metal-based complexes in medicine and chemotherapy. Consequently, metal-drug interaction is becoming a fascinating topic for research in medical science (Anacona *et al.*, 2018; Magyari *et al.*, 2018; Malik *et al.*, 2017). During the late 19th century, Schiff-base transition metal chemistry gained momentum. Since then, researchers in medical science have been fascinated with metal-based drugs of Schiff bases because of their tremendous biological effects. Most metals cause toxic effects on the human body by lacking a mechanism for rejection (Elsayed *et al.*, 2018). However, rapid growth has been witnessed in research and development for synthesizing novel metal-based drugs having upgraded pharmacological characteristics. Ligands may be used to chelate free metal ions and ameliorate medical problems caused by their toxicity. There are several biological applications for Schiff base metal complexes, including analgesic, anti-inflammatory, antitumor, antibacterial, antimicrobial, and antifungal. It has been established that some drugs have higher activity when administered as metal complexes rather than free organic compounds (Anacona *et al.*, 2014; Shaygan *et al.*, 2018). Schiff base and their metal complexes are discussed in this report as comparable antibacterial studies. Schiff base metal complexes have potential biological activity having a lone pair electron that anchors bio-molecules within living organisms.

1.1.4 The Application of Schiff Bases and Their Metal Complexes to Other Fields

In addition to their biomedical applications, Schiff base metal complexes have important industrial, chemical, and electronic applications. Their corrosion-inhibitory properties are good in the material science field (Chafiq *et al.*, 2019). During this process, a monolayer spontaneously forms on the surface to be protected. In a variety

of synthetic chemical processes, several Schiff base metal complexes exhibit outstanding catalytic activity at high temperatures (> 100 °C) and in the presence of moisture. They are described in several research reports as being used in both homogeneous and heterogeneous catalysis. Some life molecules, such as enzymes and biopolymers, are synthesized by the active participation of Schiff bases and metal complexes in many biological systems (Uddin *et al.*, 2020). In recent years, researchers have been increasingly interested in metal complexes in which Schiff bases play a crucial role as ligands, based on reports in several scientific publications. Many potentiometric sensors utilize Schiff base ligands for specific metal ions having excellent selectivity, stability, and sensitivity.

Schiff bases and metal complexes play a vital role in the sectors of modern technology because of their thermochromic and photochromic characteristics (Bar *et al.,* 2021). These molecules can be used in optical computers to measure and control radiation intensity, imaging systems, and molecular memory storage devices. Due to their photochromic properties, they serve as photo stabilizers, solar collector dyes, and solar filters. Due to their thermal stability, Schiff bases can also be used as stationary phases in chromatography (Acet *et al.*, 2018).

1.1.5   Surfactants under Investigation

In recent years, pharmacists are interested in designing and preparing new chemotherapeutics inspired by biomedical approaches to inorganic chemistry. Metals are vital in medicine since a large number of contemporary drugs are coordination compounds that have significantly contributed to pharmacology. Many metal complexes are utilized for a variety of therapeutic purposes, including antiviral, analgesic, antibacterial, antitubercular, anticancer, and anti-inflammatory (Abu-Dief & Mohamed, 2015; Nazirkar *et al.*, 2019; Nyawade *et al.*, 2020). With a focus on surfactant activity, we are aiming to change the biological profile of such metal complexes by changing ligand behavior.

The term surfactant refers to an amphiphilic organic compound used in various applications, including wetting agents, emulsifiers, solubilizers, fabric softeners, mineral concentrators, corrosion inhibitors, cleaning detergents, and crop protection

(Chowdhury *et al.*, 2019). The biological activity of pharmaceuticals is greatly affected by the amphiphilic nature of surfactants (Skocibusic *et al.*, 2015). There is a significant issue with conventional drugs' biological activities related to their solubility in vivo in aqueous medium, which can have a significant effect on their performance. The addition of surfactants to drug formulations can have a variety of impacts, such as causing solid drugs to dissolve and deaggregate as well as enhancing the permeability to the lipid layer in the cell membranes (Solanki *et al.*, 2019). The molecular structure of surfactants consists of polar head groups and hydrophobic carbon chain tail groups. Surfactants have the inherent ability to rearrange molecules into a variety of structures, including micelles, monolayers, bilayers, and other shapes. Thus, the aggregates can respond differently regarding their physicochemical profiles (Gawali & Usmani, 2019). The foundations of many physical, chemical and biological systems are comprised of surfactants. There are many applications for them, including as antiseptics in cosmetics (Ziklo *et al.*, 2021), as a surface-active agent in detergents (Zhou *et al.*, 2017), germicides (Verma *et al.*, 2015), and pharmaceutical industries. Since surfactants are antifungal, antibacterial, and antiviral, they are used by the pharmaceutical industry to enhance drug activity (Öztürk *et al.*, 2020). Schiff base metal complexes (Metallo-surfactants) are surfactants with metal ions at their head and hydrocarbon chains at their tail (Kaur *et al.*, 2018). In order to achieve the desired outcomes, drugs are generally administered in complex forms in vivo. Surfactant-based drugs can interact with proteins in a complex way that affects the mechanism of drug metabolism together with enzymes (Saraf *et al.*, 2018). Metal complexes have amphiphilic properties, which make them useful for magnetic, catalytic, and biological applications (Schattschneider *et al.*, 2019; Toth *et al.*, 2019; Wagay *et al.*, 2016). This research contributes to current therapeutic approaches in drug delivery by considering all these aspects of surfactant-based drugs. In modern pharmacology, antibiotic resistance has become a significant problem; consequently, new chemotherapeutics, especially antibiotics, are needed to develop. The bacterial resistance is a result of the evolution of novel bacterial strains with various enzymatic actions on host cells. There are only options for improving drug activities by complexation or adding prodrugs such as surfactants or surfactant-based modified molecules (Kushnazarova *et al.*, 2021).

Dodecylamine

Dodecylamine is a main fatty amine with twelve carbon atoms as the tail group and free amino head group in linear hydrocarbon chain.The water solubility of the free (non-protonated) form is extremely low. It is frequently made via ammonolysis of dodecanoic/lauric acid; (a fatty acid) followed by catalytic hydrogenation using Raney nickel or cobalt and copper chromite catalysts. In some specialized applications, dodecylamine and its derivatives, such bis (3-aminopropyl) dodecylamine, N-dodecyl-1, 3-propane diamine, and coco-amine acetate, may be employed as disinfectants. Bis (3-aminopropyl) dodecylamine, a typical derivative of dodecylamine in the form of triamine, has a variety of properties, including broad-spectrum activity against both Gram-negative and Gram-positive bacteria, high efficacy even in heavy organic soilings like protein or blood, good surface activity, compatibility with some anionic surfactants, and activity against TB and other viruses (such as Hepatitis-B). Dodecylamine contains amine groups that act as a site for the condensing of carbonyl groups to form the Schiff base and as an anchoring site for metal ions. The structure of dodecylamine is depicted in Figure 1 as follows.

H_2N
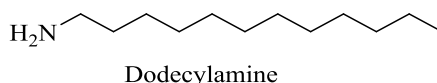
Dodecylamine

Figure 1: Structure of Dodecylamine

1.1.6 Schiff Base Preparations with Pyrrole Derivatives

Biochemical reactions rely heavily on heterocyclic compounds, which can be found in nature in large quantities. Pyrrole belongs to a five-membered heterocyclic aromatic compound with a distinctive nutty odor. The intensive application of this compound has earned it its position in many fields of chemistry. Many pyrrole-based heterocyclic compounds possess various pharmacological properties, including antimicrobial, anticancer, antiviral, anti-HIV, antifungal, and other therapeutic properties (Sakthivel *et al.*, 2020). Pyrrole and many of its derivatives are found in varieties of natural products such as vitamin B12, bile pigments like bilirubin and biliverdin, and the porphyrins of heme, chlorophyll, chlorins, bacteriochlorins, and porphyrinogens, etc. Because of their numerous biological activities, chemists are

highly interested in heterocyclic compounds with five members, including pyrrole and its derivatives (Adhikari *et al.*, 2023). This study, therefore, considers the aldehyde derivatives of pyrrole. Thus, in the present study, pyrrole-2-carboxaldehyde and pyrrole-3-carboxaldehyde have synthesized novel Schiff bases with dodecylamine. The Schiff base condensation reaction with the -NH_2 group of dodecylamine is most effective with the presence of the aldehyde group in the pyrrole derivatives. Figure 2 displays the chemical structures of these compounds.

Pyrrole-2-carboxaldehyde   Pyrrole-3-carboxaldehyde

(a)   (b)
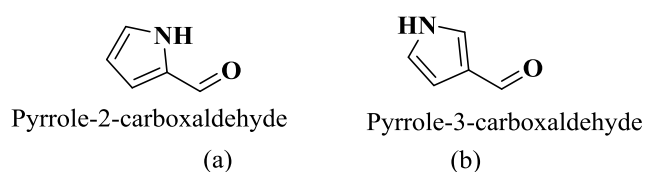
Figure 2: Structures of (a) Pyrrole-2-carboxaldehyde   (b) Pyrrole-3-carboxaldehyde

1.1.7   Schiff Bases Derived from Dodecylamine

Schiff Base Ligands:

Multidrug therapy is considered a new evolving technique to prevail over bacterial infections. Many of the previous antibiotics are under bacterial resistance, which causes a substantial burden to the human population. In the days of penicillin, this was only the drug to treat bacterial infections, but in the coming days, as the report says, many antibiotics have lost their effectiveness against common bacterial infections (Li & Webster, 2017; Luepke *et al.*, 2017). In the present investigation, we have worked on synthesizing pyrrole-derived Schiff bases by interacting with dodecylamine, pyrrole-2-carboxaldehyde, and pyrrole-3-carboxaldehyde compounds. This aims to enrich the medical library with a new class of antibiotics and better activities. Schiff base ligands have attracted significant and increasing interest for researchers due to complex formation behavior with metals. They possess various donor sites that facilitate coordination properties. The presence of aldehydes and amino groups in such compounds is the essential formulation for preparing Schiff base ligands. Further, the various pharmaceutical importances of Schiff base ligands attracted us to do research work in this field. The structure of Schiff base ligands is given in Figures 4 - 5.
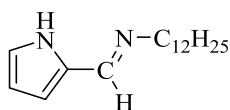
Figure 3: Structure of DDAP2C Schiff base Ligand
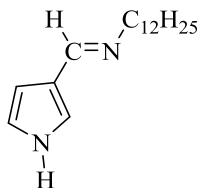
Figure 4: Structure of HL (DDAP3C) Schiff base Ligand

1.1.8 Metallo-elements Selected for Investigation

Metallic ions play various roles in life-critical processes, from structural to catalytic. Since transition metal ions have close-lying energy bands due to partially filled d-orbitals, they are rich in chemistry and act as unique agents in various biological processes. It is a significant aspect of medicinal bioinorganic chemistry to recognize, understand at the molecular level, and treat diseases caused by insufficient metal-ion function. Metabolic functions and the immune system of living organisms require some metals in trace and ultra-trace amounts that significantly impact the physiological profiles of bio-molecules that act at the molecular level in the cell (Al-Fartusie & Mohssan, 2017). As a result, such metals play critical roles in the body for structural, electrochemical, and catalytic activities. Metal-based drugs are now becoming a pioneering research work in medical science, even though metals have been used for medical purposes for centuries. Various diseases are caused by these metals, at high and low concentrations, due to the poisoning of living bodies. The unique properties of transition metals enable them to coordinate with ligands and form stable complexes in biological systems (Zayed *et al.*, 2014). Many pieces of evidence in the living system support the idea that increased concentrations of some metal ions block the transport site for others, resulting in the depletion of some of these metal ions. Besides many drugs, several human food ingredients contain bio-molecules that are bio-stimulators and bio-ligands that can coordinate some metallo-elements and alter their homeostasis behavior (Palmer & Skaar, 2016). The present study investigates four 3d-metals, including Ni(II), Co(II), Cu(II) & Zn(II), to form stable complexes. The partially filled d-orbitals of these metals play a significant role in their coordination behavior with ligands.

1.1.8.1 Cobalt

The Cobalt metal belongs to the first-row transition metal series, with three states of oxidation; +1, +2, and +3. Although it is precarious in its +3 oxidation state, its role in biology is crucial. Cobalt is most stable in its +2 oxidation state and plays a significant role in biological systems. It is needed for life in tiny amounts and forms a key component of vitamin B12 (cyanocobalamin), which is responsible for building proteins and regulating DNA. Anemia in pregnant women is treated with cobalt since it stimulates the production of red blood cells (RBC). Its high concentration, however, may cause human health problems (Shaygan *et al.*, 2018). Many kinds of literature uncover imperative bio-functions of cobalt complexes, such as antibacterial, antitumor, and more.

1.1.8.2 Nickel

Nickel, the earth's 7th most abundant transition metal, exists mainly in the +2 oxidation state in its complexes. It played a memorable part in material science. A fascinating area of research in material science is the alloying behavior of nickel with many other metals and nonmetals. Numerous geometries and coordination numbers are possible for Ni^{+2} in the complex. The most common geometries for nickel complexes are square planar, tetrahedral, and octahedral. The enzyme chemistry in biomedical research emphasizes nickel as a critical component of numerous enzymes in the human body, without which normal metabolic functioning is unthinkable (Raj *et al.*, 2017). Many works of literature explain the multifunctional bio-activities of Schiff bases nickel complexes; hence, the study has included nickel.

1.1.8.3 Copper

Copper is a member of the 3d-transition metal series, and its coordination chemistry depends on its two accessible oxidation states, +1 and +2. Due to its oxidative properties, bio-essential activity, and participation in complex synthesis in many biological processes, it is a necessary element (Yusuf *et al.*, 2021). When anemia was shown to develop from copper-deficient diets in animals, and the addition of copper salts remedied this problem, it was initially recognized as a necessary biological

element in the 1920s (Luca *et al.*, 2019). In several enzymes, it acts as a catalytic constituent. All living organisms need copper in trace amounts to keep their cells functioning correctly. However, excessive copper concentration is highly poisonous because of its chemical reactivity. Two fatal inherited conditions induced by malfunctioning copper absorption are Wilson's disease and Menkes kinky hair disease (Latorre *et al.*, 2019). It forms complexes without crystal field stabilization energy in its +1 oxidation state, which has a diamagnetic d^{10} electronic configuration. Its reductive activation towards molecular oxygen proves the biological relevancy of its complexes. Its +2 oxidation state exists as an electronic configuration d^9, making it suitable for coordination with different ligands for complex formations which range from square planar to distorted octahedral geometries. Its complexes are considered the best candidate for incorporation into pharmaceutical industries because of its crystal field stabilization energy, making it less labile towards the ligand exchange phenomenon. The +3 oxidation state of this metal, however, is relatively rare.

1.1.8.4 Zinc

As a result of its complete d-shell electronic configuration, zinc is often found in +2 oxidation states in its coordination complexes. The Zn(II) ions have no crystal field stabilization energy with the d^{10} configuration, and no biological reactions are evidenced to oxidize or reduce these ions. The Zn(II) complexes generally have four coordinated tetrahedral geometry, although six coordinated octahedral geometry has also been observed in various complexes. It is an indispensable metallo-element for all forms of life. Proteins and enzymes often form stable complexes with the d^{10} electronic configuration of zinc. It plays a vital role in biological systems for maintaining vitamin A levels in the blood by releasing it from the liver (Chasapis *et al.*, 2020). It is believed that zinc helps insulin to be synthesized and stored in β-cells. Numerous metabolic enzymes and regulatory proteins utilize it as an essential cofactor. Several enzymes function only in the presence of zinc. Its usefulness in biological systems and antiseptic properties make it widely valuable for cosmetics. Many research outcomes revealed that zinc complexes had been identified as potential drug candidates in clinical practices in bioinorganic chemistry. However, zinc in excess in the human body develops toxic effects and disturbs the normal functioning of metalloproteins (Lee, 2018).

1.1.9 Theoretical Background of Characterization Techniques

1.1.9.1 Elemental Microanalysis

Elemental (CHN) microanalysis aids in the determination of structure by providing the percentage composition of the elements that are relevant to find the molecular formula. Its information is also accessible and helpful in ascertaining the structure and purity of the synthesized compounds.

1.1.9.2 Conductivity Measurement

Measuring conductivity is a crucial physical tool to learn more about how metal complexes develop in coordination chemistry. Chelation of ligands with metal ions is indicated by changes in conductance values from ligand to complex formation. Electrolytic and non-electrolytic compounds can be differentiated based on conductivity measurements, which helps to calculate solution concentrations. Conductivity measurements are very useful for surfactant analysis to determine critical micelle concentrations (CMCs), and degree of dissociation (α), which in turn can be used to calculate properties like Gibbs free energy, entropy, and enthalpy of micellization.

1.1.9.3 Electronic Absorption Spectra (EAS) Study

Electronic absorption spectroscopy, often known as UV-visible spectroscopy, is a vital instrumental technique that coordination chemists use to gather crucial data regarding the structural features of complexes. An interaction between light and matter is the basis of the UV-Visible spectroscopy. In this Spectroscopy, ultraviolet light or visible light is absorbed by chemical compounds, producing distinct spectra. When matter absorbs ultraviolet radiation, the electrons present in it undergo excitation then jump from a ground state to an excited state and again de-excitation that results into the production of a spectrum which helps to characterize the chemical compounds.

1.1.9.4 FT-IR Spectral Study

The FT-IR spectral analysis is another crucial instrumental tool for characterizing ligands and metal complexes. It provides information on functional groups, other building components, and the metal-ligand bonding parameter. The instrument utilizes infrared radiation of the electromagnetic spectrum to detect vibrations in the bonds within compounds, resulting in the collection of a wealth of information. The presence of different structural components in the molecules can be determined by processing the data obtained from the IR bands. The bands caused by metal-ligand coordination are primarily seen in the far infrared range around 500 cm^{-1}.

1.1.9.5 ^{1}H & ^{13}C NMR Spectral Studies

The structure of Schiff base ligands and metal complexes can be better understood using the ^{1}H and ^{13}C NMR spectral data. A chemical researcher can only build an unknown compound's appropriate structure using NMR spectroscopy, a contemporary experimental tool. By comparing their ^{1}H and ^{13}C NMR spectrum data, it is possible to determine the binding mechanism of the ligand with metal centers in diamagnetic complexes.

1.1.9.6 ESI-MS Spectral Study

Mass spectrometry is another crucial instrumental tool to determine the exact molecular mass of the prepared compounds. The relationship between molecular mass and microanalytical data reveals the chemical formula of the compounds. Recently mass spectrometry using electrospray ionization technique is also called ESI-MS. Due to the soft ionization approach and the low level of compound fragmentation, this is better for developing molecular ion peaks. Since the metal ions in LC-MS may corrode the column, it is also appropriate for determining the molecular mass of metal complexes.

1.1.9.7 TGA/DTA Study

At various phases of temperature ranges, the decomposition profiles of the complexes were observed. The complexes' thermograms show the curve area change corresponding to their disintegration at various temperatures.

1.1.9.8 X-ray Powder Diffraction Study

Powder diffraction is a scientific instrumentation method that uses X-rays as electromagnetic radiation to characterize the structural makeup of materials by striking powder or microcrystalline samples. The X-ray powder diffractometer is the particular instrument used for this investigation.

Since single-crystal growth attempts were unsuccessful in our study, the compound's structure and crystallinity were examined using the powder diffraction technique. The observation of diffractograms of the compounds can achieve several crystalline parameters.

1.1.9.9 Surface Morphology Analysis

The scanning electron microscope (SEM) creates a surface image by scanning the surface of solid materials with a focussed beam of high-energy electrons. Different signals containing details on the surface topography, chemical composition, and crystalline structure are produced due to the high-energy electronic interaction with the atoms in molecules (Rao *et al.*, 2020). This surface-level interaction dissipates secondary and backscattered electrons, which are used for imaging sample compounds. The topographic information is conveyed by secondary electrons generated within a few nm from the surface. The backscattered electrons have significantly stronger interactions and come from far deeper in the sample (Inkson, 2016).

1.2   Rational

Researchers in the pharmaceutical industry are deeply concerned about the active participation of drug substances in therapeutic outcomes. Drug development is a

challenging task in medical science because there is a need to find potentially valuable drugs for treating diseases. The threat of rising antibiotic resistance to human health compels the scientific world to review medications so that the proper insight can be given for modifying previous drugs. The normal physiological function of the human body runs with the essential metallo-elements in trace and ultra-trace amounts. The literature search revealed no reports on the Schiff bases of pyrrole (pyrrole-2-carbaldehyde and pyrrole-3-carbaldehyde) and surfactant (dodecylamine). The new hope for better therapeutic substances in clinical practices will be metal complexes of new Schiff bases produced from pyrrole derivatives and surfactant dodecylamine.

1.3   Objectives

1.3.1   General Objective

Developing more efficient and safer antibiotics leads to designs and modifications of existing drug libraries. Drug resistance has become a significant issue in treating many infectious diseases caused by bacteria and other causative agents in recent years (More *et al.*, 2017), according to current research publications about drug substances. Schiff base complexes have a wide range of applications in a variety of scientific fields. Many chemotherapeutic agents are on the market; however, pathogenic organisms are becoming resistant to these drugs, creating a global threat in medical science. Therefore, it is essential to find chemotherapeutic agents that are safer and more effective. The present study aimed to synthesize, characterize, and evaluate biological significance of the new Schiff base ligands and their metal complexes.

1.3.2 Specific Objectives

This research work aims to accomplish the following specific objectives:
- Synthesis of new Schiff base ligands using pyrrole-2-carboxaldehyde, pyrrole-3-carboxaldehyde, and dodecylamine and analysis of their structures using spectroscopic techniques, including FTIR, ^{1}H & ^{13}C NMR, MS, MALDI-TOF, UV-visible (EAS), TGA/DTA, magnetometry, elemental analysis, and X-ray powder diffraction.

- Synthesis of metal complexes of prepared ligands using Ni(II), Co(II), Cu(II) ,and Zn(II), salts.

- The characterization of synthesized metal complexes using spectroscopic techniques such as FTIR, 1H & 13C NMR, MS, MALDI-TOF, UV-visible (EAS), TGA/DTA, magnetometry, powder diffraction, and elemental analysis.

- The investigation of physical parameters of synthesized compounds, such as melting points and conductivity.

- Identification of the surface topography and elemental composition of ligands and metal complexes using scanning electron microscopy (SEM-EDX) study.

- Screening of synthesized ligands and metal complexes for antibacterial activities.

CHAPTER 2

2. LITERATURE REVIEW

2.1   General Overview

This chapter search for earlier studies that had been conducted on Schiff base and metal complexes. They are versatilely applied in a variety of sciences, so much research is being conducted in this area, and its scope is expanding rapidly. The history of almost one hundred and fifty-five years of study in Schiff bases and their transition metal complexes forecast the scientific interest in this field, which has grown enormously in recent years. It is worth saying that coordination chemistry advances due to research of this sort. Over the recent decades, chemistry has been conducted substantial research on the synthesis, characterization, and biological uses of Schiff bases and metal complexes. Modern chemistry was founded by Hugo Schiff, who discovered the pioneer compound Schiff base. As a result of Prof. Wohler's work, vis-vitalis theory is ruled out, demonstrating that organic and inorganic matter has no metaphysical differences. The outstanding contribution of Berzelius, Wohler and Hugo Schiff achieved a paradigm shift in how we view organic compounds. Prof. Schiff memorized himself with the phrase: "Remember, I descend from Berzelius because Berzelius taught chemistry to the old Wohler, and the old Wohler taught me." A German native, Prof. Schiff has continued his research and study in Italy and established himself as an Italian chemist (Hossain *et al.*, 2018; Miroslaw, 2020). Many researchers worked on this area of study in the years after Schiff's groundbreaking discovery in 1864, and they were successful in synthesizing and structural design of this group of compounds.

As evidence of the continued study of Schiff bases, (Kaban & Fidaner, 1990) synthesized a novel Schiff base ligand by condensing hetarylcarboxaldehydes with p-phenetidine and characterized by spectral analyses. (Kasselouri *et al.*, 1993) prepared four octahedral Mn(II), Co(II), Ni(II), and Cu(II) complexes and one tetrahedral Zn(II) complex of new Schiff base ligand 1,2-bis(2'-pyridylmethyleneimino)benzene that was derived from 2-pyridine carboxaldehyde and 1,2-phenylenediamine. Various physical and spectral techniques have characterized them. The Cu(II) and $V^{IV}O$

complexes of an open chain (1:2) Schiff-base ligand (H2L1), derived by the template condensation of diaminomaleonitrile (DMN) and salicylaldehyde and dicopper(II) complexes of (2:2) macrocyclic Schiff-base ligands derived by template condensation of diformylphenols and diaminomaleonitrile have been synthesized by (MacLachlan *et al.*, 1996). Their crystal structures were studied through X-ray diffraction. After the fruitful applications of Schiff bases and metal complexes in multiple disciplines of science, the work has sped up from the beginning of the 21st century.

Based on recent studies, Schiff base organic compounds are the most employed ligands in coordination chemistry. Due to the potential interest of researchers in various interdisciplinary fields, the research field concerning the coordination compound with the azomethine group as a vital part is widely expansive. Metal coordination with organic ligands dramatically changes metal complexes' physiological and pharmacological behaviors (Chaurasia *et al.*, 2018). Chelation also makes the compounds stable. Schiff bases generally have the potential of drugs used as chemotherapeutic agents in medical science. Chemotherapy generally means the treatment of disease with chemicals. When chemicals are used against infectious diseases, the process is antimicrobial chemotherapy. In addition to their chemotherapeutic applications, they have also played significant roles in other fields. Schiff base and its metal complexes are being studied in research because of their simple preparative methods and easy structural designs. This literature review sheds light on some fields of interest to Schiff bases and metal complexes based on their applications.

2.2   Applications in Pharmaceuticals and Biomedicine

Many research outcomes describe the possibility of using Schiff bases as potential drug candidates or diagnostic probes and analytical tools in therapeutic and biological fields. Additionally, Schiff bases are present in various natural, semi-synthetic, and synthetic chemical compounds and contribute to their biological activities. Several review articles have summarized the significant applications of Schiff bases and their metal complexes, including (Hameed *et al.*, 2017; Mohapatra *et al.*, 2018; Pervaiz *et al.*, 2021; Sakthivel *et al.*, 2020). Due to their impressive biomedical applications, many Schiff base metal complexes can be used as successful models of biological

compounds with great potential. Several of their applications include anticancer (Bahron *et al.*, 2019; Mohamed *et al.*, 2015). antibacterial (Fathi *et al.*, 2021; Palanimurugan *et al.*, 2019), antiviral (Abdel-Rahman *et al.*, 2016), antifungal (Joshi *et al.*, 2020; Patil *et al.*, 2015), analgesics (Murtaza *et al.*, 2014), and others.

Many drugs contain a cyclic system of salicylaldehyde is a vital drug component (Iftikhar *et al.*, 2018). Some piperazine derivatives have antimalarial properties as well. Thus, (Keypour *et al.*, 2017) synthesized two new Schiff base ligands, H_2L^1 and H_2L^2 from the condensation of 2- hydroxybenzaldehyde or 2-hydroxy-3-methoxybenzaldehyde with 2, 2'-(piperazine-1,4-diylbis (methylene))dianiline, respectively to widen the applications of this class of compounds. Furthermore, they studied the biological activity and structure of the ligand metalized with metal ions (Co^{+2}, and Cu^{+2}) forming four macroacyclic Schiff-base complexes. It was found that cobalt complexes possess better antibacterial activity against Gram-positive than Gram-negative bacteria. Furthermore, both cobalt complexes were effective against the three human cancer cell lines including H1299, A2780 and U87 MG, and were more potent than standard doxorubicin in U87 MG cell line. H_2L^1 and H_2L^2 ligand structure is represented in Figure 5.
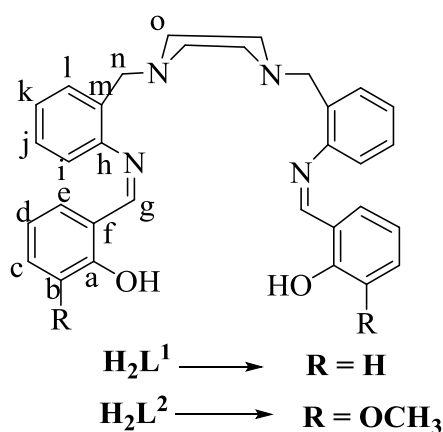
Figure 5: Chemical structure of of piperazine Schiff base ligand $\mathbf{H_2L^1}$ and $\mathbf{H_2L^2}$

It has been reported that 3,3-diaminobenzidine, and creatinine constitute a binuclear tetradentate Schiff base ligand and that four transition metal complexes with Co^{2+}, Cu^{2+}, Ni^{2+}, and Zn^{2+} have been synthesized (Radha *et al.*, 2020). Electrochemical, spectral, and analytical studies established the structures of ligands and their metal complexes. Based on the antifungal and antibacterial evaluation of the ligands and

their metal complexes, the metal complexes demonstrated higher antibacterial and antifungal activity than the free ligand.
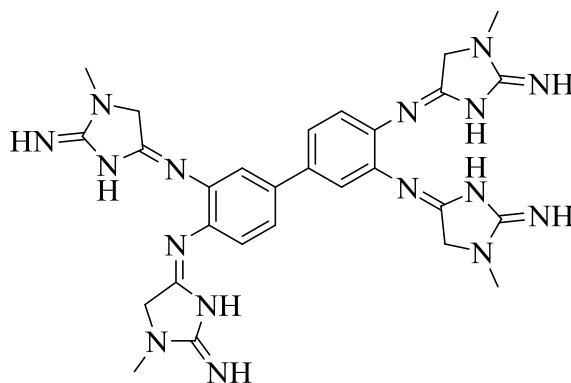
Figure 6: Structure of binucleated tetra dentate Schiff base ligand

The adverse effects of urease on human health include the development of peptic ulcers, stomach cancers, etc. The Urease inhibitory properties are also found in the transition metal complexes of some Schiff bases. It was reported by (Cui *et al.*, 2016) that four Schiff base ligands H_2L1-4 can be obtained by reacting 2-amino-3-(4-hydroxyphenyl) propanoic acid (Tyrosine) with 2-hydroxy-1-naphthaldehyde (H_2L1), 3,5-dibromo-2-hydroxybenzaldehyde (H_2L3), and 2-amino-3-phenylpropanoic acid (L-Phenylalanine) with 2-hydroxy-1-naphthaldehyde (H_2L2), and the 5-chloro-2-hydroxybenzaldehyde (H_2L4).

To get the respective complexes, they were metalized with transition metal copper. Based on their evaluation of the inhibitory activity on jack bean urease, they have a more substantial effect and enhanced inhibitory power. The predicted structure of the Schiff base ligands is shown in Figure 7.
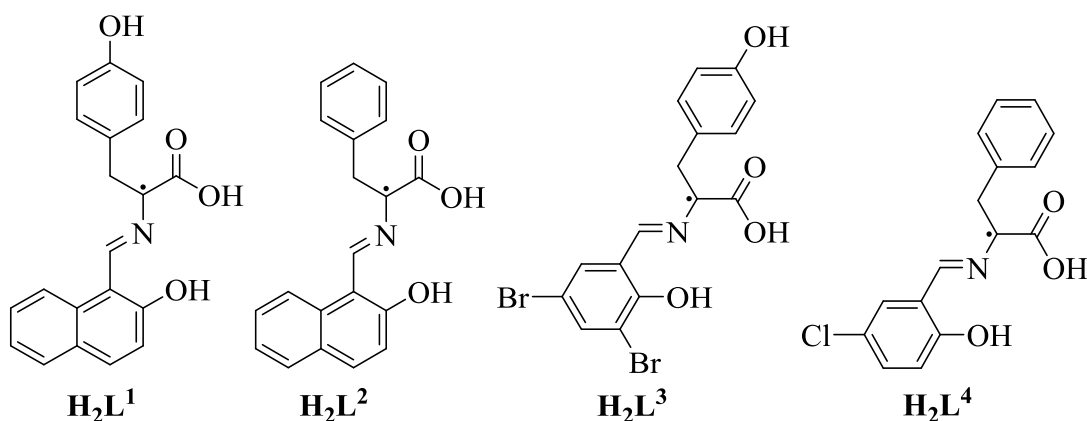
Figure 7: Structure of four Schiff base ligands H_2L1, H_2L2, H_2L3, and H_2L4

Many metal complexes and Schiff bases are reported to have anticancer activity. There are medicinal properties associated with benzamides and their derivatives, including antibacterial, antifungal, analgesic, antihelmintic, anti-inflammatory, antimalarial, antitumor, and antiallergic properties. They are also used in the preparation of aromatic ligands. In the same way, thiophene derivatives have many therapeutic applications in medicinal chemistry. It has been reported that Ni(II), Co(II), Cu(II), and Zn(II) complexes of general composition M(L)$_2$ of Schiff base (Figure 8) obtained from the condensation of L-histidine with Thiophene-2-carbaldehyde. Copper complex exhibited promising anticancer activity against human ovarian cancer cells (John *et al.*, 2019).
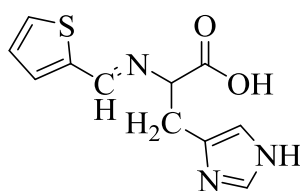
Figure 8: Structure of Schiff base ligand of L-histidine

In their study, (Lapasam *et al.*, 2019) described the synthesis of a series of nine mononuclear complexes of p-cymene ruthenium, Cp* rhodium and Cp* iridium with pyridyl azine derived ligands L1, L2 and L3. These Schiff bases and metal complexes possess interesting antibacterial properties against *Escherichia coli, Staphylococcus aureus*; and *Klebsiella pneumonia* but the metal complexes were more effective than the ligands.

It has been reported that (Abdulghani & Hussain, 2015) have synthesized twelve metal complexes with Co(II), Cd(II), Ni(II), Cu(II), Pt(IV), and Pd(II) ions using two Schiff base prepared by condensing cefotaxime with isatin (L$_I$), and 4-N, N-dimethylaminobenzaldehyde (L$_{II}$). In the cephalosporin class, cefotaxime is a β-lactam antibiotic with higher antibacterial properties. In this work, the authors have attempted to enhance antibacterial activity by forming Schiff base and metal complexes. The compounds were tested for their *in vitro* antibacterial potency against pathogenic bacteria. According to the results, the metal complexes show superior antibacterial properties than Schiff bases. It was found that bacteria type, functional

groups of ligands, and type of metal ion all contributed to the biological activity of the prepared compounds.

There are three new transition metal complexes (Fe (III), Cu (II), and Zn (II) ions) of the 4-(benzylideneamino)-5-phenyl-4H-1,-2,4-triazole-3-thiol ligand (L) derived from 4-amino-5-phenyl-1,2,4-triazole-3-thiol and benzaldehyde. Physical measurements and spectral techniques have been used to propose their structures. Based on *in vitro* antibacterial and antifungal studies, metal complexes exhibit higher antimicrobial activities than free ligands (Mahmoud *et al.*, 2021) and the zinc complex was the most potent antibacterial and antifungal agent.

The synthesis of four metal complexes Ni(II), Cu(II), Co(II), and Zn(II) has been accomplished using Schiff bases formed from 4-aminoantipyrine acetamide and m-phenylenediamine (Dhanaraj & Raj, 2020). The tetrahedral geometry was proposed for the Zn(II) complex and square planar geometry for the Co(II), Ni(II), and Cu(II) complexes. Compounds of this class have been tested for antibacterial, antifungal, DNA cleavage, and anticancer properties. There was promising evidence that the complexes were antibacterial and antifungal. Furthermore, Cu(II) complex provoked the most remarkable cytotoxicity in SK-MEL-28 cells.

According to (Nyawade *et al.*, 2020), pyrrole-2-carboxaldehyde was directly condensed with the solution of the amino acid (l-methionine (L1), l-histidine (L2) and l-tryptophan (L3) in KOH(aq)) (1.0 mmol, 5.0 mL)/ethanol (5.0 mL) mixture to form three tridentate Schiff bases amino acids. Schiff bases L1, L2, and L3 were then complexed with palladium metal to produce Pd(II) complexes C1, C2, and C3 respectively. According to the experimental results, Pd(II) complexes of Schiff bases amino acids have a square planar geometry. According to *in vitro* antibacterial studies of Schiff bases amino acids and their Pd(II) complexes with pathogenic bacterial strains, the complexes have more incredible antibacterial efficiency than their ligands. The complexes C2 and C3 were better than C1 based on antibacterial activity.

The Ni(II) and Pd(II) complexes of Schiff base have been investigated by (Satheesh *et al.*, 2015) for their antibacterial and antifungal activities. In this study, 2-(3,4-dimethoxyphenyl) ethanamine were refluxed with 2-hydroxy benzaldehyde, and 2'-

hydroxy acetophenone for 1.5-2.0 hours at room temperature to prepare the Schiff base ligand L^1H and L^2H respectively as the following reaction **Scheme 2**.
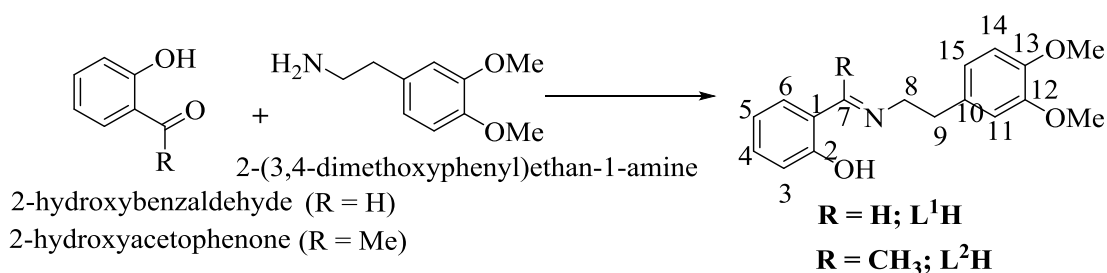
Scheme 2: Synthesis of Schiff base ligands L^1H and L^2H

Based on a fair evaluation of antibacterial activities, the new ligands and complexes have demonstrated higher antibacterial activity against *P. desmolyticum* and *S. aureus*, and moderate activity against *E. coli* and *K. aerogenes*. Moreover, Schiff bases and their derived complexes were more potent antifungal agents against *A. flavus*, as compared with *C. albicans*. In screening these new compounds, complex **2** and ligand L^1H showed the most potent antibacterial and antifungal properties.

Organic compounds based on triazoles and their derivatives have been reported to have enzyme inhibition activity and biological functions. In their work, (Sumrra *et al.*, 2021) used two mono-Schiff bases (**L1**) and (**L2**), and one bis-Schiff base (**L3**) for synthesizing 24 different complexes of transition metals [VO(IV), Cr(III), Mn(II), Fe(II), Co(II), Ni(II), Cu(II), and Zn(II)]. According to the *in vitro* antibacterial results, *Halomonas salina* displayed significant antibacterial activity, while *Chromohalobacter salexigens* demonstrated the least activity. Furthermore, all the compounds had dual inhibitory effects against AChE and BChE. In terms of activity against *BChE* and *AChE* enzymes, compounds (15) and (1) displayed the greatest activity, respectively among the synthesized metal complexes.

Several studies report improved pharmacological properties for the Schiff bases prepared from sulfonamide drugs. (Mondal *et al.*, 2016) synthesized different Schiff bases by condensing 2-hydroxynaphthaldehyde with different sulfonamides [sulfapyridine (SPY), sulfadiazine (SDZ), sulfaguanidine (SGN), sulfamerazine (SMZ), and (sufathiazole (STZ)]. They were characterized by using various

spectroscopic data to gain more insight into antimicrobial action. Based on the antibacterial study, the Schiff bases of STZ and SGN are much more active than their parent sulfonamides with good drug-like properties. Besides, the Schiff bases exhibited a positive response to the cytotoxicity and molecular ducking examination.

Six new metformin Schiff base oxovanadium(IV) complexes have been prepared with each of salicylaldehyde (HL1), 2,4-dihydroxybenzaldehyde (H2L3), 3,4-dihydroxybenzaldehyde (H2L5), 2,3-dihydroxybenzaldehyde (H2L2), 2,5-dihydroxybenzaldehyde (H2L4), and 2-hydroxynaphthaldehyde (HL6), and investigated for their antidiabetic activities in mice (Mahmoud *et al.*, 2016). The result showed that the complexes **1** (HL[1]); and **4** (H$_2$L[4]); have a potential blood glucose-lowering effect even better than metformin.

(Latif *et al.*, 2019) reported the synthesis of the three metal complexes including Cu(II), Ni(II), and Zn(II) of the Schiff base ligand synthesized from the condensation of 4-(dimethylamino)benzaldehyde and S-benzyldithiocarbazate. All the complexes containing Schiff bases displayed a bidentate uni-negative ligand, giving a square-planar structure with Ni(II) and Cu(II) and a tetrahedral structure with Zn(II). Antibacterial tests showed that complexes were more effective than free ligands against bacteria. The Zn(II) showed moderate antibacterial activity, while Cu(II) and Ni(II) complexes were highly effective. Copper complexes are predicted to be more powerful and less toxic than other anticancer agents. Various biomolecules related to important physiological activities are associated with copper, making it a biologically relevant metal. The anticancer effects of Schiff base copper complexes of general formula [Cu(HL)(pdc)]2 (**1**) and [Cu(L')$_2$]$_2$ (**2**), where HL = 2-([2-(piperazine yl)ethylimino]methyl)phenol, pdc = py-2,5-dicarboxylate and HL' = 2-(((2-(di-isopropylamino) ethyl)imino)methyl)phenol, have been investigated by (Manna *et al.*, 2019), against human breast (MCF7) cancer cell lines, and the results showed significant anticancer effects of complex **1** compared to **2** in vitro.

2.3   Catalytic Applications

Transition metal complexes can catalyze various organic transformations, vital for oxidative processes followed in laboratory synthesis and chemical industries. Since Schiff bases and their metal complexes are used in more expansive areas as valuable

catalysts, they have been extensively investigated in recent years. It has been reported that Schiff base compounds can stabilize many metals in different oxidation states and influence the performance of metals in many catalytic transformations.

Because of their low cost, simple synthesis, and chemical and thermal stability, the Schiff bases and their transition metal derivatives are known to have catalytic activity for the oxidation of alcohols and alkenes in numerous synthetic organic processes. The transition metal complexes of dithiocarbazate Schiff base (abbreviated as NiSBdiAP, CuSBdiAP, CoSBdiAP, FeSBdiAP, MnSBdiAP, and ZnSBdiAP, in which SBdiAP represents the Schiff base) were synthesized by (Alshaheri *et al.*, 2017). The ligands were prepared by condensing S-Benzyldithiocarbazate with 2, 6-diacetylpyridine. The resulting compounds were examined for their ability to oxidize cyclohexane in the presence of tert-butyl hydroperoxide into the respective cyclohexanol and cyclohexanone catalytically. Extensive research revealed that the iron complex of SBdiAP Schiff base ligand has a superior catalytic activity to other compounds.

Several lanthanide and ruthenium compounds are also known to have remarkable catalytic efficiency in many organic synthetic chemical processes and establish themselves as a very excellent catalyst. In a similar study, (Cen *et al.*, 2018) synthesized a series of lanthanide complexes stabilized by Schiff-base ligands that have been successfully synthesized through protonolysis reaction using the readily available $Ln[N(SiMe_3)_2]_3$ (Ln = La, Gd) as the precursors. All complexes exhibited fantastic catalytic activities for ε-caprolactone polymerization through the ring-opening process.

Many transition metal complexes have been identified as catalysts for the transfer hydrogenation of ketones (Buldurun & Özdemir, 2019). According to the cited paper, four novels Ru(II)-Schiff base complexes catalyzed the transfer hydrogenation of ketones to alcohols in the presence of isopropanol/KOH. This catalyst was found to have excellent catalytic results than other standard catalysts that were very hard to achieve or even impossible.

In industrial applications, rhodium and iridium complexes can serve as catalysts to lead chemical reactions very efficiently. According to (Siangwata *et al.*, 2016), through Schiff base condensation reaction, monometallic and heterobimetallic Rh(I) complexes with N, O- bidentate chelating aryl and ferrocenyl ligands have been synthesized and evaluated for their catalytic properties. As a result of studies, it was shown that the complex could catalyze the conversion of 1-octene towards aldehydes in the hydroformylation reaction with outstanding chemoselectivity.

In recent years, vanadium complexes have gained immense interest in coordination chemistry due to their multifaceted properties. For this work, (Kargar et al., 2021) synthesized and characterized a dioxovanadium (v) complex with a tridentate ONO Schiff base, obtained by condensing 4-aminobenzohydrazide and 3-ethoxysalicylaldehyde. Its crystal structure was also determined. Furthermore, synthesized vanadium complexes were studied for their catalytic properties in the selective oxidation of the alkyl and aryl sulfides to the respective sulfones in the presence of 30% aqueous H_2O_2 in ethanol. This study demonstrated that the dioxovanadium complex could act as an effective, less time-consuming, higher yield-producing and extra-selective catalyst to oxidize the alkyl and aryl sulfides to the corresponding sulfones.

2.4   Applications in Modern Technologies

Recently, metal-containing organic polymers incorporating Schiff base complexes have gained considerable attention because of their novel electronic, magnetic, and catalytic properties. Metals can act as good sensors and building blocks of supramolecular structures due to their coordination ability within polymer backbones. In addition to their biological relevance, Schiff base metal complexes have also been found to be helpful in modern technological advancements. A more efficient way of capturing solar energy using organic polymers, which emit no greenhouse gases or air pollutants, can help tackle the over-exploitation of fossil fuels and increasing air pollution problems. This literature review is presented here to summarize some of the significance of Schiff base metal complexes in the modern field of science. As a class of valuable chemicals, Schiff base metal complexes have been popularized in recent years as optical computers used to measure and control radiation intensity in imaging

systems and for molecular storage as organic materials in reversible optical memories and biological photodetectors.

According to many research studies, the polymers of Schiff base metal complexes may be used as organic photovoltaic materials having good stability, electroactivity, and electrical conductivity (Nitschke *et al.*, 2021). The π-electron conjugated system allows for substantial charge carrier mobility and electron delocalization throughout the polymer chain. The performance of organic solar cells using substituted Schiff base polymers has improved.

In order to study the photosensitizer for photovoltaic applications (Shehata *et al.*, 2019) synthesized Zn (II) complex (ZnL$_2$) with pyridyl Schiff base obtained by condensing salicyldehyde and aminopyridine. The thermal evaporation method has been successfully used to grow ZnL$_2$ thin films on glass, quartz, and silicon, and the optical properties of these films have been measured using spectrophotometry. According to the final results, the Au/ZnL$_2$/p-Si/Al heterojunction performed very well for low and high illumination light, indicating that ZnL$_2$ could be used as a photosensitizer in photovoltaics and optoelectronics.

(Dineshkumar & Muthusamy, 2015) synthesized and characterized the cross-linked rigid structured Schiff base polymers, and studied their optical, electrical, and thermal properties. For this, they synthesized three Schiff base diol monomers including 4-bromo-2-{[(2 hydroxyphenyl)imino]methyl}phenol (BHB2AP), 4-bromo-2-{[(3-hydroxyphenyl)imino]methyl}phenol (BHB3AP) and 4- bromo-2-{[(4-hydroxyphenyl)imino]methyl}phenol (BHB4AP) were synthesized by condensing 5-bromo-2-hydroxybenzaldehyde with 2-aminophenol, 3-aminophenol, and 4-aminophenol respectively by taking equimolar quantities in the alcoholic medium. Then the Schiff base diol monomers were converted into their polymers through the oxidative polycondensation reaction in an aqueous alkaline medium using NaOCl as an oxidant. Different analytical techniques were applied to investigate the optical, electrical, and thermal properties of the synthesized polymers. As a result of poly-conjugated structures, the synthesized polymers exhibit lower band gaps than monomers, allowing them to be used as semiconducting materials in electronics, optoelectronics, and photovoltaics. Moreover, the synthesized polymers have good

thermal stability, making them potential candidates for applications in aerospace and high-temperature environments.

When chemical species are exposed to electromagnetic radiation in the ultraviolet or visible range, a reversible and abrupt change in their photochemical behavior occurs. This phenomenon is known as photochromism. There is a difference in the absorption frequency of light between different chemical species. When radiation is absorbed, it produces a photochemically stable but thermodynamically metastable state with a different color than the original (Bar *et al.*, 2021). The color-changing lenses for sunglasses worn as eyeglasses are one of the significant applications of photochromism. Schiff bases can behave as a model for showing photochromism (Chai *et al.*, 2018). Schiff base compounds act as photostabilizer dyes for solar filters and collectors because of their photochromic characteristics.Additionally, they are utilized in optical sound recording technology.

In the study by (Weng *et al.*, 2019), typical photochromic properties with fluorescence emission from the conjugated structure of Schiff-based dithienylethene derivative **DTEN**. The Schiff-base ligand **DTEN** was prepared by refluxing, the mixture of 1-(5-chloro-2-methyl-3-thienyl)-2-(5-formyl-2-methyl-3-thienyl) cyclopentene and 3-hydroxy-2-naphthoic acid hydrazide in ethanol for 12 h. According to authors it is the first gated photochromic system that is regulated by Ni^{2+}. The different binding modes of Al^{3+} and Ni^{2+} with compound **DTEN** allow both the initial and photostationary states of **DTEN** to be used as fluorescent probes for Al^{3+} at different wavelengths in aqueous solutions.
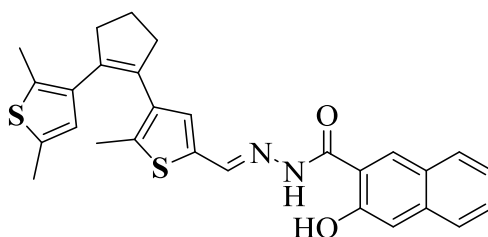
Figure 9: Structure of Schiff-based dithienylethene derivative **DTEN**

In a related study by (Kang *et al.*, 2021), they developed a novel composite hydrogel mainly based on oxidized hydroxyethyl cellulose and allyl co-polymer. The oxidized

hydroxyethyl cellulose molecular chains were then used for Schiff bases, borate bonds, and hydrogen bonds to create a unique mechanical property, while allyl spirooxazine derivatives were used to endow oxidized hydroxyethyl cellulose-based transparent hydrogels with photo and pH sensitivity. This designed oxidized hydroxyethyl cellulose-based hydrogel has potential applications in the development of safe, fashionable, and pH-detectable contact lenses

(Shu *et al.*, 2021) reported a multi-stimuli-responsive compound DDHAC with Et_2N-substituted salicylaldehyde Schiff base skeleton. The compound DDHAC was synthesized by stirring solution of 3-amino-7-diethylaminocoumarin, 4-(diethylamino)-2 hydroxybenzaldehyde in EtOH for 2 h at room temperature, and adding CH_3COOH. Initially 3-amino-7-diethylaminocoumarin was prepared by stirring 7-diethylamino-3-nitrocoumarin 4 h at room temperature in the presence of stannous chloride dihydrate and conc. HCl, and then diluting in iced water. This molecule displayed mechanochromism and thermochromism properties due to its structural flexibility. Additionally, the Et_2N group provided DDHAC with the capability to respond to protonation, allowing it to distinguish $CHCl_3$ from organic solvents when irradiated with UV light.
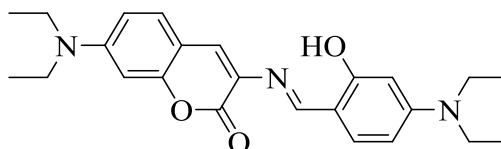
Figure 10: Structure of Schiff base molecule DDHAC

2.5 Surfactant and Corrosion Inhibition Applications

The crucial materials utilized in several industrial and engineering applications are iron and its alloys (steel). Although their constant usage in industrial processes necessitates cleaning the metal surface, acid solutions are employed to eliminate undesired scale and corrosion products. The metal may suffer severe damage due to this corrosion, which also deteriorates its quality. Some organic inhibitors with donor atoms are needed to protect the metal surface from acid attack. Some Schiff base compounds with imine groups and donor atoms like nitrogen, oxygen, and sulfur work well to stop the corrosion of metal surfaces in acidic media.

30

(Bedir *et al.*, 2021) prepared two ethoxylated nonionic surfactants (L400 and L600) based on Schiff base are prepared from polyoxyethylene, glyoxalic acid, and phenylenediamine. They investigated corrosion inhibition behavior on carbon steel/1.0 M HCl interface using electrochemical impedance spectroscopy (EIS) and Tafel techniques and complemented with microscopic analysis methods. Their investigation found the high corrosion inhibition effect on carbon steel due to the presence of the effective electronic adsorption centers (N, O, and π bond). The synthesized Schiff base showed effective inhibitive capabilities of L600 than L400 for mild steel, and its effectiveness rises with inhibitor concentration.

Some benzidine-based Schiff bases, such as bis(4(dimethylamino)benzylidene) biphenyl4,4′-diamine (DBB), Bis(4-methoxy benzylidene)biphenyl-4,4′-diamine (MBB) and Bis(4-chlorobenzylidene)biphenyl-4,4′-diamine (CBB) were evaluated for inhibition efficiency on carbon steel (CS) corrosion in 1.0 M HCl aqueous media. The inhibition efficiency increases with the concentration of Schiff bases and rises as temperature increases, suggesting chemical adsorption mechanism. The inhibitory effectiveness and adsorption behavior have been studied using gravimetric and electrochemical techniques (Bedair *et al.*, 2020).

The effectiveness of two benzohydrazide Schiff bases (B1 and B2) as corrosion inhibitors of carbon steel plate in a 1.0 M HCl solution was studied by (Shahabi *et al.*, 2019). The study found a fantastic corrosion inhibition effect. They explained the remarkable efficiency of Schiff base inhibition (based on WL results) because of the adhesive adsorption of the inhibitor molecules on the surface of carbon steel (Kashyap *et al.*, 2018) prepared Ni(II), Zn(II), Co(II), and Cu(II) complexes of Schiff base prepared from m-hydroxybenzaldehyde and 4-amino antipyrine in methanol and examined their corrosion inhibition impact on mild steel in acidic solution by electrochemical impedance spectroscopic (EIS) measurements. The collected data showed that these complexes were effective at inhibiting corrosion, and the Ni(II) complex was an excellent corrosion inhibitor.

As a donor atom in Schiff bases, alkoxy group exhibits a strong affinity for the surfaces of aluminium alloys. Using Tafel polarization, electrochemical impedance spectroscopy (EIS), weight loss measurement, the ferrocenyl Schiff bases such as 4,40

-((((ethane-1,2-diylbis(oxy))bis(4,1-phenylene))bis(methaneylylidene))
bis(azaneylylidene))bisferrocene (**Fcua**), 4,40 -((((ethane-1,2-diylbis(oxy))bis(2-
methoxy-1,4-phenylene)) bis(methaneylylidene))bis(azaneylylidene))bisferrocene
(**Fcub**) and 4,40 -((((ethane-1,2-diylbis(oxy))bis(2-ethoxy-1,4
phenylene))bis(methaneylylidene))bis(azaneylylidene))bis ferrocene (**Fcuc**) were
examined as a corrosion inhibitor for aluminium alloy AA2219-T6 in acidic medium.
The analysis has identified the Schiff base compounds as a reliable aluminium alloy
corrosion inhibitor (Nazir *et al.*, 2020).

Fcua (R = H)
Fcub (R = OCH$_3$)
Fcuc (R = OC$_2$H$_5$)
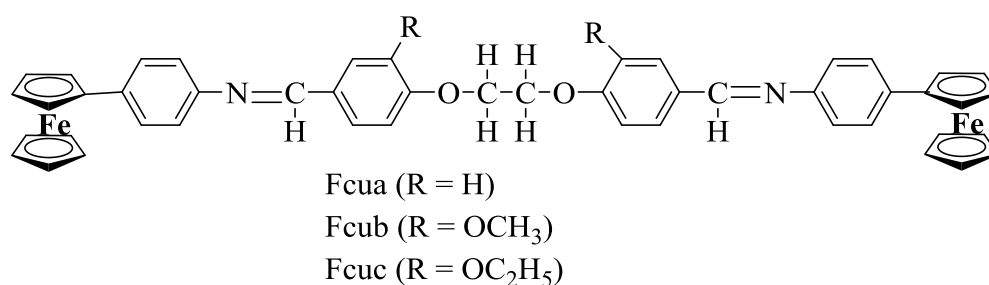
Figure 11: Structure of ferrocenyl Schiff bases (Fcua, Fcub, Fcuc)

Applications in medicine and pharmaceuticals are possible for oxyzepine molecules.
Numerous investigations have established the excellent biological activity of
heterocyclic residues containing Schiff bases. (Praveen *et al.*, 2021) synthesized novel
heterocyclic compounds tert-butyl 4-[(4-methyl phenyl) carbonyl] piperazine-1-
carboxylate [TBMPCPC] and investigated its corrosion inhibition property for carbon
steel in 1M HCl solution by Electrochemical and quantum chemical techniques. The
study showed that the synthetic chemical TBMPCPC had good corrosion-inhibiting
properties. The chemical adsorption of inhibitor molecules on the carbon steel's
surfaces was the reason for the inhibitory activity of the inhibitor.

Metal surface corrosion is significantly related to material loss in technological
processes. One of the main factors contributing to corrosion is the saline medium.
Numerous dissolved organic and inorganic substances can be found in the formed
water created during petroleum extraction in deep oil wells. Since these compounds
can aggressively corrode material constituents, inhibitors are frequently utilized to
prevent it. Corrosion inhibitors reduce corrosion rate by blocking active sites and
increasing adsorption, which prolongs the equipment's life. The organic Schiff bases
based on Chitosan have been employed successfully as corrosion inhibitors in oil and

gas operations. (Chauhan *et al.*, 2020) have prepared a new family of Schiff base as Chitosan-cinnamaldehyde Schiff base (Cinn-Cht) and assessed their ability to prevent corrosion on carbon steel in 15% HCl. The results demonstrated good corrosion inhibition characteristics, which are explained by the Cinn-Cht molecules' remarkable ability to adsorb on the metal surface. The inhibition efficiency increases with the inhibitor concentration. The adsorption of the inhibitor on the metal surfaces was of mixed tye of physical and chemical adsorption.

(Hegazy *et al.*, 2015), synthesized a new series of cationic Schiff bases surfactants such as 1-dodecyl-2-(phenethylimino)-1-methylpyrrolidin-1-ium bromide (A), 1-dodecyl-2-((2-hydroxyethyl)imino)-1-methylpyrrolidin-1-ium bromide (B), and 1-dodecyl-2- ((4-hydroxyphenyl)imino)-1-methylpyrrolidin-1-ium bromide (C). They used the weight loss, potentiodynamic polarization, and electrochemical impedance spectroscopy methods to assess the corrosion inhibitory impact on carbon steel pipelines in oil and gas wells applications (1M HCl). It was found that the inhibition efficiency increases by increasing the inhibitor concentration, exposure time, and temperature. The inhibition efficiency of three cationic surfactants follows the order: C > A > B.

2.6   Research Gap

Various organic and inorganic ligands exhibit coordinating properties with metal ions, leading to the discovery of coordination compounds. Since metal complexes first came into the limelight and opened up new fields of research for inorganic chemists, much progress has been achieved in the synthesis and characterization of these compounds. There has been an increasing interest in developing biofunctional model compounds that can save human lives, aside from their diverse properties. A lot of attention has been paid to biomedical applications without understanding how to functionalize them. A further limitation of the existing literature is that there are very few studies that have examined the pharmacological activity of surfactant-based metal complexes. Surfactant properties such as critical micelle concentration, conductivity and surface tension of the complexes also influence drug profile of the compounds. So, in order to address all this, we correlated surfactant properties with biological profiling of the synthesized compounds.

CHAPTER 3

3. MATERIALS AND METHODS

This chapter outlines the chemicals and other materials required to synthesize new Schiff base ligands and metal complexes. Here, the numerous physical, analytical, and spectral approaches used for the characterization will be covered, along with the specifics of the antibacterial activity investigation. The steps involved in synthesizing Schiff base ligands and their metal complexes will be covered in depth. The information regarding the crystallinity of the compounds will be provided by the X-ray powder diffraction analysis, which will be presented in the appropriate subchapter. Here, the methodology for the in-depth investigation of antibacterial activity will also be provided.

3.1   Materials / Reagents

All the chemicals and reagents utilized for the experiment were of analytical quality and used without additional purification. Main seed compounds were purchased from pharmaceuticals and international standard companies through local market dealers. The chemical dodecylamine (Laurylamine) was procured from Spectrochem, Mumbai, India. The pyrrole-2-carboxaldehyde (P2C) in a pure form was obtained from Sigma-Aldrich, Germany. The pyrrole-3-carboxaldehyde (P3C) was procured from Alfa Aesar. All the chloride salts of cobalt, nickel, copper, and zinc were purchased from Merck. The ethanol and MHN agar were procured from Qualigens, Merck, and Himedia co. respectively. The synthesis was carried out using distilled ethanol as a solvent, and standard techniques were used to distill ethanol before using it. The metal complexes were synthesized using four metal chloride salts ($MCl_2.xH_2O$, M = Ni(II), Cu(II), Co(II), and Zn(II). Due to the significantly lower solubility of dodecylamine (DDA) in water, absolute ethanol was used for this purpose. The microbiology laboratories at Birat Medical College Teaching Hospital and Suraksha Hospital, Biratnagar, provided the clinical strains of human pathogenic bacteria species required for the antibacterial sensitivity study. Table A1 summarizes the list of chemicals and reagents used to synthesize Schiff bases and metal complexes. Table A2 includes a list of the equipment and glass apparatus utilized in the experiment.

3.2 Synthesis of Schiff Base Ligands

Out of many synthetic techniques for producing Schiff bases, solvent-free synthesis using a microwave irradiation technique is the most modern and quick method that promotes green chemistry but has certain limitations on its application (El-Wahab *et al.*, 2020; Seewan *et al.*, 2018). Reflux method synthesis, on the other hand, is regarded as a conventional procedure but is frequently employed in research. The chemical reactions of seed compounds in their stoichiometric ratios produced two Schiff base ligands.

3.2.1 Schiff base ligand DDAP2C

Initially, a warm and uniformly stirred P2C (10 mmol, 0.951 g) in 20 mL ethanol was mixed with a well-stirred DDA (10 mmol, 1.8535 g) solution in 20 mL of ethanol. The mixture solution was refluxed at 30 °C for 6 hours and then slowly cooled through the diffusion method (Srivastava *et al.*, 2021). A reddish-brown solid (75% yield) was produced at room temperature by volume reduction. The ligand was dried over anhydrous $CaCl_2$ after being recrystallized in pure ethanol. For the subsequent stages of work, the product was maintained in an airtight vial and kept in a refrigerator.

3.2.2 Schiff Base Ligand HL (DDAP3C)

The equimolar mixture (1:1) of laurylamine (LA) and pyrrole-3-carboxaldehyde (P3C) was refluxed in an ethanol solvent to prepare the novel Schiff base ligand (E)-N-dodecyl-1-(1H-pyrrol-3-yl)methanimine. In order to complete this procedure, 15 mL of ethanol was first used to prepare a solution of P3C (4 mmol, 0.3804 g), followed by another 15 mL of ethanol to prepare a solution of LA (4 mmol, 0.7414 g). In a 100 mL round-bottom flask, the two solutions were mixed and stirred magnetically. The mixture was refluxed for seven hours at 30 °C then it was allowed to cool at room temperature. As a result, an orange solid was obtained. The solid substance was filtered, recrystallized using ethanol, and dried over anhydrous $CaCl_2$. The solid was kept in the refrigerator in an airtight vial.

3.3   Metal Complexes Synthesis

Standard procedures reported in the literature were used to synthesize metal complexes (Kargar *et al.*, 2021; Kargar & Fallah-Mehrjardi, 2021; Ommenya *et al.*, 2020; Shebl *et al.*, 2017). In our study, the ligand and suitable metal chloride salts were mixed and refluxed in the estimated volume of ethanol under a constant stirring condition utilizing a magnetic stirrer. The crystalline product obtained was dried using a desiccator and stored in an airtight vial in the refrigerator till its future use.

3.3.1   Metal Complexes of DDAP2C Schiff Base Ligand

In separate tests, 10 mL of an ethanolic solution containing one half (0.5) mmol of metal chloride salts was added dropwise to a hot, uniformly stirring solution of DDAP2C (1 mmol, 0.2624 g) in ethanol. The mixture was then refluxed for several hours under a hot condition. After cooling, the precipitates of various colored metal complexes were collected, filtered, and washed with ethanol. The metal complexes were recrystallized and kept in an airtight vial in the refrigerator for future use.

3.3.1.1 Synthesis of Co-DDAP2C

The standard procedure for synthesizing metal complexes is described in subunit 3.3.1. The 10 mL ethanolic solution of $CoCl_2.6H_2O$ (0.5 mmol, 0.1189 g) salt was used to prepare the Co-DDAP2C complex. As a result of reducing the volume of solution in normal atmospheric conditions, a coffee-colored solid was precipitated. The solid was filtered and washed with ethanol and kept in a refrigerator using an airtight vial for future use.

3.3.1.2 Synthesis of Ni-DDAP2C

The general process for synthesizing metal complexes is described in subunit 3.3.1. In order to prepare the Ni-DDAP2C complex, a 10 mL ethanolic solution of $NiCl_2.6H_2O$ (0.5 mmol, 0.1188 g) salt was used. The light green solid was obtained after the volume reduction of the solution. The solid was filtered and washed with ethanol and kept in a refrigerator with an airtight vial for future use.

3.3.1.3 Synthesis of Cu-DDAP2C

The general process for synthesizing metal complexes is described in subunit 3.3.1. In order to prepare the Cu-DDAP2C complex, a 10 mL ethanolic solution of $CuCl_2.2H2O$ salt (0.5 mmol, 0.0853 g) was used. When the volume of the refluxed solution was reduced, a solid of a black color precipitated. The solid black product was recovered by filtration and washed using ethanol. It was kept in the refrigerator in an airtight vial until its future use.

3.3.1.4 Synthesis of Zn-DDAP2C

The general process for synthesizing metal complexes is described in subunit 3.3.1. In order to prepare the Zn-DDAP2C complex, a 10 mL ethanolic solution of $ZnCl_2$ (0.5 mmol, 0.0681 g) salt was used. The leaf brown-colored solid was precipitated after the volume reduction of the solution. The solid was filtered and washed with ethanol and kept in the refrigerator in an airtight vial until its future use.

3.3.2   Metal Complexes of HL (DDAP3C)

The Schiff base ligand in this category was prepared following the procedure described in section 3.2.2. Salts of Co(II), Ni(II), Cu(II), and Zn(II) were used to prepare the corresponding complexes. A hot solution of metal salts dissolved in ethanol was added to the heated and uniformly stirred ligand (0.1312 g, 0.5 mmol) in 10 mL of ethanol. The mixture was refluxed using a Liebig water condenser for a number of hours. The simple indicator for the complex development was the physical change observed in the mixture solution. The subsequent units describe the specific reaction conditions followed in the complex formation.

3.3.2.1   Synthesis of Co-DDAP3C / Complex1

To the hot, uniformly stirred ligand solution (0.5 mmol, 0.1312 g) in 15 mL, ethanol was added a hot solution of $CoCl_2.6H_2O$ (0.0595 g, 0.25 mmol) in 10 mL ethanol. The mixed solution was continuously stirred while being refluxed for three to four

hours under a hot water bath. The purpose of the stirring is to homogenize the molecules and promote the bonding of ligand with metal ions. The green-colored Co-HL complex was obtained by reducing the volume of solution. The solid was filtered, washed with ethanol, and dried in the desiccator. The complex was kept in the refrigerator in an airtight vial until its future use.

3.3.2.2 Synthesis of Ni-DDAP3C / Complex3

The general procedure for synthesizing metal complexes is depicted in the sub unit 3.3.2. For the Ni-HL complex, 10 mL ethanolic solution of $NiCl_2.6H_2O$ (0.25 mmol, 0.0594 g) salt was used. Greenish yellow colored solid was separated after the volume reduction of the solution. The solid was filtered and washed with ethanol and kept in the refrigerator in an airtight vial until its future use.

3.3.2.3 Synthesis of Cu-DDAP3C / Complex4

The general procedure for synthesizing metal complexes is depicted in the sub unit 3.3.2. For the Cu-HL complex, 10 mL ethanolic solution of $CuCl_2.2H_2O$ (0.25 mmol, 0.0426 g) salt was used. The green-colored solid product was separated after the volume reduction of the solution. The solid was filtered and washed with ethanol and kept in the refrigerator in an airtight vial until its future use.

3.3.2.4 Synthesis of Zn-DDAP3C / Complex2

The general procedure for synthesizing metal complexes is depicted in the sub unit 3.3.2. For the Zn-HL complex, 10 mL ethanolic solution of $ZnCl_2$ (0.25 mmol, 0.0341 g) salt was used. A reddish brown-colored solid was separated after the volume reduction of the solution. The solid was filtered and washed with ethanol and kept in the refrigerator in an airtight vial until its future use.

3.4   Characterization Techniques

The physical and spectroscopic characterization of synthesized compounds provides the critical information required for structure elucidation and stereochemistry.

Elemental microanalysis, melting point, conductivity measurement, FT-IR, electronic absorption spectral study, ^{1}H & ^{13}C NMR, ESI-MS, MALDI-TOF, XRPD study, SEM-EDX, and TGA/DTA analysis are some of the characterization techniques used in the current work. The relevant subchapters will discuss below.

3.4.1   Elemental Microanalysis

A Thermo Finnigan Flash EA1112 Series CHN analyzer was used in SAIF IIT Bombay, India to determine the CHN % of the synthesized compounds.

3.4.2   Conductivity Measurement

The conductivity measurement was performed using an auto-ranging digital conductivity/TDS meter TCM 15+ in the Chemistry Department of Mahendra Morang Adarsh Multiple Campus, Biratnagar.

3.4.3   Electronic Absorption Spectra (EAS) and Magnetic Moment Study

The study was conducted using a quartz cuvette in an Agilent Cary 5000 UV-visible spectrophotometer in the 200–800 nm wavelength regions, and data were collected from SAIF Cochin, India. The Lakeshore VSM 7410 model equipment was used to analyze the magnetic moment of the metal complexes, and the data were gathered from SAIF-IIT Madras, India.

3.4.4   FT-IR Spectral Study

The FT-IR spectra were recorded in a Thermo Nicolet Avatar 370 FT-IR spectrophotometer with a KBr matrix operating in the 4000-400 cm^{-1} range in SAIF-STIC Cochin, India.

3.4.5 ^{1}H & ^{13}C NMR Spectral Studies

In the present study, the 1H & 13C NMR spectra were recorded using Bruker Avance III, 400 MHz spectrometers, with DMSO-d6 as the working solvent and TMS as the internal reference standard chemical in SAIF-STIC Cochin, India.

3.4.6 ESI-MS and MALDI-TOF-MS Spectral Study

For the current study, ESI-MS spectra of Schiff base ligands in the mass range of 200 to 1100 were acquired in positive mode on an Agilent Q-TOF mass spectrometer outfitted with a source of electron spray ionization at SAIF-CDRI Lucknow, India. In other studies, a MALDI-TOF: Bruker Autoflex max LRF apparatus was used at SAIF- STIC Cochin, India, to record the mass spectra of the metal complexes.

3.4.7 TGA/DTA Study

In the current study, the compounds' thermal events (TGA/DTA) were captured at SAIF-STIC Cochin, India, utilizing a Perkin-Elmer thermal analyzer and linear heating rates of 10 and 20 °C per minute within the range of 40 to 750 °C

3.4.8 X-ray Powder Diffraction Study

Since single-crystal growth attempts were unsuccessful in our study, the compound's' structure and crystallinity were examined using the powder diffraction technique. The observation of diffractograms of the compounds can achieve several crystalline parameters. The X-ray powder diffraction (PXRD) patterns were captured at SAIF, STIC Cochin, India, using an X-ray diffractometer of Bruker AXS D8 Advance having a radiation source of monochromatized Cu-Kα line at a 1.5406 A° wavelength. The measurements were carried out within 2θ (3 to 80°) range. The X'pert Highscore Plus and Origin software were used to solve the raw data to produce the compound's diffractograms, and to gather further crystallographic data.

3.4.9 Surface Morphology Study

JEOL 6390LA/OXFORD XMXN SEM-EDX microscope was used to collect the micrographs and measure the EDX components of the compounds under investigation.

3.5 Molecular Modeling Study

Molecular modeling involves designing molecular graphics and optimizing the molecular geometry of proposed structures through computer simulations. In our study, the 3D molecular modeling of the proposed structure of the metal complexes and Schiff base ligands was achieved using the CsChemOffice Ultra 16 programs and ArgusLab 4.0.1 edition software (Gaber *et al.*, 2018; Kavitha *et al.*, 2019). The molecular modeling software ChemDraw is used to sketch the chemical structures of molecules. Further, it is supported by many tools for designing 2D and 3D shapes of the molecules. ArgusLab is a software program for building molecular models in a graphic format. The different features in this software allow for modification of the molecular model by optimizing geometry, calculating the energy, creating surfaces, and performing Gaussian calculations. It helps visualize molecular orbitals, electron densities, electrostatic potentials, and spin densities on a molecule's surface. Electron density mapped by electrostatic potential can also be observed on the surface of molecules. It is also supplemented by numerous computations of molecular characteristics, such as the single point energy calculation and the geometry optimization calculation to sketch the stable molecular shape of the suggested molecules.

3.6 Antibacterial Activity Study

One of the main medications used to treat many different diseases, antibiotics are regarded as modern medicine's "wonder pill" (Hutchings *et al.*, 2019; Tyers & Wright, 2019; Wright, 2017). Antibiotics are a common prescription drug among doctors. The overdose and the misuse of antibiotics are the factors in the failure of this drug (Ammar *et al.*, 2021; Hasan *et al.*, 2021; Kumar *et al.*, 2019). Therefore, it is crucial to revive them using novel drug designs or their complexation with different

transition metals. Schiff bases and their transition metal complexes can potentially be valuable antibiotics, as revealed by the literature review search outlined in chapter 2. This family of compounds is regarded as a valuable pharmacophore in pharmaceutical science since they have potential pharmacological efficiency.

The synthesized Schiff bases and their transition metal complexes have been investigated in the present study for their qualitative and quantitative antibacterial properties. It has been carried out using a modified Kirby-Bauer paper disc diffusion technique. Further quantitative analysis of the compounds was conducted using minimum inhibitory concentrations (MICs).

3.6.1   Equipment Sterilization

The procedure of sterilization eliminates all varieties of microorganisms from the objects. It can be accomplished using various methods, including heat exposure, chemical treatment, high pressure, or a delicate membrane filtration procedure. In the current study, all necessary equipment was first carefully cleaned using detergents and distilled water, then rinsed with acetone, and finally sterilized in a hot air oven at 200 °C for two hours. They were maintained in laminar flow until their future use.

3.6.2   Media Preparation Procedure

The nutrient agar medium has been utilized for most antibacterial studies since it includes enough nutrients to support the improved growth of microorganisms. The nutritional agar suspension was made following the instructions provided by the manufacturing company. The agar suspension, petri dish, and other glass equipment were autoclaved for 15 minutes at 120 °C. After cooling for a short while, the autoclaved suspension was gently poured into each Petri plate. The plates were kept under UV laminar flow to maintain a sterile atmosphere and avoid bacterial contamination. The plates were left in the sterile area until the agar had solidified.

3.6.3 Preparation of Culture

The antibacterial investigation has been conducted both on gram-positive and gram-negative pathogenic bacteria. They were *Escherichia coli (E. coli), Klebsiella pneumonia (K. pneumonia), Pseudomonas aerugenosa (P. aeruginosa)*, *Enterococci*, and *Staphylococcus aureus (S. aureus)*. The microbiological laboratory at Biratnagar Teaching Hospital in Biratnagar, Nepal, and Suraksha Hospital Pvt. Ltd., provided a new culture of these clinical bacterial strains.

3.6.4 Organism Information

Escherichia coli

It is a gram-negative, nonsporulating bacterium, normally rod-shaped, and around 2 μm long. According to morphological evidence, bacterial cells have a diameter that ranges from 0.25 to 1 μm and a cell volume of 0.6 to 0.7 $μm^3$. It is a member of the Enterobacteriaceae family. Its cell wall consists of a thin peptidoglycan layer and an outer membrane. Since this outer membrane of the organism acts as a barrier to antibacterial agents, most antibiotics are resistant to this organism.

Nearly a hundred strains of *E. coli* bacteria have been identified and isolated, which remain in the large intestine of many mammals, including humans. Most strains that contribute to food digestion and control pathogenic bacteria are safe for humans. Some of the strains support the synthesis of the B complex and the metabolism of vitamins. However, some *E. coli* strains cause acute food poisoning that leads to enterohemorrhagic diarrhea. The blood vessels are damaged, and the cells lining of the large intestines wall are destroyed by this bacterial strain, resulting in internal bleeding. For small children, such conditions are dangerous and pose a death risk (Aijuka *et al.*, 2018). People having weaker immune systems, like elderly or younger children, are much more vulnerable to this bacterial strain. In the present study, antibiotics were tested against clinical strains of human pathogenic *E. coli*.

Klebsiella pneumoniae

Klebsiella pneumoniae is a rod-shaped, nonmotile, and gram-negative bacterium of the Enterobacteriaceae family. Edwin Klebs, a German microbiologist, investigated this organism in the 19th century and gave it the name *Klebsiella*. This bacteria ordinarily resides human intestine, where it does not cause diseases. Clinically speaking, it is regarded as a human pathogenic organism that results explicitly in lung damage. The most prevalent illness brought on by this bacterium is bronchitis (also known as bronchopneumonia), which, in its acute form, can be fatal death of people.

Additionally, *Klebsiella* can infect the urinary tract, lower biliary tract, surgical incision sites, and bloodstream. The majority of middle-aged and older individuals are more vulnerable to this illness. Klebsiella infections typically do not occur in healthy individuals. Patients needing long courses of medications and external equipment like ventilators or intravenous catheters are especially at risk for contracting this infection. The spread of bacteria through the atmosphere is unknown; however, it can be spread from person to person or through contaminated environments less commonly. According to a recent study report, antibiotic resistance is significantly dangerous during the treatment of this organism.

Staphylococcus aureus

In 1880, Scottish surgeon Sir Alexander Ogston found *Staphylococcus aureus* in the fluid from surgical abscesses. It is a member of the Staphylococcaceae bacterial family and is a coccal gram-positive bacterium. In all types of cultural media, it grows very well. It is a facultative anaerobic bacterium that can grow without oxygen. Skin and superficial tissues of the body are the most commonly infected by this organism. In addition to respiratory infections, such as sinusitis, it can also cause food poisoning. The medical literature refers to this bacterium as S. aureus, and its groups appeared as grape-like clusters. Morphologically, *S. aureus* is small, nonmotile, and round-shaped cocci. Air droplets act as a means of transmission for this pathogenic organism. When infected individuals cough or sneeze, the bacterial suspension of tiny droplets of saliva or mucous spreads in the air and then spread to other people. Direct contact with objects that are contaminated with bacteria is another typical mode of

transmission. About 30% of healthy people carry this organism in their pharynx, noses, and skin.

It can also cause other infections, such as pneumonia, meningitis, osteomyelitis, and endocarditis, in addition to the most typical skin infection. The Fever, chills, and hypotension are symptoms of a blood infection caused by a pathogenic organism, *S. aureus*. Usually, skin infections result in pus-filled abscesses that drain pus. This bacterium causes food poisoning by putting a toxin into the food, which can cause severe nausea and vomiting in those who consume it.

Recent years have seen an increased antibacterial resistance to *S. aureus* strains, making this bacterium more likely to spread in hospitals and community settings (Sipahi *et al.*, 2017).

Enterococcus

A significant genus of lactic acid bacteria belonging to the phylum Bacillota is called Enterococcus. Gram-positive enterococci frequently appear in pairs (diplococci) or short chains, and they are hard to differentiate from streptococci based solely on morphological traits.

As facultative anaerobic organisms, enterococci may carry out cellular respiration in both oxygen-rich and oxygen-poor situations. Enterococci can survive in a variety of harsh environmental circumstances, including high sodium chloride concentrations (6.5%), extreme temperatures (10–45 °C), and a pH range of 4.6–9.9.

UTIs, bacteremia, bacterial endocarditis, diverticulitis, meningitis, and spontaneous bacterial peritonitis are among the significant clinical infections caused by Enterococcus. Ampicillin, penicillin, and vancomycin can all be used to treat these bacteria's sensitive strains. Even in circumstances of vancomycin resistance, urinary tract infections can be particularly treated with nitrofurantoin.

Pseudomonas aerugenosa

Pseudomonas aeruginosa is a widespread rod-shaped, gram-negative, aerobic-facultatively anaerobic bacteria that can harm both plants and animals, including humans. *P. aeruginosa* is a multidrug-resistant pathogen and a species of considerable medical significance. It is known for its widespread distribution, intrinsically sophisticated mechanisms of antibiotic resistance, and association with serious illnesses, including hospital-acquired infections like ventilator-associated pneumonia and various sepsis syndromes.
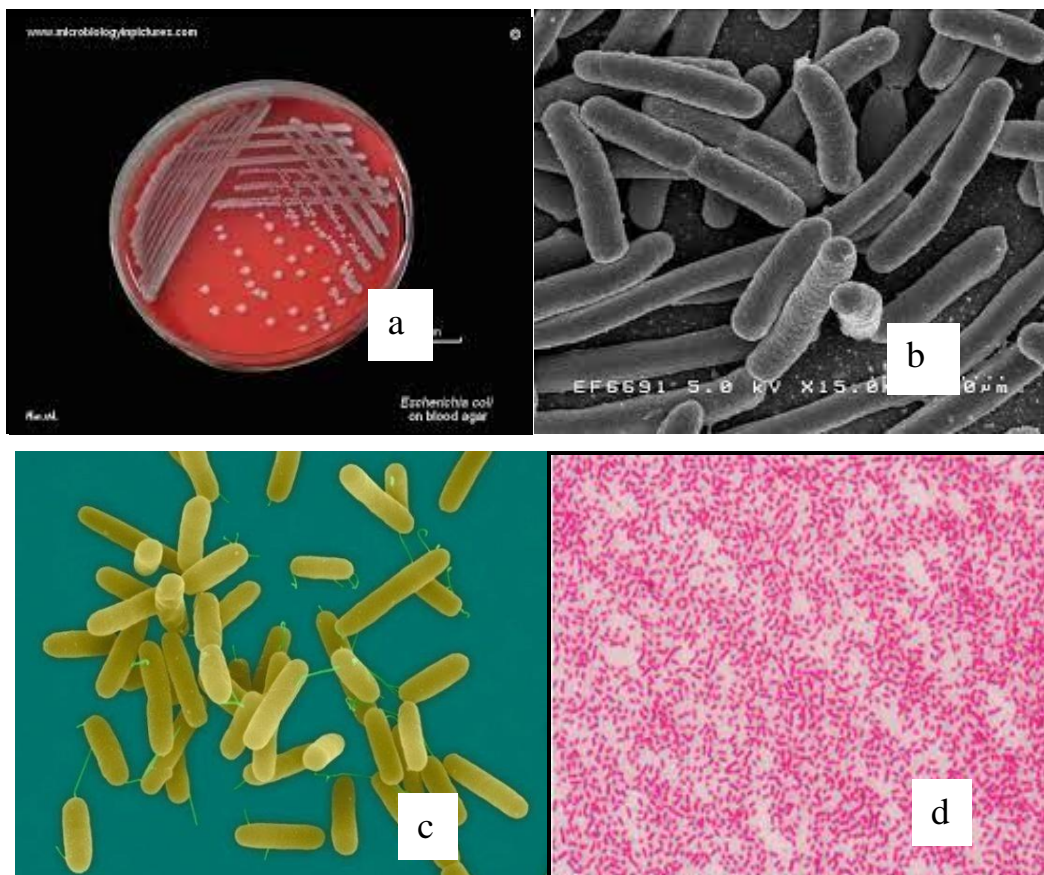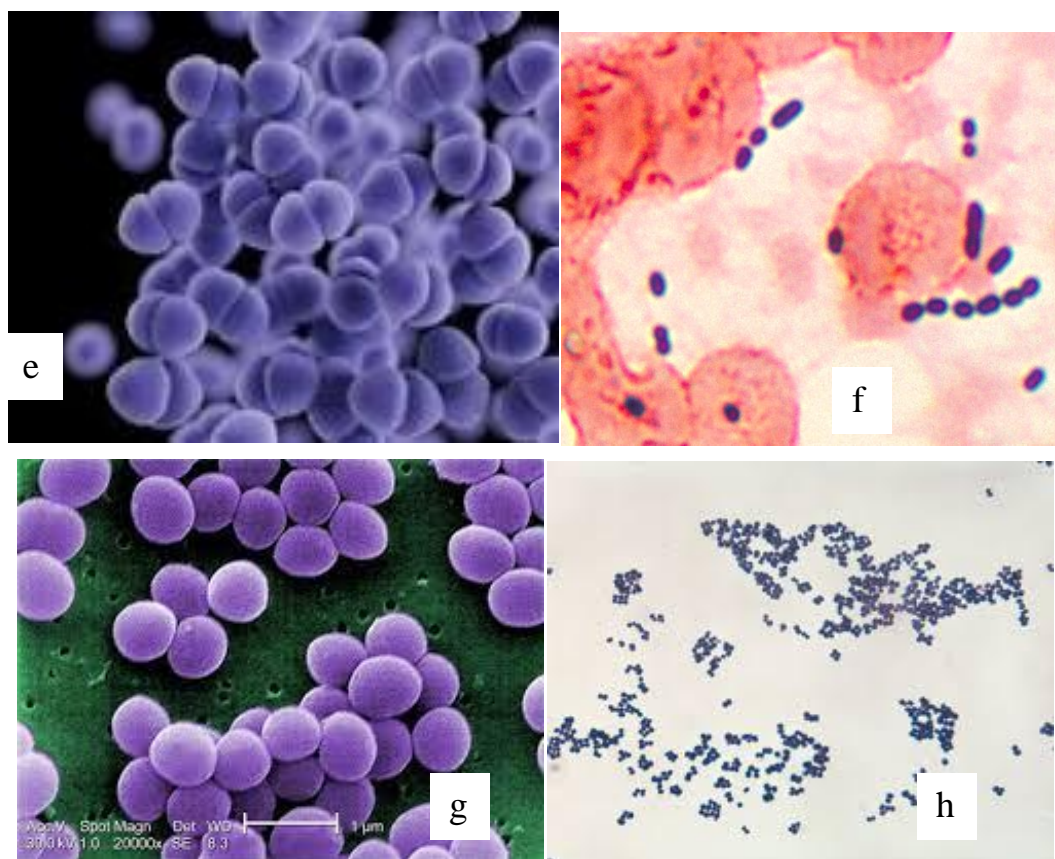
Figure 12: *E. coli* (a&b), *P. aeruginosa* (c), *K. pneumonia* (d), *Enterococcus* (e&f), *S.aureus* (g&h) (*Source: Internet*)

3.6.5   Paper Disc Preparation

Paper discs were prepared using Whatman filter paper no. 1. The filter paper was sized to 5 and 6 mm using a paper punching machine. The paper disc was heated to eliminate the moisture and activate the absorption capacity. In order to load the synthesized compounds on the disc, the disc was sterilized first.

3.6.6   Loading of Chemicals

Capillary tube was used to load the paper disc with synthesized compounds at different concentrations prepared in DMSO solvent. In order to absorb the maximum amount of solution, the loaded paper was dried with hot air through a hair drier machine.

3.6.7 Inoculation of Organism and Measurement of Growth Inhibition Zone

A few bacteria colonies were homogenously suspended in tryptone soy broth and maintained for two hours at 37 °C for homogeneous growth. Then, using a sterile stick swab, the bacterial culture was swabbed on agar media. Plates were incubated for 24 - 36 hours at 37 °C with loaded paper discs after being stuck onto swabbed media. To compare the inhibition zone, the positive and negative control drug discs were also stuck to the media. The antibiogram zone measurement scale was used to examine and measure the diameter of the zone of inhibition.

CHAPTER 4

4. RESULTS AND DISCUSSION

4.1 Measurements of physical properties

Measurements of their physical characteristics, such as color, solubility, melting point, and conductivity, can be used to understand the behavior of metal complexes better. These are necessary to gather evidence that supports theories about how ligands and complexes develop during chemical reactions. The various chemicals each have distinctive physical characteristics, and a thorough study of these characteristics aids in defining the reaction's mechanism and anticipating the compound's nature.

4.1.1 Colour

The degenerate d-orbitals of metal ions interact with the electron cloud of the ligand to split it into several energy levels that correspond to the geometrical shape of the complexes. When these complexes are exposed to electromagnetic radiation, the typical energy absorption and electronic transition occur from lower to higher energy levels. The chemical complex emits spectral energy complementary to the absorbed electromagnetic radiation as it absorbs the radiation at the visible region of the spectrum. As a result, it produces color from the complexes. The variable range of electronic absorption, whether by π bonding, nonbonding, or free electrons, causes the change of color of the complexes. In general, auxochromes enable the chromophores to exhibit electronic absorption in the UV-visible region, which gives the substances their distinctive color. Color intensity further enhances with conjugation. The metal complexes show different colors due to the electronic absorption of their free electrons. Based on Table 5-6, different colors of synthesized compounds can be identified.

4.1.2 Melting Points and Solubility

Chemicals have a characteristic solubility and melting point. In addition to water, various organic solvents were tested for the solubility of the ligands and metal complexes. Data on their solubility are listed in Table A3. The analysis of solubility data showed that the ligands and metal complexes were soluble in organic solvents but insoluble in water. Metal complexes were partially soluble in ethanol but soluble in DMSO and DMF, while ligands were soluble in ethanol, DMSO, and DMF. The melting points were determined by filling a finely powdered sample in a glass capillary and heating it in a Gallen Kamp melting point apparatus and a VEEGO ASD-10013 programmable melting point apparatus.

4.1.3 Conductivity Measurement

The conductivity data determines whether the complexes are electrolytes or non-electrolytes. In this study, the conductivities of complexes at M/1000 concentration were measured at room temperature, and their data are shown in Table 1. The data analysis revealed the varieties of metal complexes. Most are 1:1 electrolytes with conductivity values between 50 to 100 Ω^{-1} $mol^{-1}cm^2$ while Co-HL with 108.8 Ω^{-1} $mol^{-1}cm^2$ is a 1:2 electrolyte (Ali *et al.*, 2013).

Table 1: Molar conductivity (Λ_M) and geometry

S.N.	Compounds	Geometry	Λ_M (Ω^{-1} $mol^{-1}cm^2$)
1	DDAP2C	-	7.5
2	HL (DDAP3C)	-	5.6
3	Co-DDAP2C	Octahedral	61.2
4	Ni-DDAP2C	Octahedral	64.5
5	Cu-DDAP2C	Tetrahedral, Dinuclear	75.8
6	Zn-DDAP2C	Octahedral	43.2
7	Co-HL (Complex1)	Octahedral	108.8
8	Ni-HL (Complex3)	Octahedral	67.5
9	Cu-HL (Complex4)	Tetrahedral	45.5
10	Zn-HL (Complex2)	Distorted trigonal bipyramidal	83.6

4.2   Conductivity study

4.2.1. Critical Micelle Concentration (CMC) Study of DDA and Metal Complexes of DDAP2C at 298.15 K

After adequately mixing the components at constant temperatures, the conductivity of each dilution was measured. The change in conductivity with the concentration of the surfactant and Metallo-surfactant (metal complexes) is graphically shown in Figures 13-15. Specific conductivity increases with concentration with a fixed slope, and at a particular concentration, the slope changes. The CMC is determined, as a result of the point of intersection of the two linear changes in the plot. The CMC and other parameters obtained for the surfactant and metal complexes are presented in Table 2. At 298.15 K, the conductivity was measured three times, and the precision of the CMC value was found to be within a 2-3% error range.

In comparison to the dodecylamine (surfactant) (1.53×10^{-2} M), which is similar to the CMC of the surfactant dodecyl ammonium chloride, the metal complexes have substantially lower CMC values. The lower CMC of metal complexes relative to surfactants may be due to two factors. The first factor that could account for this drop in CMC of metal complexes is the rise in hydrophobicity brought on by hydrocarbon chains, which encourages the tendency for micellization (Wagay *et al.*, 2019). The second factor could be that the dissolution of the Metallo-surfactants frequently results in forming ions and surface active molecules. The CMC value should generally rise as electronegativity increases and ionic radius decreases during the period, but zinc defies the pattern and has a lower CMC than a nickel. Although zinc is on the right side than a nickel in the periodic table, its electronegativity value of 1.65 is lower than that of nickel's (1.91), leading to a higher ionic radius of 74 pm for zinc than for nickel (70 pm). It is reasonable to anticipate that a change in electronegativity will likewise result in a change in the ionic character. This results in an increase in the ionic strength surrounding the micelles, resulting in a sort of screening effect that decreases the repulsion between polar head groups, encourages micellization, and lowers CMC values (Veeralakshmi *et al.*, 2014). Zinc ions have larger ionic radii than nickel ions, making them less hydrated. As a result, there is greater metal penetration into the micelle, which lowers the CMC by reducing

electrostatic repulsion. Finally, it has been ascertained that the 3d metal complexes of the surfactant have higher micellization capacities than typical synthetic organic surfactants. This behavior is governed by the interaction of ionic radii, the electronegativity of metal ions, and the hydrophobic chain of the surfactant (Mehta & Kaur, 2013). The pseudo-phase separation model was used to calculate the free energy of micellization for the complexes (Caleb Noble Chandar *et al.*, 2013).

$$\Delta G°_m = (2 - \alpha)RTlnCMC$$

Where α, R, and T stand for the degree of micellar ionization, the gas constant, and absolute temperature, respectively. ΔG^o_m was negative for all complexes but became less negative as Zn-DDAP2C, Ni-DDAP2C, and DDA were descending in order. The negative ΔG^o_m indicates the spontaneous micellization process, but the process becomes less spontaneous in descending order of Zn-DDAP2C, Ni-DDAP2C, and DDA corresponding to their energy. Larger metal ions in surfactants result in higher head polarity, and as head polarity rises in a metal surfactant, so does the negative Gibbs free energy of micellization. Micellization of metal-based surfactants is more favorable with this result. Similarly The CMC and other parameters obtained for the cobalt and copper complexes (Co-DDAP2C & Cu-DDAP2C) are presented in Table 2 and the graph plotted between concentrations versus conductivity for them are given in Figures 16-17.

Table 2: Physical parameters of DDA and metal complexes of DDAP2C ligand in ethanol at 298.15 K

Compounds	S_2 (µS cm^{-1} l·mole^{-1})	S_1 (µS cm^{-1} l·mole^{-1})	α=S2/S1	CMC (mole L^{-1})	ΔG^o_m (kJmol^{-1})
DDA	240	633	0.379	1.53 x 10^{-2}	-16.79
Ni-DDAP2C	6.27 x 10^4	6.98 x 10^4	0.898	1.002 x 10^{-3}	-18.86
Co-DDAP2C	9962	3.66 x 10^4	0.272	5.14 x 10^{-4}	-32.42
Cu-DDAP2C	2.96 x 10^4	4.77 x 10^4	0.621	4.14 x 10^{-4}	-26.61
Zn-DDAP2C	4.63 x 10^4	4.96 x 10^4	0.933	3.85 x 10^{-4}	-20.79

premicellar slope (S1), postmicellar slope (S2), critical micelle concentration (CMC), Gibbs free energy of micellization (ΔG^o_m), and degree of dissociation (α)

Figure 13: Plot of conductivity versus concentration of dodecylamine (DDA)
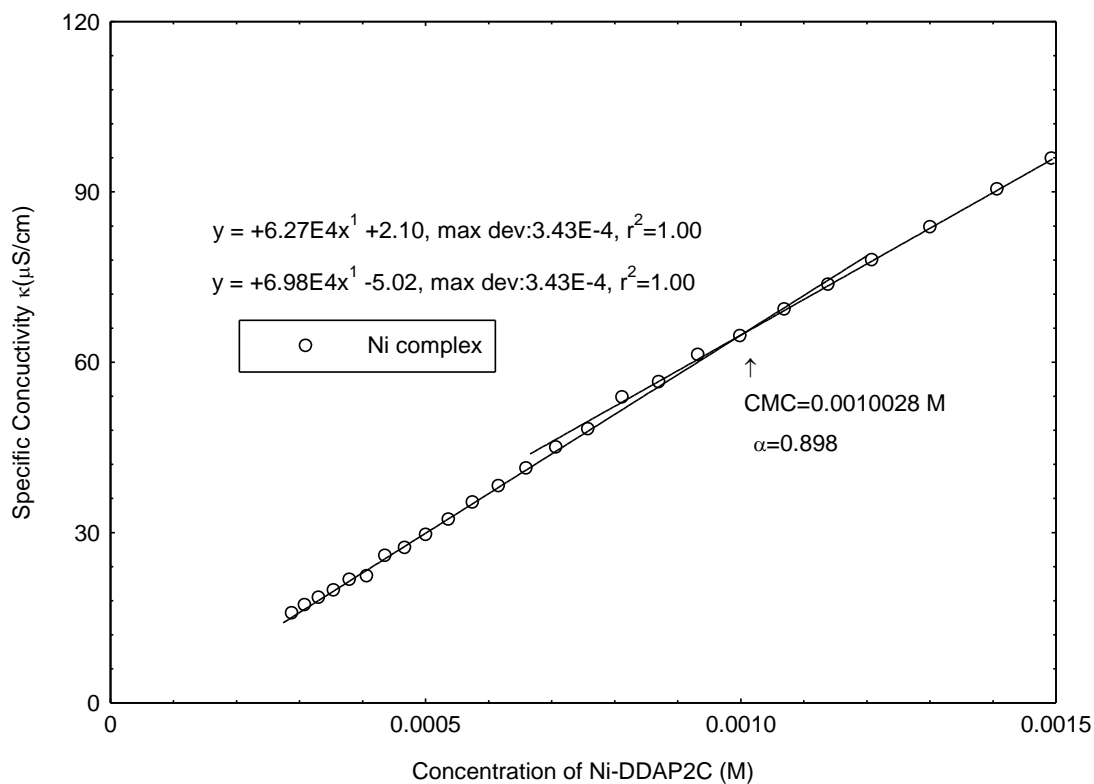
Figure 14: Plot of conductivity versus concentration of Ni-DDAP2C
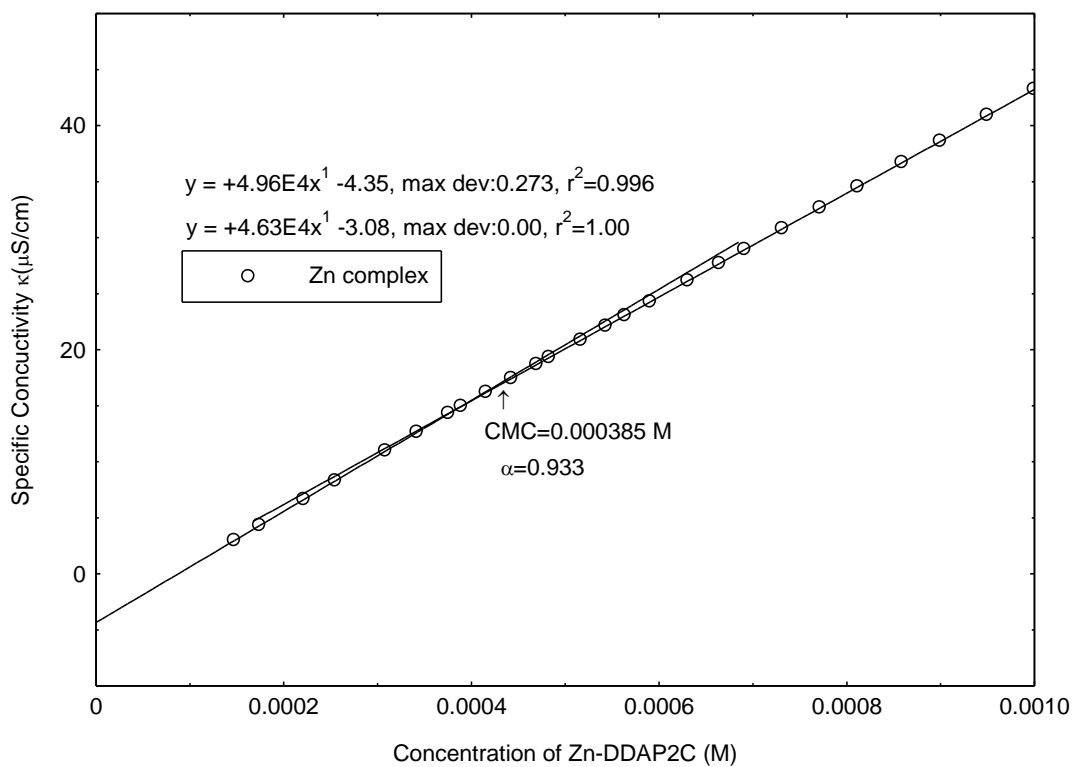
Figure 15: Plot of conductivity versus concentration of Zn-DDAP2C
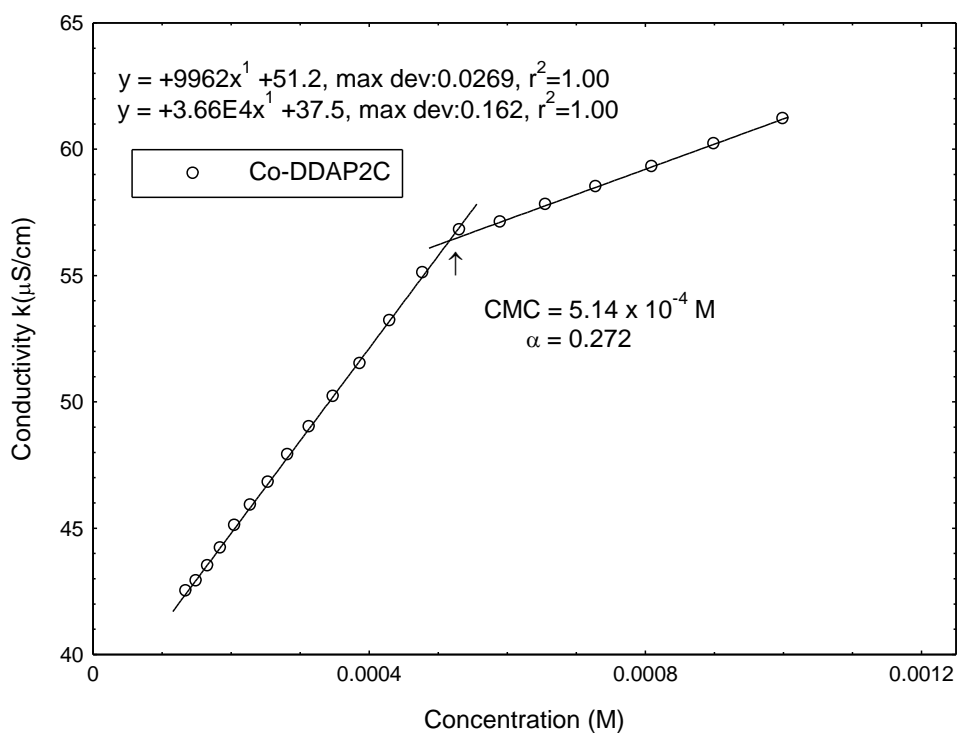
Figure 16: Plot of conductivity versus concentration of Co-DDAP2C

54
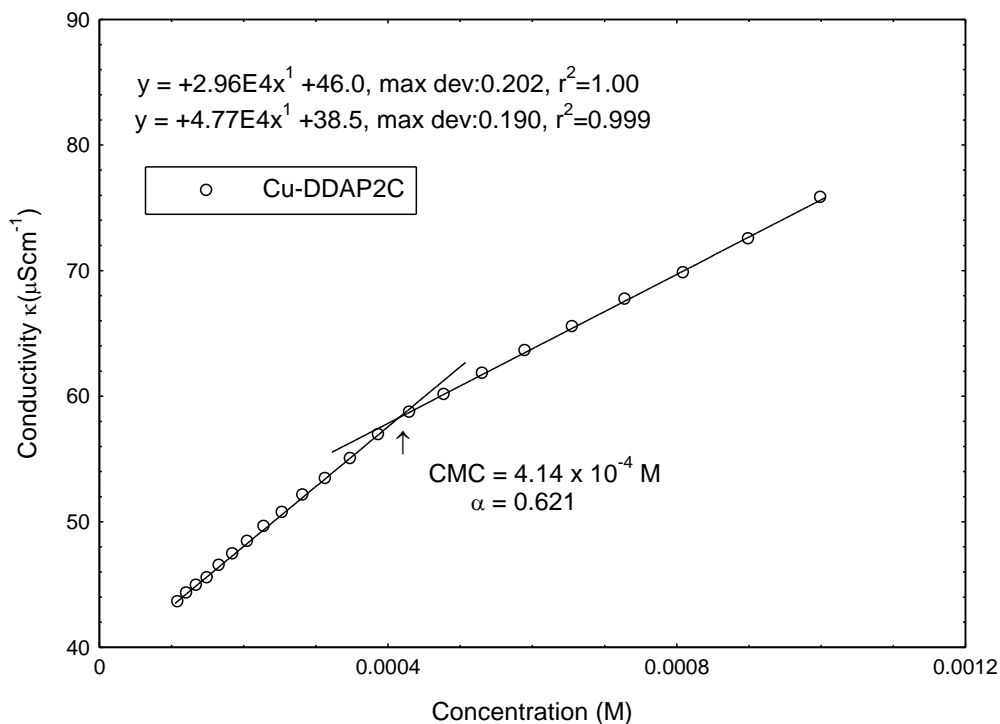
Figure 17: Plot of conductivity versus concentration of Cu-DDAP2C

4.2.2 Critical Micelle Concentration (CMC) Study of DDA and Metal Complexes of HL (DDAP3C) at 298 K

The specific conductivities of LA (DDA) and its metal complexes 1 and 2 were evaluated at 298 K at various concentrations in order to determine the degree of micellization (α) and critical micelle concentration (CMC). The conductivity versus concentration plot shows two straight lines denoting the pre-micellar zone and the post-micellar zone. The CMC is indicated by the intersection of the two straight lines in the plot, and the degree of micellization (α) is represented with the slope ratio between the post- and pre-micellar regions. The computed values of CMC and (α) are displayed in Table 3, and the conductivity-concentration plots are illustrated in Figures 18-19. We have previously documented the CMC value for LA in the literature (1.5×10^{-2} M) at 298 K (Adhikari *et al.*, 2022) and the CMC of the complexes mentioned here is lower than this value. As calculated, complexes **1** and **2** have CMC values of $3.21 \ 10^{-4}$ M and $1.98 \ 10^{-4}$ M, respectively. The electrolytic nature of the complexes as well as changes in the electronegativity and size of the metal ions can all be used to explain the variations in the CMC of the complexes. The rise in the CMC of metal complexes is typically brought by a decrease in the ionic

radii and an increase in the electronegativity of the metals. The ionic radius of Zn^{+2} is more significant than that of Co^{+2}, and Zn is less electronegative than Co. Thus, the CMC trend of this study supported our prediction. When the ionic concentration around micelles is higher, polar head groups are less likely to repel each other, micellization is easy, and CMC is significantly lower concerning larger ionic size (Chandar *et al.*, 2009; Nagaraj *et al.*, 2015). The given equation was used to compute the Gibbs free energy of micellization ($G°_m$):

$$\Delta G°_m = (2 - \alpha) \, RT \, ln(CMC)$$

It was found that this value ($\Delta G°_m$) was negative, indicating spontaneous micellization. In our investigation, compound **2** exhibited a higher negative ($G°_m$) due to easier micellization. These findings showed that Metallo-surfactants have a higher tendency to micellize (Mehta *et al.*, 2012). Similarlrly, the calculated values of CMC and (α) for complex **3** and **4** are presented in Table 3, and the conductivity-concentration plots are illustrated in Figures 20-21.

Table 3: Physical parameters of DDA and metal complexes of DDAP3C ligand in DMSO at 298 K

Compounds	S_1 ($\mu S \, cm^{-1} \, l \cdot mole^{-1}$)	S_2 ($\mu S \, cm^{-1} \, l \cdot mole^{-1}$)	$\alpha = S2/S1$	CMC (mole L^{-1})	$\Delta G°_m$ (kJmol^{-1})
LA (DDA)	633	240	0.379	1.53×10^{-2}	-16.79
Complex **1**	3.98×10^4	1.34×10^4	0.337	3.21×10^{-4}	-33.14
Complex **2**	6.42×10^4	1.02×10^4	0.159	1.98×10^{-4}	-38.89
Complex **3**	3.44×10^4	1.72×10^4	0.500	5.47×10^{-4}	-27.91
Complex **4**	5.44×10^4	1.36×10^4	0.250	2.99×10^{-4}	-35.18

premicellar slope (S1), postmicellar slope (S2), critical micelle concentration (CMC),

Gibbs free energy of micellization ($\Delta G°_m$), and degree of dissociation (α)

Complex **1** (Co-complex), Complex **2** (Zn-complex), Complex **3** (Ni-complex),

Complex **4** (Cu-complex),
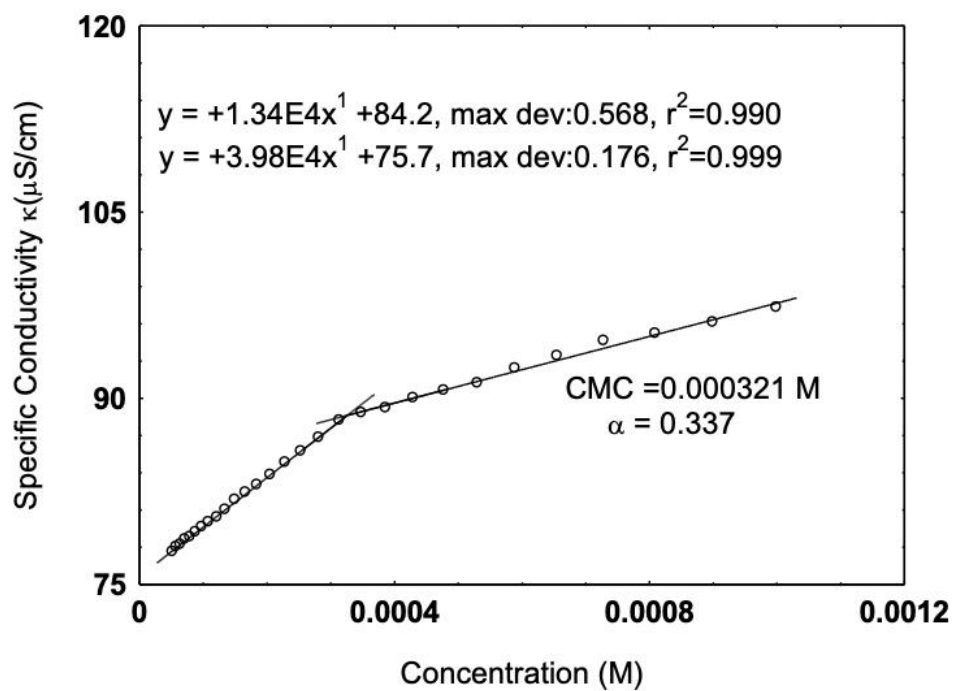
Figure 18: Plot of conductivity versus concentration of Complex **1**
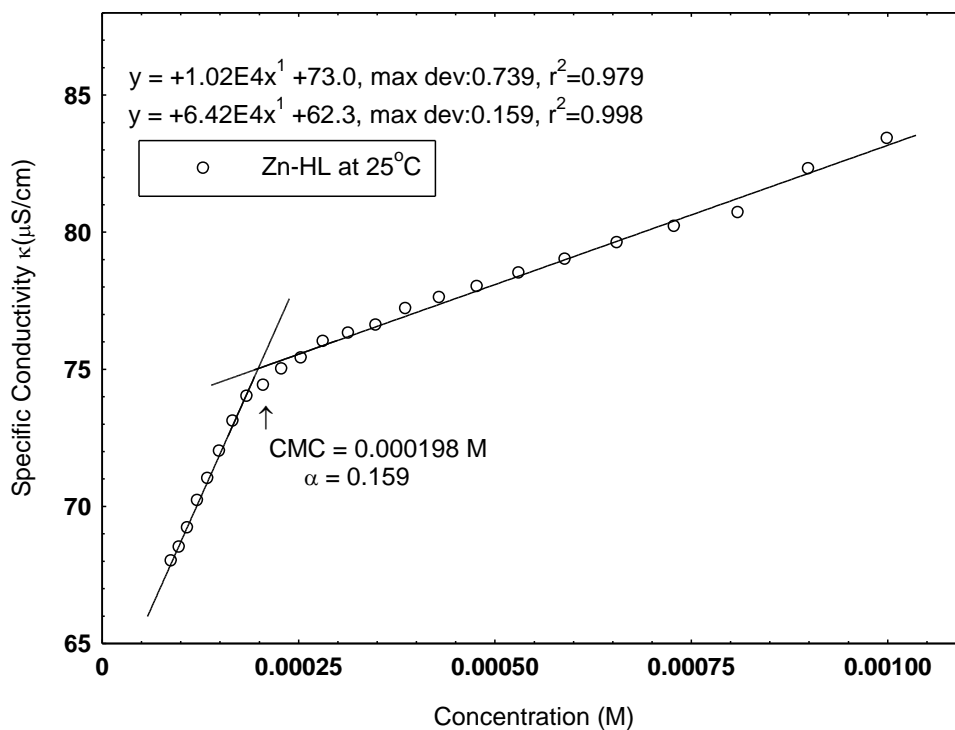
Figure 19: Plot of conductivity versus concentration of Complex **2**
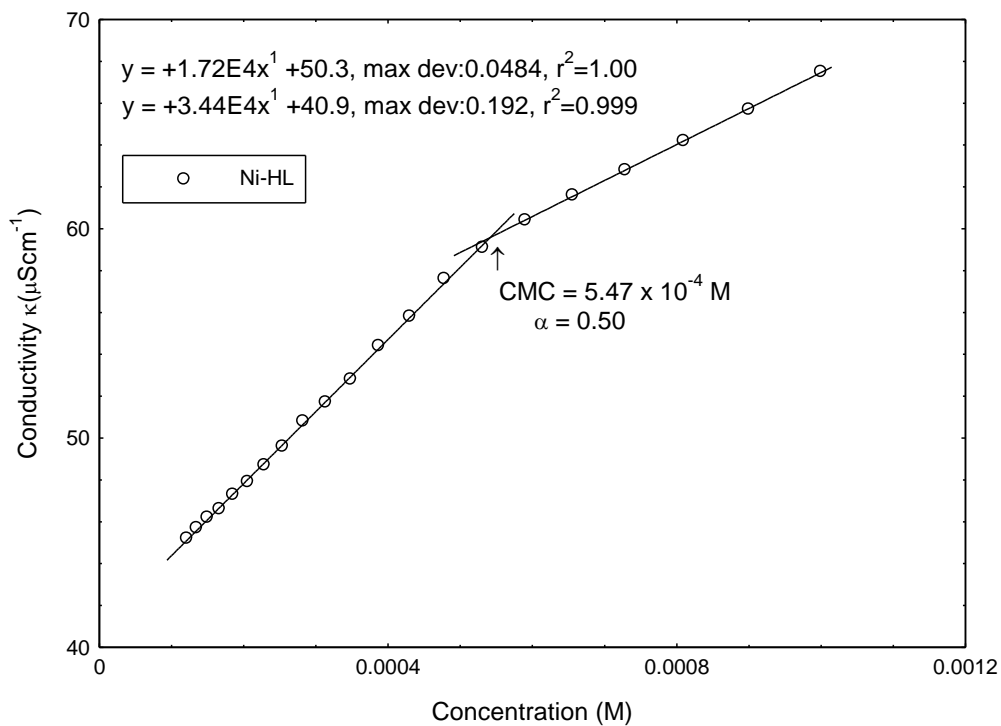
Figure 20: Plot of conductivity versus concentration of Complex **3**
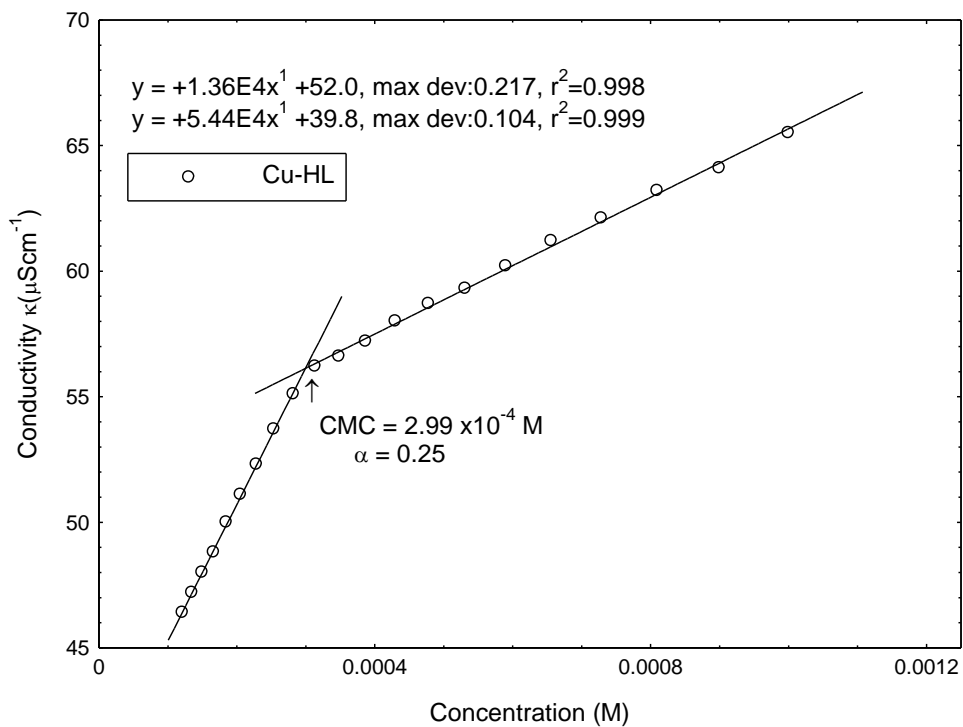
Figure 21: Plot of conductivity versus concentration of Complex **4**

4.2.3 Critical Micelle Concentration (CMC) Study of LA (DDA), Complex1 and Complex2 at 308 K & 318 K

The conductivity against concentration plots for **LA** (**DDA**), complex **1**, and complex **2** at 308 K and 318 K are displayed in Figures 22-27. Before and after CMC, the specific conductivity values changed. The conductivity declines after the CMC point as a result of the development of micelles with lesser ionic mobility (Bhattarai, 2015). The physicochemical data generated from conductivity vs concentration plots are listed in Table 4. The CMC values for **LA** and complexes **1** and **2** were lowest at a lower temperature of 308 K and highest at a higher temperature of 318 K. Prior research revealed that **LA** (1.5 10^{-2} M) has a higher CMC value than complexes **1** (3.21 10^{-4} M) and **2** (1.98 10^{-4} M) (Adhikari *et al.*, 2023). At a specific temperature, the Gibbs free energy of micellization increased from **LA** to complex **1** and then to complex **2,** and was negative for all (Table 4), confirming spontaneity.

Table 4: Physical parameters of DDA, Complex **1** and Complex **2** in DMSO at 308 and 318 K

Compounds	T (K)	CMC (mol L^{-1})	ΔG_m^o (kJ/mol)	$\alpha = S_2/S_1$	Std. Dev. in Linear Fit (SD)
LA	308	4.02×10^{-2}	-12.50	0.48	0.1200
	318	4.68×10^{-2}	-12.21	0.49	0.1703
Complex 1	308	3.59×10^{-4}	-32.09	0.42	0.1738
	318	4.33×10^{-4}	-31.33	0.47	0.7464
Complex 2	308	2.64×10^{-4}	-34.16	0.38	0.2744
	318	3.76×10^{-4}	-32.94	0.42	0.0561

Figure 22: Plot of conductivity versus concentration of **LA (DDA)** at 308 K
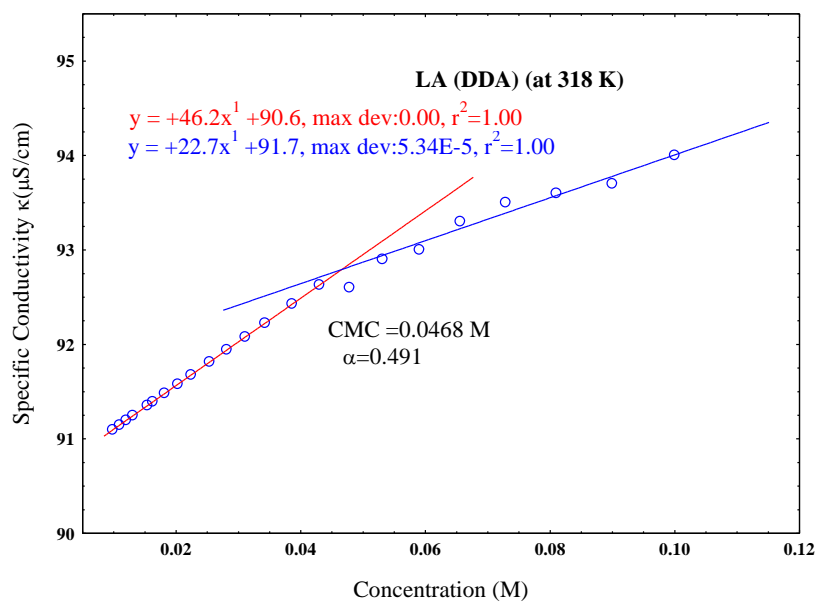
Figure 23: Plot of conductivity versus concentration of **LA (DDA)** at 318 K
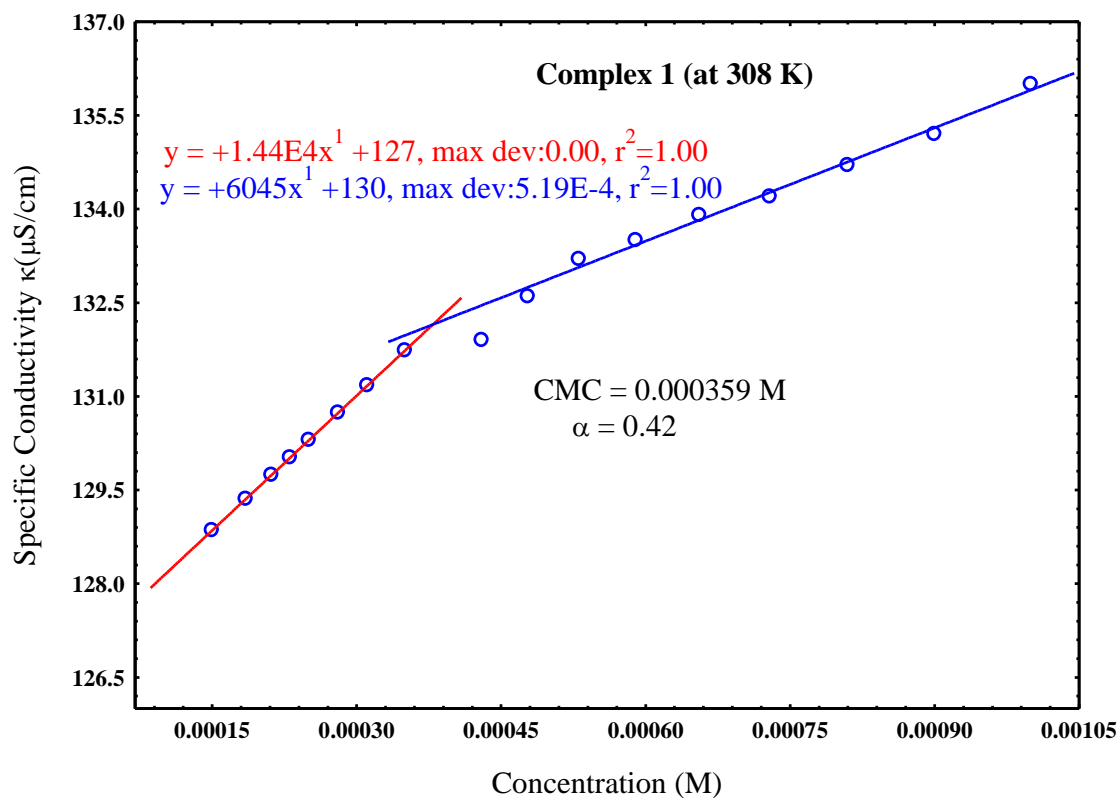
Figure 24: Plot of conductivity versus concentration of Complex **1** at 308 K
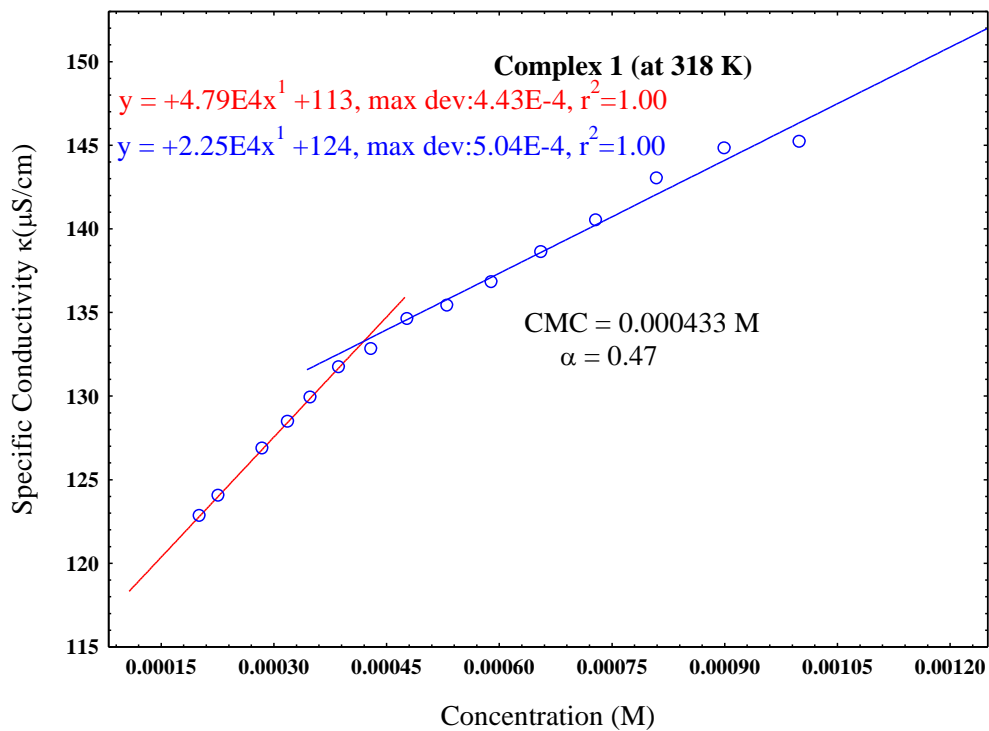
Figure 25: Plot of conductivity versus concentration of Complex **1** at 318 K
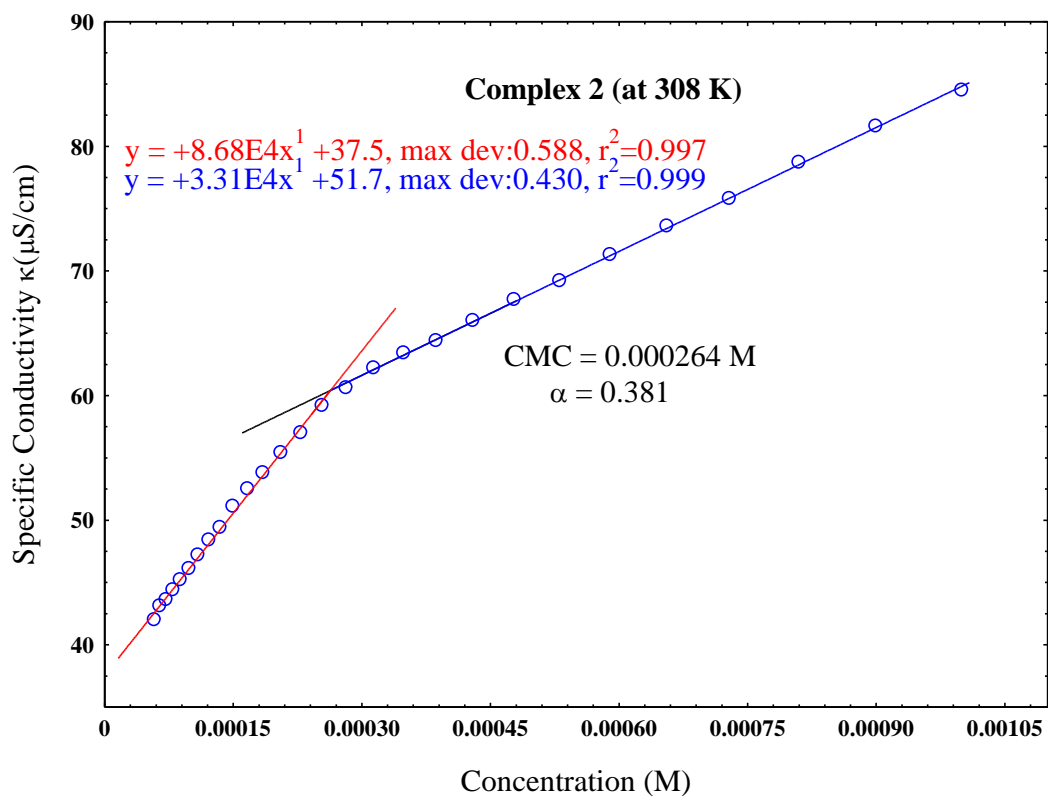
Figure 26: Plot of conductivity versus concentration of Complex **2** at 308 K
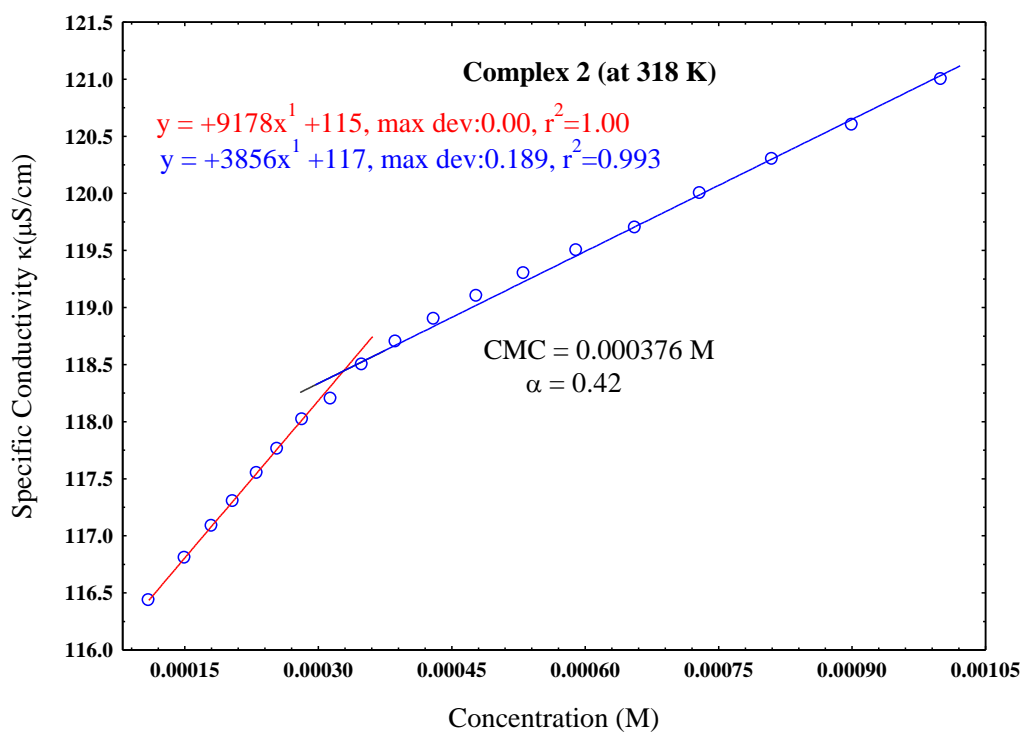
Figure 27: Plot of conductivity versus concentration of Complex **2** at 318 K

4.3   Microanalytical Results

Elemental analysis is a method of quantitatively or qualitatively determining the presence of carbon, hydrogen, nitrogen, and sulfur in organic matrices and other types of materials rapidly. The CHNS analysis is a low-cost method that can give essential details on the composition and purity of chemical compounds. The microanalytical results of the Schiff base ligands and their metal complexes in our study are presented in Table 5-6. The microanalytical findings are very compatible with the suggested stoichiometry of the compounds.

Table 5: Micro-analytical and Physical data of the Schiff base ligand DDAP2C and its complexes

Compounds	Empirical Formula	Formula Wt.	Yield %	Color	M.Pt. (°C)	Calculated (Found) (%)		
						C	H	N
DDAP2C	$C_{17}H_{30}N_2$	262	82	Reddish Brown	58-59	77.80 (77.33)	11.52 (11.36)	10.67 (10.47)
Ni-DDAP2C	$C_{17}H_{35}ClN_2NiO_3$	410	78	Light Green	170-175	49.85 (49.57)	8.65 (8. 35)	6.84 (6. 89)
Zn-DDAP2C	$C_{17}H_{35}ClN_2O_3Zn$	416	84	Leaf Brown	105-107	49.05 (48.77)	8.47 (8. 96)	6.73 (6. 40)
Co-DDAP2C	$C_{34}H_{72}Cl_2CoN_4O_7$	778.79	72	Coffee Colour	193.2-194.5	52.44 (51.97)	9.32 (9.61)	7.19 (7.29)
Cu-DDAP2C	$C_{34}H_{76}Cl_2Cu_2N_4O_8$	864.97	74	Black	158-160	47.21 (47.95)	8.62 (8.04)	6.48 (6.14)

Table 6: Micro-analytical and physical data of the Schiff base ligand DDAP3C and its complexes

Compounds	Empirical Formula	Formula Wt.	Yield %	Color	M.Pt. (°C)	Calculated (Found) (%)		
						C	H	N
HL (DDAP3C)	$C_{17}H_{30}N_2$	262	80	Light Orange	67-69	77.80 (77.91)	11.52 (11.31)	10.67 (10.48)
Complex **1**	$C_{34}H_{66}Cl_2CoN_4O_3$	708	75	Green	70-76	57.78 (58.02)	9.13 (9.25)	7.93 (7.81)
Complex **2**	$C_{34}H_{66}Cl_2N_4O_3Zn$	714	68	Reddish Brown	68-70	57.26 (57.34)	9.05 (8.95)	7.86 (7.80)
Complex **3**	$C_{34}H_{65}Cl_2N_4NiO_{2.5}$	699.5	76	Greenish yellow	120	58.38 (58.85)	9.37 (9.75)	8.01 (7.91)
Complex **4**	$C_{34}H_{62}CuN_4O$	606.4	82	Green	123.5	67.34 (66.99)	10.30 (10.83)	9.24 (8.96)

4.4 Spectroscopy: Results and Discussion

4.4.1 FT-IR Spectral Study

4.4.1.1 FT-IR Spectra of DDAP2C and Metal Complexes

Comparing Schiff base ligands and metal complexes based on their FT-IR spectra provides essential information regarding the interaction between metals and ligands and the coordination mode of the ligand with the metals (El-Sonbati *et al.*, 2019). In our study, the bidentate DDAP2C ligand revealed a variety of FT-IR spectral bands corresponding to the groups it contains. These bands were shifted and, in some cases, even decreased after coordination with the metal ions. The broad absorption bands at 3163 cm^{-1} (DDAP2C) and 3127 cm^{-1} (Cu-DDAP2C) complex in the FT-IR spectra are attributed to the ν(N-H) stretching bands (Hashem *et al.*, 2021). Metal complexes don't have a pyrrole N-H stretching vibration band at 3163 cm^{-1} (Co-DDAP2C, Ni-DDAP2C, Zn-DDAP2C), providing strong evidence that the N-H moiety is deprotonated during complexation (Aboafia *et al.*, 2018; Anacona *et al.*, 2014; Festus *et al.*, 2019). In the spectra of DDAP2C ligand and metal complexes, the CH$_3$ group exhibits symmetric and asymmetric ν(C-H) stretching frequencies around 3000 cm^{-1} (Murugaiyan *et al.*, 2019). Significant variations in absorption frequencies are noticed at lower frequencies below 600 cm^{-1} and between 1775 and 1200 cm^{-1}. A

strong absorption band at 1648 cm^{-1} for the DDAP2C is attributed to the azomethine ν(C=N) stretch that has shifted to lower or higher wavenumbers in different metal complexes (Abu-khadra *et al.*, 2016; Diab *et al.*, 2019; Hashem *et al.*, 2021). The related ν(C=N) stretching frequencies for metal complexes display absorption bands within wave numbers 1622-1660 cm^{-1}. The respective IR spectral bands for the ν(C=N) stretch of Co-DDAP2C, Ni-DDAP2C, Cu-DDAP2C, and Zn-DDAP2C were observed at 1627, 1629, 1660, and 1622 cm^{-1}. All the complexes have shown a shift in the absorption band for the ν(C=N) stretch to lower wave numbers, and the Cu-DDAP2C has shifted to a higher value, demonstrating their participation with metal ions during coordination. In the IR spectrum of DDAP2C, the ν(C-N) stretching frequency for amine groups has changed from 1366 cm^{-1} to 1386 cm^{-1} for the Co-DDAP2C complex, 1385 cm^{-1} for the Ni-DDAP2C complex, 1376 cm^{-1} for the Cu-DDAP2C complex, and 1378 cm^{-1} for the Zn-DDAP2C complex, respectively. These changes nicely support the involvement of the said group in the coordination process with metal ions (El-Sonbati *et al.*, 2019; N. F. Mahmoud *et al.*, 2021). After complex formation, there was a minor change in the ν(Ar-C=C) stretching vibrational bands of DDAP2C at 1553, 1470, and 1421 cm^{-1}. The metal complexes also showed weaker bands at 422 cm^{-1} for Co-DDAP2C, 452 cm^{-1} for Ni-DDAP2C, 419 cm^{-1} for Cu-DDAP2C, and 466 cm^{-1} for Zn-DDAP2C in addition to these distinct absorption bands, which can be attributed to ν(M-N) stretching vibrations (Aggoun *et al.*, 2021). These comprehensive data suggest that the azomethine-N and amine-N of the pyrrole moiety of the ligand are responsible for the ligand-metal interaction. A summary of FT-IR data is presented in Table 7, and spectral diagrams are shown in Figures 28-32.

Table 7: FTIR spectral data of DDAP2C Schiff base ligand and its complexes in cm^{-1}

Complex	ν(NH)	ν(C=N) (imine)	ν (C-H)	ν (Ar-C=C)	ν (C-N)	ν(M-N)	ρ_w H$_2$O Coordinated
DDAP2C	3163	1648	2927, 2848	1421,1470 ,1553	1366	-	-
Ni-DDAP2C	-	1629	2924, 2854	1469, 1511	1385	452	3440
Zn-DDAP2C	-	1622	2924, 2848	1476	1378	466	3447
Co-DDAP2C		1627	2921, 2851	1466	1386	420	3552
Cu-DDAP2C	3127	1660	2920, 2850	1463, 1521	1376	422	3443
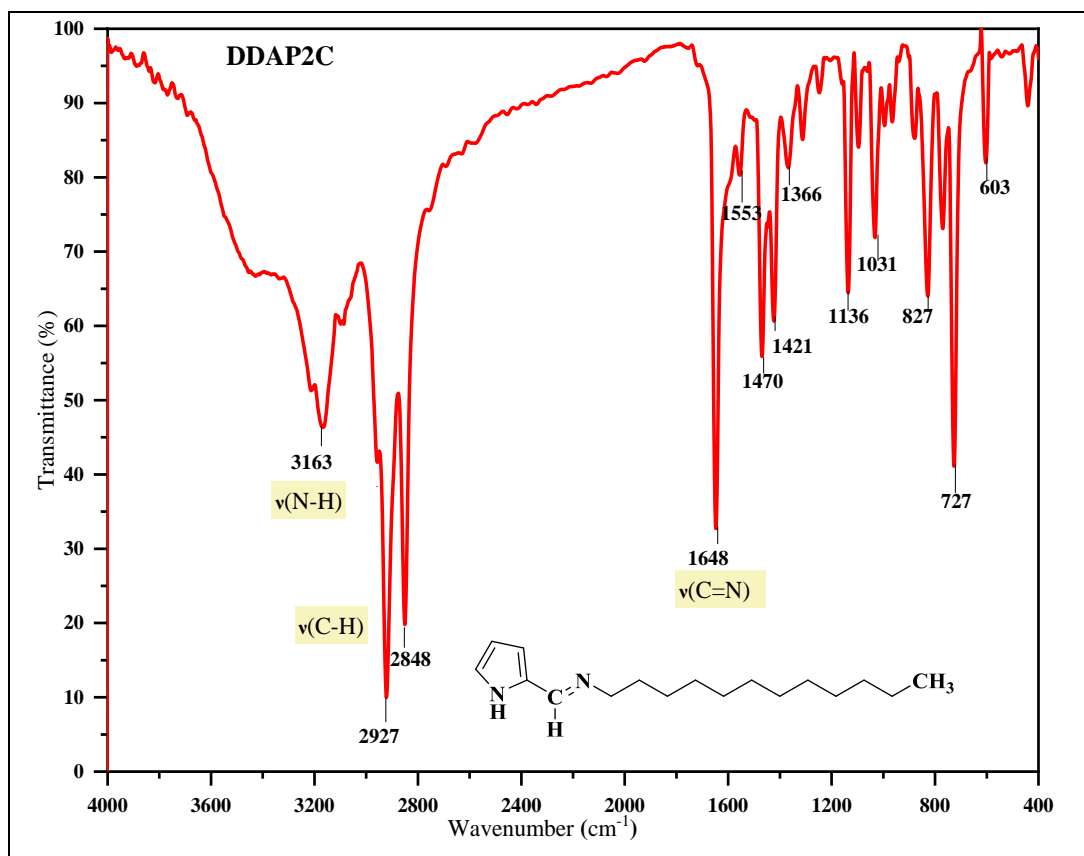
Figure 28: FT-IR spectrum of DDAP2C ligand
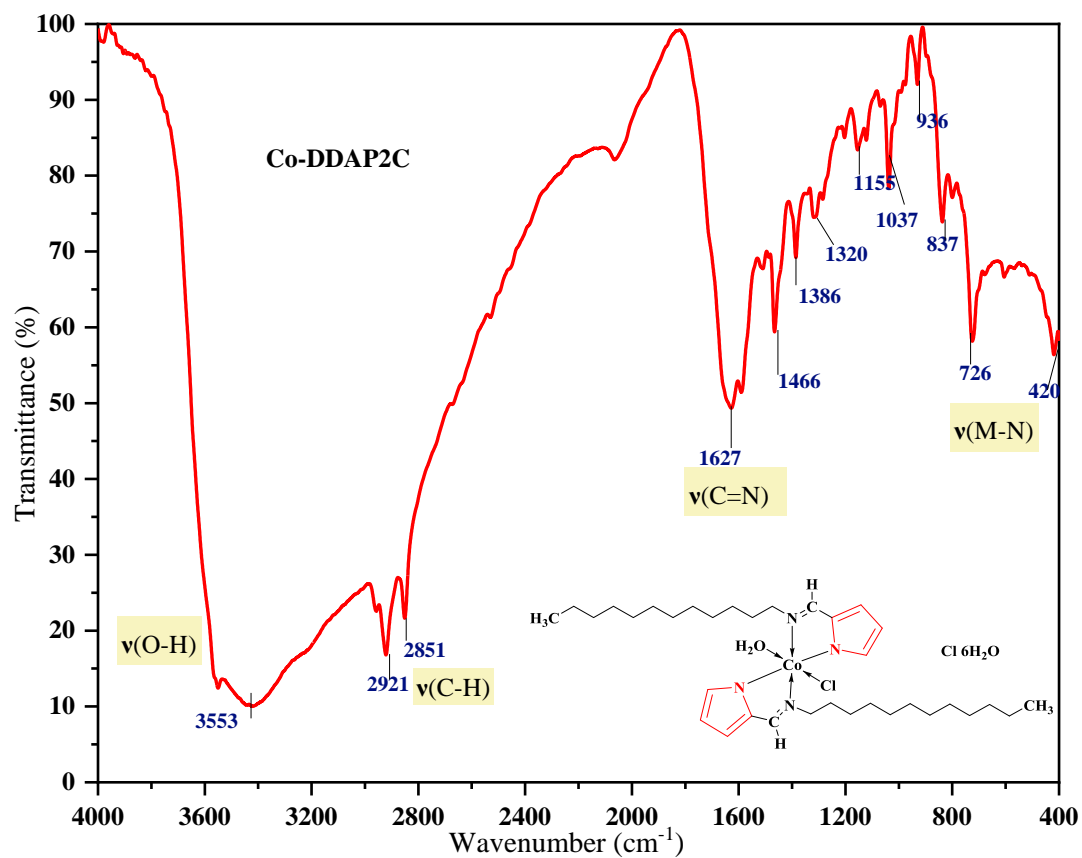
Figure 29: FT-IR spectrum of Co-DDAP2C complex
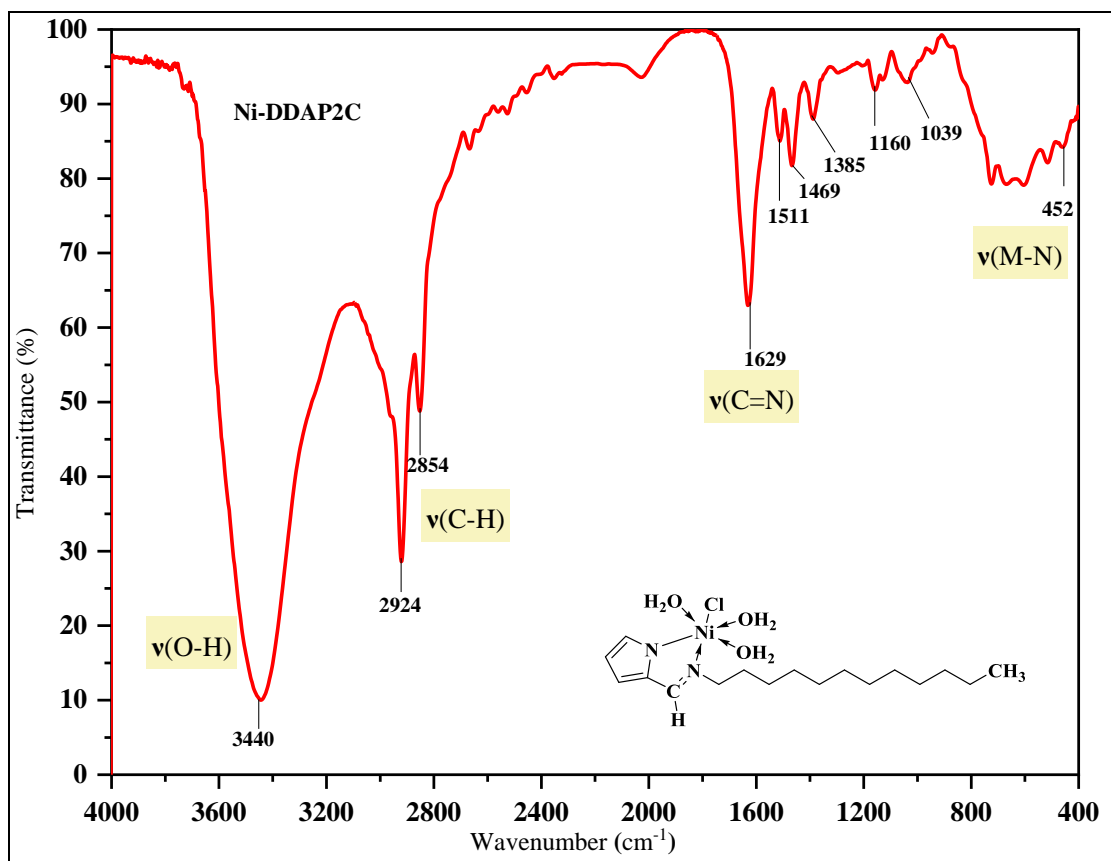
Figure 30: FT-IR spectrum of Ni-DDAP2C complex
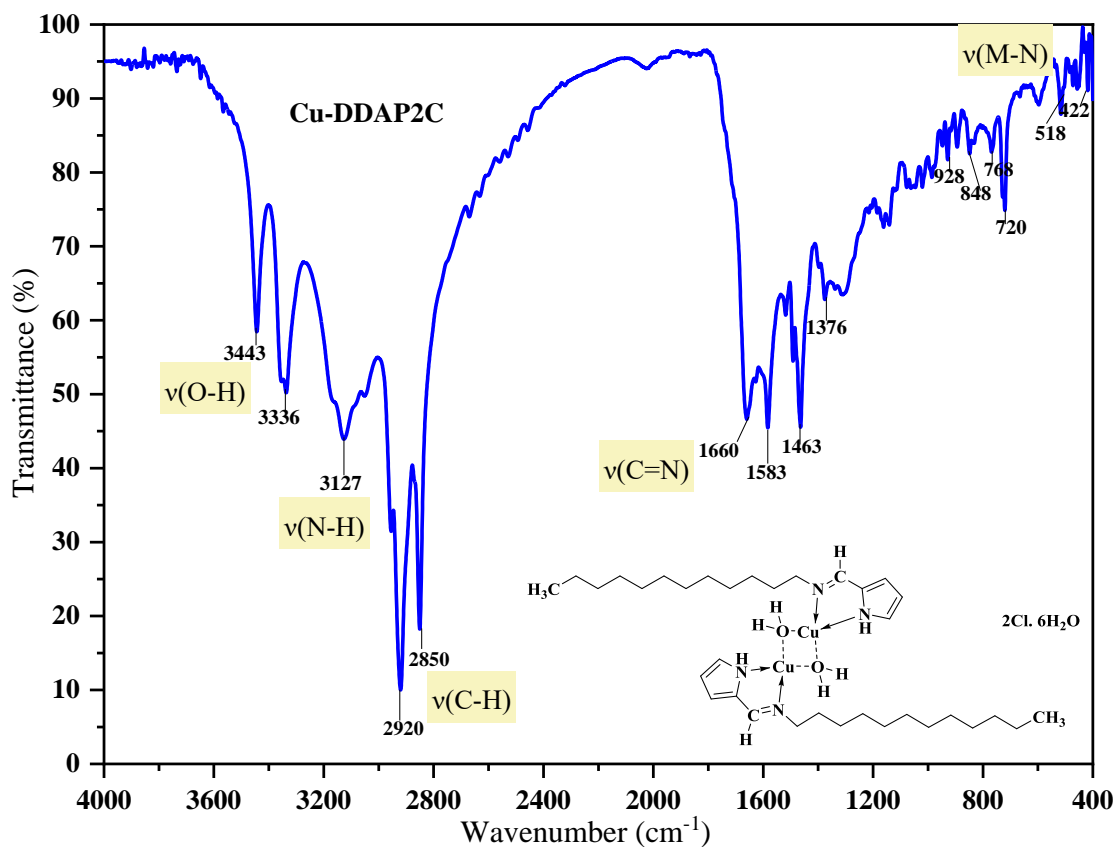
Figure 31: FT-IR spectrum of Cu-DDAP2C complex
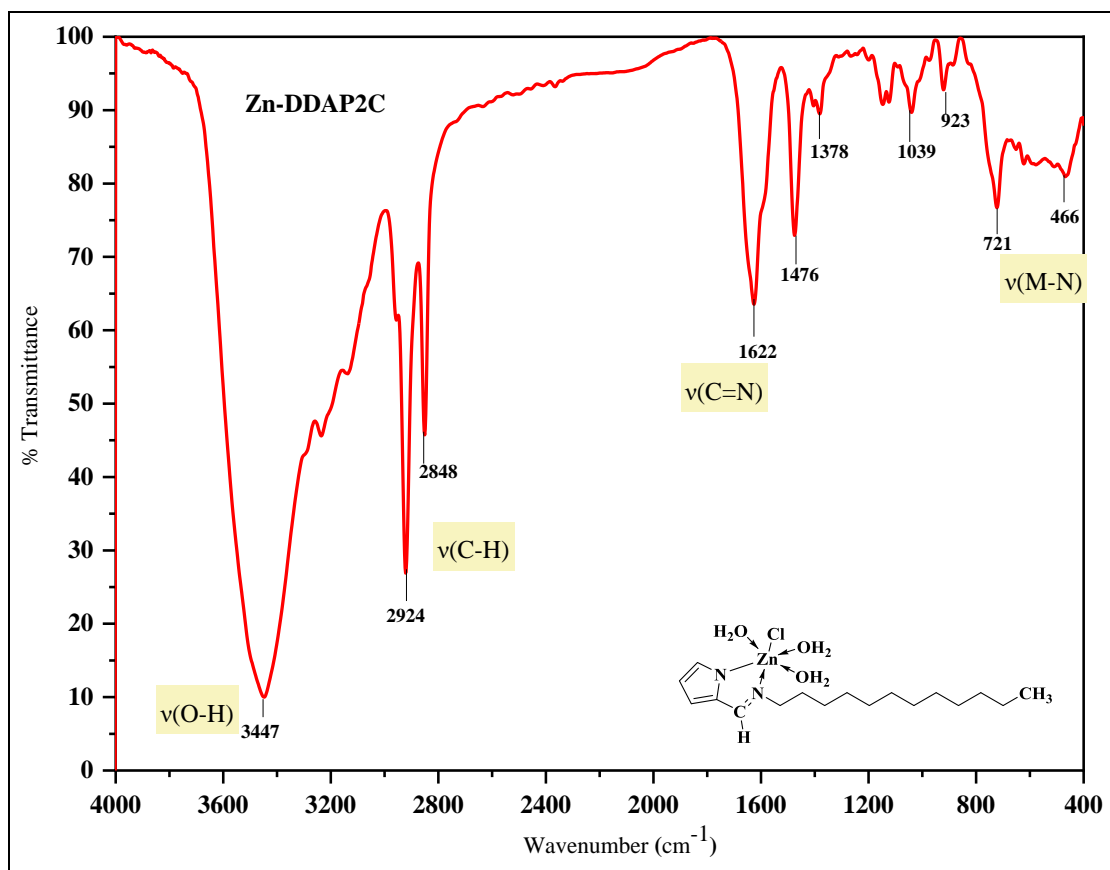
Figure 32: FT-IR spectrum of Zn-DDAP2C complex

4.4.1.2 FT-IR Spectra of DDAP3C and Metal Complexes

The crucial IR bands (4000-400 cm-1) were identified in the spectra to evaluate the bonding sites of the ligand when coordinated with metal ions. Table 8 provides a summary of the reported FT-IR outcomes. According to a study of the band locations in the infrared spectra of HL and its complexes, the HL behaves as a neutral bidentate N, N donor ligand with azomethine-N and pyrrole-N serving as coordination sites. Figures 33–37 display a collection of FT-IR spectra. When the azomethine group complexed with metal, the $v(HC=N)$ stretching vibration band changed to higher wave numbers, suggesting that the nitrogen was bonded to the metal ions. In the HL spectrum, the $v(HC=N)$ appeared at 1644 cm^{-1} and then shifted upwards to 1653 cm^{-1}, 1664 cm^{-1}, 1665 cm^{-1}, and 1659 cm^{-1} for the respective complexes 1, 2, 3, and 4. This variance may be a consequence of the +I effect generated by the long-chain alkyl group in the surfactant moiety (Kaur *et al.*, 2016; Tawfik & Zaky, 2015). The participation of the pyrrole ring nitrogen in the complexation was shown by the v(N-

H) stretching vibration band for ligand HL at 3131 cm^{-1} and metal complexes at 3134, 3222, 3147, and 3129 cm^{-1}. A minor shift in complexes **1**, **3**, and **4** indicates no loss of H atoms even after complexation, whereas complex **2** may have a more significant shift in the ν(N-H) stretching vibration due to hydrogen bonding. The overlap of coordinated water and metal ions was justified by the observation of a new band in the IR spectrum at higher wave numbers of complexes **1** (3551 cm^{-1}), **3** (3580, 3609 cm^{-1}), and **4** (3449 cm^{-1}) (Ali *et al.*, 2015; Bhaskar *et al.*, 2020). Further, in complexes **1**, **3**, and **4**, another sharp peak corresponds to the bending vibration of the coordinated H$_2$O at 961, 966, and 928 cm^{-1}. The absorption bands seen in the lower wavenumber region of the spectra provided the most compelling and convincing evidence for M-O and M-N coordination in the complexes. Complex **1** was found to have absorption bands at 416 cm^{-1} and 448 cm^{-1}, respectively, reflecting the ν (M-N) stretch associated with coordination with azomethine nitrogen and pyrrole ring nitrogen. The ν(M-O) stretching vibration was confirmed by a new band at 549 cm^{-1}. Complex **2** exhibited a ν(M–N) stretching band at 418 cm^{-1}. The ν(M–N) stretch was detected at 410 cm^{-1} and 451 cm^{-1} for complex **3** because of metal bonding with azomethine nitrogen and pyrrole ring nitrogen, respectively. The ν(M–O) stretching band was observed at 605 cm^{-1}. The IR absorption bands for the complex **4** were seen at 603 cm^{-1} and 475 cm^{-1}, corresponding to the ν(M–O) and ν(M–N) stretching vibrations, respectively. These significant characteristic bands and their transitions in position from free ligands to metal complexes provide strong evidence for the proposed structure of these complexes (Prabhakara *et al.*, 2016; Vamsikrishna *et al.*, 2020).

Table 8: FTIR spectral data of   DDAP3C Schiff base ligand and its complexes in cm^{-1}

Compounds	v(NH)	v(C=N) (imine)	v (C-H)	v (C=C)	v (C-N)	v(M-N)	v(M-O)	v(H$_2$O)/δ(H$_2$O) Coordinated
HL	3131	1644	2916, 2847	1470, 1511	1375	-		-
Complex **1**	3134	1653	2910, 2848	1470, 1513	1376	416	549	3551, 961
Complex **2**	3222	1664	2922, 2851	1466, 1519	1380	418	-	-
Complex **3**	3147	1665	2919, 2850	1467, 1518	1305	410,451	605	3580,3609, 966
Complex **4**	3129	1659	2921, 2852	1466, 1584	1375	475	603	3338,3449, 928
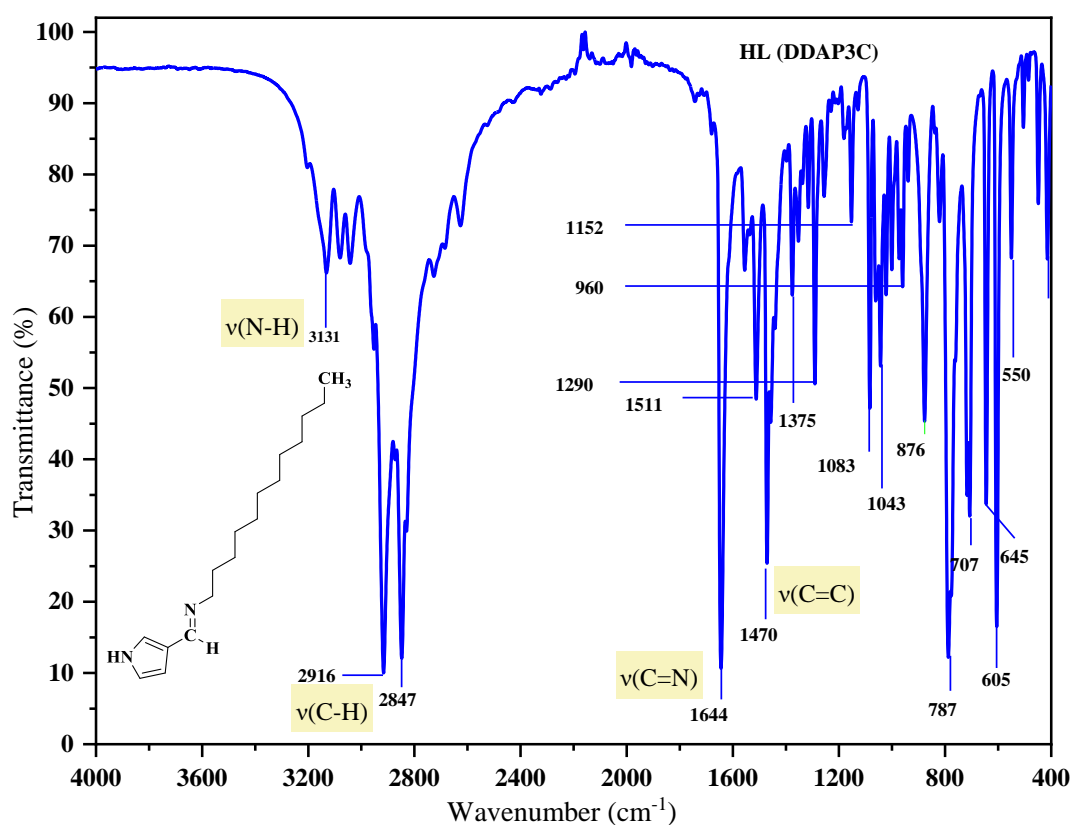
Figure 33: FT-IR spectrum of DDAP3C ligand
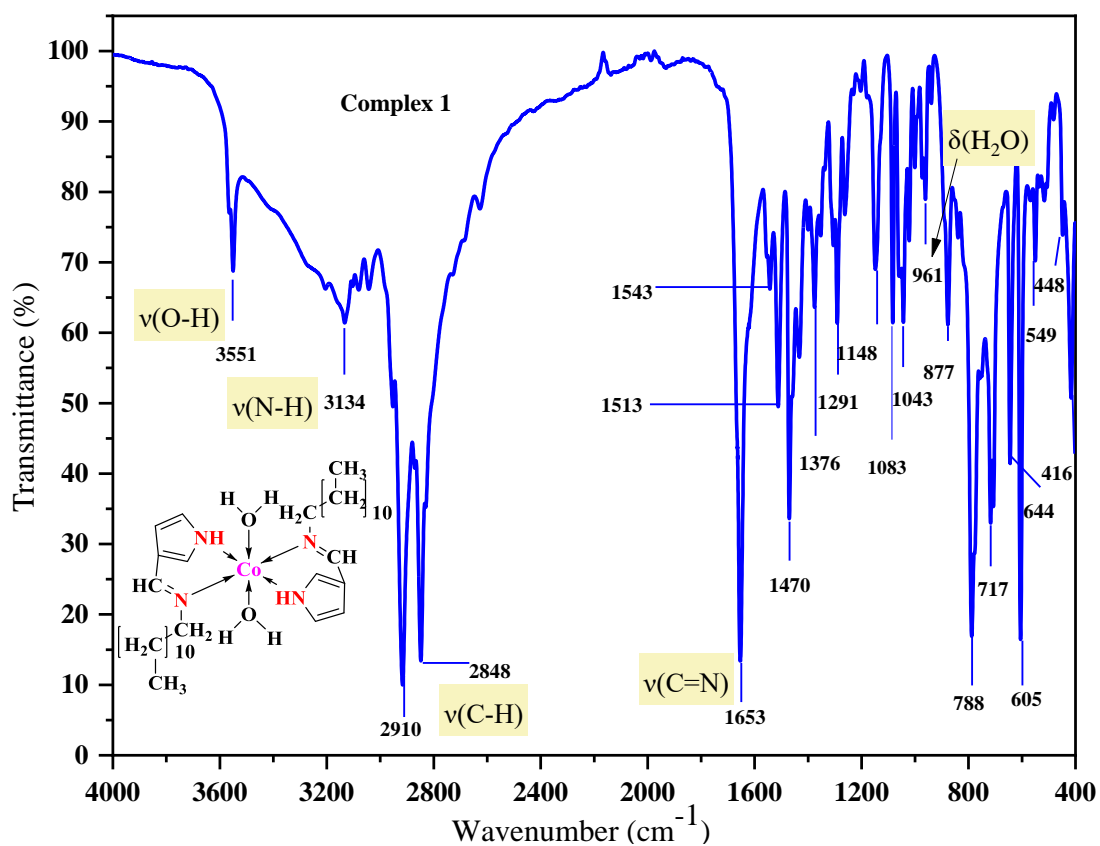
Figure 34: FT-IR spectrum of Co-DDAP3C complex

Figure 35: FT-IR spectrum of Zn-DDAP3C complex

71

Figure 36: FT-IR spectrum of Ni-DDAP3C complex

Figure 37: FT-IR spectrum of Cu-DDAP3C complex

4.4.2 ^{1}H & ^{13}C NMR Spectral Studies

The carbon-hydrogen framework present in organic ligands and metal complexes can be identified by NMR spectroscopy. Protons in molecules have diverse electronic environments; therefore, depending on the degree of their shielding and deshielding effects, they exhibit resonance peaks at various parts of the spectrum. The NMR signal is delivered by shielded protons in the region of low chemical shift value and by deshielded protons in the region of high chemical shift value (Bruch, 1996; Tampieri *et al.*, 2020). Additionally, splitting signals into multiplets provides vital information about the kinds of protons present in the molecule. Sometimes, the signal loss in the NMR spectrum of the metal complexes concerning the ligand also conveys crucial information regarding the point of ligand interaction with the metal center (Gondia & Sharma, 2018).

4.4.2.1 ^{1}H NMR Spectra of DDAP2C Schiff Base and Zn-DDAP2C Complex

The ^{1}H NMR spectral analysis supports the formation of the diamagnetic Zn-DDAP2C complex and the Schiff base (DDAP2C) ligand. The spectrum comparison reveals the binding patterns of the ligand to metal ions. There is a correlation between the integral intensities of each signal in the ^{1}H NMR spectra of the DDAP2C and Zn-DDAP2C complexes and the number of various protons present. In our work, the DDAP2C showed a signal at 8.041 ppm ascribed to the azomethine proton (-CH=N), which shows that the Schiff base ligand has been formed. The Zn-DDAP2C signal was shifted downfield to 8.486 ppm, showing that azomethine nitrogen was involved in the complex formation process (El-Hamid *et al.*, 2019; Kuate *et al.*, 2020). For DDAP2C, the pyrrole ring protons resonate between 6.088 and 6.852 ppm, while for the Zn-DDAP2C complex, they were shifted to the downfield in the range of 6.455 to 7.664 ppm (El-Razek *et al.*, 2019). A singlet at 11.296 ppm was found in the pyrrole NH proton of DDAP2C, and its removal in the ^{1}HNMR spectra of Zn-DDAP2C indicates that pyrrole NH proton deprotonation occurred in a complexation with zinc-nitrogen binding (Kumar *et al.*, 2016; Nami *et al.*, 2016; Tyagi *et al.*, 2015). The 1HNMR spectral data of ligand and metal complex are documented in Table 9, and their 1HNMR spectra are given in Figs. 38-39.

Table 9 ^{1}H NMR spectral data of DDAP2C and Zn-DDAP2C

Compounds	Chemical shift (δ)ppm	Assignment
DDAP2C	8.041	Azomethine proton
	6.088-6.852	Pyrrole ring protons
	11.296	Pyrrole NH proton
	3.425-3.470	Methylene protons near the pyrrole NH group
	1.240-1.579	Methylene protons
	0.838-0.872	Methyl protons
Zn-DDAP2C	8.486	Azomethine proton
	6.455-7.664	Pyrrole ring protons
	2.735-3.581	Methylene protons near the pyrrole NH group
	1.240-1.640	Methylene protons
	0.838-0.869	Methyl proton
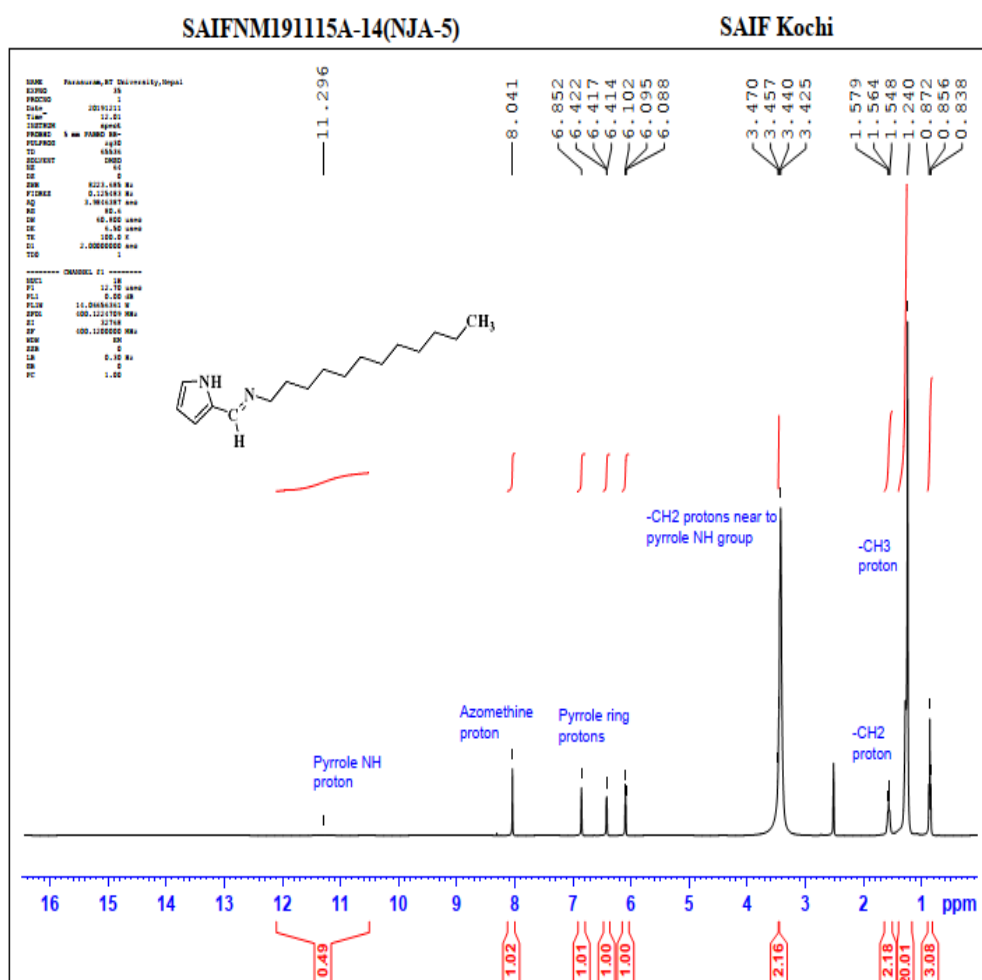
Figure 38: ^{1}HNMR Spectrum of DDAP2C ligand
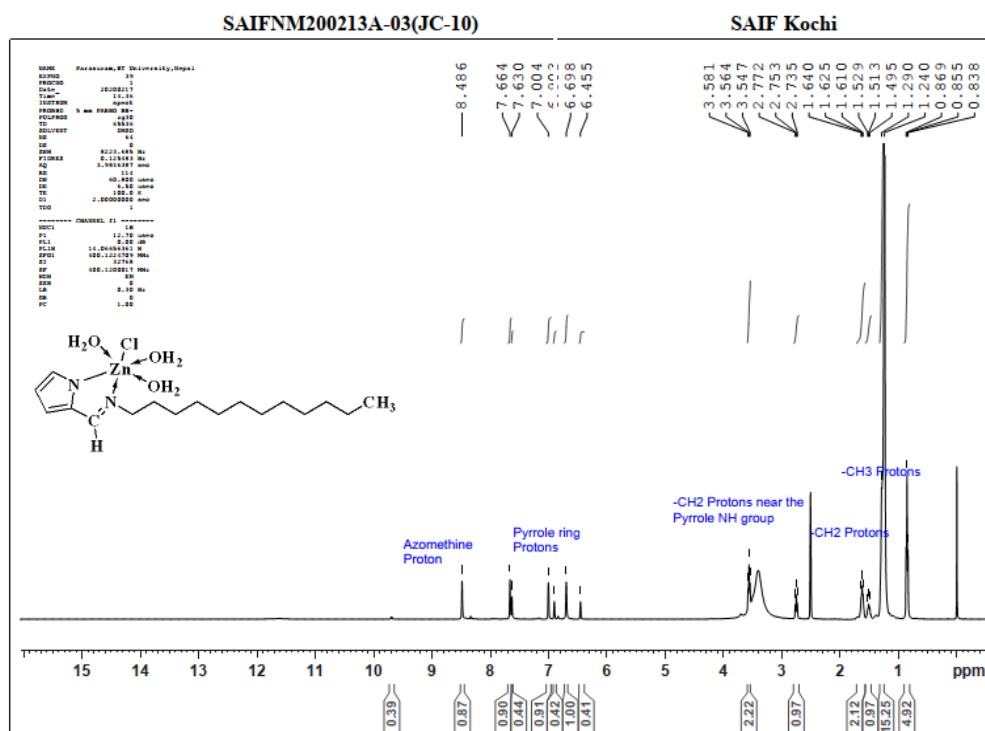
Figure 39: ^{1}HNMR Spectrum of Zn-DDAP2C complex

4.4.2.2 ^{1}H NMR Spectra of DDAP3C Schiff Base and Zn-DDAP3C Complex

The ^{1}H NMR spectral investigations also contributed to a greater comprehension of the HL ligand formation. To establish the binding mechanism of HL to the metal centers, the ^{1}H NMR spectra of the diamagnetic complex **2** and the HL ligand were recorded in the DMSO-d6 solvent. A singlet from the azomethine proton (-N=CH-) was visible in the spectra of HL, indicating that the Schiff base had formed (Sumrra *et al.*, 2020; Yeğiner *et al.*, 2017). This peak for complex **2** has changed from 8.1 ppm to 8.5 ppm in the downfield, which may be due to lone pair electrons contributing to the central metal ion and formation of the (Zn←N) linkage (Almasi *et al.*, 2020). For HL, the pyrrole N-H proton resonated at 7.11 ppm as a singlet, which then shifted downfield to 7.77 ppm after complexation. Other remarkable 1H NMR signals for HL include signals at 6.75 (s, H-(2a/2b)), 6.34 (s, H-4), and 3.33-3.39. (H_{H2O}). These peaks in the spectra of complex **2** were nearly in the exact location and showed only slight variation, suggesting the linkage of HL to Zn^{+2} through the azomethine moiety. The ^{1}H and ^{13}C NMR spectrum data of complex **2** and HL are presented in Table 10, and their spectra are displayed in Figures 40 and 41, respectively.

Table 10: [1]H spectral data of DDAP3C and Zn-DDAP3C and ^{13}C NMR spectral data of DDAP3C

H	Ligand (HL) / DDAP3C δ (ppm)	Complex 2 / Zn-DDAP3C δ (ppm)	C	Ligand (HL) / DDAP3C δ (ppm)
H-1	7.11 (s, J = 1.01 Hz, 1H)	7.77 (s, J = 1.01 Hz, 1H)	C-2a	122.51
H-(2a/2b)	6.75 (s, J = 1.00 Hz, 1H)	7.05 (s, J = 1.00 Hz, 1H)	C-2b	119.04
H-4	6.34 (s, J = 1.02 Hz, 1H)	6.77 (s, J = 1.05 Hz, 1H)	C-3	121.3
H-5	8.11 (s, J = 1.03 Hz, 1H)	8.56 (s, J = 0.96 Hz, 1H)	C-4	108.2
(H-6 & 7)	1.51/1.53 (m, J = 2.01 Hz, 2H)	1.64 (m, J = 2.07 Hz)	C-5	155
	-	-	C-6	60.69
(H-8) – (H-15)	1.23-1.26 (m, J = 14.02)	1.24-1.29 (m, J = 14.61 Hz)	C-7	30.74
H-16	1.52	-	C-8	26.71
H-17	0.83-0.86 (t, J = 3.1 Hz, 3H)	0.83-0.87 (t, J = 4.11 Hz)	(C-9) – (C-14)	28.59-28.93
H(H2O)	3.33-3.39	3.58-3.61 (broad, J = 2.31 Hz)	C-15	31.18
			C-16	21.98
			C-17	13.84

Figure 40: ^{1}H NMR Spectrum of DDAP3C ligand
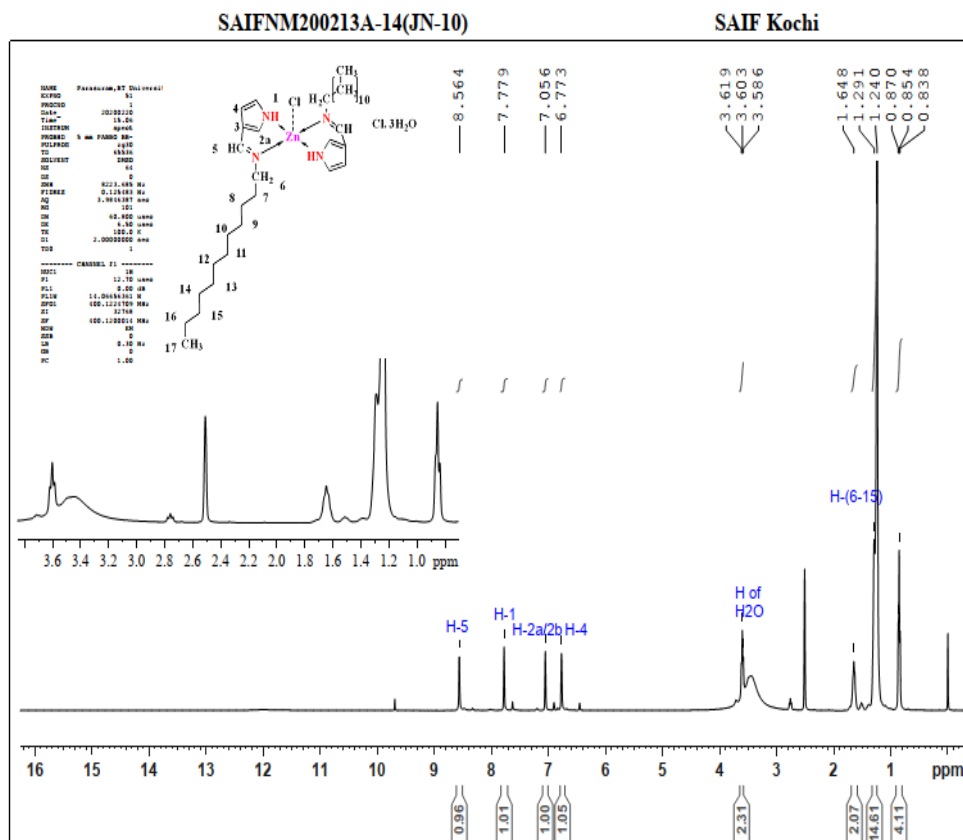
Figure 41: ^{1}HNMR Spectrum of Zn-DDAP3C complex

4.4.2.3 ^{13}C NMR Spectra of DDAP2C Schiff Base and Zn-DDAP2C Complex

The ^{13}C NMR spectral analysis provides information about molecules' numerous carbon atoms and their electronic surroundings. In the ^{13}C NMR spectral investigation of the DDAP2C, the azomethine carbon (C=N) resonated at 151.398 ppm (Vinusha *et al.*, 2019). The carbons in the pyrrole ring produced 13C NMR peaks at 108.686-129.947 ppm for DDAP2C, which were shifted to 105.924 -128.339 ppm for Zn-DDAP2C in the 13CNMR spectrum (Rawat *et al.*, 2017). The methyl carbons in DDAP2C exhibited a signal at δ 13.896 ppm, and methylene carbons showed signals within δ 22.055-60.316 ppm. The 13C NMR spectra of the Zn-DDAP2C showed no significant difference in the chemical shifts for these carbons. The spectra recorded for DDAP2C and Zn-DDAP2C are shown in Figs. 42 and 43, respectively, and their spectral data are listed in Table 11.

Table 11 ^{13}C NMR spectral data of DDAP2C ligand and Zn-DDAP2C

Comp.	Assignment	Chemical shift (δ) ppm
DDAP2C	CH=N	151.3
	Pyrrole ring carbon	108.6, 113, 121.7, 129.9
	Methylene carbon near the pyrrole NH group	60.3
	Methylene carbons	22, 26.7, 28.6, 28.9, 294, 30.7, 31.2
	CH$_3$	13.8
Zn-DDAP2C	Pyrrole ring carbons	105.9, 106.8, 120.7, 120.8, 122.3, 128.3
	Methylene carbons	21.9, 25.6, 28.4, 28.5, 28.5, 28.7, 28.8, 28.8, 28.8, 31.1
	CH$_3$	13.8
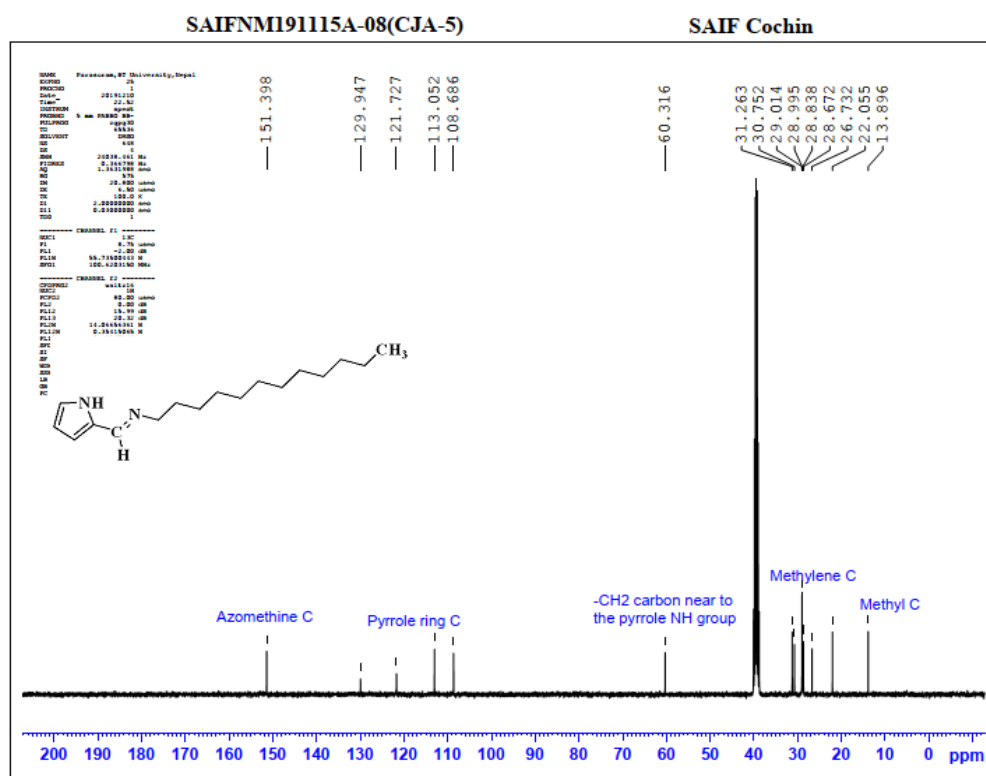
Figure 42: ^{13}C NMR Spectrum of DDAP2C ligand
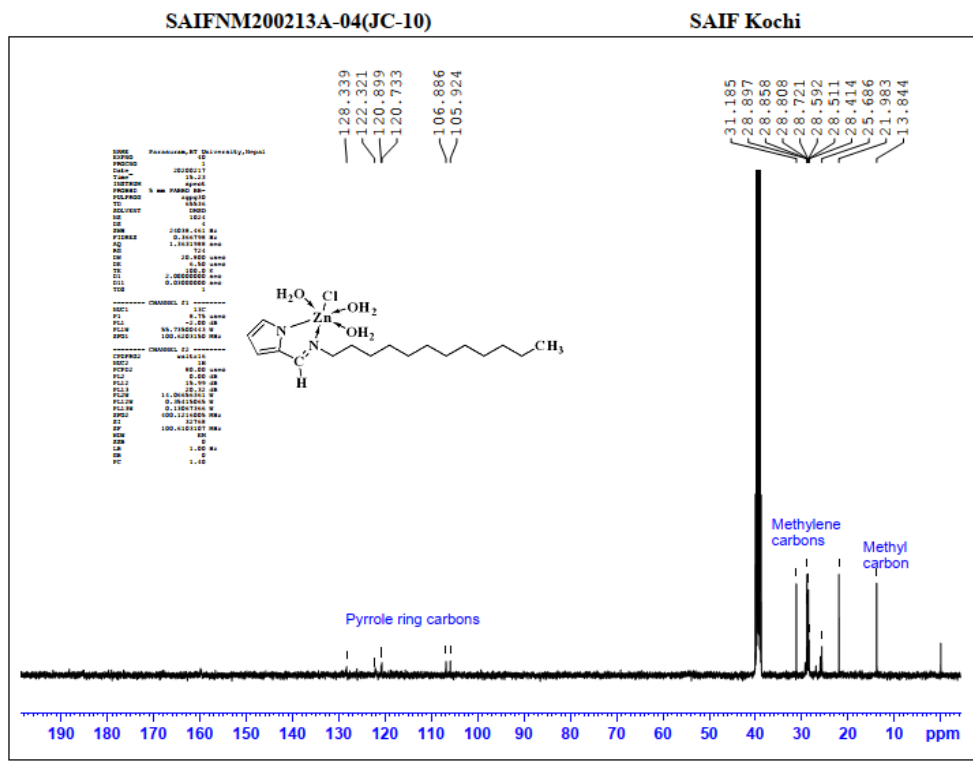
Figure 43: ^{13}CNMR Spectrum of Zn-DDAP2C complex

4.4.2.4 ^{13}C NMR Spectra of DDAP3C Schiff Base Ligand

The ^{13}C NMR spectrum can also provide evidence that ligands are formed. In the ^{13}C NMR spectrum of the HL Schiff base, a signal is observed at 155 ppm, which is attributed to azomethine carbon (C-5). The carbons in the pyrrole ring exhibited signals at 122.51 ppm (C-2a), 119.04 ppm (C-2b), 121.3 ppm (C-3), and 108.2 ppm (C-4). The methylene and methyl carbons of the hydrocarbon chain of the surfactant part of the molecule showed a range of signals from 13.84 ppm to 60.69 ppm. The ^{13}C NMR spectra of HL are depicted in Figure 44, and its spectral data are listed in Table 10.
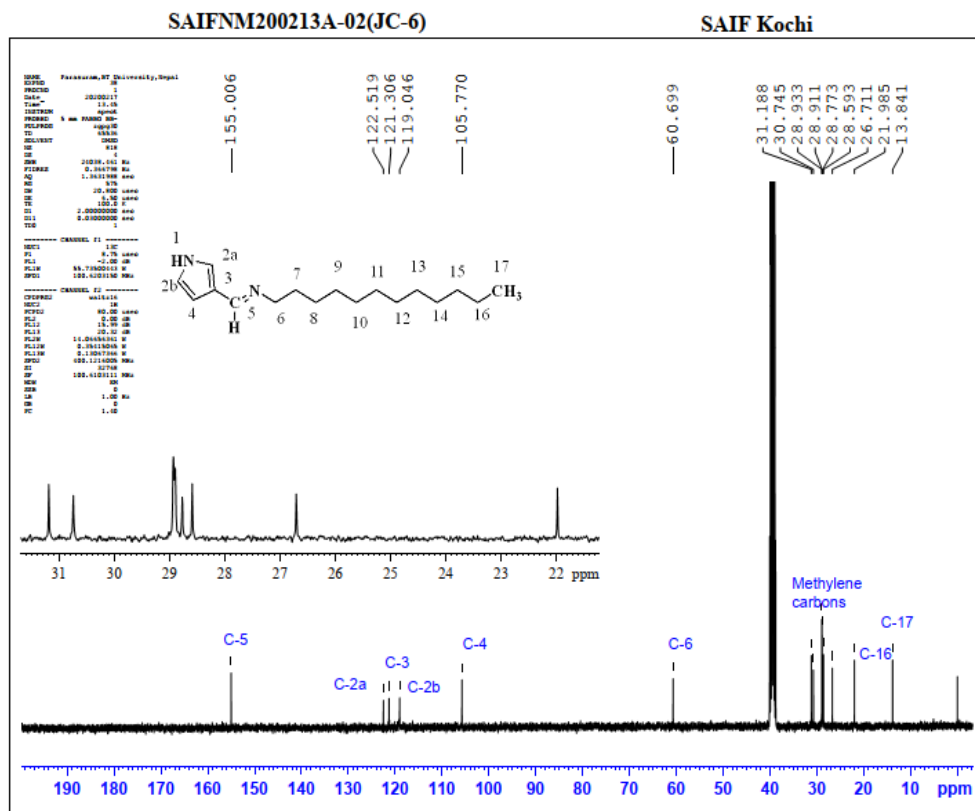
Figure 44: ^{13}C NMR Spectrum of DDAP3C ligand

4.4.3 Mass Spectral Study

4.4.3.1 Mass Spectra of DDAP2C and Metal Complexes

The mass spectra of the DDAP2C and its metal complexes were obtained to compare their stoichiometric composition. The base peak for DDAP2C is represented by the [M$^{·+}$+H] peak, which was recorded at m/z 263. At m/z 264, the [M$^{·+}$+2H] peak for DDAP2C was recorded. Therefore, the molecular mass of DDAP2C was determined to be 262 amu using the nitrogen rule. The spectra also reported other fragment peaks at m/z 187 and 186. Similarly, the Ni-DDAP2C and Zn-DDAP2C produced the [M·+] peaks at m/z 410 and 416, respectively, which is consistent with the proposed molecular formula. The predicted molecular formula of the compounds is supported by all of these mass spectral peak values for DDAP2C and its investigated metal complexes (Naureen *et al.*, 2021). For metal complex Co-DDAP2C, the molecular ion peak appears at m/z 776.9 which is compatible with their predicted molecular formula

(Table 5). Likewise, the Co-DDAP2C delivers fragment ion peaks at m/z 699, 593, 545, 506, and 453 with considerable intensity. The Cu-DDAP2C shows a strong base peak at 864.6 m/z with a relative intensity of 1990 (a.u.) and a molecular ion peak at 865.7 m/z with a considerable relative intensity of 705 (a.u.). According to this, a molecular mass of 866 m/z was determined, which is consistent with its predicted value. Likewise, the Cu-DDAP2C exhibits fragment ion peaks at m/z 776, 699, 622, 540, and 465 (Pervaiz *et al.*, 2018). A series of mass spectra of ligands and their metal complexes are exhibited in Figures 45 - 49 and their spectral data are documented in Table 5.
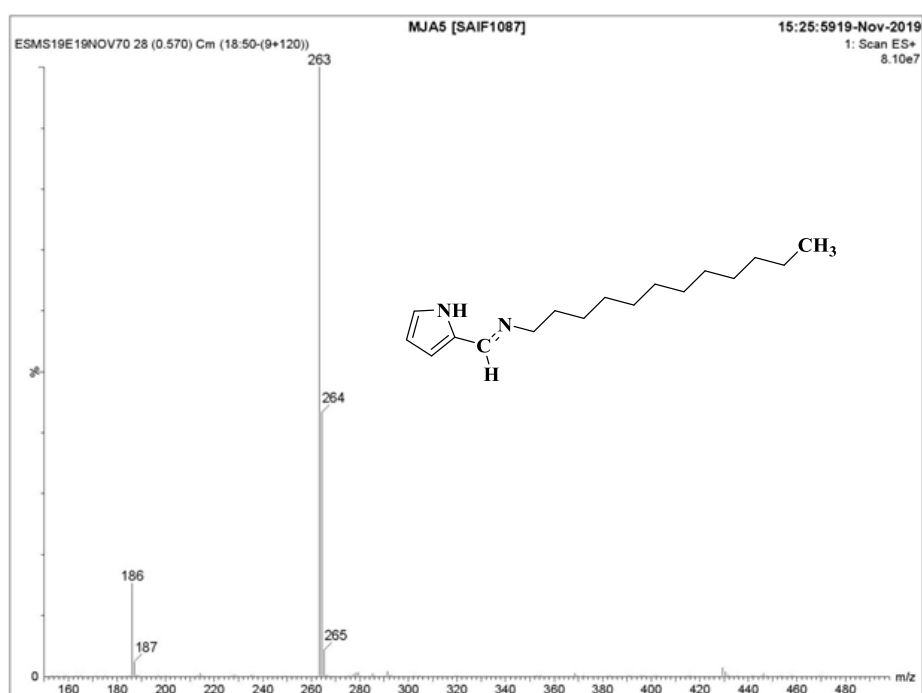
Figure 45: Mass spectrum of DDAP2C ligand
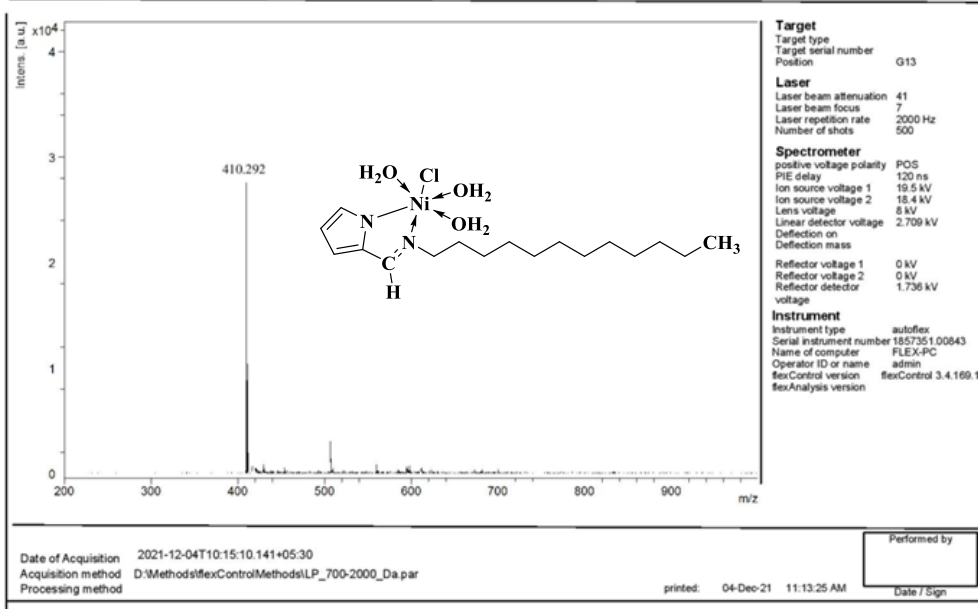
Figure 46: Mass spectrum of Ni-DDAP2C complex
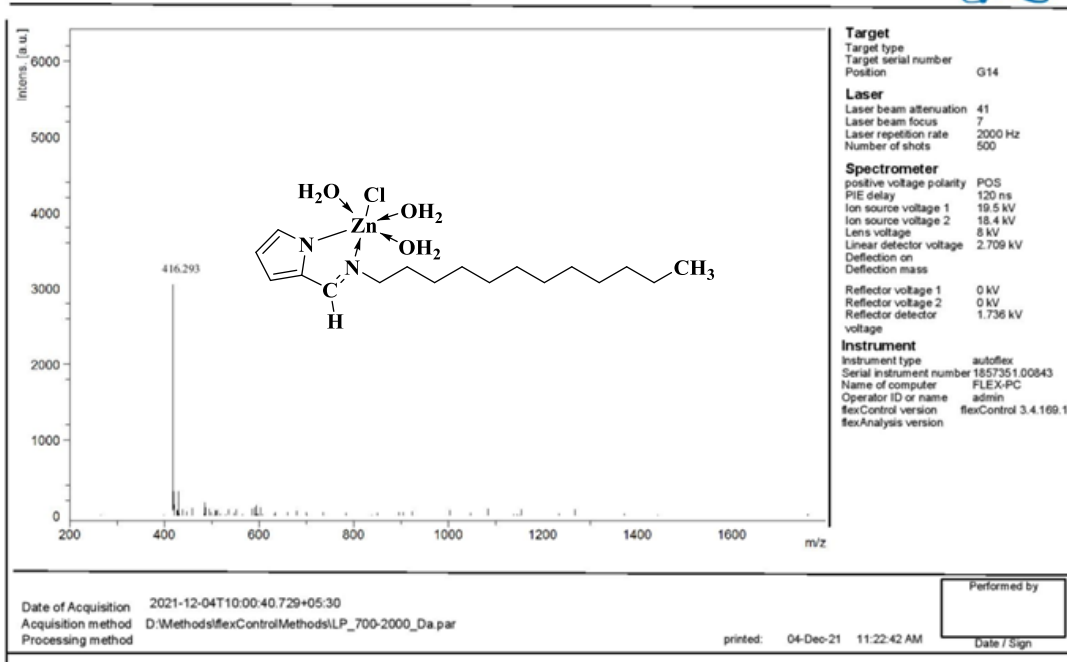
Figure 47: Mass spectrum of Zn-DDAP2C complex
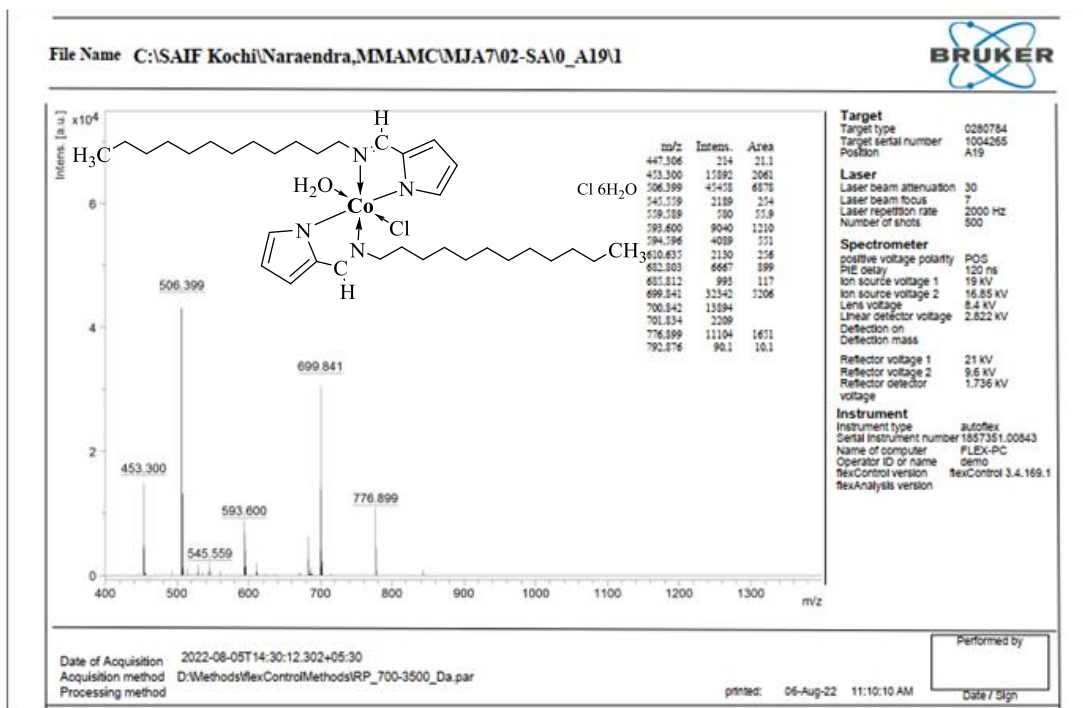
Figure 48: Mass spectrum of Co-DDAP2C complex
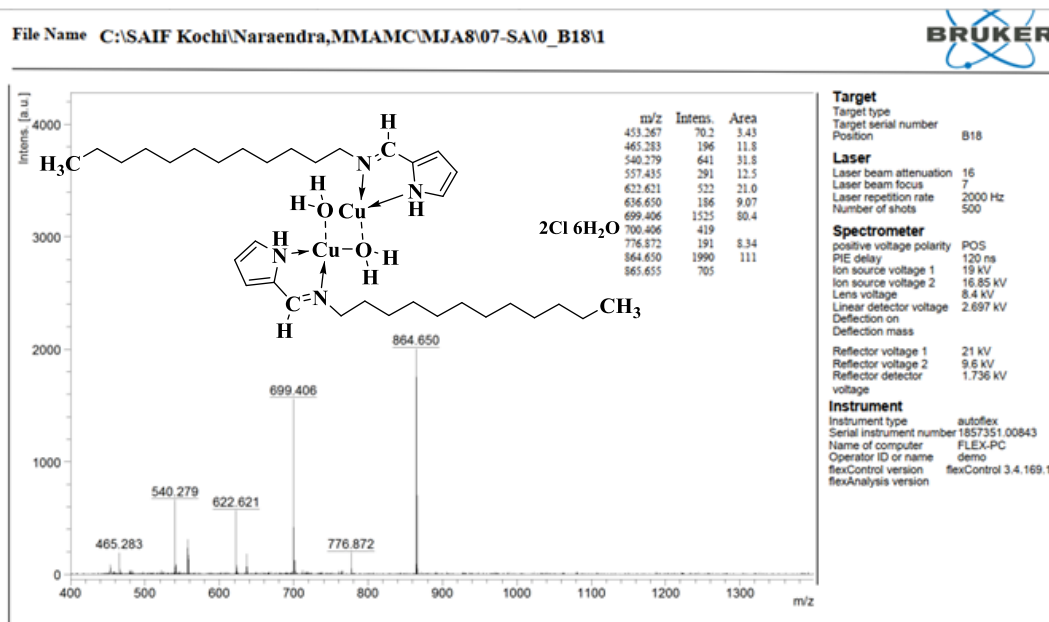
Figure 49: Mass spectrum of Cu-DDAP2C complex

4.4.3.2 Mass Spectra of DDAP3C and Metal Complexes

The $[M^{\cdot+}+H]$ peak, identified in the HL spectrum at 263 m/z, has a high intensity. Therefore, according to the nitrogen rule, the HL must have a molecular mass of 262

83

m/z. The fragment peaks for HL were recorded at m/z 186, 187, and 235. Two significant peaks could be seen in the MALDI-TOF mass spectra of complex 1: a strong base peak at 610.56 m/z with a relative intensity of 6454 (a.u.) and a weak molecular ion peak at 707.65 m/z with a relative intensity of 165 (a.u.). Based on this, a molecular mass of 708 m/z was determined, which is consistent with its predicted value. Additionally, fragment peaks with varying intensities were found at m/z 446, 453, 523, 582, and 593. A $[M^{·+}-2H]$ peak was observed at 711.466 m/z in the mass spectrum of complex **2**. Consequently, its molecular mass was confirmed to be 714 m/z, which agrees with its calculated molecular mass. Various fragment peaks were also detected at m/z 449, 469, 487, and 655. The mass spectra for complexes **3** (Ni-DDAP3C) and **4** (Cu-DDAP3C) showed the molecular ion peaks at m/z 700.3 and 611.4, respectively, which are relevant to their proposed molecular formula (Table 6). The fragment ion peaks for Ni-DDAP3C are observed at m/z 699, 610, 579, 565, and 451. Similarly, the Cu-DDAP3C exhibits fragment ion peaks at m/z 610, 586, 469, and 445. In light of this, the mass spectrum data largely corroborated the suggested molecular formula for all complexes (Kareem *et al.*, 2020; Zoubi *et al.*, 2017). The mass spectra of HL (DDAP3C) and its metal complexes are displayed in Figs 50-54, and their spectral data are listed in Table 6.
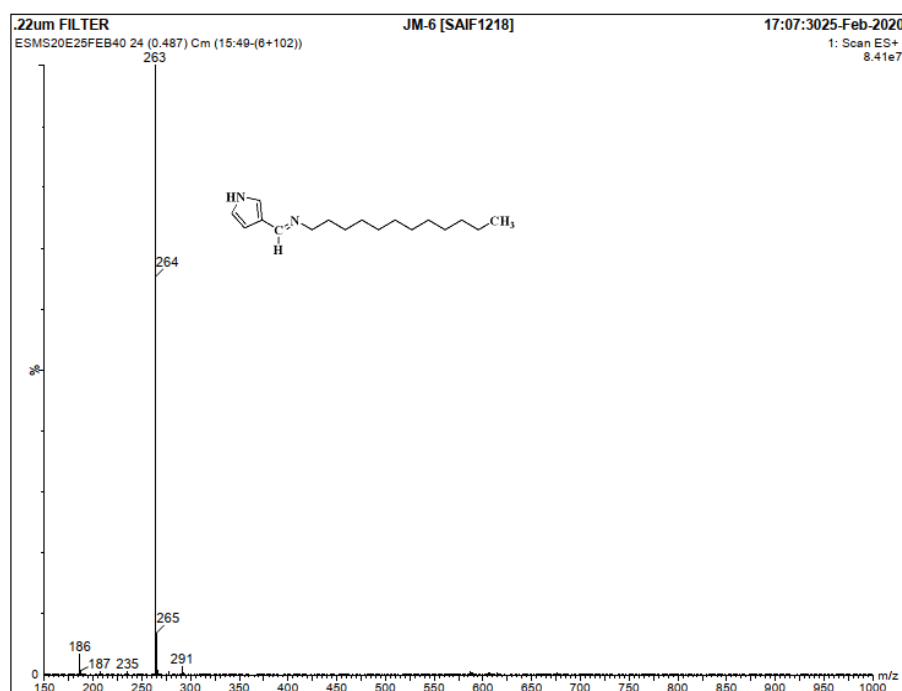
Figure 50: Mass spectrum of DDAP3C ligand
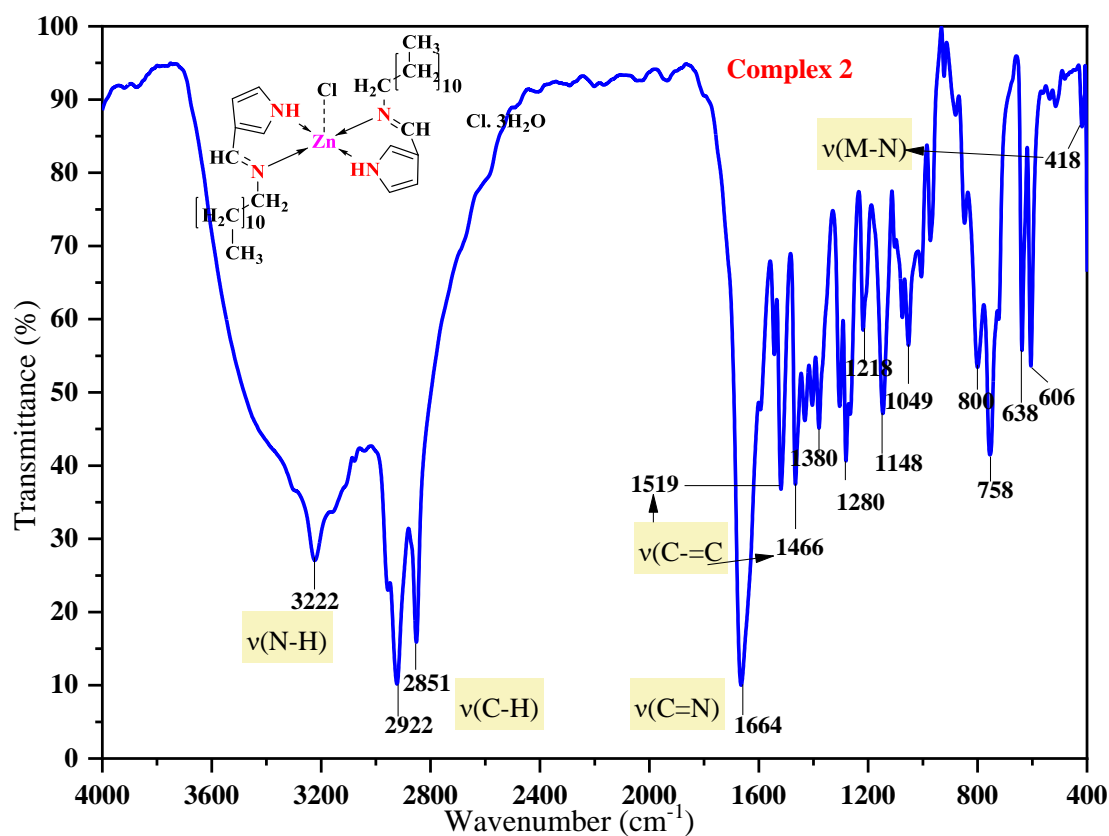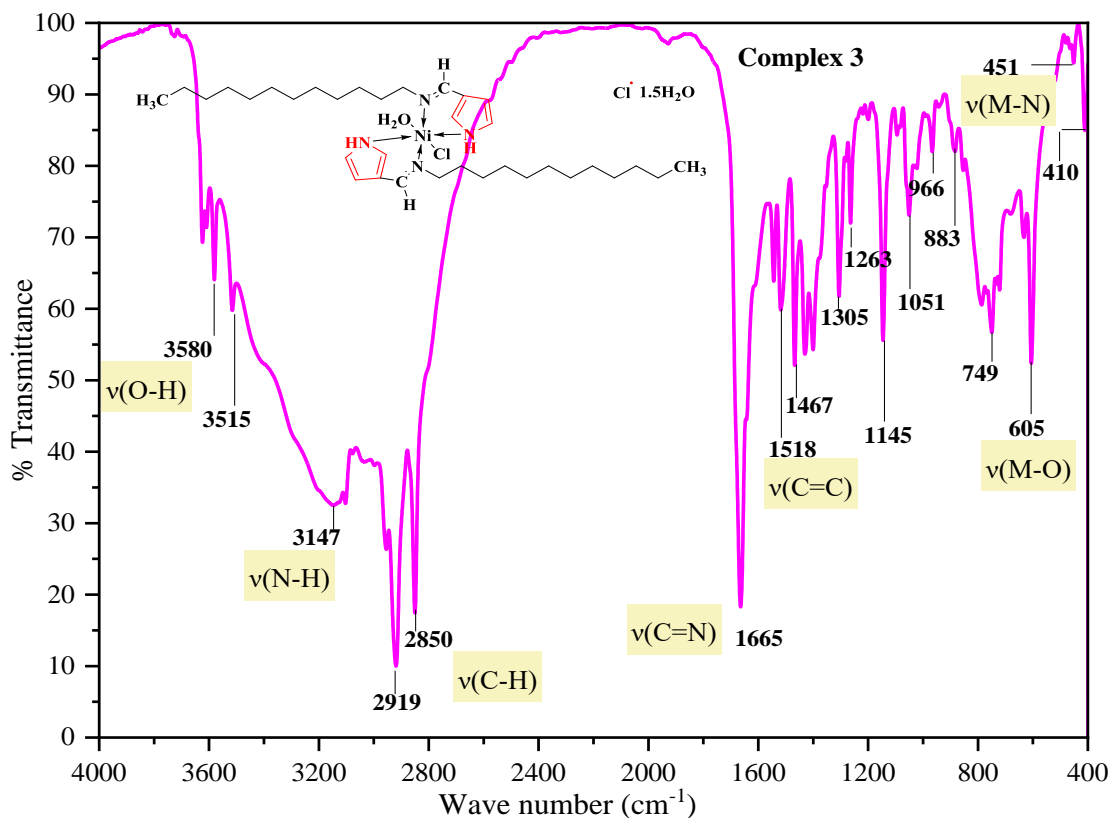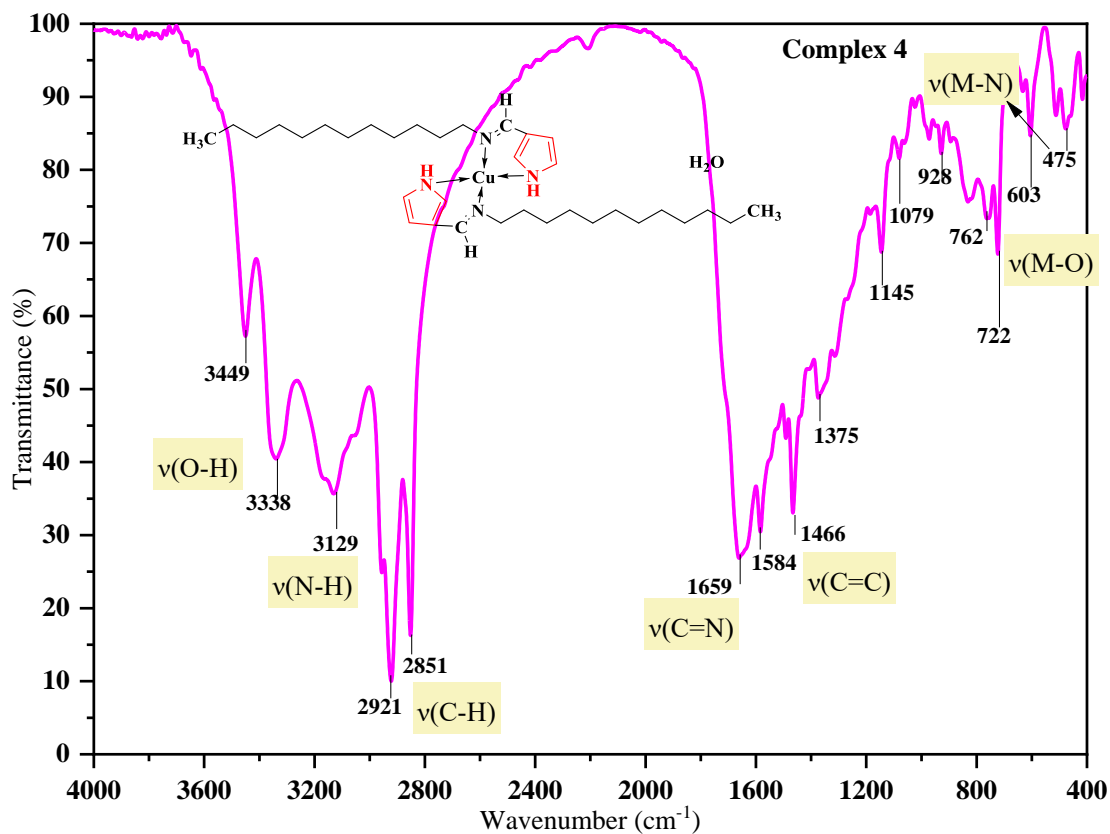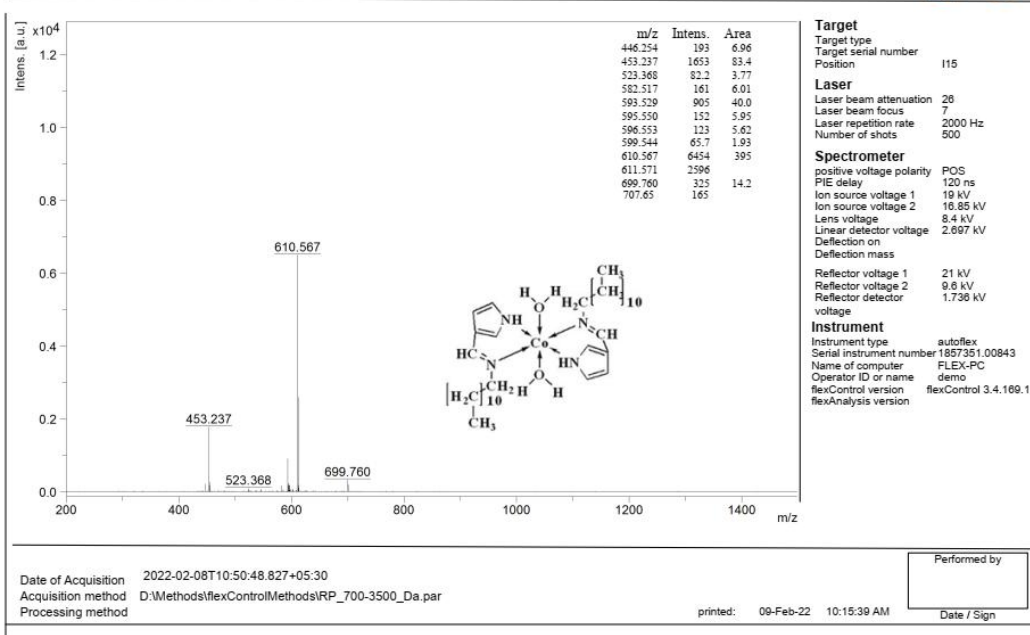
Figure 51: Mass spectrum of Co-DDAP3C complex
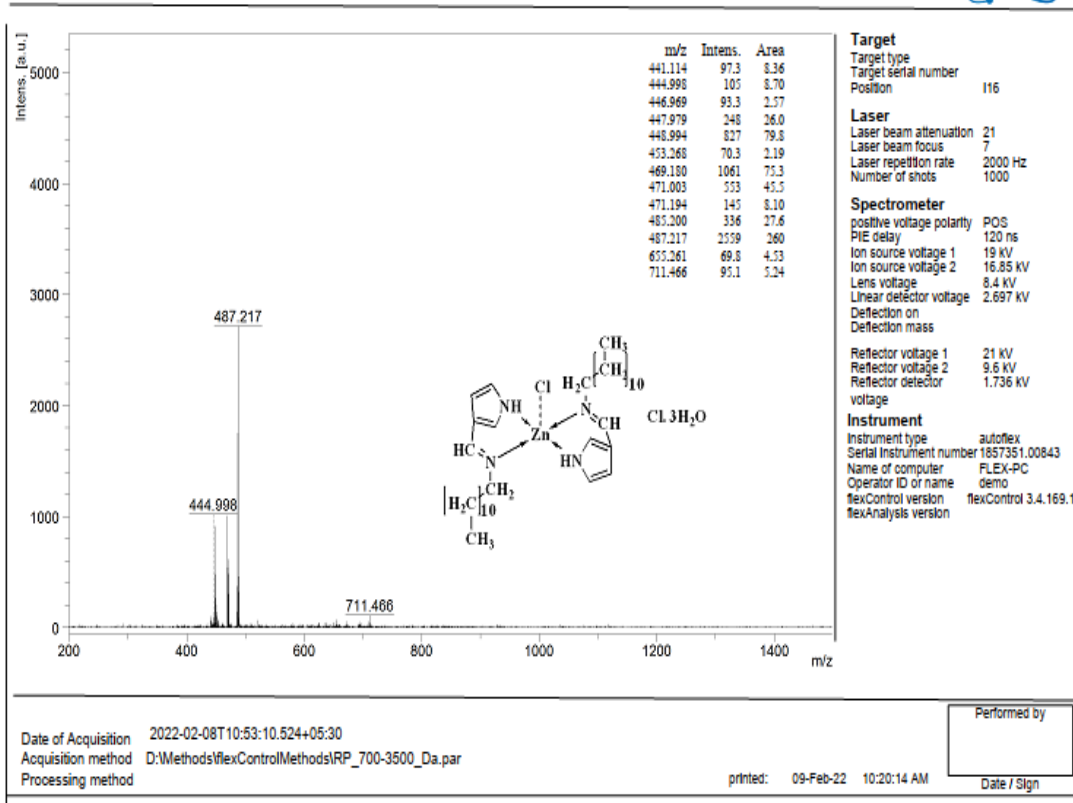
Figure 52: Mass spectrum of Zn-DDAP3C complex
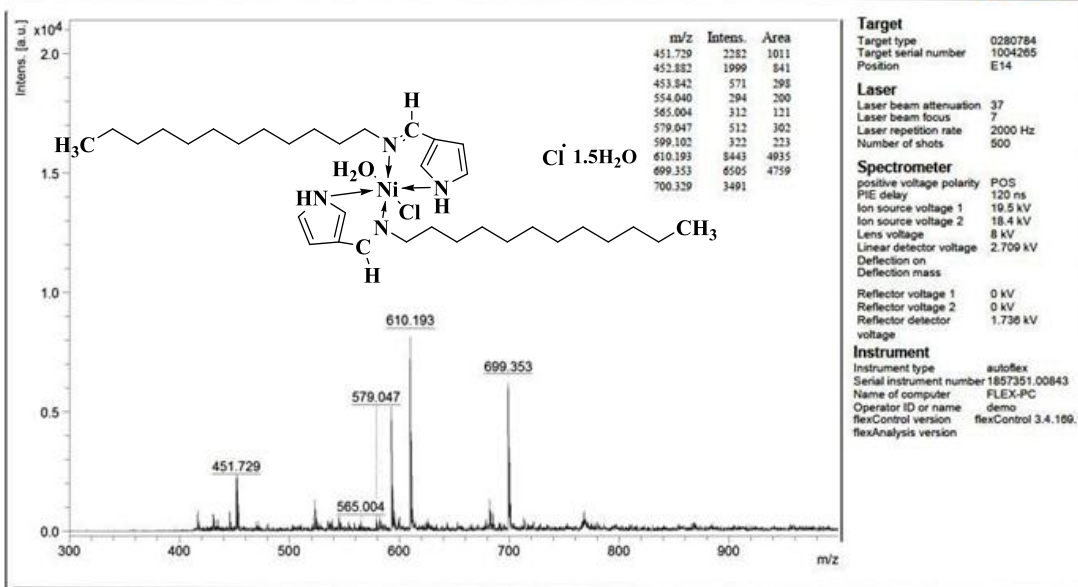
Figure 53: Mass spectrum of Ni-DDAP3C complex
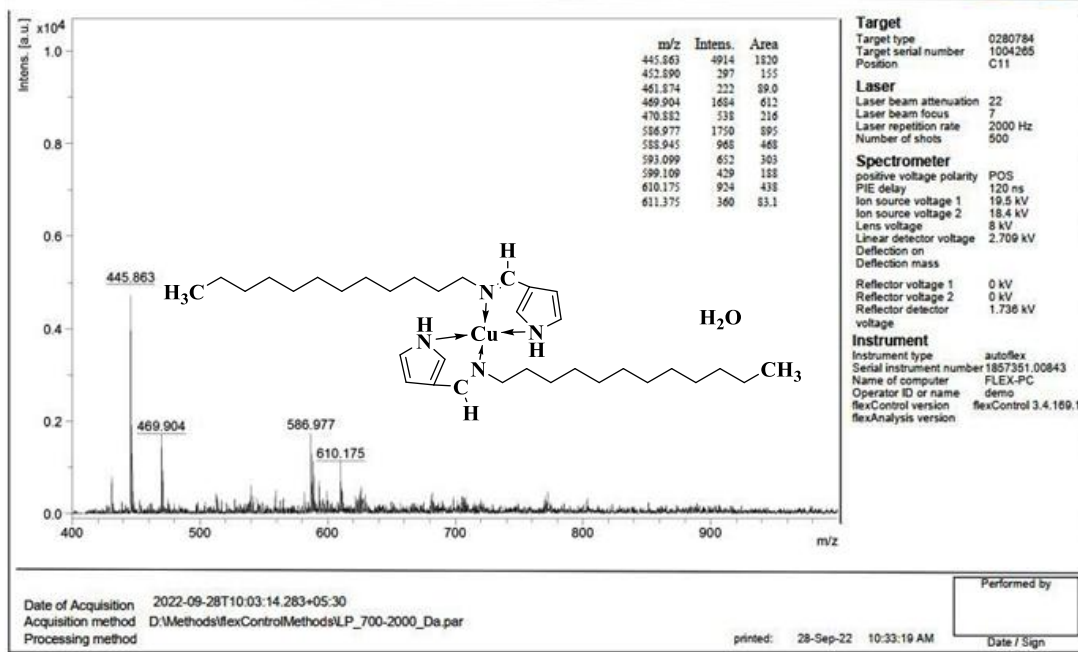
Figure 54: Mass spectrum of Cu-DDAP3C complex

4.4.4 Electronic Absorption Spectra (EAS) and Magnetic Moment Study

4.4.4.1 EAS of DDAP2C and Metal Complexes

Three bands were observed at 283, 325, and 346 nm for the Schiff base ligand DDAP2C. The absorption band at 283 nm is exhibited as a result of the $\pi\to\pi^*$ transition in aromatic ring. The band at 325 nm is visible due to the $n\to\pi^*$ transition of free electrons in the nitrogen atom of the azomethine group (Canpolat & Kaya, 2005). Interaction between the aromatic ring and the azomethine group leads to intra-ligand charge transfer (ILCT), resulting in the electronic absorption band for the ligand at 346 nm.

Five absorption bands at 294, 322, 441, 548, and 627 nm were observed in the electronic absorption spectra of the Ni-DDAP2C complex (El-Gammal $et\ al.$, 2021; Noorussabah $et\ al.$, 2020). The band at 294 nm is generated by the $n\to\pi^*$ transition, and LMCT (ligand metal charge transfer) band is exhibited at 322 nm. The $n\to\pi^*$ transition band for the DDAP2C ligand has shifted bathochromically in the Ni-DDAP2C complex. The transitions $^3A_{2g} \to {}^3T_{1g}$ (P), $^3A_{2g} \to {}^3T_{1g}$ (F), and $^3A_{2g} \to {}^3T_{2g}$ have been given the bands at 441, 548, and 627 nm, respectively. These transitions demonstrate that the Ni-DDAP2C complex has an octahedral structure (Fekri $et\ al.$, 2017). Its magnetic moment data of 2.95 BM further supports this conclusion. The complex Zn-DDAP2C exhibited three absorption bands at 443, 321, and 285 nm, corresponding to the LMCT, $n\to \pi^*$, and $\pi\to\pi^*$ transitions. The d-d transition band was missing in the zinc complex because of its entire d^{10} electronic configuration (Dhanaraj & Johnson, 2015; Mendu $et\ al.$, 2015). Six coordination numbers have been ascribed to the Zn-DDAP2C complex, which was also suggested by the thermal analysis to contain three water molecules as a structural component. The Zn-DDAP2C complex has been proposed as an octahedral geometry based on analytical, thermal, spectral, and conductance data (Saif $et\ al.$, 2016). The two absorption bands at 304 nm and 344 nm for the Co-DDAP2C complex represent the $n\to\pi^*$ and ligand-to-metal charge transfer (LMCT) band. The high-spin octahedral Co(II) complex exhibited two bands at 430 and 455 nm. These were attributed to the spin-allowed transitions $^4T_{1g}$ (F) $\to {}^4T_{1g}$ (P) (Turan $et\ al.$, 2019). The octahedral geometry of the cobalt complex is supported by these values and magnetic moment data (4.5 BM). The Cu-DDAP2C

exhibited absorption bands at 309 and 455 nm in the UV spectrum. The first at 309 nm was due to n→ π * transition. The transition band focused in the high wavelength region at 455 nm was assigned for the $^2T_2 \rightarrow ^2E$ transition revealing tetrahedral environment around both of the copper center (Belal *et al.*, 2015; Ikram *et al.*, 2015). The magnetic moment value of Cu-DDAP2C, 1.83 B.M, further supports the tetrahedral geometry of the compound.The electronic absorption spectra for DDAP2C and its complexes are depicted in Fig. 55 (a, b, c, d, e), and their data with magnetic moments are documented in Table 12.

Table 12: Electronic absorption spectral data of DDAP2C and its metal complexes

No.	Comp.	Peak positions (nm)	Assignment
1	DDAP2C	283	π→π* ,
		325	n→ π * ,
		346	intra ligand charge transfer band
2	Ni-DDAP2C	294	n→π*
		322	(LMCT) band
		441	$^3A_{2g} \rightarrow ^3T_{1g}(P)$
		548	$^3A_{2g} \rightarrow ^3T_{1g}(F)$
		627	$^3A_{2g} \rightarrow ^3T_{2g}$
3	Zn-DDAP2C	285	π→π*
		321	n→ π *
		443	(LMCT) band
4	Co-DDAP2C	304	n→π*
		344	(LMCT) band
		430 - 455	$^4T_{1g} (F) \rightarrow ^4T_{1g} (P)$
5	Cu-DDAP2C	309	n→π*
		455	$^2T_2 \rightarrow ^2E$
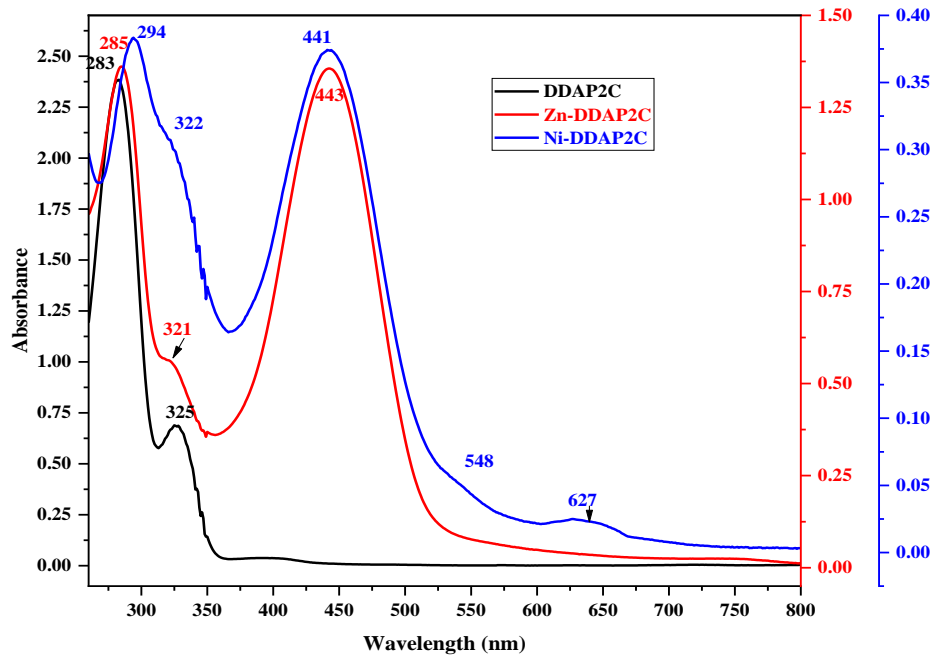
Figure 55: Electronic absorption spectra of (a) DDAP2C, (b) Zn-DDAP2C, (c) Ni-DDAP2C
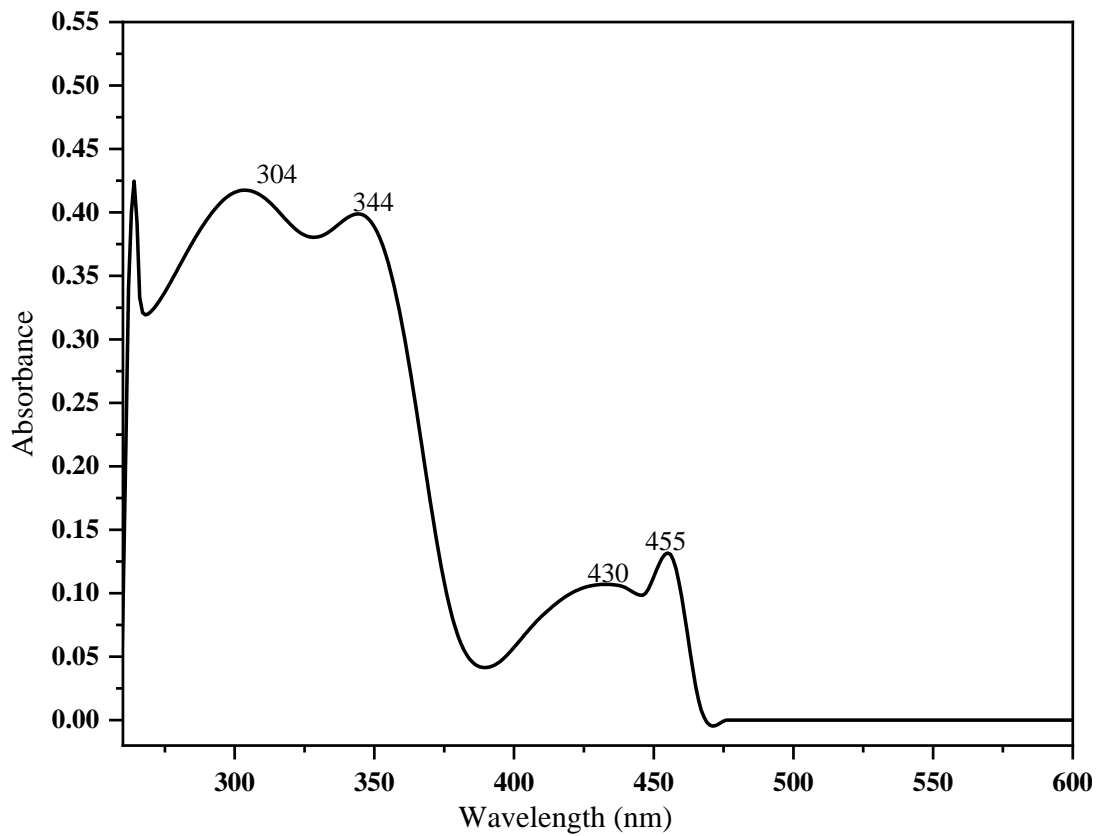
(a)
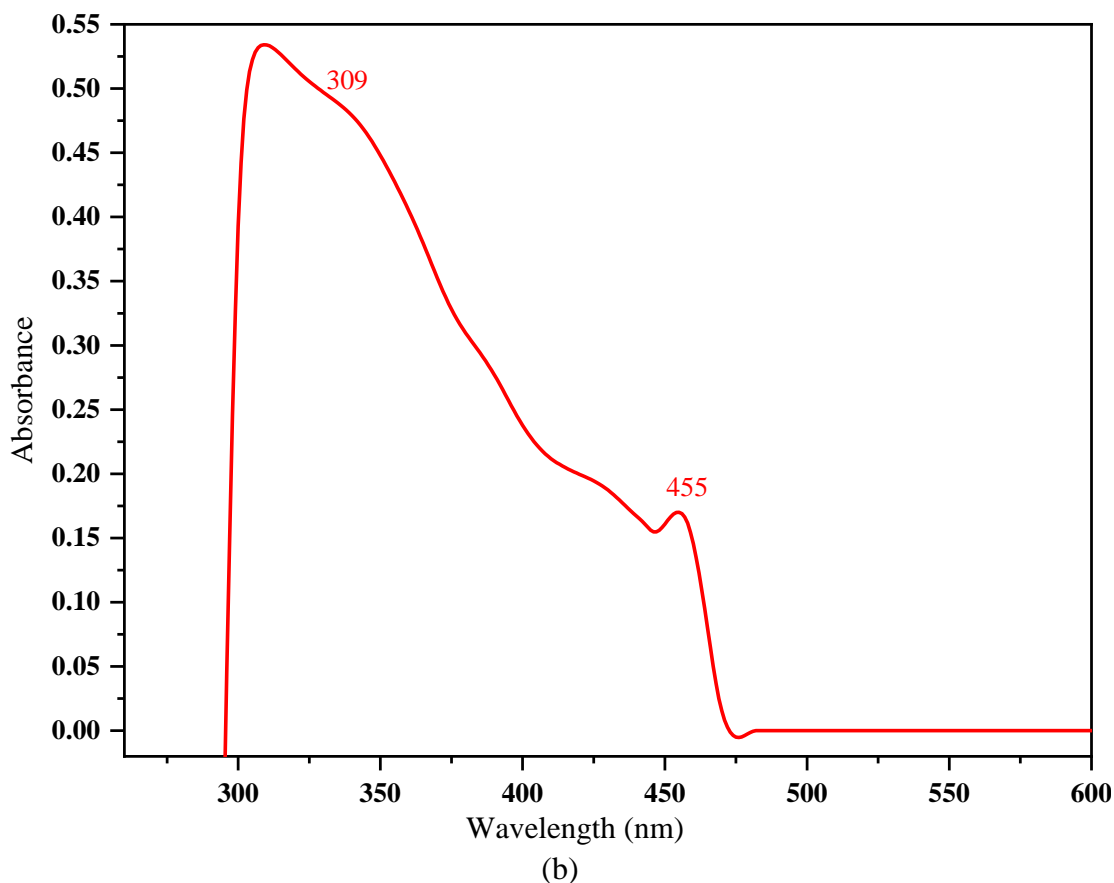
Figure 56: Electronic absorption spectra of (a) Co-DDAP2C, (b) Cu-DDAP2C

4.4.4.2   EAS of DDAP3C and Metal Complexes

The ultraviolet region of the spectrum showed two separate absorption bands for **HL**. The first band was observed at 275 nm as a result of the $\pi\rightarrow\pi^*$ electronic transition in the pyrrole ring. This intense band was present in the spectra of complexes 1 and 2, at wavelengths of 268 nm and 286 nm, respectively. The second band for HL at 373 nm is caused by the $\pi\rightarrow\pi^*$ and $n\rightarrow\pi^*$ transition in the azomethine group (Kavitha *et al.*, 2020). These absorption bands were also found in the spectra of complexes 1 and 2 at 350 nm and 392 nm (Rao *et al.*, 2020). The octahedral geometry of complex **1** was established by its UV-visible spectral data and magnetic moment data (4.2 BM) (Venkateswarlu *et al.*, 2019). The visible spectra of complex **1** were found to contain three absorption bands. The assigned electronic transitions for these absorption bands at 444 nm, 552 nm, and 661 nm, are $^4T_{1g}(F)\rightarrow{}^4T_{1g}(P)$, $^4T_{1g}(F)\rightarrow{}^4A_{2g}(F)$, and $^4T_{1g}(F)\rightarrow{}^4T_{2g}(F)$, respectively; which are in agreement with the octahedral structure of the complex **1**. The UV-visible spectra of complex 2 showed the presence of two

bands at 286 nm and 392 nm, which represent the π→π* and n→π* transitions, respectively. The band at 392 nm could broaden as a result of the interaction between the ligand-to-metal charge transfer (LMCT) and the n→π* transition band. The complete d^{10} electronic configuration of zinc causes to inhibit the d-d transition that is not displayed in its absorption spectrum. In addition, the structural component of this complex was identified as $3H_2O$ molecules by FT-IR, ^1H NMR, and thermal analysis. These indications, along with UV-visible and molar conductivity data, suggested that complex **2** has distorted trigonal bipyramidal geometry (Vlasenko *et al.*, 2018). The complex**3** (Ni-DDAP3C) exhibited four absorption bands at 308, 440, 590, and 666 nm assigned to n→π*, $^3A_{2g}$→$^3T_{1g}(P)$, $^3A_{2g}$→$^3T_{1g}(F)$, and $^3A_{2g}$ (F)→$^3T_{2g}$ (F) transitions, respectively, which indicated octahedral geometry for the nickel complex with 2.83 B.M. of magnetic moment value (Singh *et al.*, 2017). The complex **4** (Cu-DDAP3C) exhibited two absorption bands at 303, 457 nm in the electronic absorption spectrum.The first band is caused by the n→π* transition whereas the band at 457 nm can be assigned to the d-d transitions in the form of $^2T_2$ → ^2E transition, exhibiting the tetrahedral geometry of the copper complex. The 1.85 B. M. magnetic moment (μ) value further corroborates this assertion (Parsaee *et al.*, 2017). The UV-visible spectral data are given in Table 13, and the spectra are shown in Figure 57 (a, b, c,).

Table 13: Electronic absorption spectral data of DDAP3C and its metal complexes

No.	Compounds	Peak positions (nm)	Assignment
1	HL	275	π→π* ,
		373	n→ π *
2	Complex **1**	268	π →π*
		350	n→ π *
		444	$^4T_{1g}$ (F) →$^4T_{1g}$ (P)
		552	$^4T_{1g}$ (F) →$^4A_{2g}$ (F)
		661	$^4T_{1g}$ (F) → $^4T_{2g}$ (F)
3	Complex **2**	286	π→π*
		392	n→π*
4	Complex **3**	308	n→π*
		440	$^3A_{2g}$→$^3T_{1g}(P)$
		590	$^3A_{2g}$→$^3T_{1g}(F)$
		666	$^3A_{2g}$→$^3T_{2g}$
5	Complex **4**	303	n→π*
		457	$^2T_2$→ ^2E
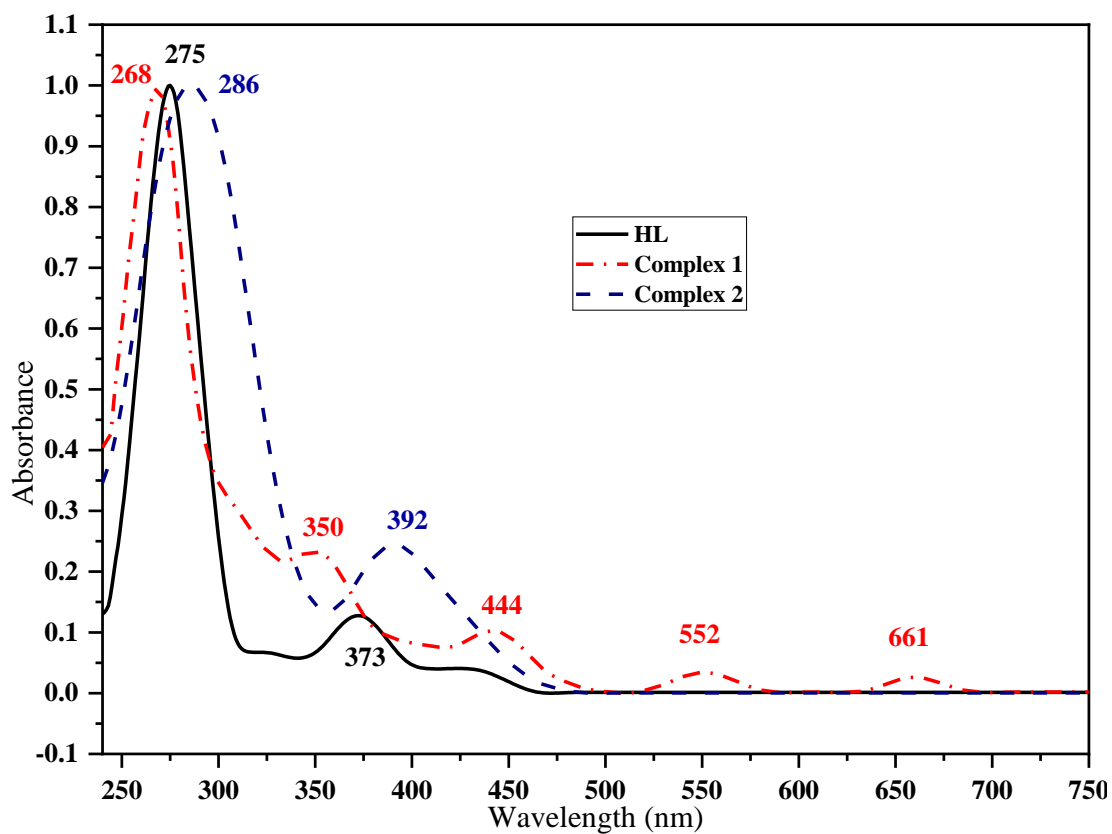
Figure 57: Electronic absorption spectra of (a) DDAP3C, (b) Co-DDAP3C, (c) Zn-DDAP3C

(a)

92
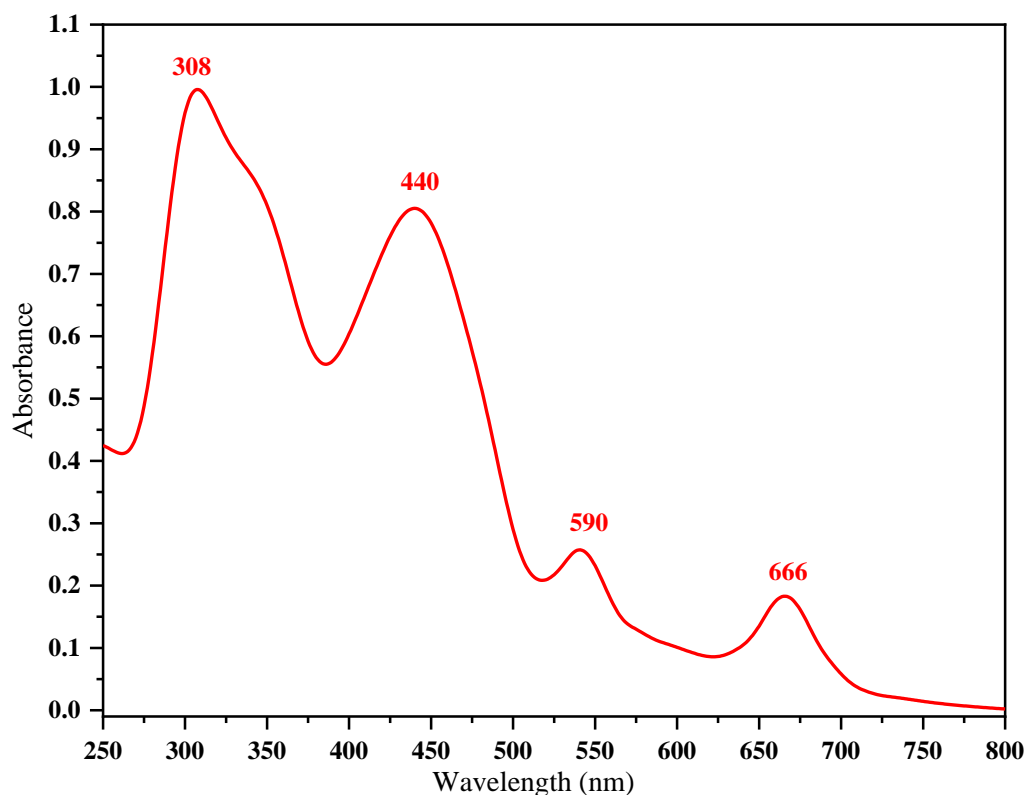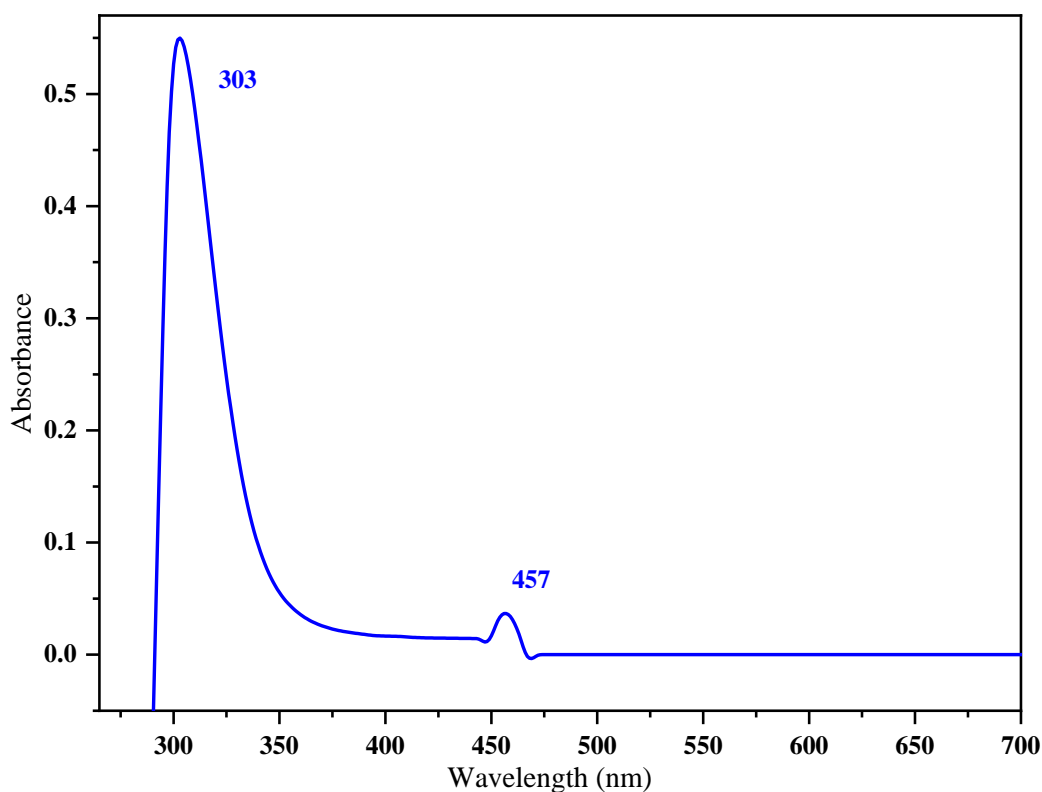
(b)

Figure 58: Electronic absorption spectra of (a) Ni-DDAP3C, (b) Cu-DDAP3C

4.5 Thermal Analysis

Thermal analysis techniques have been widely used in recent years to characterize chemicals by detecting changes in properties at high temperatures as a function of increasing temperature. Heat-sensitive physical and chemical properties of complexes are thoroughly investigated in these techniques. The primary uses of measurements are to ascertain substances' mineral composition and assess their thermal stability. Temperature-dependent changes in the weight of substances are measured by thermogravimetric Analysis (TGA) (De Blasio, 2019; Deboucha *et al.*, 2017; Saadatkhah *et al.*, 2019). An instrument that measures the thermal events of chemicals is known as a thermal analyzer. The sample under study is heated at a controlled rate in a nitrogen atmosphere, and the mass loss of the constituents is noted as a function of temperature. The results of a thermogravimetric run can be displayed as either (i) a weight against temperature curve, known as a thermogravimetric (TG) curve, or (ii) a rate of weight loss versus temperature curve, known as a differential thermogravimetric (DTG) curve. The weight of the chemicals in the thermogram can

93

be scaled either as a percentage of the overall weight or as an accurate weight scale. The differential thermogravimetric (DTG) curve calculates the rate of weight loss, and its relationship to the thermogravimetric (TG) curve provides a method for examining the physicochemical characteristics of the substances. The maximum peak in the DTG curve is identical to the point of maximum slope in the TG curve, whereas the curved portion of the TG curve corresponds to the apex of the DTG curve. The stability of the intermediates is evaluated by the height of the curve above the line at (dw/dt = 0). Any variation in the rate of weight loss can be shown as a trough in the DTG curve, which denotes two consecutive thermal reactions, or as a shoulder to a peak, which indicates two overlapping thermal reactions. Although the thermal events in the TG curve are occasionally not resolved well, they are easier to observe in the DTG curve. Thermogravimetric data help to determine the kinetic parameters of the thermal reactions involving weight gain or loss. For determination of the kinetic parameters, it is more practical and advantageous than traditional isothermal investigations. Nearly all the kinetic parameters can be assessed with a single sample and much less thermal data.

Using several integrating approximations, (Coats & Redfern, 1963) created a well-known equation to compute the kinetic parameters from thermal data. Here is the Coats-Redfern equation:

$$ln\left[-\frac{ln(1-\alpha)}{T^2}\right] = ln\left[\frac{AR}{\beta E^*}\right] - \frac{E^*}{RT}$$

Where α represents fraction decomposed ($\alpha = \frac{w_i - w_t}{w_i - w_f}$, where w_i = initial weight of the sample, w_t = weight of the sample at T K, w_f = final weight of the sample) at temperature *T* K, β denotes linear heating rate, (*dT/dt*). E* and A are the activation energy and Arrhenius pre-exponential factor, respectively. R represents a general gas constant. By changing the data into the equation for a straight line (y = mx + c), a linear plot of the left side of the Coats-Redfern equation $ln\left[-\frac{ln(1-\alpha)}{T^2}\right]$ versus 1000/T results in a straight line. The activation energy parameter is provided by the slope (E*/R), and the intercept can be used to compute the pre-exponential factor (A) (Bouzerafa *et al.*, 2017; Morgan *et al.*, 2017; Suleman *et al.*, 2020). The present study

used the Coats-Redfern equation to compute many kinetic parameters. The following formulae have been used to calculate the additional thermodynamic parameters, including the entropy of activation (ΔS^*), enthalpy of activation (ΔH^*), and energy of activation (ΔG^*):

$$\Delta S^* = R ln \left[\frac{Ah}{k_B T}\right]$$

$$\Delta H^* = E^* - RT$$

$$\Delta G^* = \Delta H^* - T\Delta S^*$$

In the above equation, k_B stands for the Boltzmann constant, and h for Plank's constant.

4.5.1 TGA/DTA Study of Metal Complexes of DDAP2C

The synthesized metal complexes were subjected to a thermogravimetric analysis in a nitrogen environment, with a linear heating rate of 20 °C/min over the temperature range of 40 to 750 °C (Ahmad *et al.*, 2020). In this work, the TGA/DTA plots were examined to determine the thermal and kinetic parameters, and the results are presented in Table 14. The findings matched the structures that other analytical data had suggested. The TGA plot for Ni-DDAP2C (Fig. 59) displayed a four-stage of decomposition with temperatures ranging from 108.15 to 602.07 °C. The coordinated water molecules lost during the first decomposition phase resulted in a mass loss of 0.36 mg (6.18%) over 108.15 °C and 204.98 °C (Buldurun, 2019; Emam *et al.*, 2016). The second stage, which takes place in the 266.3–375.16 °C temperature range, partially involves a mass of 1.763 mg (34.199%) with a loss of ligand. The exothermal impact was noticed in this phase with a T_{DTG} and T_{DTA} peaks at 338.17 and 357.80 °C, respectively (Croitor *et al.*, 2021). The third decomposing phase was detected in the temperature range of 386.01-443.05 °C, with a T_{DTG} peak at 413.60 °C, and the loss of the ligand part had a mass of 0.711 mg (21.77%). The ultimate loss of the ligand moiety is represented by the fourth and final phase decomposition, which occurred between 493.01 and 602.07 °C with the $T_{DTG} = 567.31$ °C, and a solid nickel oxide residue was left behind (El-Megharbel *et al.*, 2016). The thermogram showed a horizontal plateau after 602.07°C, confirming the change.

The TGA plot of Zn-DDAP2C (Fig. 60) showed five decomposing phases with different shoulder peaks. With T_{DTG} = 188.82 °C, the first decomposing step ranging 158.09- 214.42 °C results in the loss of three coordinated water molecules, equivalent to a mass loss of 0.143 mg (2.56%) (Sherif & Abdel-Kader, 2018). In the second phase of decomposition, between 319.06 and 384.83 °C, the loss of 0.906 mg (17.98%) of mass was observed, which may have been caused by a partial loss of the ligand. This stage consists of a shoulder peak at T_{DTG} = 359.49 °C and an exothermal T_{DTA} peak at 372.05 °C. The third decomposition was completed in the range of 394.02-464.36 °C, with a corresponding T_{DTG} peak at 443.48 °C. This step may be because the ligand component was lost, with a mass loss of 1.084 mg (27.01%) (Sevgi *et al.*, 2018; Turan *et al.*, 2019). The loss of a ligand moiety with a mass loss of 0.824mg (32.04%) is represented by the fourth decomposition observed in the 500.73- 575.61°C with T_{DTG} = 531.95 °C. The fifth and final decomposition step took place between 607.58 and 723.32 °C, with T_{DTG} at 651.69 °C, which reflects the total loss of the ligand component, leaving a solid residue ZnO. The horizontal TGA curve segment verified this after 723.32 °C. This step has been completed with an exothermal effect and the peak of T_{DTA} at 651.69 °C.

Four decomposing phases were observed in the thermogram of Co-DDAP2C, ranging in temperature from 191.3 to 614.2 °C. The first disintegrating step between 191.3 and 276 °C causes a mass loss of 0.3691 mg (14.57%), equal to three coordinated water molecules being lost. when the T_{DTG} is 250.3 °C (Buldurun *et al.*, 2020). A mass loss of 0.3798 mg (18.06%) was detected in the second step of disintegration between 287.76 and 363.28 °C, with a T_{DTG} at 316.3 °C, which may have been driven by the loss of the ligand moiety partially. Decomposition of the third phase occurred in the temperature range of 387.3-480.4 °C, with ligand loss of 0.3673 mg (22.18%) having a T_{DTG} peak at 405.9 °C. The fourth and last decomposition stage occurred between 529.6 and 614.2 °C, with a shoulder peak at 571.4 °C, a T_{DTG} at 553.7 °C and a T_{DTA} peak at 562.4 °C, reflecting the complete loss of the ligand component (0.8448 mg, 76.44%), leaving a solid cobalt oxide residue. A horizontal plateau in the thermogram after at 614.2 °C confirmed this transition. The thermograms of Co-DDAP2C are exhibited in Figure 61.

A three-step decomposition pattern with temperatures ranging from 134.35 to 612.39 °C was observed on the Cu-DDAP2C thermogram (Fig. 62). The first disintegrating phase occurred between 134.36 and 200.96 °C, with a T_{DTG} at 178.3 °C leading to a mass loss of 0.1883 mg (10.42%), equivalent to three water molecules lost. The partial loss of the ligand moiety may be the cause of the mass loss of 0.1796 mg (12.04%) that was observed during the second stage of decomposition, which took place between 268.24 and 351.08 °C with a T_{DTG} at 317.1 °C. The third and final decomposition was observed at 433.88-612.39°C, indicating the complete loss of the ligand component (0.5229 mg, 44.58%), leaving a solid CuO residue (Osypiuk *et al.*, 2020). This step was completed with a T_{DTA} peak at 357.80 °C, and a T_{DTG} peak at 338.17 °C, indicating the exothermic process. The horizontal portion seen after at 612.39 °C in the thermogram confirmed the solid residue of CuO.

Kinetic Parameter

TGA/DTA plots were analyzed to extract the kinetics and thermodynamic properties of metal complexes and the results are presented in Table 15.
These details have come to light:

(1) The activation energy (E*) increased with each successive stage, suggesting a reduced rate of complex breakdown. A slower pace of ligand disintegration in the metal complex indicates that the complex is more thermally stable.

(2) Entropy of activation (ΔS*) values in most decomposition phases were negative, indicating more ordered complexes than reactants with slower reaction processes. Additionally, the nonspontaneous decomposition process was suggested by the negative values in the decomposition stages (Alturiqi *et al.*, 2020).

(3) The negative enthalpy (ΔH*) for all decomposition steps revealed that the decompositions are exothermic (M. A. Mahmoud & Abou-elmagd, 2020).

(4) The fact that the value of ΔG* was positive at every step demonstrates that the decomposition was nonspontaneous (Howsaui *et al.*, 2021).

Table 14: Thermal decomposition data of metal complexes of DDAP2C ligand

Complex	Steps	Δm % found (Cal.)	T_i	T_f	T_{DTG}	Mass loss	T_{DTA}	Peak
							DTA	
Ni-DDAP2C	1	6.18	108.15	204.98	173.71	0.36	-	-
	2	34.199	266.3	375.16	338.97	1.763	357.80	Exo
	3	21.77	386.01	443.05	413.60	0.711	-	-
	4	57.326	493.01	602.07	567.31	1.252	569.96	Exo
Zn-DDAP2C	1	2.56	158.09	214.42	188.82	0.143	-	-
	2	17.98	319.06	384.83	359.49	0.906	372.05	Exo
	3	27.01	394.02	464.36	443.48	1.084	-	-
	4	32.04	500.73	575.61	531.95	0.824	-	-
	5	93.56	607.58	723.32	651.69	1.394	-	-
Co-DDAP2C	1	14.57	191.31	276.002	250.3	0.3691	-	-
	2	18.06	287.76	363.28	316.3	0.3798	-	-
	3	22.18	387.29	480.44	405.9	0.3673		
	4	76.44	529.62	614.23	553.7	0.8449	562.4	Exo
Cu-DDAP2C	1	10.42	134.36	200.96	178.3	0.1883	-	
	2	12.04	268.24	351.08	317.1	0.1796	-	
	3	44.58	433.88	612.39	510.3	0.5229	506.2	Exo

Table 15: Kinetic and thermodynamic parameters of metal complexes of DDAP2C ligand

Comp.	Step	r	A (s^{-1})	T_{max} (K)	E^* (J/mol)	ΔS^* (J/K.mol)	ΔH^* (kJ/mol)	ΔG^* (kJ/mol)
Ni-DDAP2C	1	-0.99317	1316.62	446.71	877.460	-188.556	-2.836	81.393
	2	-0.99159	709.818	611.97	550.886	-196.331	-4.537	115.599
	3	-0.99082	446.783	686.60	280.348	-201.115	-5.428	132.658
	4	-0.99141	338.531	840.31	270.704	-205.101	-6.715	165.633
Zn-DDAP2C	1	-0.99078	279.439	461.82	249.836	-201.719	-3.589	89.568
	2	-0.99168	560.628	632.49	331.812	-198.546	-4.927	120.651
	3	-0.99178	477.918	716.48	342.869	-200.909	-5.614	138.333
	4	-0.99083	338.896	804.95	258.898	-204.735	-6.433	158.368
	5	-0.99178	281.035	924.69	252.247	-207.445	-7.436	184.134
Co-DDAP2C	1	-0.9915	9.58×10^2	523.4	585.2	-192.51	-3.77	97.00
	2	-0.9900	7.24×10^2	589.4	534.8	-195.82	-4.37	111.06
	3	-0.99011	5.19×10^2	679.1	433.5	-199.77	-5.21	130.44
	4	-0.99007	2.79×10^2	826.8	205.02	-206.56	-6.67	164.12
Cu-DDAP2C	1	-0.99607	1.38×10^3	451.4	593.7	-188.24	-3.16	81.82
	2	-0.99163	7.77×10^2	590.2	565.8	-195.25	-4.34	110.90
	3	-0.99014	4.76×10^2	783.4	561.86	-201.67	-5.95	152.05
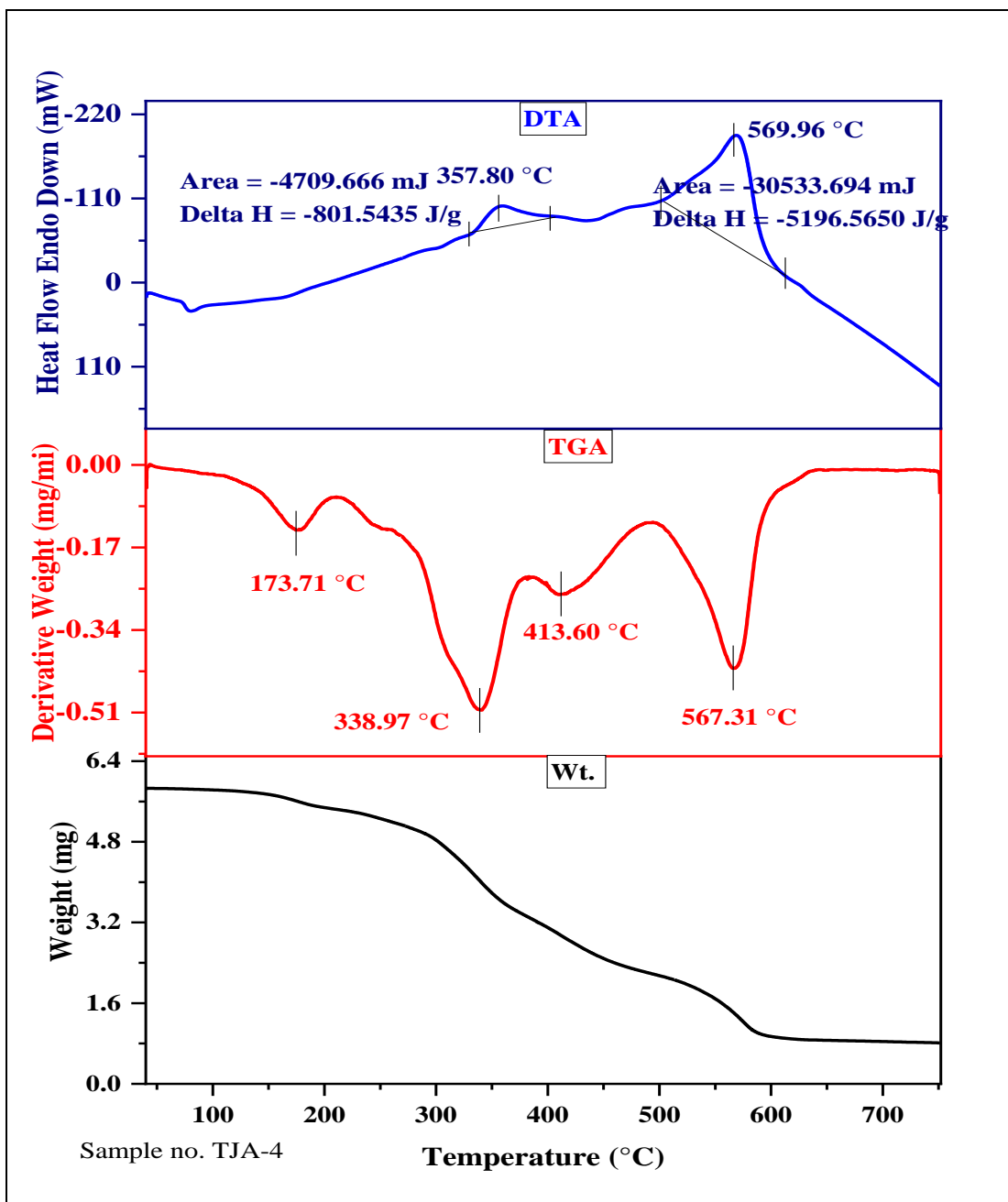
Figure 59: Thermogram of Ni-DDAP2C
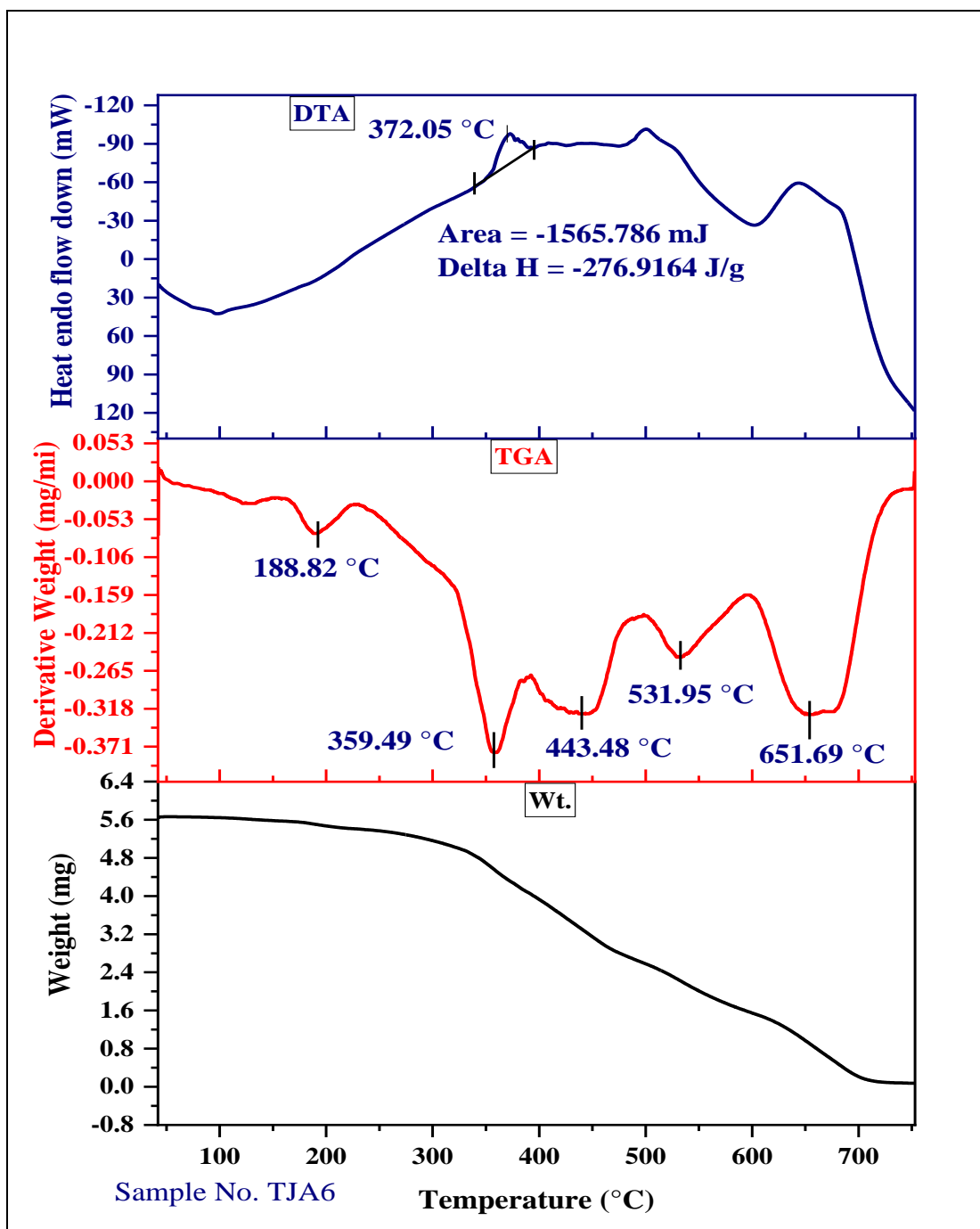
Figure 60: Thermogram of Zn-DDAP2C

100
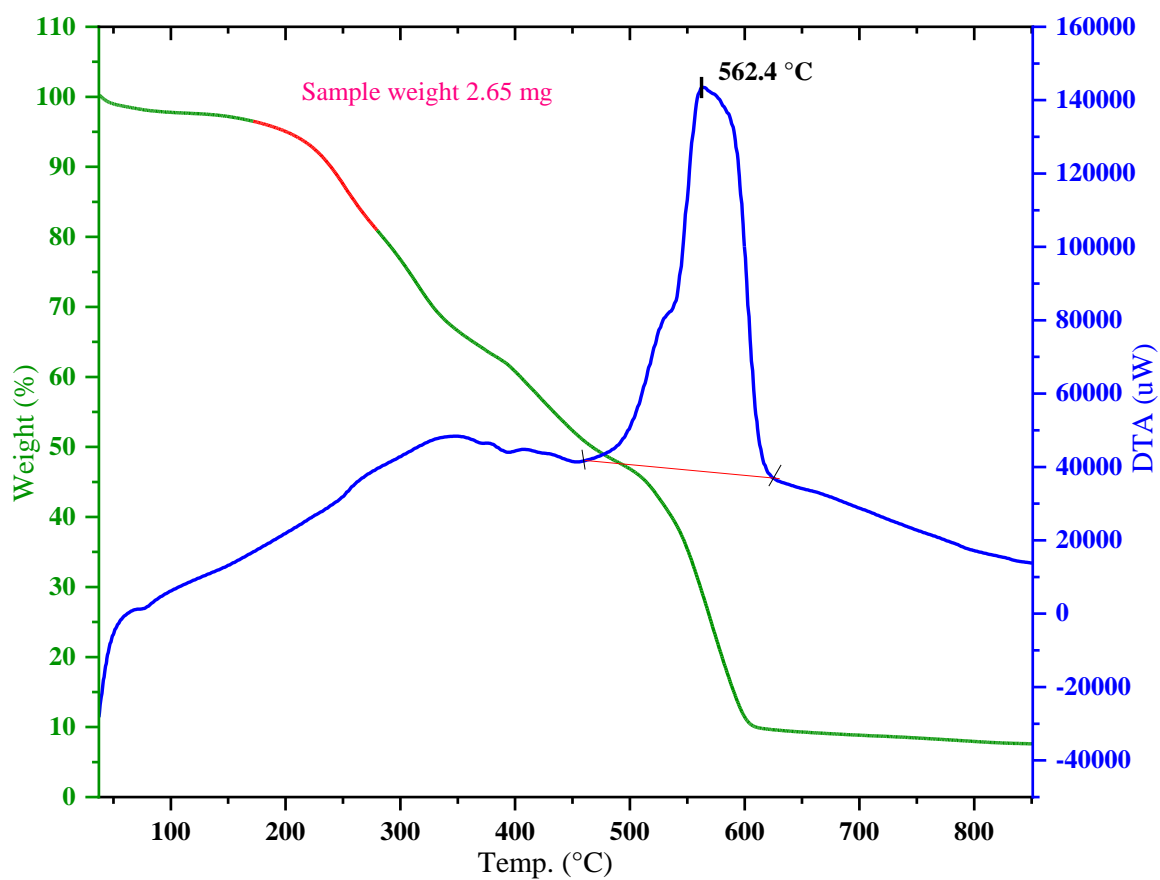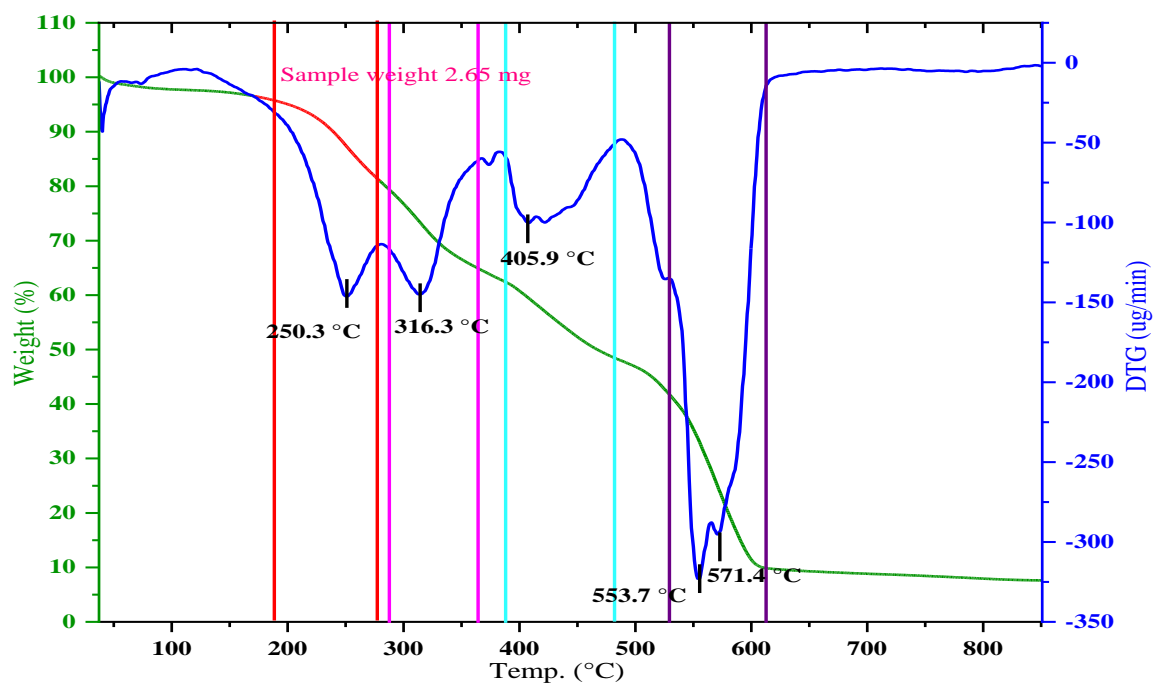
Figure 61: Thermogram of Co-DDAP2C
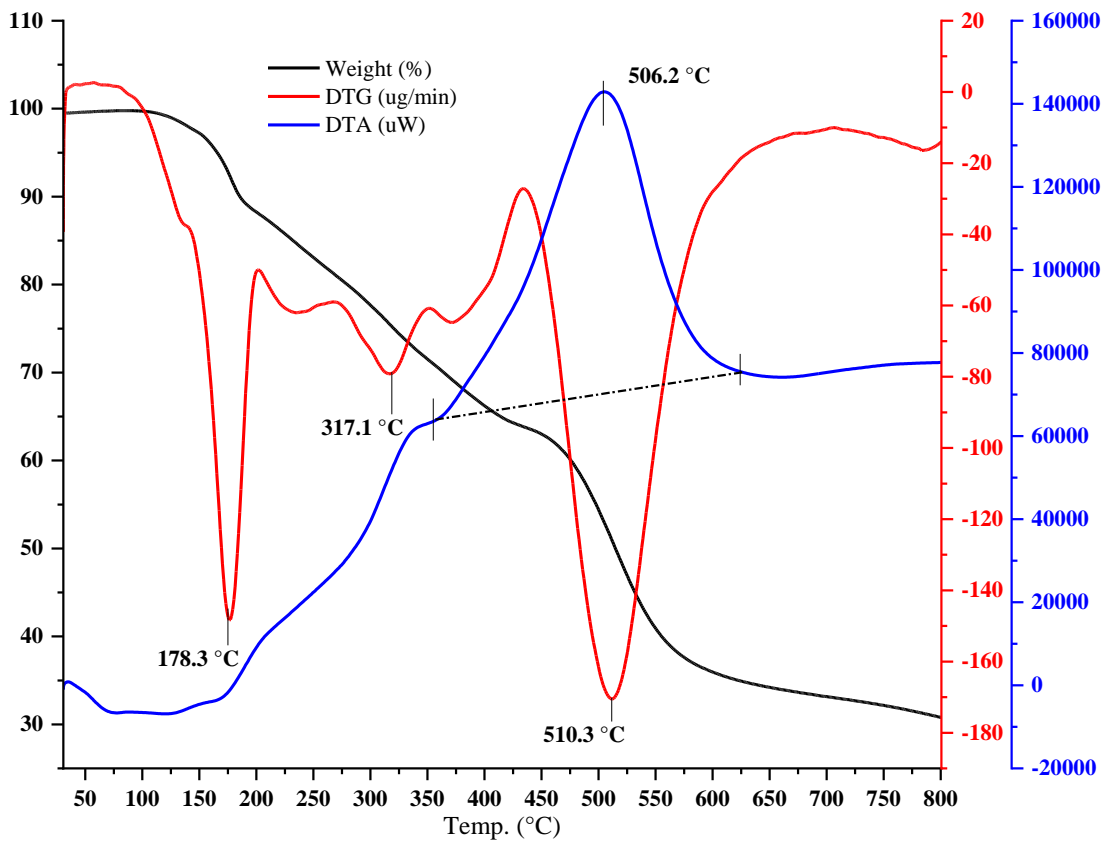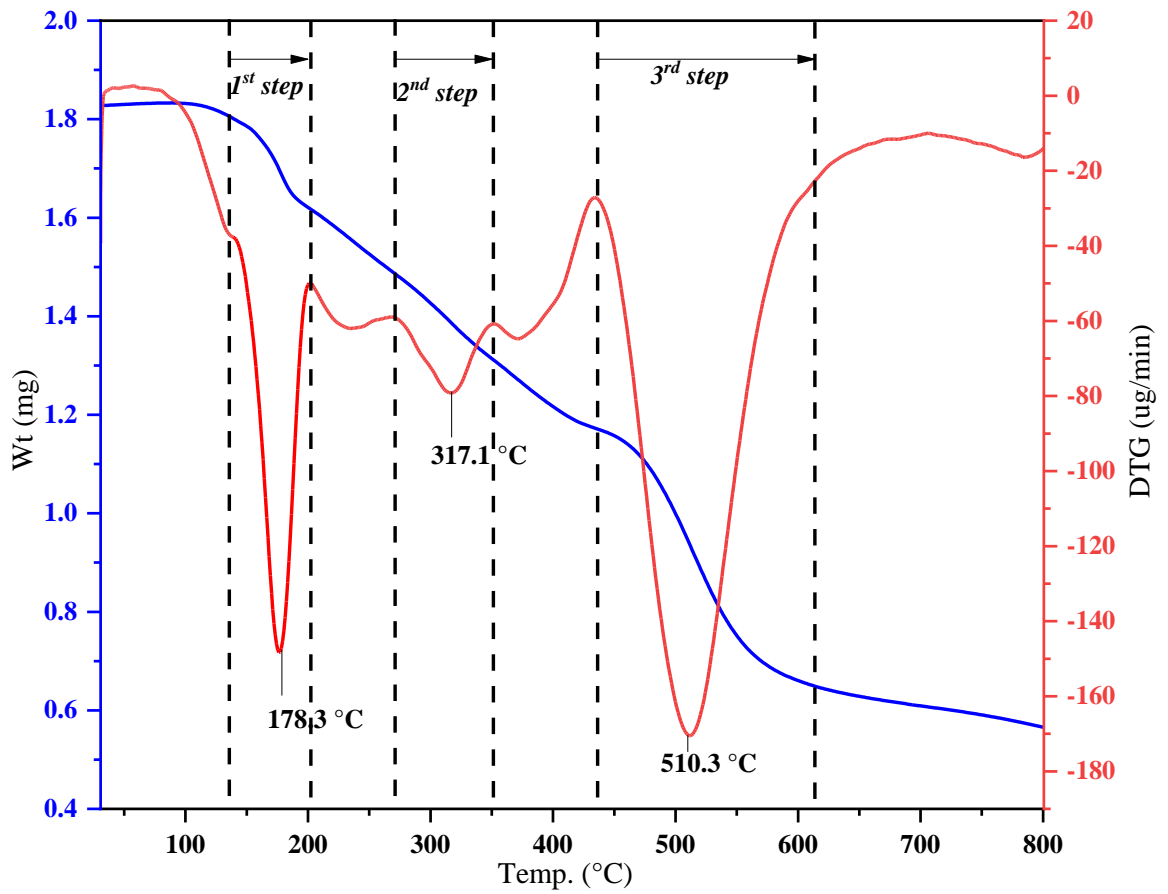
Figure 62: Thermogram of Cu-DDAP2C

4.5.2 TGA/DTA Study of Metal Complexes of DDAP3C

The thermogravimetric Analysis (TGA) was carried out in an N_2 environment between 40 and 730 °C at a linear heating rate of 10 °C/min (Aghaei *et al.*, 2020). The TGA/DTA outcomes are listed in Table 16, and Figures 63 and 64 show thermograms depicting different disintegration stages. Among the three phases of decomposition of complex **1**, the first occurred within 73.6 - 147.4 °C, having the peak of T_{DTG} at 118.1 °C. This decomposition might result from losing 2Cl atoms and H_2O molecules from the outer sphere. In the second phase of disintegration at 152.3 - 250.6 °C, coordinated H_2O and a portion of the ligand moiety was lost. This action resulted in a mass loss of 1.1364 mg (26.05%) and with a peak of T_{DTG} at 198.5 °C. With a mass loss of 0.4098 mg (17.74%) and a T_{DTG} peak at 412.7 °C in the third stage, the whole ligand moiety was removed entirely, leaving a solid cobalt oxide residue. Among the four decomposition steps of complex **2**, the first step took place at 73.6 - 147.4 °C, with the T_{DTG} peak at 118.1 °C. This action suggests a mass loss of 0.108 mg (1.55%), which corresponds to the loss of an atom of Cl and H_2O from the outer sphere. The loss of a portion of the ligand moiety and coordinated Cl-atoms in the second stage of breakdown at 156.64 - 250.43 °C range with the T_{DTG} peak at 209.09 °C associated with a shoulder peak of less intensity. Eliminating the ligand part relates to a mass loss of 1.69 mg (33.13%) in the third step of decomposition at 342.07 - 474.57 °C with a T_{DTG} peak at 429.42 °C. The whole ligand portion is eliminated in the fourth and final breakdown stage, which occurs between 551.07 and 700.11 °C with a T_{DTG} peak at 634.46 °C that corresponds with a mass loss of 2.718 mg (92.11%), leaving a solid residue of ZnO (Mahdy *et al.*, 2021). The horizontal segment displayed after 700.11 °C in the thermogram depicts the residue of the ZnO solid.

The first of the four decomposition phases for complex **3** (Ni-DDAP3C) began at 114.93 and completed at 176.45 °C, with the T_{DTG} peak occurring at 147.2 °C. The loss of 2Cl atoms and H_2O molecules from the outer sphere may cause the 0.3809 mg (6.18%) mass loss that occurred in this step. The coordinated H_2O and a portion of the ligand moiety were lost during the second stage of disintegration, which occurred at 244.21-356.33 °C, with a T_{DTG} peak at 296.6 °C, this activity caused a mass loss of

0.8315 mg (15.19%).In the third decomposition phase at 369.83 - 483.29 °C with a T_{DTG} peak at 422.6 °C, there was a mass loss of 0.9097 mg (19.81%), indicating the elimination of the ligand moiety. The fourth and final breakdown stage occurs between 495.60 and 620.21°C with a T_{DTG} peak at 548.3 °C. It corresponds to a mass loss of 2.1211 mg (58.44%), eliminating the whole ligand moiety and leaving a solid nickel oxide residue (Ashok *et al.*, 2020). The confirmation of the NiO residue was assured by the appearance of the horizontal portion after 620.21°C in the thermogram. The thermograms of complex **3** are depicted in Fig. 65.

Among four, the initial decomposition phase of complex **4** (Cu-DDAP3C) occurred between 89.98 and 168.52 °C, with the T_{DTG} peak occurring at 119.8 °C. This activity predicts a mass loss of 0.1986 mg (5.47%), representing the loss of water molecule from the outer sphere. The second stage of decomposition, which occurs between 238.73 and 312.76 °C with a mass loss of 0.3182 mg (13.27%) with the T_{DTG} peak at 282.9 °C, results in the loss of the ligand part. There was a mass loss of 0.3019 mg (15.79%) in the third decomposition step at 349.95 - 398.39 °C with a T_{DTG} peak at 371.2 °C and a T_{DTA} peak at 375 °C, suggesting the loss of a portion of ligand moiety. The entire ligand moiety is removed in the fourth and final decomposition stage, occurring at 522.85-668.44°C, corresponding to a mass loss of 0.8692 mg (66.70%), leaving a solid CuO residue (Kurt *et al.*, 2020). This step has been completed with a T_{DTG} at 599.8 °C and the peak of T_{DTA} at 605.6 °C showing an exothermal empact. The horizontal portion in the thermogram of complex **4** confirms the rest mass of the copper oxide. The thermograms of complex **4** are displayed in Fig. 66.

Kinetic Parameter

The kinetic and thermodynamic parameters of the metal complexes of the ligand have been extracted from thermogravimetric (TG) and differential thermal analysis (DTA) curves. These parameters such as the energy of activation (E∗), enthalpy change (ΔH∗), entropy change (ΔS∗), and Gibbs free energy change (ΔG∗) of each decomposition step are evaluated by employing the Coast-Redfern equation and the computed values for the decomposition steps for all four complexes are summarized in Table 17. The E* value increases successively in each decomposition step of complex **1**, indicating a decreasing decomposition rate. The ligand moiety

decomposition rate in the metal complex slowed down, pointing to more excellent thermal stability. Covalent bonds in complexes contribute to their stability, producing high activation energy (E*) for decomposition (Chaudhary *et al.*, 2021).The positive values of Gibbs free energy change (ΔG*) for complex **2** indicated a nonspontaneous thermal process. The negative *Δ*S* values for the decomposition steps in complexes indicate an ordered activated complex over reactants or a slower reaction (Yaşar *et al.*, 2021). Moreover, negative values in the decomposition steps also showed a nonspontaneous decomposition process. The enthalpy change value (ΔH*) is positive in all decomposition steps, indicating that the decomposition process is endothermic (Elsenety *et al.*, 2020). Figures 65& 66 exhibit the thermograms of complexes **3** and **4**.

Table 16: Thermal decomposition data of metal complexes of DDAP3C ligand

Complexes	TG range (°C)						DTA
	Steps	Δm % found (Cal.)	T_i	T_f	T_{DTG}	Mass loss	T_{DTA}
Complex **1**	1	3.86	73.57	147.35	118.13	0.17	-
(Co-complex)	2	26.05	152.31	250.62	198.54	1.14	
	3	17.74	378.05	476.31	412.68	0.40	422.89
Complex **2**	1	1.55	67.77	132.65	100.91	0.10	-
(Zn-complex)	2	13.21	156.64	250.43	209.09	0.90	195.27
	3	33.13	342.07	474.57	429.42	1.69	445.36
	4	92.11	551.07	700.11	634.46	2.72	637.19
Complex **3**	1	6.18	114.93	176.45	147.2	0.3809	-
(Ni-complex)	2	15.19	244.21	356.33	296.6	0.8315	-
	3	19.81	369.83	483.29	422.6	0.9097	-
	4	58.44	495.60	620.21	548.3	2.1211	-
Complex **4**	1	5.47	89.98	168.52	119.8	0.1986	-
(Cu-complex)	2	13.27	238.73	312.76	282.9	0.3182	-
	3	15.79	349.95	398.39	371.2	0.3019	375
	4	66.70	522.85	668.44	599.8	0.8692	605.6

Table 17: Kinetic and thermodynamic parameters of metal complexes of DDAP3C ligand

Complexes	Step	r	A (s^{-1})	T_{max} (K)	E^* (kJ/mol)	ΔS^* (J/K.mol)	ΔH^* (kJ/mol)	ΔG^* (kJ/mol)
Complex **1**	1	-0.99490	6.32 x 10^{10}	391.28	86.13	-40.40	82.88	98.68
(Co-complex)	2	-0.98210	8.09 x 10^{10}	471.69	108.39	-39.89	104.46	123.28
	3	-0.98387	3.85 x 10^{10}	685.83	153.15	-49.19	147.45	181.19
Complex **2**	1	-0.99142	3.75 x 10^{10}	374.06	82.89	- 44.35	79.78	96.36
(Zn-complex)	2	-0.99335	9.78 x 10^{9}	482.24	100.59	-57.65	96.59	124.39
	3	-0.9962	4.29 x 10^{8}	702.57	126.27	- 86.77	120.43	181.39
	4	-0.99907	1.72 x 10^{12}	907.61	226.83	-19.94	219.28	240.08
Complex **3**	1	-0.99077	1.55 x 10^{3}	420.35	0.7706	-186.69	-2.72	75.75
(Ni-complex)	2	-0.99007	7.73 x 10^{2}	569.75	0.7479	-194.99	-3.98	107.11
	3	-0.99017	5.37 x 10^{2}	695.75	0.4727	-199.69	-5.31	133.62
	4	-0.99043	3.33 x 10^{2}	821.45	0.2676	-205.05	-6.56	161.88
Complex **4**	1	-0.99026	1.66 x 10^{3}	392.9	0.8503	-185.55	-2.42	70.49
(Cu-complex)	2	-0.99105	8.07 x 10^{2}	556.05	0.4801	-194.44	-4.14	103.98
	3	-0.99054	4.85 x 10^{2}	644.35	0.2724	-199.89	-5.08	123.71
	4	-0.99060	3.52 x 10^{2}	872.95	0.3312	-205.09	-6.93	172.11
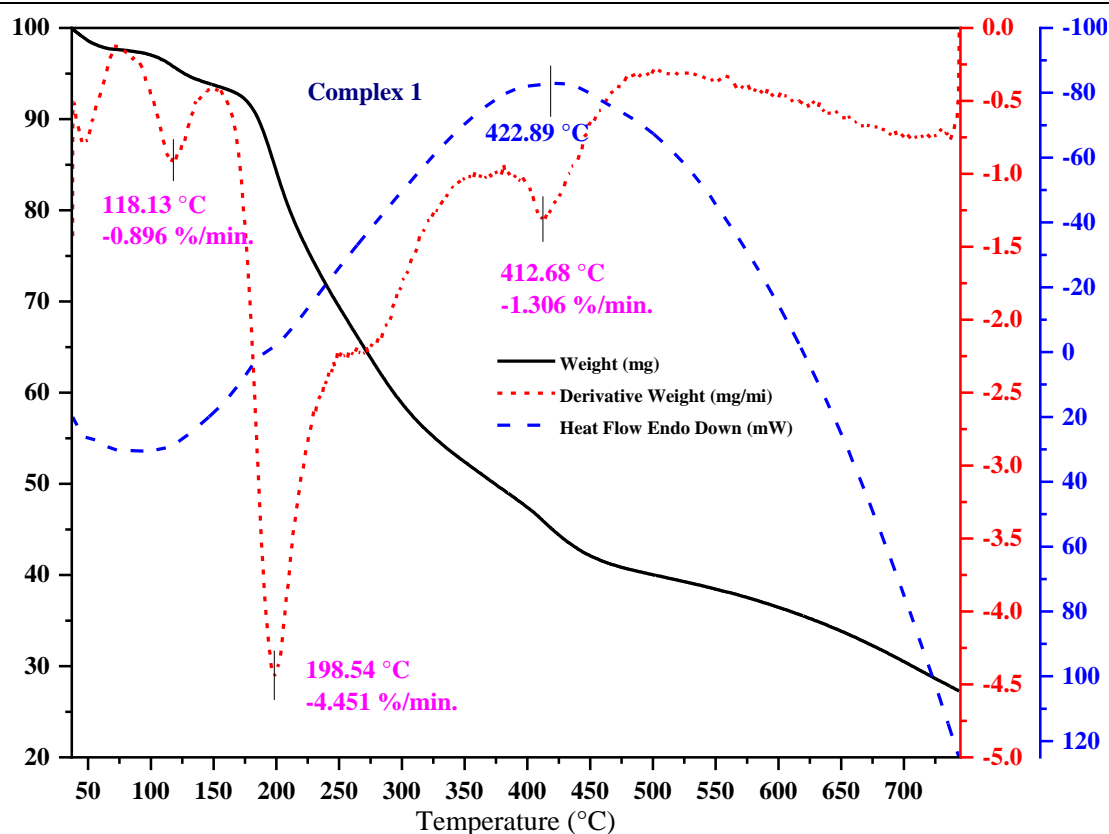
Figure 63: Thermogram of Co-DDAP3C

106
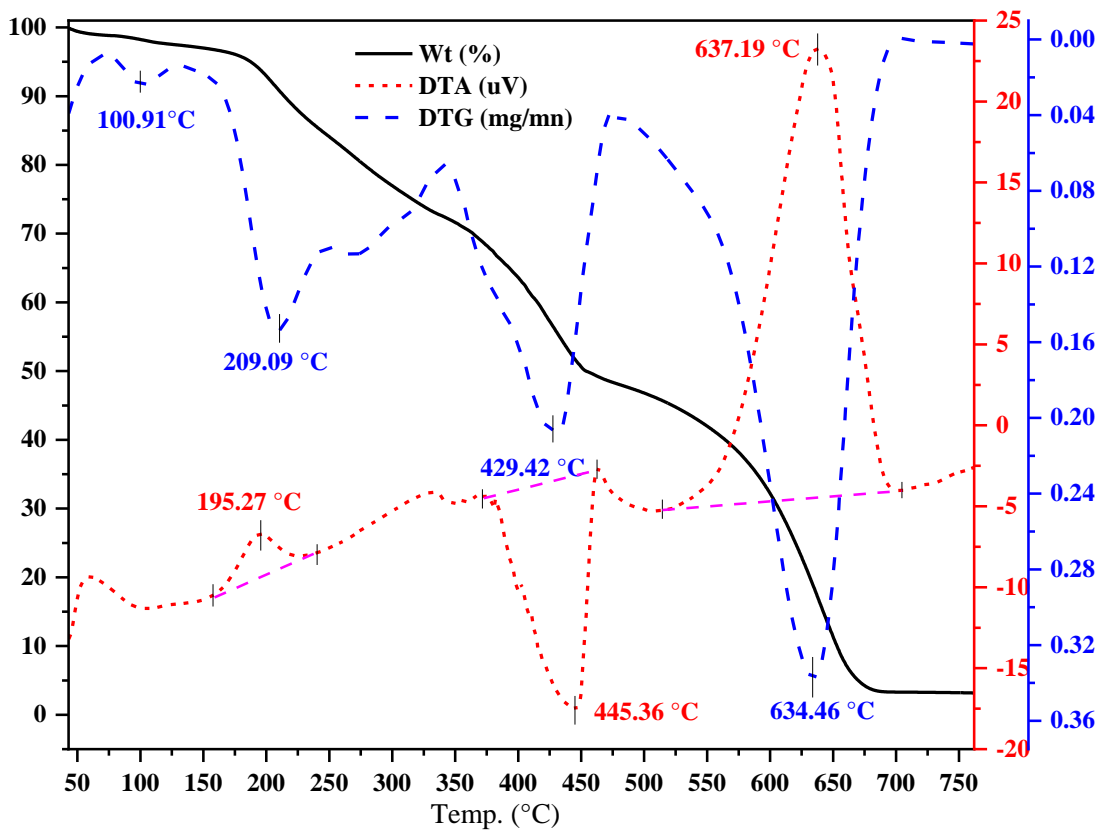
Figure 64: Thermogram of Zn-DDAP3C
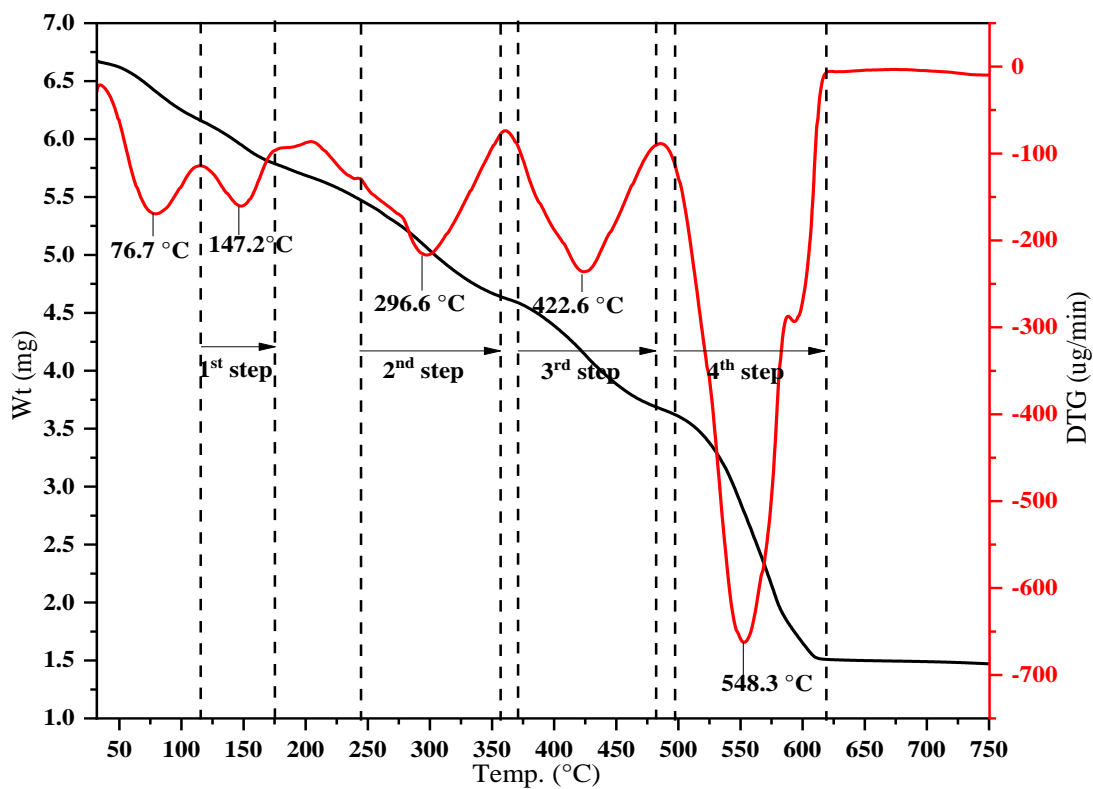
Figure 65: Thermogram of Ni-DDAP3C

107

werenano
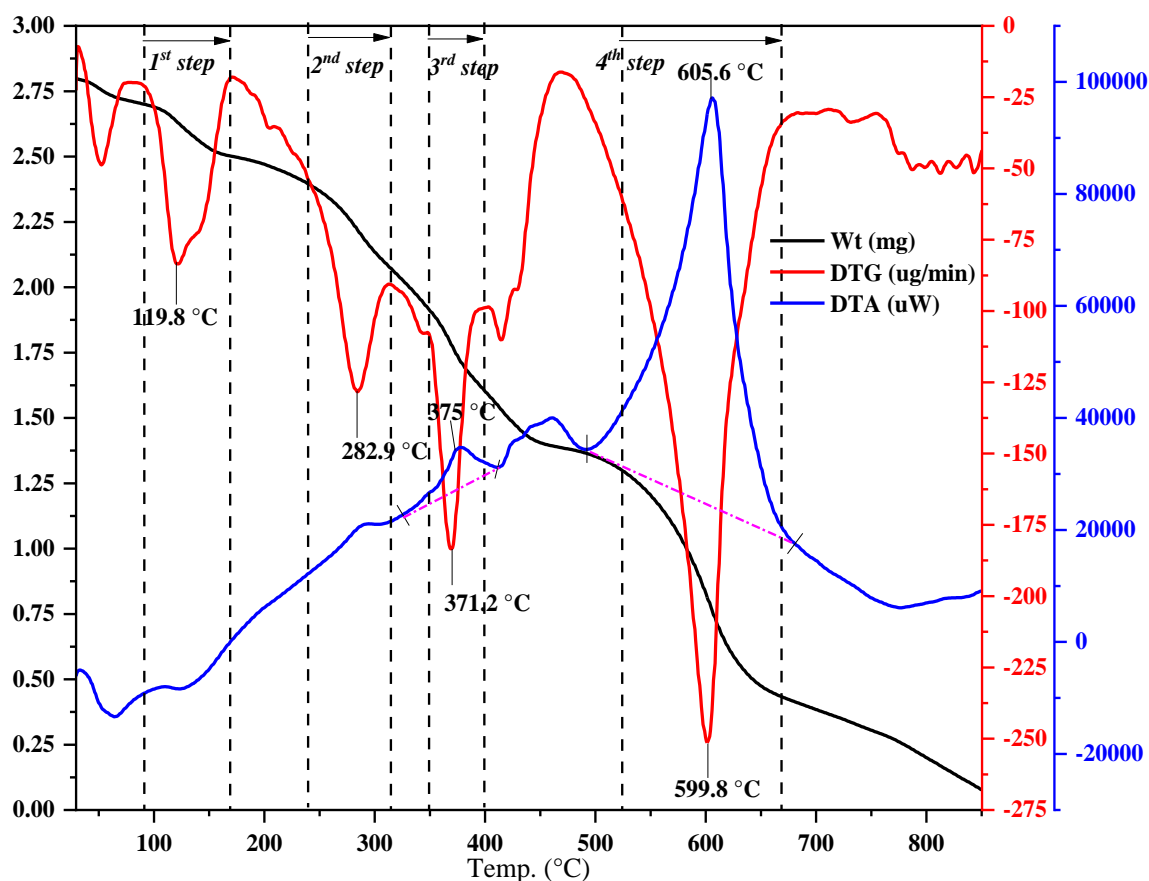
Figure 66: Thermogram of Cu-DDAP3C

4.6   X-ray Powder Diffraction (XRPD) Study

In the discipline of coordination chemistry, the analysis of compounds using X-ray powder diffraction has shown to be an invaluable tool for complex characterization. Determining the crystal structure using powder diffraction data is far more complicated and challenging than single crystal data. This difficulty is because the three-dimensional crystallographic information collapses into the single-dimensional powder diffraction pattern. The synthesis of a single crystal for all chemical compounds is not possible, despite the single-crystal approach being considerably more suited and straightforward than the powder diffraction analysis for structure determination.

4.6.1 XRPD Study of Metal Complexes of DDAP2C

The Powder X-ray diffraction analysis was performed to determine the crystal characteristics of DDAP2C ligand and its transition metal complexes because single-crystal formation proved ineffective. In order to comprehend the lattice dynamics of the compounds, the patterns of PXRD of the compounds were assessed in the 3-80° (2θ) range. It gives a precise idea of the solid's purity and reveals its distinct crystal structure. The diffractogram showed significant peaks, which suggested that the material was crystalline. The full width at half maximum (FWHM) of the refined diffraction peaks was used to calculate the particle size (El-Shwiniy *et al.*, 2021). The DDAP2C diffractogram displayed 7 reflection peaks with intense peak at 7.54429° and an associated d spacing value of 0.05068 Å. The average crystallite size of 8.4581 nm proved that it was nanocrystalline. The diffractogram for Ni-DDAP2C also showed 8 reflection peaks, with the highest intensity peak at 24.5929° and having a d-spacing value of 0.16405 Å. The average crystallite size of the complex is 35.8373 nm, representing its nanocrystalline nature. Similarly, thirteen reflection peaks have been identified in the diffractogram of Zn-DDAP2C, with the high intensity peak being at 4.0995° and a corresponding d-spacing value of 0.02755 Å. The average crystallite size of 53.2379 nm demonstrated its nanocrystalline nature.

Using Debye Scherrer's equation, the synthesized chemical's crystallite size (D) was calculated from PXRD patterns (Nozha *et al.*, 2020).

$$D = \left({K\lambda} / {\beta Cos\theta} \right)$$

Here, λ stands for the wavelength; θ (radians) and β stand for the diffraction angle and the full width at half maxima, respectively. K stands for the shape factor, a constant having a value of 0.9 (Özdemir, 2020). DDAP2C, Ni-DDAP2C, and Zi-DDAP2C have average crystallite sizes of 8.4581 nm, 35.8373 nm, and 53.2379 nm, respectively. Peaks with various peak intensities associated with different interplanar d-spacing values were found when the X-ray diffraction patterns were compared; this may indicate the formation of the complexes.

The value of (D), was used to calculate the dislocation density (δ) of the complexes ,which represents the number of dislocation lines in the crystal per unit area (nm^{-2}), (Ismail *et al.*, 2021). The following equation describes the relation between average crystallite size (D) and dislocation density (δ):

$$\delta = (^1/_{D^2})$$

According to calculations, the values of (δ) for Ni-DDAP2C, Zn-DDAP2C, and DDAP2C were 13.98 x 10^{-3}, 0.779 x 10^{-3}, and 0.353 x 10^{-3}, respectively. The 'δ' values of the metal complexes differ from the ligand supporting complex formation. Microstrain (ε), which was calculated using the value of the peak location (2θ) and its related FWHM, is another significant parameter that explains the differences in the lattice parameters between samples (Abou Melha *et al.*, 2021).

$$\varepsilon = ^\beta/_{4tan\theta}$$

Here, β signifies the FWHM, and θ stands for the diffraction angle in radians. For DDAP2C, Zn-DDAP2C, and Ni-DDAP2C, the measured microstrain values were 0.04340, 0.01127, and 0.01353, respectively. The varied values of ε ensure that the complexes and ligand are distinct molecules that once further affirms that the ligand is involved to form the complexes. Compared to its complexes, the ligand exhibits a considerable variation in lattice parameters across the sample. The crystallographic information as well as the refinement parameters are listed in Table 18, 19, and 20, and difractograms are shown in Figure 67.

The Co-DDAP2C diffractogram showed 8 reflection peaks with maximum peak intensity at 16.32° and the associated d spacing value of 5.43, within a range of 0–39.38° (2θ). The complex is nanocrystalline, as evidenced by the average crystallite size of 21.97 nm (Alkıs *et al.*, 2021). In the same way, the diffractogram of Cu-DDAP2C displays 11 reflection peaks within 0-43.68° (2θ), with the interplanar d-spacing value being 28.84 and the intense peak appearing at 3.06°. The average crystallite size value of 81 nm indicated that it was a nanocrystalline solid (Al-Humaidi, 2019). For Co-DDAP2C and Cu-DDAP2C, the percentage of crystallinity

within the entire XRD scan range was 31.03 and 35.14%, respectively. The crystallographic data and refinement parameters for Co-DDAP2C and Cu-DDAP2C obtained from calculations are shown in Tables 21 and 22 and difractograms are displayed in Figures 68 and 69, respectively.

Table 18: Crystallographic data of DDAP2C ligand

Position (2 theta)	FWHM	Crystallite size (nm)	Av. crystallite size (nm)	Crystallinity (%)	d- spacing	Dislocation density x 10^{-3}	Microstrain x 10^{-3}
3.838	0.86	9.2383	8.458	93.183	0.0257	11.7169	112.042
7.544	0.925	8.6017			0.0506	13.5152	61.2537
11.48	0.855	9.3304			0.0770	11.4867	37.1427
15.386	0.741	10.8079			0.1031	8.56084	23.9586
19.367	1.032	7.8043			0.1295	16.4184	26.4054
23.39	1.399	5.7954			0.1561	29.7733	29.5042
39.286	1.105	7.6286			0.2589	17.1831	13.5168

Table 19: Crystallographic data of Ni-DDAP2C

Position (2 theta)	FWHM	Crystallite size (nm)	Av. crystallite size (nm)	Crystallinity (%)	d- spacing	Dislocation density x 10^{-3}	Microstrain x 10^{-3}
4.703	0.049	160.755	35.837	46.463	0.0316	0.0386	5.2546
8.480	0.368	21.6			0.0569	2.1432	21.704
12.047	0.711	11.234			0.0808	7.9228	29.4
16.099	0.576	13.91			0.1078	5.1665	17.792
20.652	0.433	18.6			0.1380	2.8883	10.392
22.572	0.541	14.94			0.1507	4.4757	11.849
24.592	0.357	22.77			0.1640	1.928	7.1468
37.400	0.366	22.86			0.2469	1.9124	4.728

Table 20: Crystallographic data of Zn-DDAP2C

Position (2 theta)	FWHM	Crystallite size (nm)	Av. crystallite size (nm)	Crystallinity (%)	d- spacing	Dislocation density x 10^{-3}	Microstrain x 10^{-3}
4.099	0.169	46.923	53.237	53.199	0.0275	0.4541	20.6536
6.156	0.195	40.734			0.0413	0.6026	15.8464
8.307	0.318	25.009			0.0557	1.5988	19.1355
9.221	0.185	42.909			0.0619	0.5431	10.0492
11.19	0.244	32.703			0.0751	0.9349	10.8648
12.329	0.245	32.591			0.0827	0.9414	9.9042
15.312	0.549	14.591			0.1026	4.6967	17.8305
20.739	0.589	13.704			0.1386	5.3246	14.0522
22.563	0.605	13.375			0.1506	5.5896	13.2472
24.934	0.349	23.304			0.1662	1.8413	6.8901
29.322	0.130	63.040			0.1949	0.2516	2.1724
33.669	0.387	21.409			0.2230	2.1815	5.5902
46.206	0.026	321.79			0.3022	0.0096	0.2745

Table 21: Crystallographic data of Co-DDAP2C

Position 2 Theta	FWHM	Crystallite size (nm)	Average Crystallite size (nm)	d-spacing (Å)	dislocation density (δx 10^{-3} nm^{-2})	Microstrain x 10^{-3}	Crystallinity (%)
12.50	0.5206	15.3487	21.965	7.0739	4.2447	20.7395	31.03
14.47	0.3716	21.549		6.1154	2.1534	12.7705	
16.31	0.2977	26.951		5.4272	1.3767	9.06184	
20.76	0.4468	18.072		4.2746	3.0616	10.6435	
21.53	0.4002	20.204		4.1239	2.4496	9.18497	
22.70	0.3176	25.512		3.9125	1.5364	6.9012	
32.21	0.3502	23.605		2.7767	1.7945	5.2933	
39.38	0.3447	24.478		2.286	1.6689	4.2026	

Table 22: Crystallographic data of Cu-DDAP2C

Position 2 Theta	FWHM	Crystallite size (nm)	Average Crystallite size (nm)	d-spacing (Å)	dislocation density (δx 10^{-3} nm^{-2})	Microstrain x 10^{-3}	Crystallinity (%)
3.06	0.0728	109.058	88.36	28.8387	0.084	11.899	35.14
6.1	0.0890	89.318		14.4577	0.1253	7.284	
9.16	0.0927	85.945		9.6412	0.1353	5.0479	
12.22	0.0879	90.823		7.2323	0.1212	3.5833	
16.32	0.3634	22.081		5.4242	2.0508	11.054	
24.63	0.2166	37.539		3.6105	0.7096	4.328	
27.69	0.1087	75.21		3.2179	0.1767	1.9253	
34.01	0.1083	76.69		2.6338	0.17	1.5453	
37.19	0.0505	165.71		2.4154	0.0364	0.6559	
40.43	0.1387	61.011		2.2287	0.2686	1.6438	
43.67	0.0539	158.57		2.0706	0.0397	0.5876	
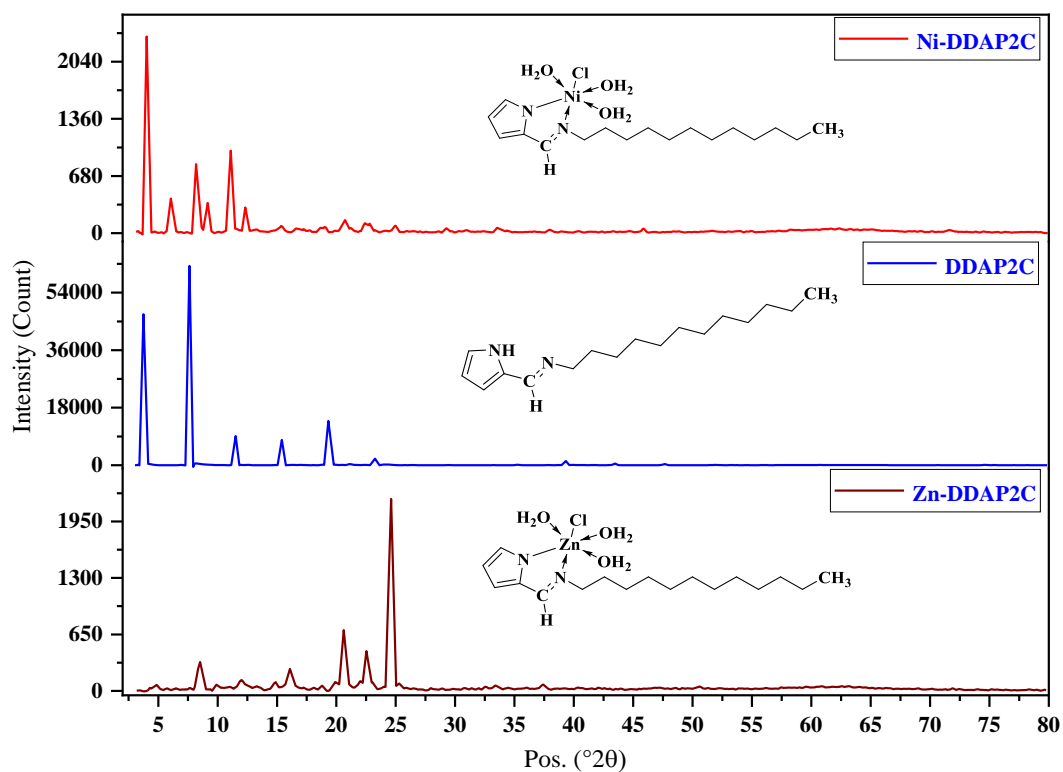
Figure 67: Diffractogram of (a) Zn-DDAP2C, (b) DDAP2C, (c) Ni-DDAP2C

113
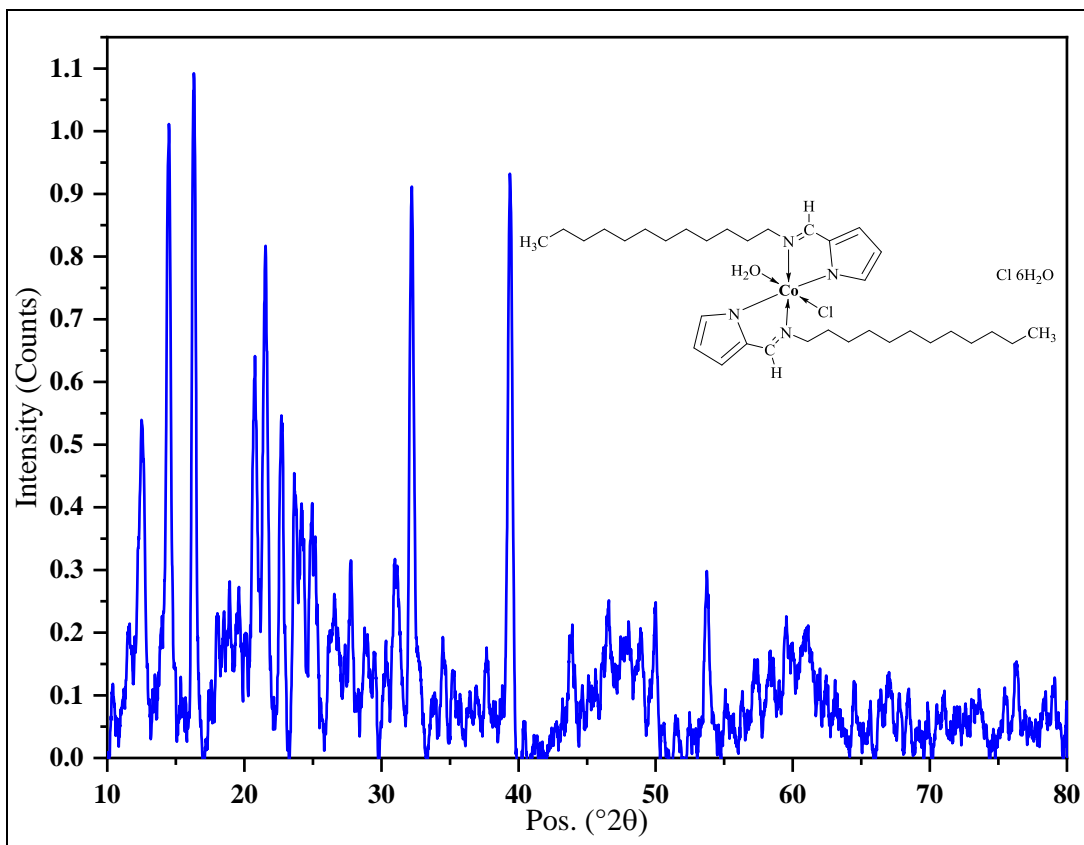
Figure 68: Diffractogram of Co-DDAP2C
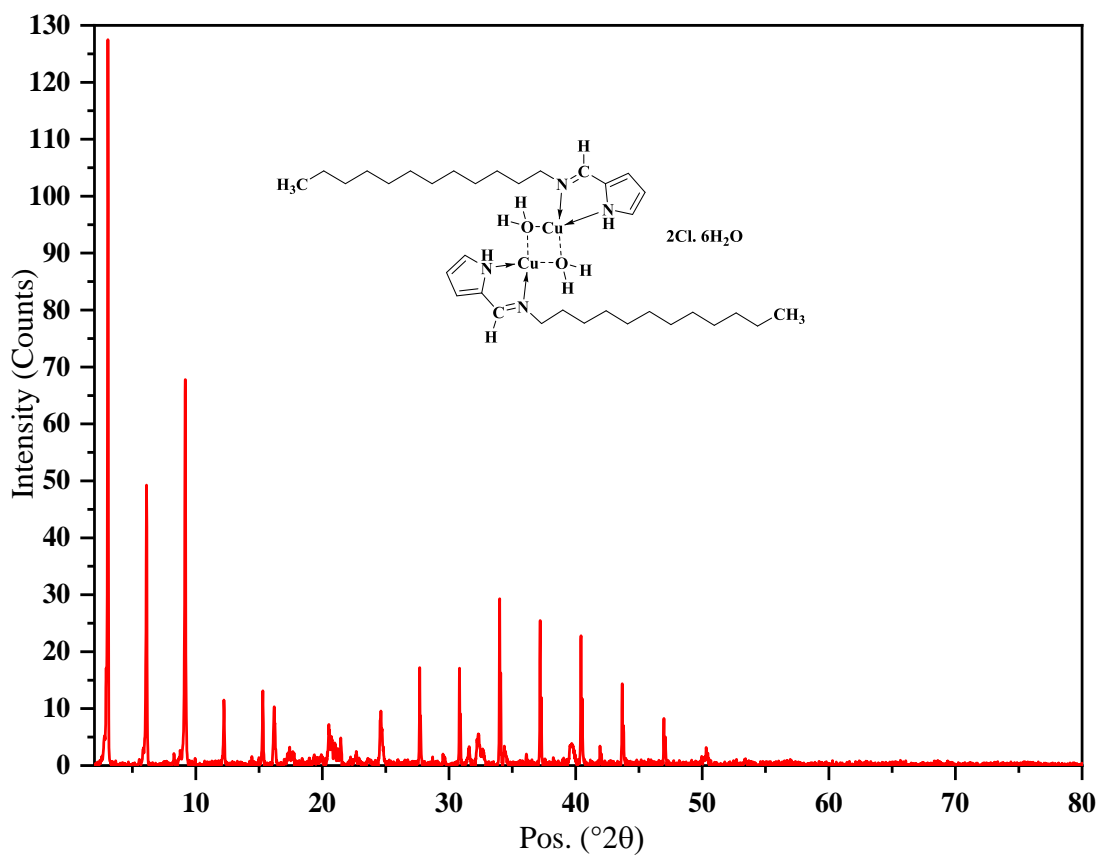
Figure 69: Diffractogram of Cu-DDAP2C

4.6.2 XRPD Study of Metal Complexes of DDAP3C

PXRD was used to estimate the crystal parameters because attempts at single-crystal development were unsuccessful, even though single-crystal X-ray crystallography (SC- XRD) is a highly reasonable method for analyzing complex structures. Figures 70, 71, and 72 exhibit the diffractogram for HL and its metal complexes. The HL diffractogram showed 13 reflection peaks between 0° and 27° in the 2θ range, with an intense peak at 10.75° and an associated d-spacing value of 0.072 Å. Similarly, the complexes **1** and **2** diffractograms also exhibited 13 and 25 reflection peaks, with the high intensity peaks at 23.54° (d = 0.157) and 11.21° (d = 0.075), respectively, throughout the whole X-ray scan range. Debye-Scherrer's equation was used to determine their average crystallite size (Devi *et al.*, 2018). The HL and complexes **1** and **2** had crystallite sizes that were, respectively, 119.88, 17.35, and 27.44 nm, indicating the nanocrystalline nature of the compounds (Al-Mohaimeed *et al.*, 2020). A reduction in crystallite size was seen, and the change in XRD patterns revealed coordination between the ligand and the metal for complex formation. The smaller crystallite size accounts for the superior antibacterial efficacy of metal complexes over the Schiff base (Palanimurugan *et al.*, 2019). The fraction of crystalline peaks across the XRD scan range is known as crystallinity. According to the calculations, these HL, complexes **1,** and **2** are 85.8, 28.7, and 58.2%, respectively. The crystallographic data and refinement parameters of HL and complexes are presented in Tables 23, 24, and 25. Microstrain (ε) is the fluctuation in the lattice parameters, and dislocation density (δ) is the number of dislocation lines in the crystal per unit area (nm^{-2}) that results in a crystallographic defect (Alshater *et al.*, 2021).

The diffractogram of complex **3** has exhibited 14 reflection peaks in the range of 2θ (0-47°), having an intense peak at 16.29°and a corresponding d-spacing of 5.44 Å. Its average crystallite size of 20.6 nm indicated that it was a nanocrystalline solid (Abouzayed *et al.*, 2020). The diffractogram for complex **4** recorded 8 reflection peaks in 2θ (0-40°) range, with a high intensity peak at 9.15° and the matching interplanar d-spacing of 9.65 Å. The value of average crystallite size 16.86 nm revealed its nanocrystalline nature (Palanimurugan & Kulandaisamy, 2018). The percentage of crystallinity across the XRD scan range for complexes **3** and **4** were 55 and 35.38%, respectively. Tables 26, 27, and 28 present the crystallographic

information and refinement parameters for complexes **3** and **4**. The difractogram images are exhibited in Figures 73 and 74, respectively.

Table 23: Crystallographic data of DDAP3C ligand

Position (2 θ)	FWHM	Crystallite size (nm)	Av. crystallite size (nm)	Crystallinity (%)	d- spacing	Dislocation density x 10^{-3}	Microstrain x 10^{-3}
5.3	0.0436	182.11	119.87	85.82	0.0356	0.0301	4.1132
5.59	0.045	176.59			0.0376	0.0320	4.0193
10.75	0.0754	105.78			0.0721	0.0893	3.4983
11.03	0.0464	171.97			0.0740	0.0338	2.0958
16.21	0.0622	129.01			0.1086	0.06	1.9052
16.37	0.0467	171.60			0.1096	0.0339	1.4186
19.64	0.1305	61.74			0.1314	0.2623	3.2908
20.25	0.255	31.64			0.1354	0.9985	6.2289
21.68	0.0608	132.90			0.1449	0.0566	1.3864
21.87	0.0606	133.32			0.1461	0.0562	1.3703
22.51	0.1453	55.71			0.1503	0.3221	3.1864
26.30	0.0777	104.99			0.1752	0.0907	1.4511
27.23	0.0809	100.97			0.1813	0.098	1.4581

Table 24: Crystallographic data of Complex **1**

Position (2 θ)	FWHM	Crystallite size (nm)	Av. crystallite size (nm)	Crystallinity (%)	d- spacing	Dislocation density x 10^{-3}	Microstrain x 10^{-3}
5.45	0.3773	21.07	17.346	28.715	0.0366	2.2514	34.5692
8.35	0.3528	22.57			0.056	1.9627	21.088
11.1	1.6276	4.9			0.0745	41.5834	73.0456
16.17	0.4984	16.09			0.1083	3.8581	15.3038
16.79	0.31	25.9			0.1124	1.4905	9.1646
18.36	1.6824	4.78			0.1229	43.7067	45.4168
20.27	0.283	28.51			0.1355	1.2301	6.9078
22.02	0.5812	13.92			0.1471	5.1581	13.035
23.54	0.3946	20.56			0.1571	2.3649	8.2623
24.41	3.3449	2.42			0.1628	169.3561	67.4578
27.14	0.3641	22.44			0.1807	1.985	6.5818
33.98	0.333	24.94			0.225	1.6072	4.7556
39.18	0.7254	11.62			0.2583	7.4007	8.8917

Table 25: Crystallographic data of Complex **2**

Position (2 θ)	FWHM	Crystallite size (nm)	Av. crystallite size (nm)	Crystallinity (%)	d-spacing	Dislocation density x 10^{-3}	Microstrain x 10^{-3}
3.11	0.1737	45.75	27.43	58.27	0.0209	0.4777	27.8729
8.82	0.2503	31.82			0.0592	0.9873	14.1553
9.49	0.4806	16.58			0.0637	3.6361	25.2672
11.20	0.3228	24.72			0.0752	1.6352	14.3537
12.46	1.0955	7.29			0.0835	18.7932	43.786
15.03	0.2192	36.55			0.1007	0.7485	7.2501
16.63	0.2944	27.26			0.1114	1.3453	8.7896
19.19	0.4623	17.42			0.1284	3.2931	11.9318
20.94	0.6194	13.04			0.14	5.8796	14.623
22.37	0.3004	26.95			0.1494	1.3765	6.63
22.58	2.0279	3.99			0.1508	62.662	44.31
24.62	0.3403	23.89			0.1642	1.7516	6.803
26.39	0.5157	15.82			0.1758	3.9941	9.5941
27.65	0.2831	28.89			0.184	1.1978	5.02
28.12	0.2645	30.96			0.1871	1.0432	4.607
30.36	0.2604	31.6			0.2017	1.0008	4.1868
31.01	0.2216	37.19			0.2059	0.7227	3.4848
32.78	0.2633	31.44			0.2174	1.0115	3.9059
33.45	0.2178	38.07			0.2217	0.6898	3.163
37.83	0.2417	34.73			0.2497	0.8289	3.0785
44.74	0.3594	23.89			0.2932	1.7508	3.8105
51.57	0.2212	39.86			0.335	0.629	1.9986
53.94	0.2872	31.027			0.3493	1.0387	2.4631
58.07	0.273	33.28			0.3739	0.9028	2.1457
60.92	0.2722	33.85			0.3904	0.8723	2.0195

Table 26: Crystallographic data of Complex **3**

Position 2 Theta	FWHM	Crystallite size (nm)	Average Crystallite size (nm)	d-spacing (Å)	dislocation density (δx 10^{-3} nm)	Microstrain x 10^{-3}	Crystallinity (%)
8.63	0.4973	16.0199	20.697	10.2322	3.8965	28.742	55
9.85	0.2056	38.7827		8.9706	0.6648	10.408	
12.15	0.3099	25.7765		7.275	1.5050	12.7	
16.28	0.4472	17.9454		5.4377	3.1052	13.635	
19.02	0.3931	20.4873		4.6617	2.3824	10.2394	
20.33	0.2255	35.7788		4.3644	0.7811	5.4892	
22.17	0.3080	26.2769		4.0055	1.4482	6.8596	
23.31	1.1646	6.9652		3.8114	20.612	24.624	
27.36	0.6243	13.096		3.2566	5.8306	11.19	
32.76	0.2593	31.926		2.7313	0.981	3.849	
33.62	1.9995	4.1503		2.6634	58.054	28.87	
37.47	0.3549	23.633		2.3977	1.7903	4.565	
40.16	0.7116	11.885		2.2432	7.0787	8.493	
47.04	0.5086	17.035		1.9301	3.4458	5.098	

Table 27: Crystallographic data of Complex **4**

Position 2 Theta	FWHM	Crystallite size (nm)	Average Crystallite size (nm)	d-spacing (Å)	dislocation density (δx 10^{-3} nm^{-2})	Microstrain x 10^{-3}	Crystallinity (%)
6.08	0.2666	29.832	16.864	14.5201	1.1236	21.902	35.38
9.15	0.2896	27.516		9.6543	1.3206	15.788	
12.23	0.3050	26.191		7.2292	1.4577	12.420	
14.38	0.3678	21.767		6.1514	2.1105	12.716	
20.44	0.6396	12.619		4.3411	6.2794	15.480	
24.09	2.3921	3.3958		3.6898	86.718	48.896	
32.12	1.6440	5.0283		2.7843	39.550	24.918	
39.87	0.9866	8.5647		2.2589	13.632	11.868	

Table 28: Crystal parameters of DDAP3C and complexes

Compounds	No. of crystalline peaks	Av. crystallite size (nm)	Crystallinity (%)	Dislocation density x 10^{-3} range	Microstrain x 10^{-3} range
HL (DDAP3C)	13	119.87	85.82	0.03-0.99	1.37-6.22
Complex **1**	13	17.35	28.71	1.23-169.35	4.75-73.04
Complex **2**	25	27.43	58.27	0.47-62.66	1.99-44.31
Complex **3**	14	20.69	55.00	0.66-58.05	3.85-28.88
Complex **4**	08	16.86	35.38	1.12-86.72	11.87-48.89
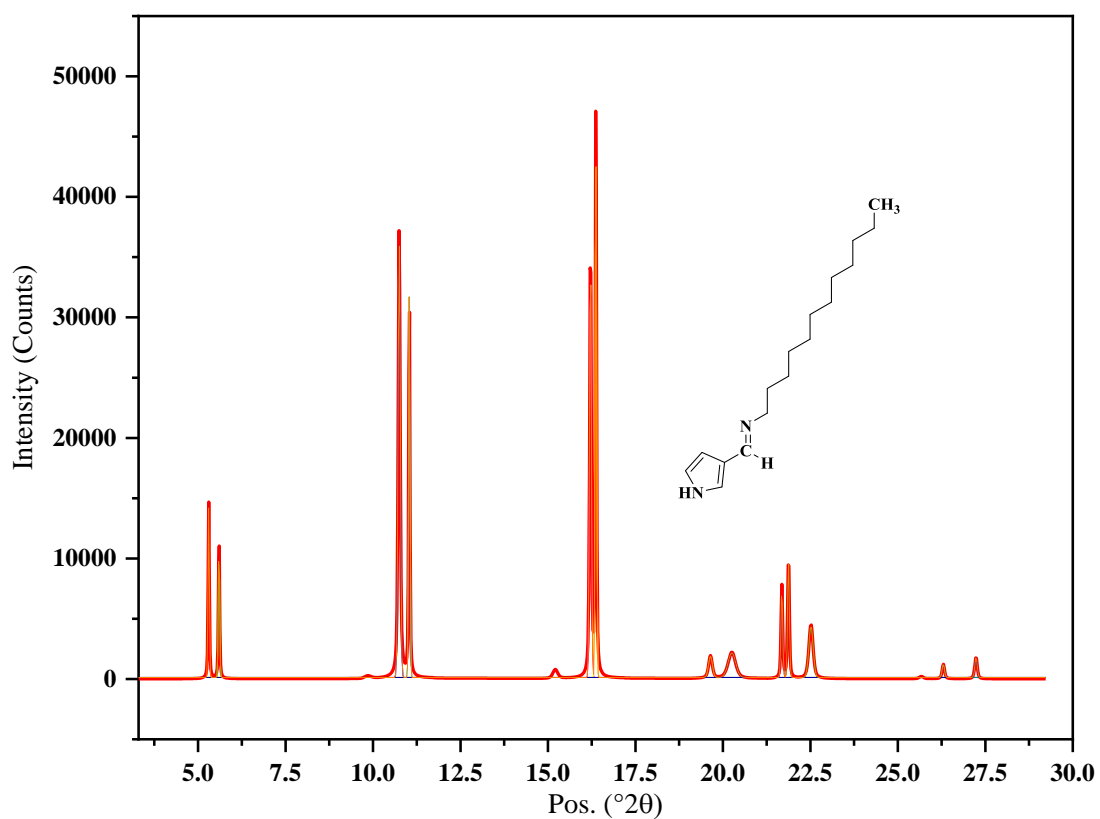
Figure 70: Diffractogram of DDAP3C ligand
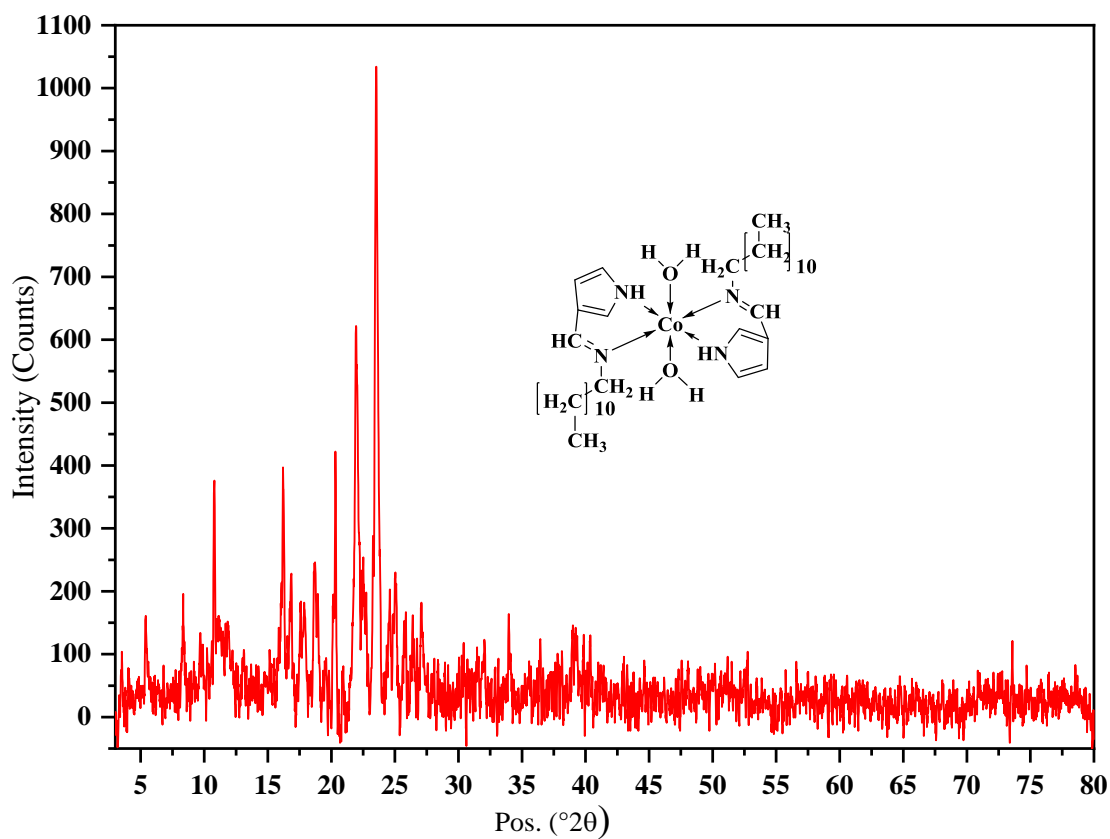
Figure 71: Diffractogram of Co-DDAP3C
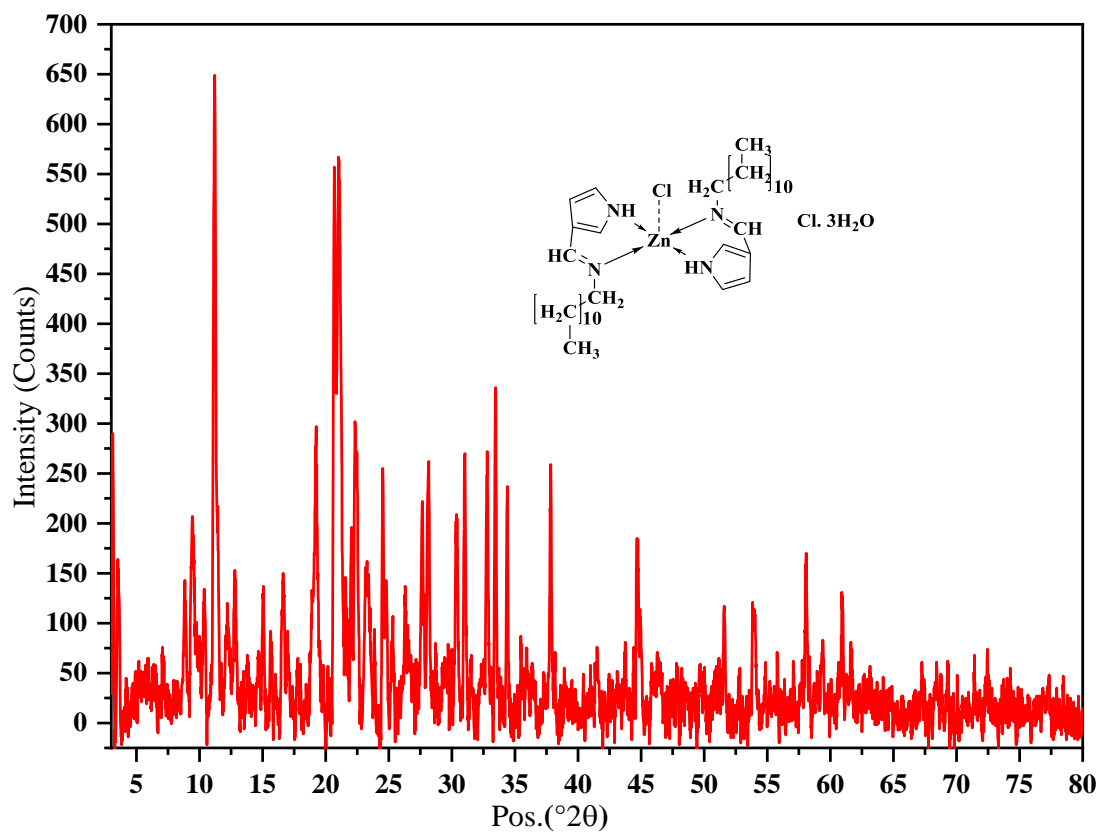
Figure 72: Diffractogram of Zn-DDAP3C

120
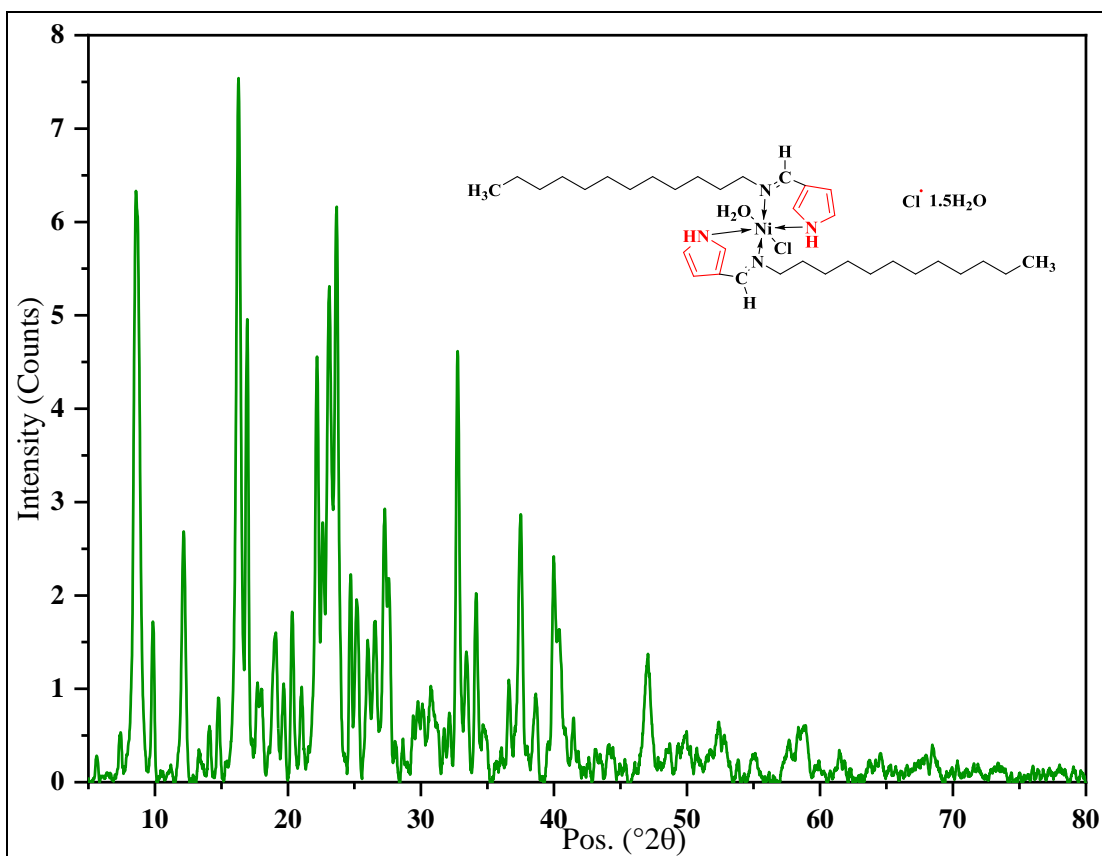
Figure73: Diffractogram of Ni-DDAP3C
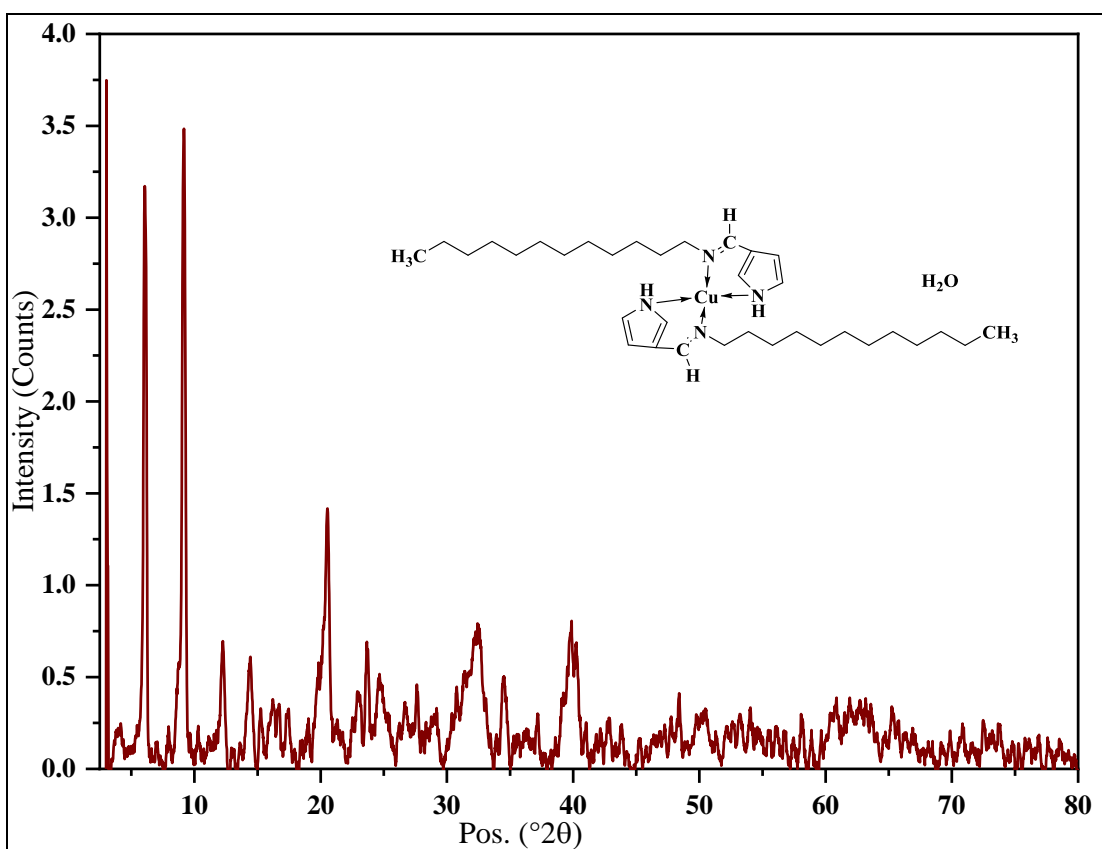
Figure 74: Diffractogram of Cu-DDAP3C

121

4.7   Scanning Electron Microscopy (SEM) and Energy Dispersive X-ray (EDX) Analysis

4.7.1   SEM and EDX Analysis of DDAP2C and Metal Complexes

Scanning electron microscopy (SEM) analysis was used to investigate how the surface topology of the metal complexes is significantly altered by the coordination of the ligand with the metal, and the SEM micrographs of DDAP2C and its complexes are displayed in Figure 75. The SEM micrograph of the DDAP2C revealed a broken ice-like structure connected to the heterogeneous matrix. Ni-DDAP2C showed a rock-like structure with a small, non-uniform matrix dispersed throughout it. The SEM micrograph of Zn-DDAP2C resembled that of broken glass, over which the uneven distribution of the matrix was seen (Alharbi *et al.*, 2021; Tadavi *et al.*, 2018).

The SEM micrograph of Co-DDAP2C appeared to have a massive block of rock smashed across its body (Ramesh *et al.*, 2019). Similarly, the SEM micrograph of the Cu-DDAP2C complex shows an uneven surface with hollow regions packed with the gravels (Kheirkhahi *et al.*, 2021).

The elemental composition of metal complexes was ascertained using the energy-dispersive X-ray diffraction analysis (EDX) method. The molecules of Ni-DDAP2C, Zn-DDAP2C, Co-DDAP2C, and Cu-DDAP2C, which are made up of vital elements including C, O, and Cl, as well as metal components, were detected in their EDX profile, which supports their predicted chemical structures. The EDX micrographs displayed various elements at different positions (Majumdar *et al.*, 2020). The complexes were further analyzed with the SEM-EDX technique, where brighter portions of the SEM micrograph of the complexes revealed the presence of Ni, Zn, Co, and Cu ions as the metal (Shah *et al.*, 2020). The EDX images of Ni-DDAP2C, Zn-DDAP2C, Co-DDAP2C, and Cu-DDAP2C are shown in Figures 76-79, and the elemental composition data are presented in Table 29.
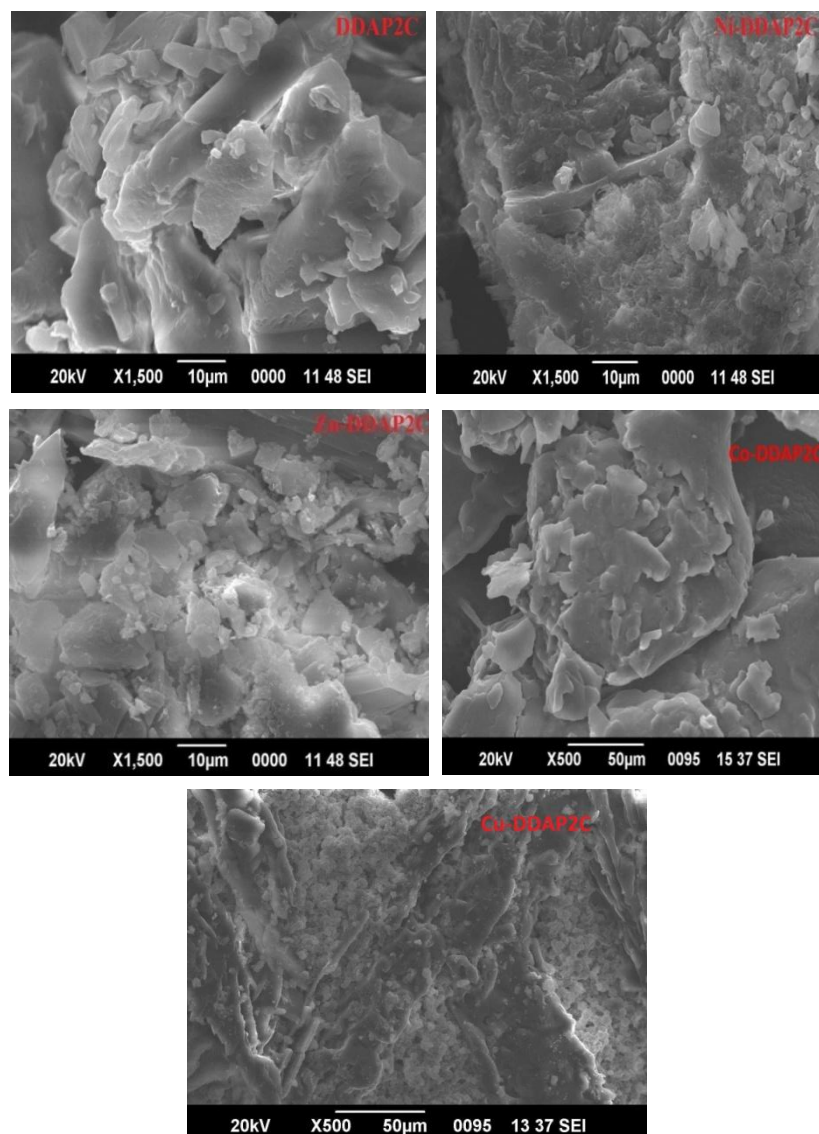
Figure 75: SEM micrograph of (a) DDAP2C, (b) Ni-DDAP2C, (c) Zn-DDAP2C, (d) Co-DDAP2C, (e) Cu-DDAP2C

Table 29: Elemental composition data of metal complexes of DDAP2C ligand from EDX analysis

Element	Ni-DDAP2C		Zn-DDAP2C		Co-DDAP2C		Cu-DDAP2C	
	Weight (%)	Atomic (%)	Weight (%)	Atomic (%)	Weight (%)	Atomic (%)	Weight (%)	Atomic (%)
C	76.11	87.59	68.39	86.8	42	55.77	42	62.2
O	8.03	6.93	3.96	3.77	34.51	34.4	20.07	22.31
Cl	11.26	4.39	15.14	6.51	19.36	8.71	21.97	11.02
Ni	4.6	1.08	-	-	-	-	-	-
Zn	-	-	12.51	2.92	-	-	-	-
Co	-	-	-	-	4.13	1.12	-	-
Cu	-	-	-	-	-	-	15.96	4.47
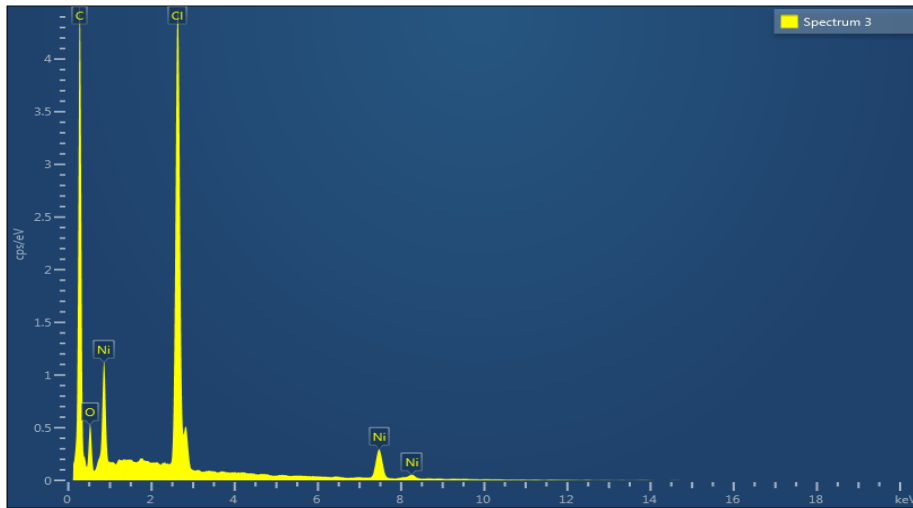
Figure 76: EDX micrograph of Ni-DDAP2C
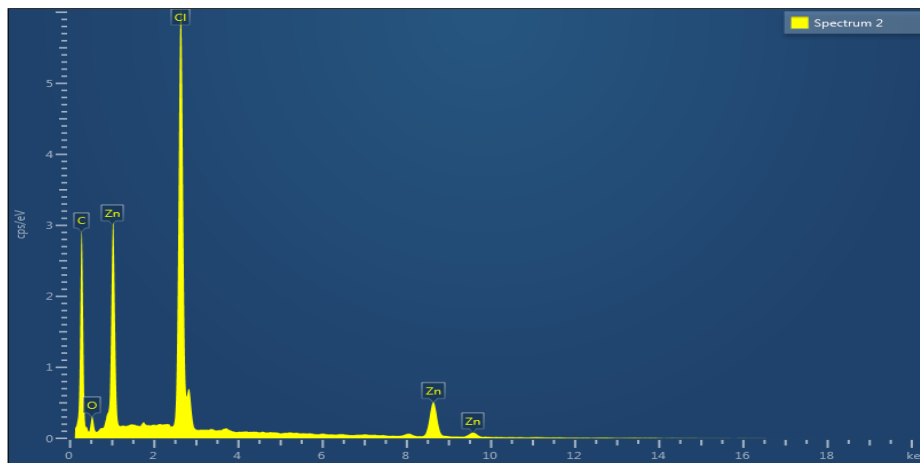
Figure 77: EDX micrograph of Zn-DDAP2C
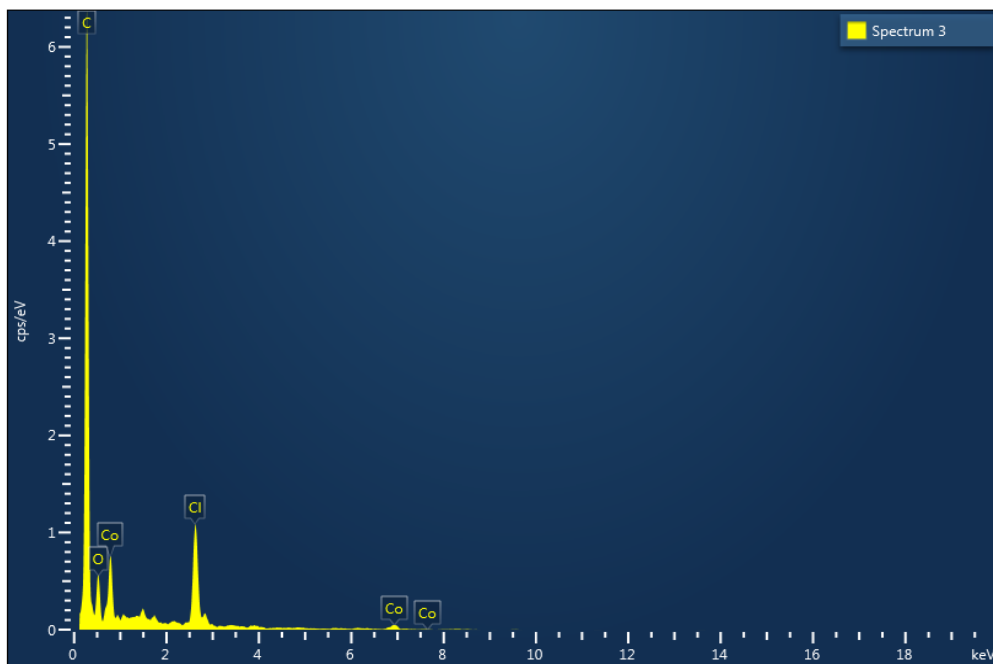
Figure 78: EDX micrograph of Co-DDAP2C

124
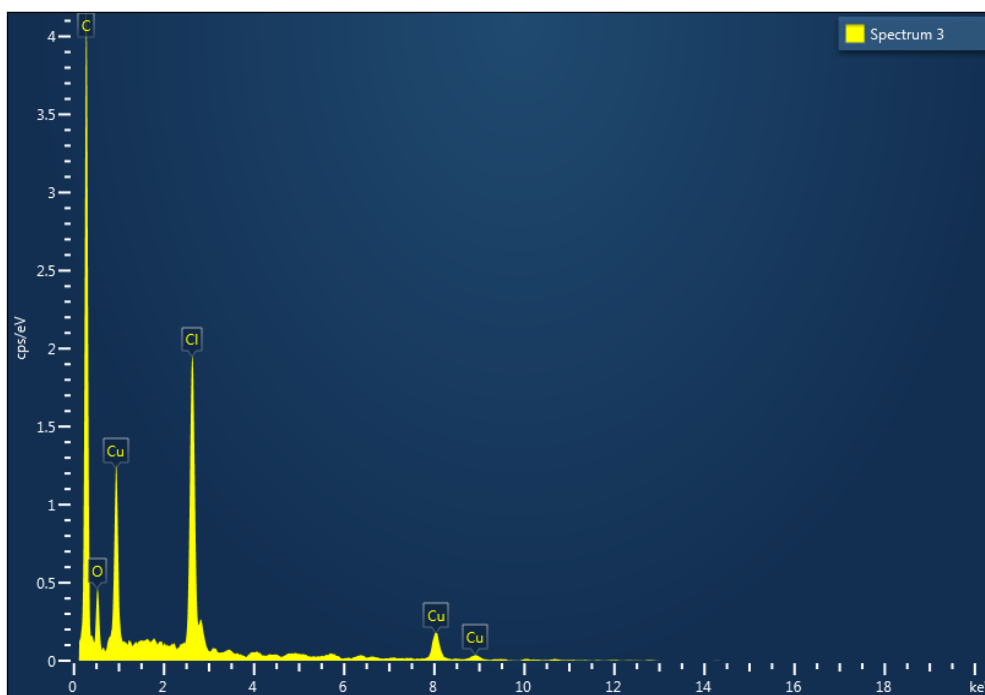
Figure 79: EDX micrograph of Cu-DDAP2C

4.7.2   SEM and EDX Analysis of DDAP3C and Metal Complexes

The SEM micrographs depict the surface morphology of the samples as examined using scanning electron microscopy (SEM), and the micrographs are depicted in Fig. 80. The micrograph of the HL ligand displayed a fragmented rock-like structure associated with an uneven distribution of rod-shaped particles. The surface of complex **1** was seen as unevenly distributed morphological mass, while the entire surface of complex **2** displayed irregularly dispersed ballast (C. Justin Dhanaraj & Jebapriya, 2020; Nagaveni *et al.*, 2018).

The SEM micrograph of complex **3** appeared to have a broken rock-like structure over which a needle-like matrix is distributed unevenly. A rough surface of irregularly shattered layers has appeared in the SEM micrograph of complex **4** (Fathima *et al.*, 2019; Kumar & Nath, 2019).

Applying electron diffraction X-ray (EDX) analysis, the elemental compositions of the produced compounds were identified. The results are shown in Table 30. The EDX investigation identified various non-metal atoms and the corresponding metals, including N, O, and Cl (Alothman *et al.*, 2019). The EDX micrographs of the

prepared complexes are illustrated in Figs 81, 82, 83, and 84. The elemental data reflect the purity of the complexes.

Table 30: Elemental composition data of metal complexes of DDAP3C ligand from EDX analysis

Element	Complex **1**		Complex **2**		Complex **3**		Complex **4**	
	Weight (%)	Atomic (%)	Weight (%)	Atomic (%)	Weight (%)	Atomic (%)	Weight (%)	Atomic (%)
C	79.54	91.42	57.18	81	62.43	83.1	53.58	76.78
O	3.02	2.61	3.09	3.29	5.24	5.24	9.5	10.22
Cl	12.17	4.74	19.07	9.15	16.01	7.22	14.01	6.8
Co	5.27	1.23	-	-	-	-	-	-
Zn	-	-	18.19	4.74	-	-	-	-
Ni	-	-	-	-	16.32	4.44	-	-
Cu	-	-	-	-	-	-	22.92	6.21
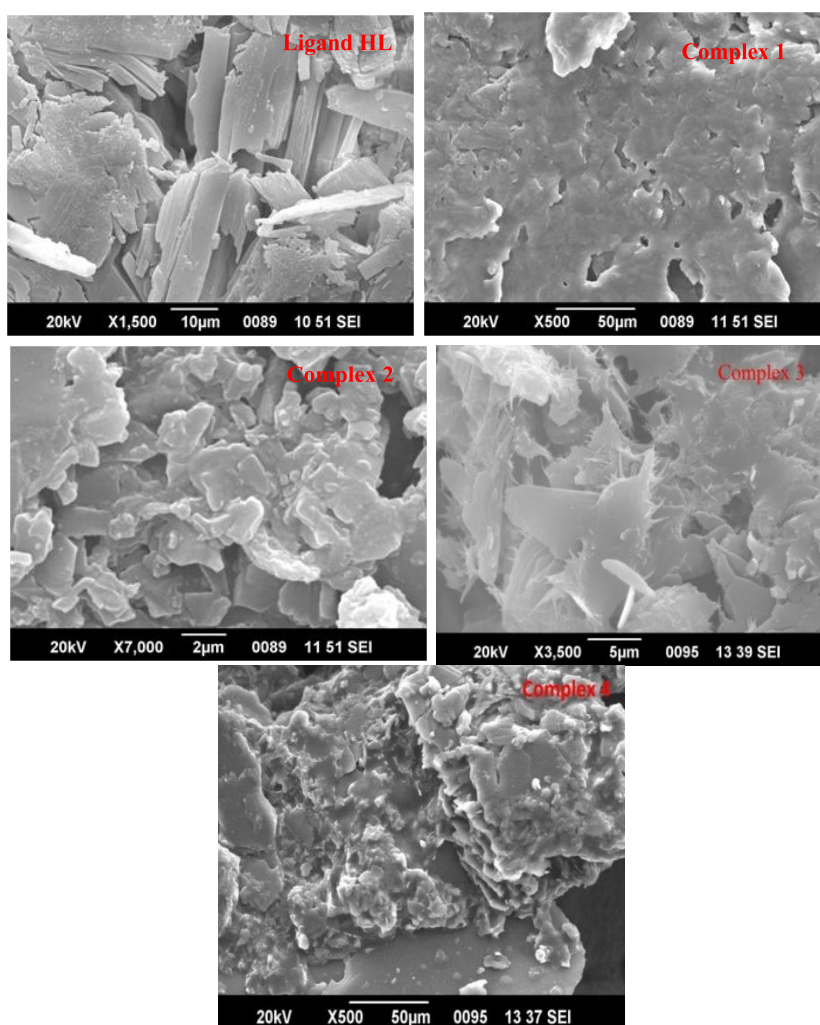
Figure 80: SEM micrograph of (a) DDAP3C, (b) Co-DDAP3C, (c) Zn-DDAP3C, (d) Ni-DDAP3C, (e) Cu-DDAP3C
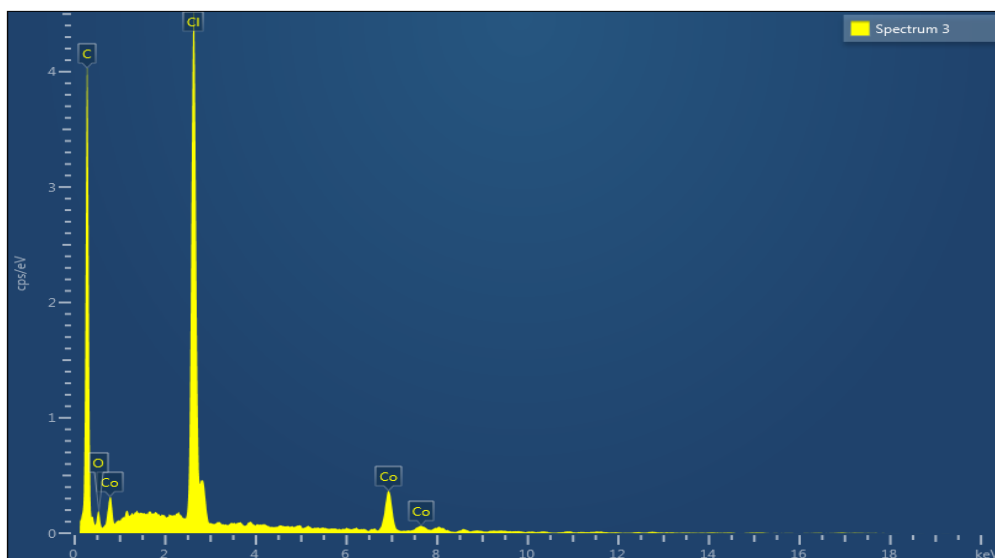
Figure 81: EDX micrograph of Co-DDAP3C
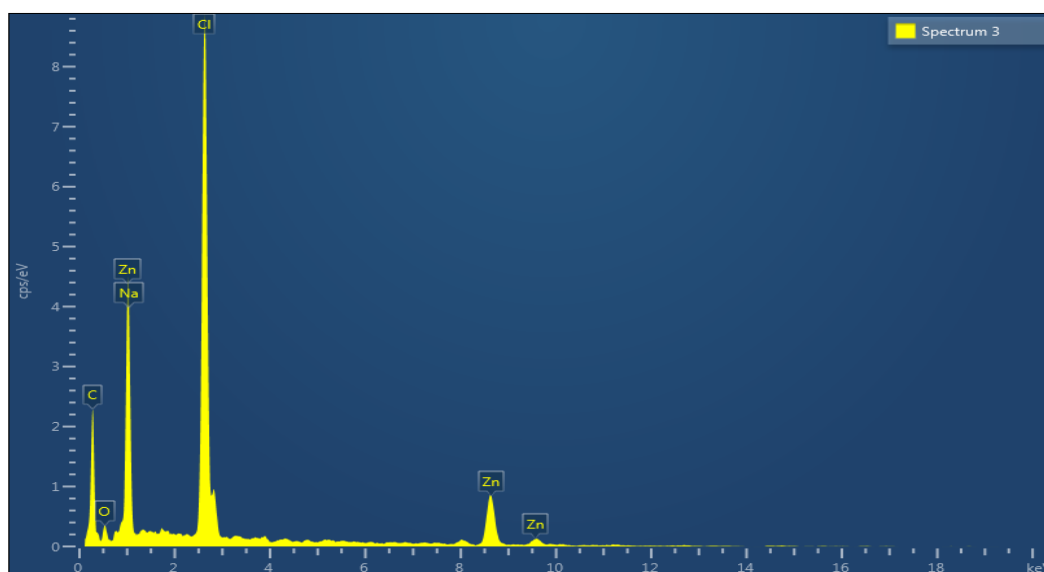
Figure 82: EDX micrograph of Zn-DDAP3C
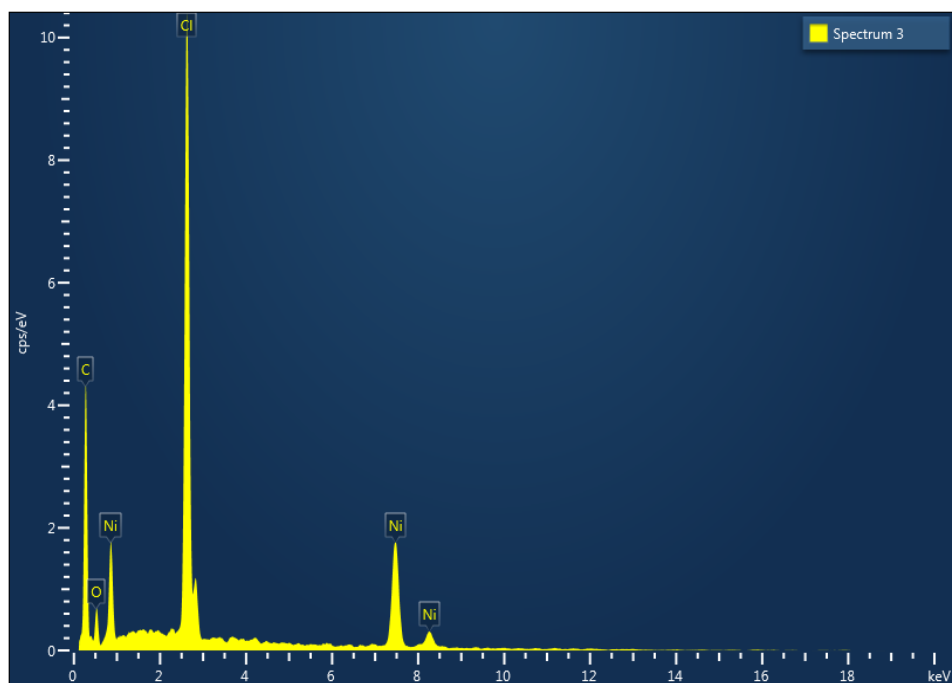
Figure 83: EDX micrograph of Ni-DDAP3C
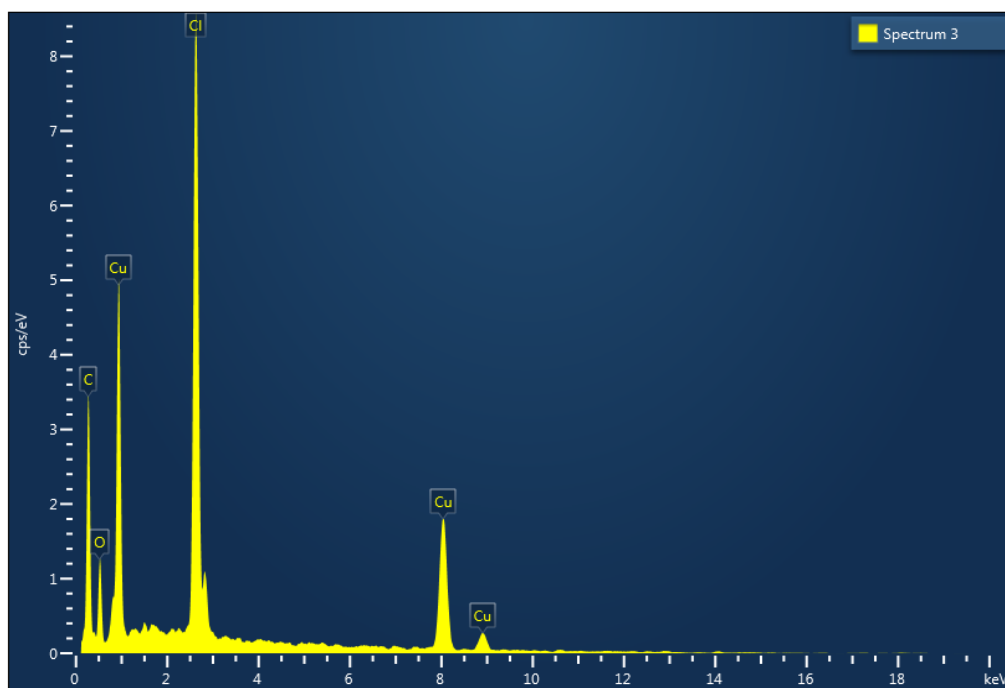
Figure 84: EDX micrograph of Cu-DDAP3C

4.8   Proposed Molecular Structures and Geometry

The molecular geometry of the complexes is suggested after a detailed study of the analytical, magnetic, and spectroscopic results, along with the use of computational software. The computer software incorporates a database and a set of principles to

create the structure of the complexes. The investigation of suggested molecular structures can exercise various bonding properties such as bond lengths, bond energies, and bond angles around the metal core. ChemDraw and the ArgusLab computer package are the computational tools used in the current work to design the molecular structure of the ligand and complexes. Based on experimental data, the potential structures of the complexes under study are displayed in Figures 86 – 93.
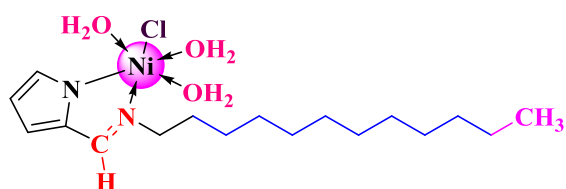
Figure 85: Proposed structure of Ni-DDAP2C complex
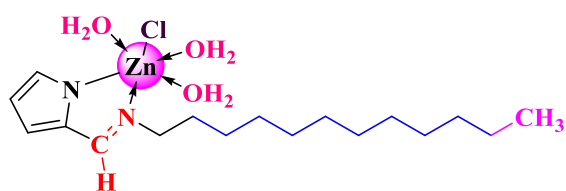
Figure 86: Proposed structure of Zn-DDAP2C complex
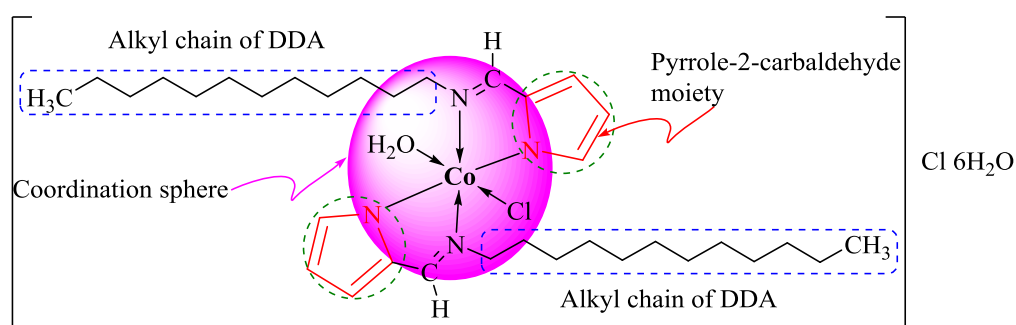
Figure 87: Proposed structure of Co-DDAP2C complex
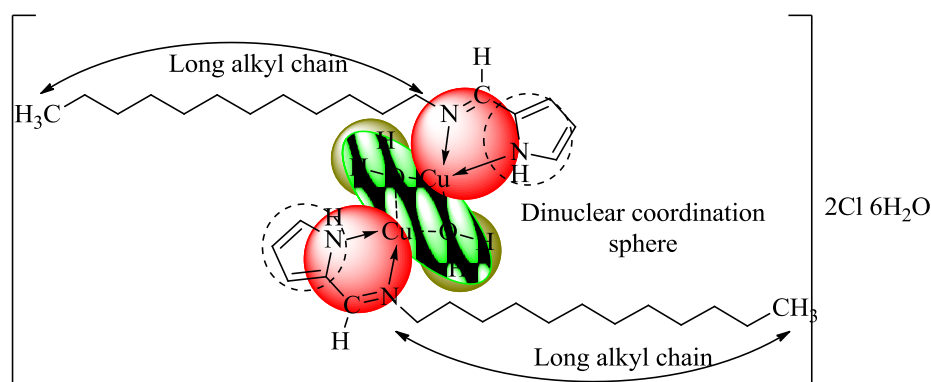
Figure 88: Proposed structure of Cu-DDAP2C complex
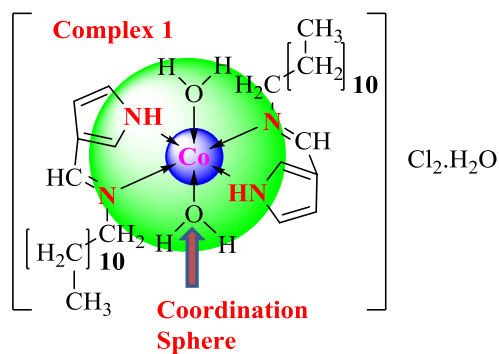
Figure 89: Proposed structure of Co-DDAP3C complex
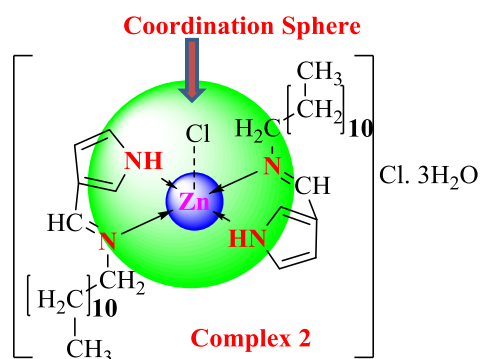
Figure 90: Proposed structure of Zn-DDAP3C complex
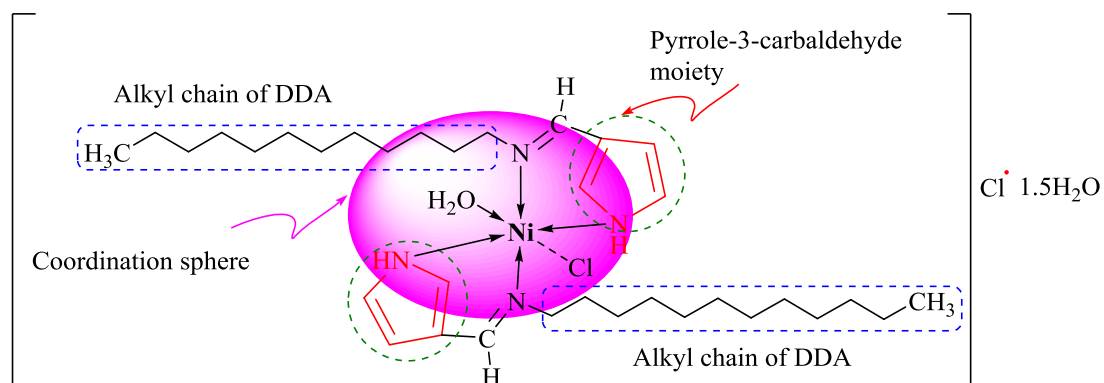
Figure 91: Proposed structure of Ni-DDAP3C complex
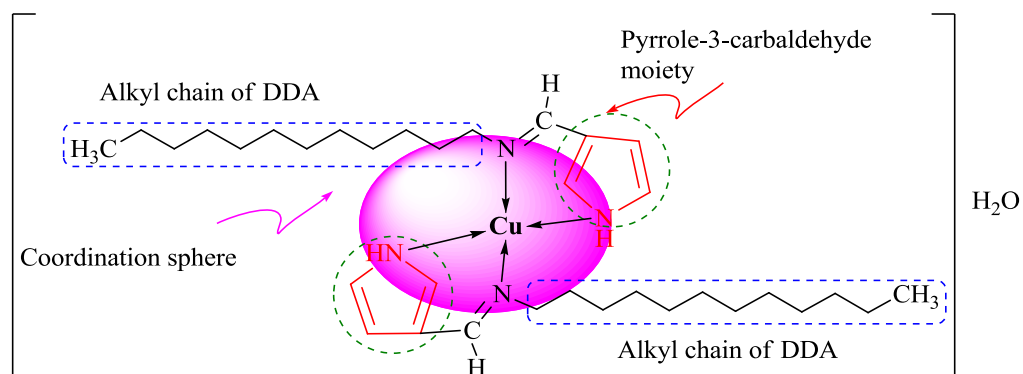
Figure 92: Proposed structure of Cu-DDAP3C complex

130

4.9   Molecular Modeling Study

Molecular modeling is a computational approach that provides a much more precise evaluation of theoretical predictions about the structure of the molecules. The best way to gain information about molecules' chemical and physical properties is to use a molecular modeling software package (Fetoh *et al.*, 2018). An understanding of the behavior of molecules can be obtained through theoretical predictions such as electron density and electrostatic potential maps. In our study, we achieved reasonable and low-energy molecular geometry by manipulating and modifying the molecular coordinates to ensure the correct stereochemistry of the complexes. Minimum energy has been found by repeating the energy minimization process several times (Bargujar *et al.*, 2017). Additional evidence for their coordination comes from the variation in metal-nitrogen bond length in the complexes compared to the ligand. The ArgusLab molecular modeling program extensively optimized the most stable conformer using molecular orbital functions PM3 (Gaber *et al.*, 2018). In CsChemOffice 3D Ultra software, MM2 calculations optimized the minimum geometrical energy of complexes, similar to those calculated in ArgusLab software.

4.9.1   Molecular Modeling Study of Metal Complexes of DDAP2C

According to the 3D structures of the metal complexes optimized by MM2 calculations, the details of the bond angles and bond lengths are provided in Table 31. The optimized structures of the metal complexes are displayed in Figures 93 to 97. The CsChem 3D Ultra software program was used to study 3D molecular modeling of the probable metal complexes, and optimized structures indicated that the Ni-DDAP2C, Co-DDAP2C, and Zn-DDAP2C complexes have octahedral geometry whereas Cu-DDAP2C has dinuclear tetrahedral structure. Several spectral techniques also support this investigation of the complex geometry. According to the energy minimization values for the metal complexes, their stability is maximum. The fact that the values of the metal-nitrogen and metal-oxygen bonds have changed in the complexes compared to the ligand further supports their coordination.
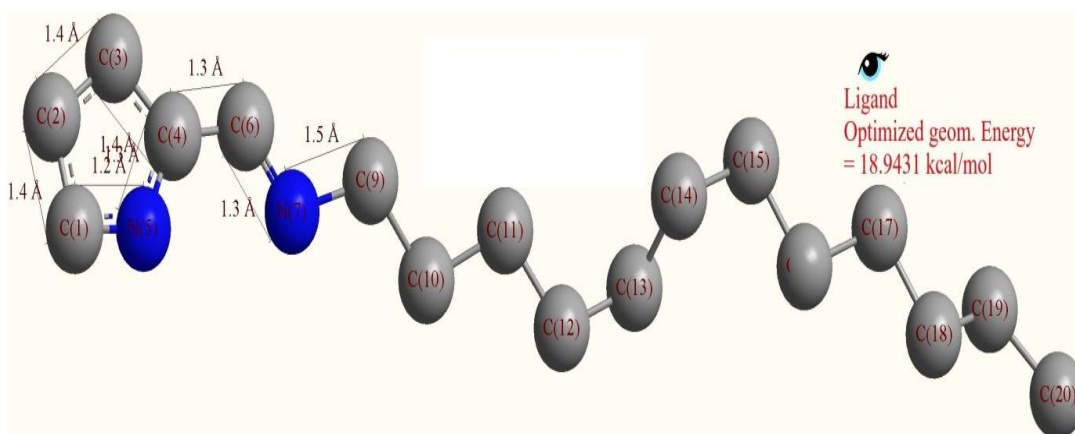
Figure 93: 3D-optimized geometrical structure of DDAP2C
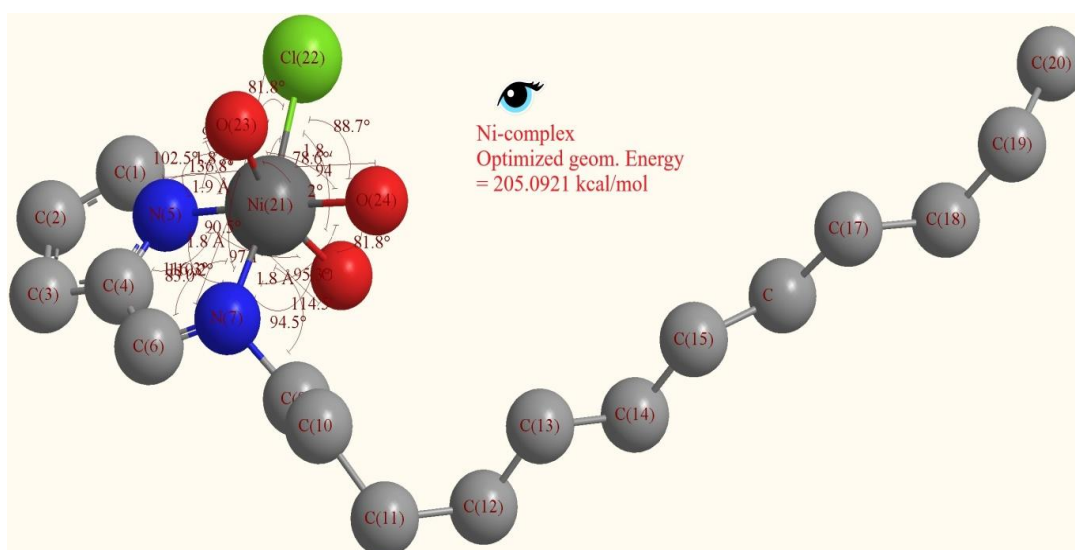
Figure 94: 3D-optimized geometrical structure of Ni-DDAP2C
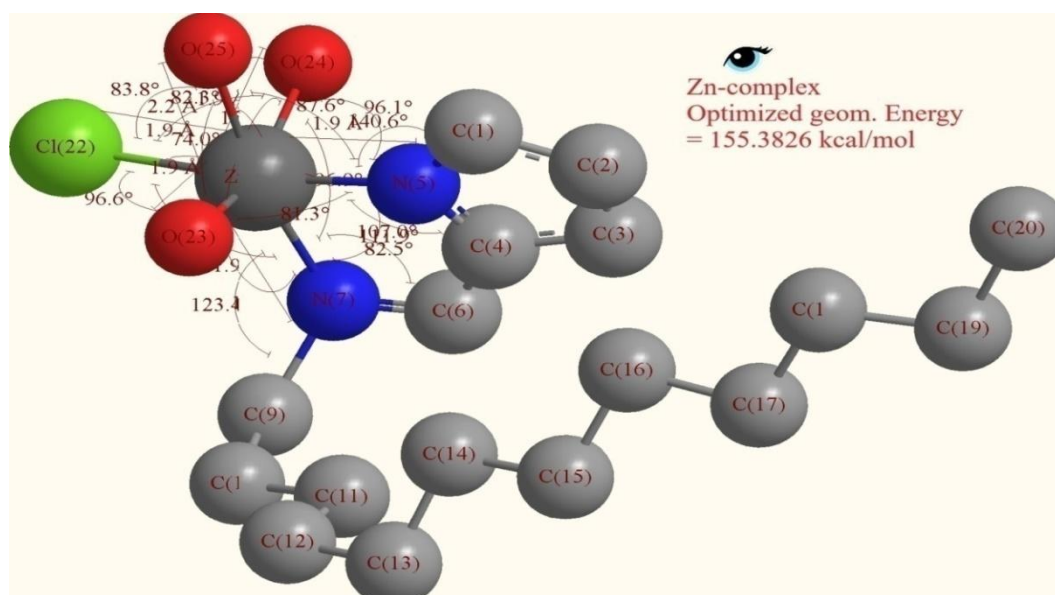
Figure 95: 3D-optimized geometrical structure of Zn-DDAP2C
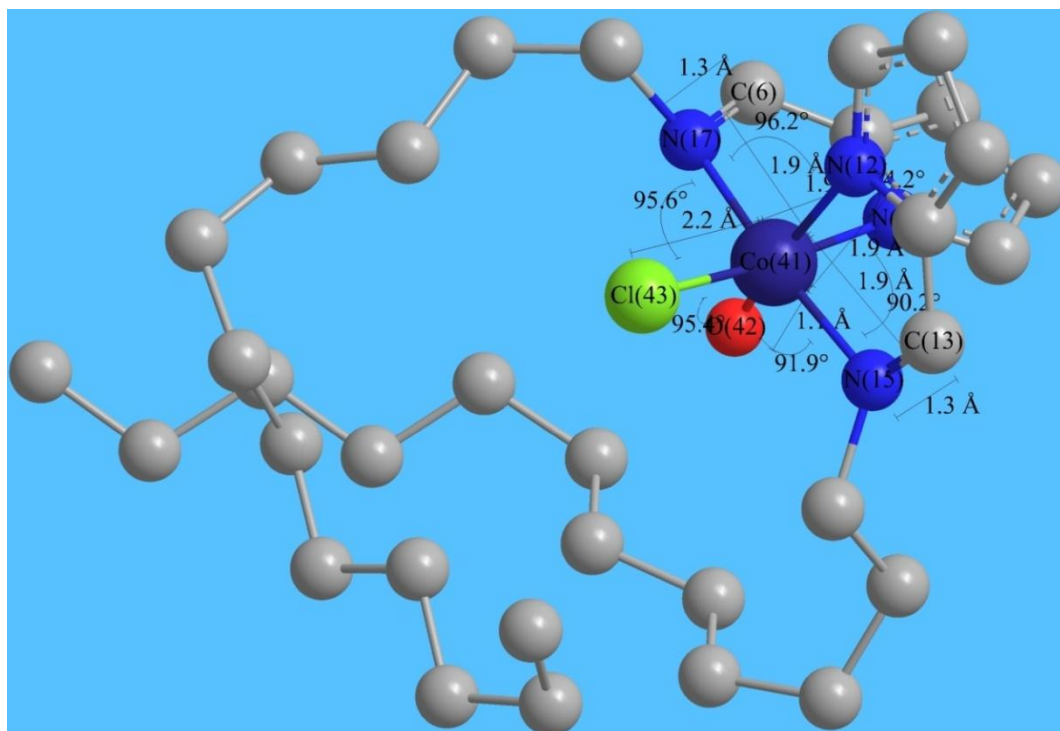
Figure 96: 3D-optimized geometrical structure of Co-DDAP2C
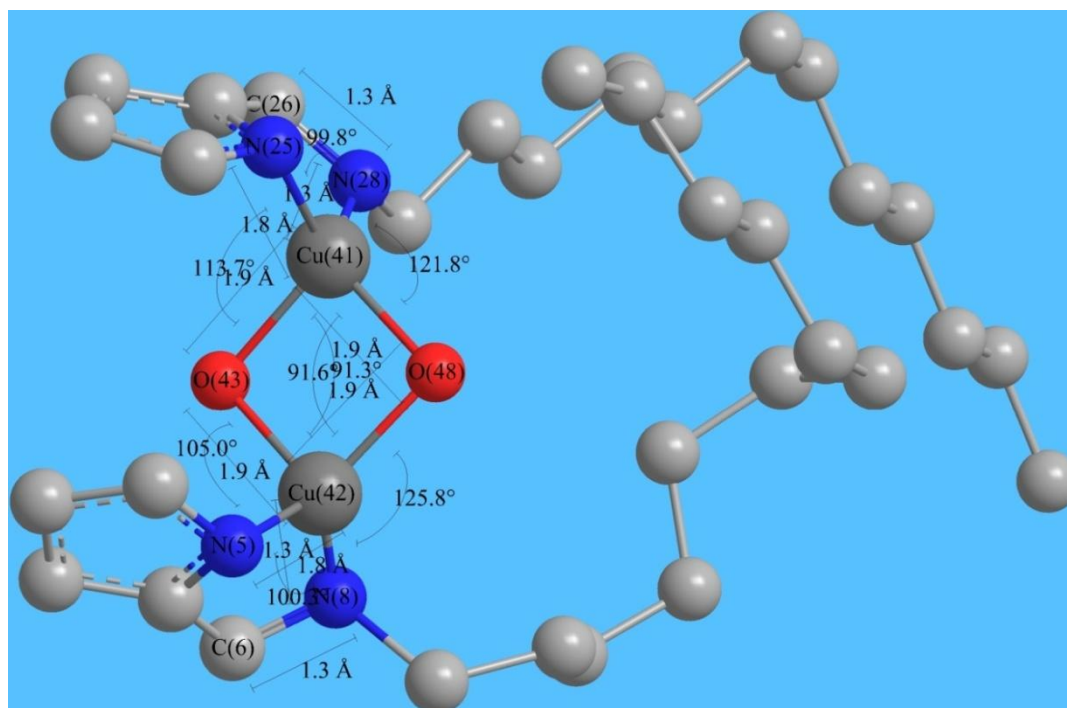
Figure 97: 3D-optimized geometrical structure of Cu-DDAP2C

Table 31: Selected bond lengths and bond angles of metal complexes of DDAP2C ligand

Complex	Bonded Atoms	Bond length (Å)	Bonded Atoms	Bond angle (°)	Final geom. energy
DDAP2C	C(1)-N(5)	1.241			18.9431
	C(4)-N(5)	1.251			kcal/mol
	C(3)-C(4)	1.376			
	C(2)-C(3)	1.366			
	C(1)-C(2)	1.372			
	N(7)-C(9)	1.471			
	C(6)-N(7)	1.278			
	C(4)-C(6)	1.344			
Ni-	O(23)-Ni(21)	1.890	O(23)-Ni(21)-O(25)	160.200	205.0921
DDAP2C	O(25)-Ni(21)	1.840	O(23)-Ni(21)-O(24)	78.639	kcal/mol
	O(24)-Ni(21)	1.826	O(23)-Ni(21)-N(5)	102.474	
	N(5)-Ni(21)	1.804	O(23)-Ni(21)-Cl(22)	81.841	
	Ni(21)-Cl(22)	2.180	O(23)-Ni(21)-N(7)	90.544	
	N(7)-Ni(21)	1.827	O(25)-Ni(21)-O(24)	81.824	
	N(7)-C(9)	1.494	O(25)-Ni(21)-N(5)	97.149	
	C(6)-N(7)	1.257	O(25)-Ni(21)-Cl(22)	94.589	
	C(4)-C(6)	1.346	O(25)-Ni(21)-N(7)	94.451	
			O(24)-Ni(21)-Cl(22)	88.693	
			O(24)-Ni(21)-N(7)	95.316	
			N(5)-Ni(21)-Cl(22)	93.103	
			N(5)-Ni(21)-N(7)	83.040	
			Cl(22)-Ni(21)-N(7)	170.549	
			Ni(21)-N(7)-C(9)	114.497	
			Ni(21)-N(7)-C(6)	116.263	
			Ni(21)-N(5)-C(1)	136.846	
			Ni(21)-N(5)-C(4)	110.205	
Zn-	O(25)-Zn(21)	1.929	O(25)-Zn(21)-O(24)	81.471	155.3826
DDAP2C	O(24)-Zn(21)	1.892	O(25)-Zn(21)-O(23)	73.981	kcal/mol
	O(23)-Zn(21)	1.918	O(25)-Zn(21)-Cl(22)	83.807	
	Zn(21)-Cl(22	2.237	O(25)-Zn(21)-N(5)	87.600	
	N(5)-Zn(21)	1.921	O(25)-Zn(21)-N(7)	169.725	
	N(7)-Zn(21)	1.934	O(24)-Zn(21)-O(23)	155.388	
	N(7)-C(9)	1.567	O(24)-Zn(21)-Cl(22)	82.273	
	C(6)-N(7)	1.285	O(24)-Zn(21)-N(5)	96.101	
	C(4)-C(6)	1.330	O(24)-Zn(21)-N(7)	96.896	
			O(23)-Zn(21)-Cl(22)	96.600	
			O(23)-Zn(21)-N(5)	81.336	

			O(23)-Zn(21)-N(7)	106.939	
			Cl(22)-Zn(21)-N(5)	171.398	
			Cl(22)-Zn(21)-N(7)	106.090	
			N(5)-Zn(21)-N(7)	82.475	
			Zn(21)-N(7)-C(9)	123.434	
			Zn(21)-N(7)-C(6)	111.925	
			C(1)-N(5)-Zn(21)	140.573	
			Zn(21)-N(5)-C(4)	106.980	
Co-DDAP2C	N(17)-C(6)	1.27, 1.260	Cl(43)-Co(41)-N(17)	95.61	345.62
	N(15)-C(13)	1.270, 1.260	O(42)-Co(41)-Cl(43)	95.36	kcal/mol
	Cl(43)-Co(41)	2.17	N(15)-Co(41)-O(42)	91.94	
	O(42)-Co(41)	1.14, 0.600	N(17)-Co(41)-N(12)	96.17	
	Co(41)-N(15)	1.87	N(5)-Co(41)-N(12)	84.17	
	Co(41)-N(5)	1.85	N(15)-Co(41)-N(5)	90.16	
	Co(41)-N(12)	1.85	-	-	
	Co(41)-N(17)	1.87	-	-	
Cu-DDAP2C	C(6)-N(8)	1.28, 1.260	N(8)-Cu(42)-N(5)	100.28	426.43
					kcal/mol
	N(5)-Cu(42)	1.85	Cu(41)-O(43)-Cu(42)	91.31	
	N(8)-Cu(42)	1.32, 1.30	Cu(41)-O(48)-Cu(42)	91.56	
	Cu(41)-N(15)	1.36, 1.30	N(28)-Cu(41)-N(25)	99.78	
	Cu(42)-O(48)	1.86	O(43)-Cu(42)-N(5)	104.96	
	Cu(42)-O(43)	1.87	O(48)-Cu(42)-N(8)	125.84	
	O(43)-Cu(41)	1.86	O(43)-Cu(41)-N(25)	113.72	
	Cu(41)-N(25)	1.85	O(48)-Cu(41)-N(28)	121.83	
	Cu(41)-N(28)	1.32, 1.30	-	-	
	C(26)-N(28)	1.28, 1.26	-	-	
	Cu(41)-O(48)	1.87	-	-	

4.9.2   Molecular Modeling Study of Metal Complexes of DDAP3C

The three-dimensional setting of the various atoms in the molecules is clearly understood by computational investigation of the compounds. When ligands formed complexes, the geometry optimization indicated structural changes. The lowest optimized energies of complexes 1, complex 2, and HL were found to be 815.28, 312.85, and 19.34 kcal/mole, respectively, after many energy optimization cycles. The details of the energy and bonding parameters determined by molecular modeling for the ligand and complexes are shown in Table 32. The azomethine bond (-HC=N)

(1.26) of the ligand HL was extended to 1.29 and 1.27 in complexes **1** and **2**, respectively. Complex **2** may be more stable than complex **1** because of its low energy (El-Boraey & El-Salamony, 2018). The bond angle and bond length are also in agreement with the distorted trigonal bipyramidal geometry of complex **2** and the octahedral geometry of complex **1**, respectively. Similarly, complex **3** revealed an octahedral geometry, and complex **4** agreed with the tetrahedral geometry after geometry optimization of the respective complexes. The table shows that complexation causes the coordinated atoms of the ligand (HL) to have less electron density and increase bond lengths (Siddappa *et al.*, 2014).

Furthermore, it was determined that the structural parameter (geometry index, τ5) of complex 2 was 1.1, rather than the ideal value of 1 for precisely trigonal-bipyramidal geometry (Addison & Rao, 1984; Hoskins & Whillans, 1973). This distortion supports pentacoordination with distorted trigonal bipyramidal geometry around the zinc atom. The optimized three-dimensional structures of HL and complexes are illustrated in Figs 98-102.
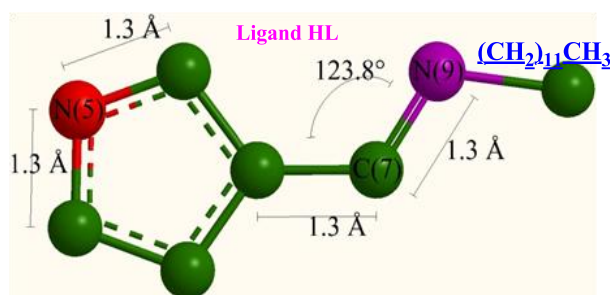
Figure 98: 3D-optimized geometrical structure of DDAP3C
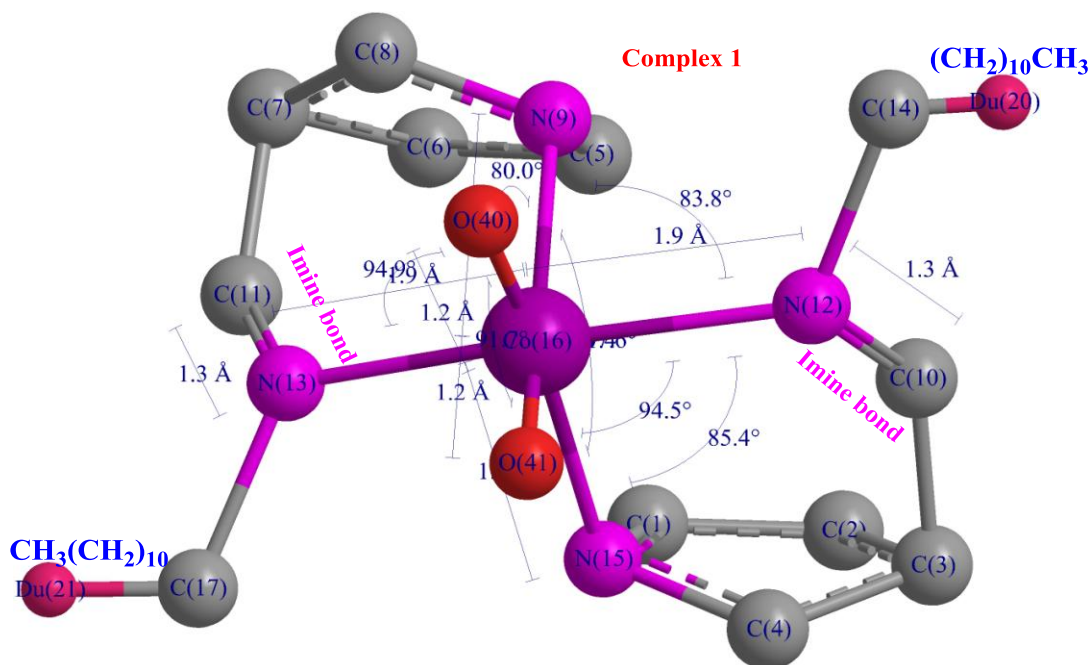
Figure 99: 3D-optimized geometrical structure of Co-DDAP3C
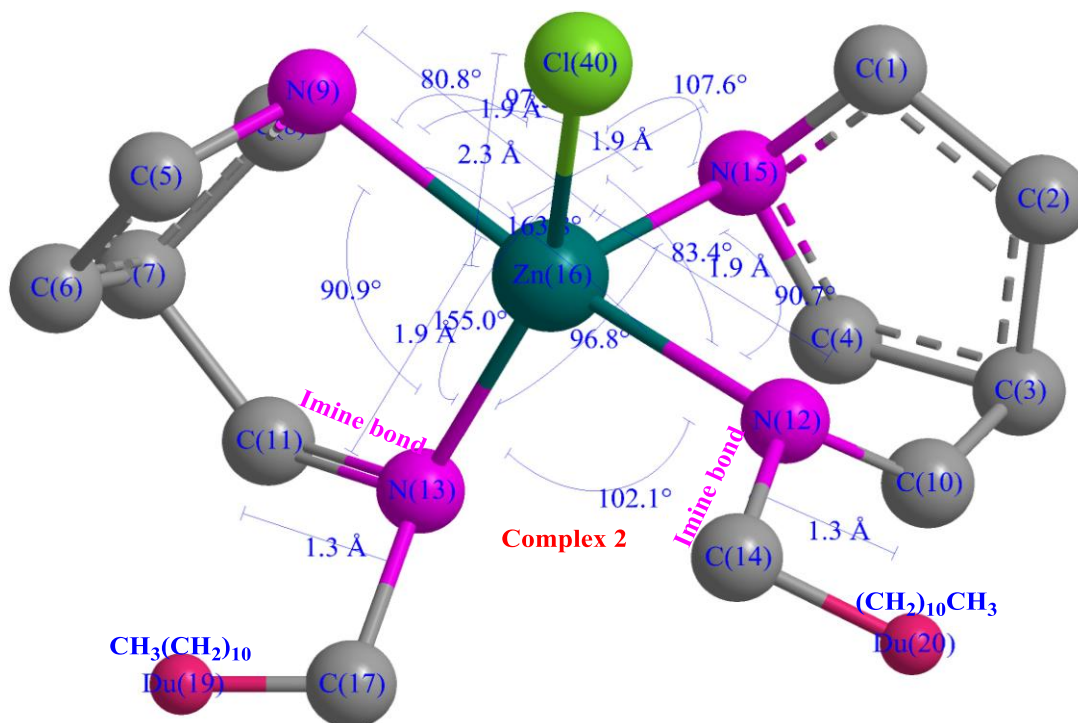
Figure 100: 3D-optimized geometrical structure of Zn-DDAP3C
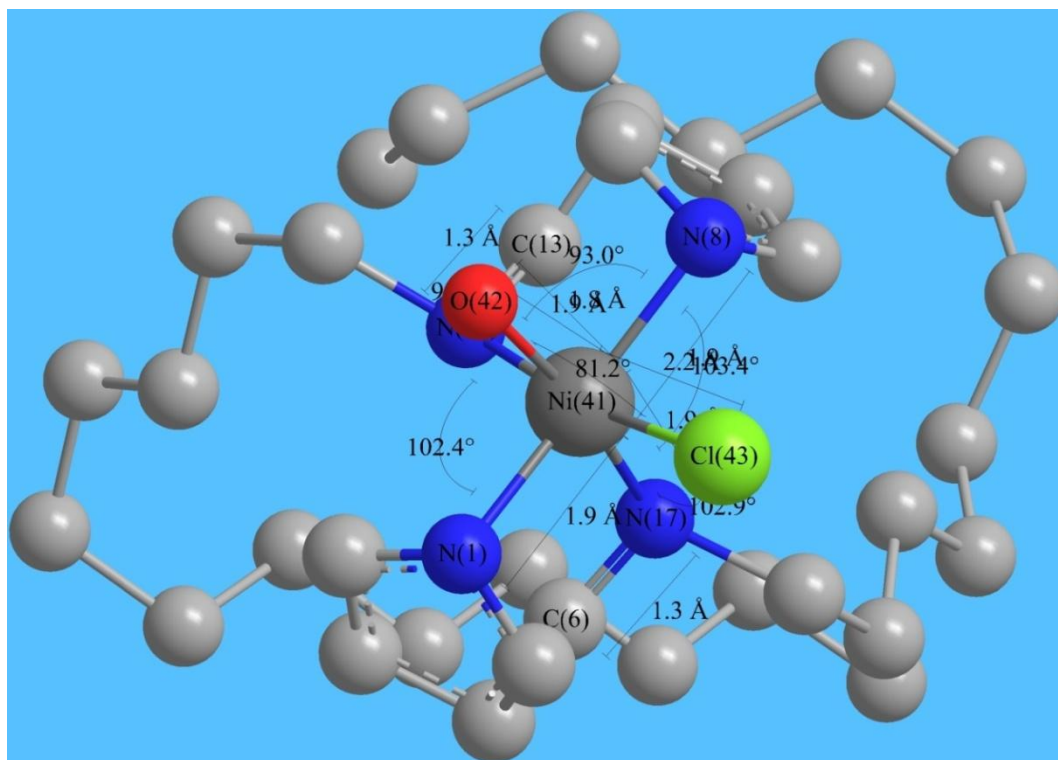
Figure 101: 3D-optimized geometrical structure of Ni-DDAP3C
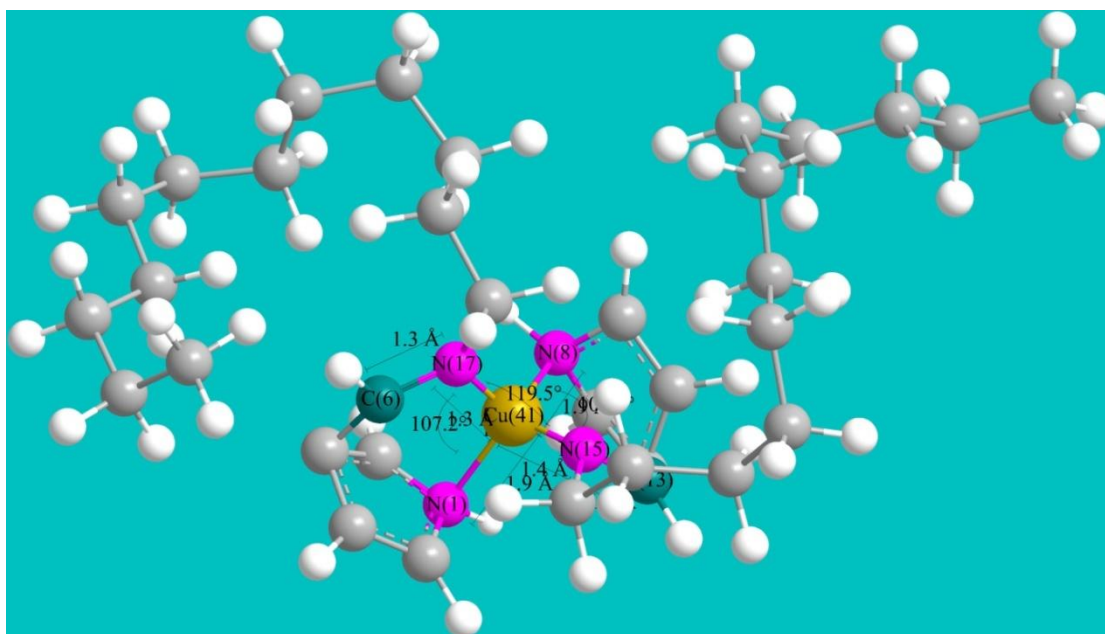
Figure 102: 3D-optimized geometrical structure of Cu-DDAP3C

Table 32: Selected bond lengths and bond angles of metal complexes of DDAP3C ligand

Compounds	Bonded Atoms	Bond length (Å)	Bonded Atoms	Bond angle (°)	Final geom. energy
HL (DDAP3C)	C(4)-N(5)	1.26			19.34 kcal/mol
	N(5)-C(1)	1.26			
	C(7)-N(9)	1.26			
	N(9)-C(10)	1.48			
Complex **1** (Co-complex)	Co(16)-N(13)	1.88	O(41)-Co(16)-O(40)	91.75	815.28 kcal/mol
	Co(16)-N(12)	1.88	N(12)-Co(16)-N(13)	161.35	
	Co(16)-O(41)	1.17	N(15)-Co(16)-N(9)	107.59	
	O(40)-Co(16)	1.17	N(13)-Co(16)-O(40)	94.93	
	Co(16)-N(9)	1.88	N(12)-Co(16)-O(41)	94.47	
	Co(16)-N(15)	1.88	N(15)-Co(16)-N(12)	85.36	
	C(11)-N(13)	1.29	O(40)-Co(16)-N(9)	80.03	
	C(10)-N(12)	1.29	N(12)-Co(16)-N(9)	83.84	
Complex **2** (Zn-complex)	Zn(16)-N(9)	1.94	N(15)-Zn(16)-N(9)	97.29	312.85 kcal/mol
	Zn(16)-N(13)	1.94	N(15)-Zn(16)-N(13)	96.82	
	Zn(16)-N(12)	1.94	N(12)-Zn(16)-N(15)	90.70	
	Zn(16)-Cl(40)	2.25	N(9)-Zn(16)-N(12)	163.81	
	N(15)-Zn(16)	1.94	N(13)-Zn(16)-N(9)	90.92	
	N(12)-C(10)	1.27	N(12)-Zn(16)-N(13)	102.1	
	N(13)-C(11)	1.27	N(13)-Zn(16)-Cl(40)	154.99	
			N(12)-Zn(16)-Cl(40)	83.36	
			N(15)-Zn(16)-Cl(40)	107.56	
			Cl(40)-Zn(16)-N(9)	80.82	
Complex **3** (Ni-complex)	Cl(43)-Ni(41)	2.16	O(42)-Ni(41)-Cl(43)	81.17	408.77 kcal/mol
	O(42)-Ni(41)	1.84	N(15)-Ni(41)-O(42)	95.04	
	N(8)-Ni(41)	1.87	N(8)-Ni(41)-N(15)	92.95	
	N(15)-Ni(41)	1.86	N(17)-Ni(41)-Cl(43)	102.87	
	N(17)-Ni(41)	1.86	N(8)-Ni(41)-N(17)	103.39	
	N(17)-C(6)	1.280, 1.260	N(15)-Ni(41)-N(1)	102.37	
	C(13)-N(15)	1.280, 1.260	-	-	
	N(1)-Ni(41)	1.87	-	-	
Complex **4** (Cu-complex)	N(17)-Cu(41)	1.34, 1.30	N(1)-Cu(41)-N(17)	107.16	421.64 kcal/mol
	Cu(41)-N(1)	1.87	N(8)-Cu(41)-N(1)	102.98	
	Cu(41)-N(8)	1.88	N(15)-Cu(41)-N(8)	105.99	
	Cu(41)-N(15)	1.36, 1.30	N(17)-Cu(41)-N(15)	119.54	
	N(15)-C(13)	1.31, 1.26			
	N(17)-C(6)	1.29, 1.26			

4.10   Antibacterial Activity Study

The most recent developments in pharmaceutical research involve using metals as a significant chemotherapeutic agent in medication systems (Arunadevi & Raman, 2020). Metals offer a synthesis template and add functions that improve medication delivery vectors (Aazam & Zaki, 2020). Pure metals are inactive biologically, but the bioavailability of metal cations and the presence of bioligands are essential factors in their activity (Aljahdali *et al.*, 2014). Metal interactions are necessary for the enhanced activity of many organic drugs (Malik *et al.*, 2018; Zafar *et al.*, 2021). Investigating the antibacterial effectiveness of Schiff base transition metal complexes against bacterial pathogens is interesting. Therefore, an investigation into the development of antibacterial activity has been carried out using new Schiff base ligands and related metal complexes.

An extensive analysis of the experimental findings from the antibacterial efficacy investigation showed a notable improvement in the effectiveness of the metal complexes and ligands against all bacterial pathogens. Antibacterial drugs work against bacterial pathogens through various mechanistic channels, such as by preventing the synthesis of proteins or by rupturing cell walls, which results in the death of the organisms (Ghanghas *et al.*, 2021). In metal complexes, the positive charge of the metal ions is distributed more widely within the chelate ring, which decreases the polarity of the metal atoms. After chelation, this charge dispersion is supported by the donor atoms of the ligand. This fact is known as Tweedy's chelation theory, which is regarded as the convincing reason for the enhanced activity of the metal complexes (Elsayed *et al.*, 2020; Fekri *et al.*, 2019; Kumaravel *et al.*, 2018). Chelation makes complexes more stable and increases their lipophilicity, facilitating their passage across the lipid layers of bacterial membranes. The metabolic pathways of organisms are disturbed by chelate complexes by deactivating several cellular enzymes (Andiappan *et al.*, 2019). The inclusion of metal ions has affected the physical characteristics of the complexes, which may also increase their biological activity. Gram-positive and gram-negative clinical (Laboratory collection) strains of bacteria were used in our investigation. The growth inhibition data was shown to vary between the various trials due to the interaction with some similar test compounds.

4.10.1 Antibacterial Activity Study of DDAP2C and Metal Complexes

Five clinical strains of bacterial pathogens were chosen for this study based on their *in vitro* interactions with the prepared ligand DDAP2C and its metal complexes. These bacterial pathogens included *S. aureus, K. pneumoniae, P. aeruginosa, Enterococci*, and *E. coli*. This study was completed by the disc diffusion technique, where the inhibition zone was compared to the positive control amikacin 30 µg/disc and DMSO, which served as a negative control (Mahato *et al.*, 2020; Mahmoud *et al.*, 2020). This was accomplished by preparing the solution of the synthesized compounds in DMSO (50, 25, and 12.5 µg/µL concentrations), which does not inhibit bacterial growth. The results of the growth inhibition values are documented in Table 33. The results are encouraging. The final results are presented in bar graphs as shown in Figs. 103-108. The findings show that, except for *S. aureus*, where the activity was comparable, the positive control amikacin had more antibacterial activity than all of the investigated compounds. At all concentrations, the Zn-DDAP2C complex displayed less antibacterial activity against *E. coli* than DDAP2C and the reference drug amikacin. By comparing the obtained antibacterial data, it was established that the ligand and its metal complexes had a better inhibitory effect on *P. aeruginosa* and *S. aureus*.

The Co-DDAP2C and Cu-DDAP2C show better antibacterial activity than the other two complexes against all pathogens at all concentrations (Ahmed *et al.*, 2021; Maiti *et al.*, 2020). The Cu-DDAP2C is the best and even better than the reference drug amikacin against *E. coli* bacteria.

MIC measurements (in µg/µL) are listed in Table 34 for each compound. It can be concluded from MIC data that all the compounds synthesized in this study have good antibacterial activity. The findings showed that metal complexes, DDA, and DDAP2C were more susceptible to *S. aureus* and *Enterococci*, and Ni-DDAP2C demonstrated a better minimum inhibitory concentration (MIC) value against all types of bacteria. According to MIC tests, the antibacterial activity against *E. coli* observes the following order: Ni-DDAP2C, Cu-DDAP2C, and Zn-DDAP2C (0.0122 µg/µL), Co-DDAP2C (0.0244 µg/µL), DDAP2C (0.0976 µg/µL), and DDA (0.7812 µg/µL). The activity data also showed that the Zn-DDAP2C and Cu-DDAP2C have the lowest MIC of 0.0122 µg/µL and are more effective against *P. aeruginosa*. The Ni-DDAP2C

complex possesses more antibacterial power against *S. aureus*, having a MIC of 0.0488 μg/μL, and the Cu-DDAP2C is the best with 0.0244 μg/μL value (Anacona *et al.*, 2021; Chandrasekar *et al.*, 2021).

Overall, the MIC data revealed that every chemical under investigation had outstanding and better antibacterial activity against every isolate and metal complexes are recommended as the most potent antibacterial compound. Two theories can explain this increased activity of complexes. Based on the overtone theory, the compound's antibacterial activity depends on its solubility in the cell membrane, which is crucial because it only allows lipid-soluble compounds to pass (Kargar *et al.*, 2021b). On the other hand, according to Tweedy's chelation theory, increased lipophilicity improves complex penetration through lipid membranes and prevents metal binding sites in the microbial enzymes (Kargar *et al.*, 2021a). Additionally, these complexes prevent the cell from respiration by deactivating enzymes involved in this process, which blocks protein synthesis and prevents the organism from growing further. The possible efficacy of the complexes against bacterial pathogens may be due to inhibiting the synthesis of peptidoglycan in the bacterial cell wall. This restriction may happen due to the inhibition of the peptidoglycan synthesis step (Bayeh *et al.*, 2020; Jiang *et al.*, 2016; Raj *et al.*, 2017).

Table 33: Antibacterial activity data of DDAP2C Schiff base ligand and metal complexes

Compounds	Diameters of the zone of inhibition in mm														
	E. coli			*K. pneumoniae*			*P. aeruginosa*			*Enterococci*			*S. aureus*		
Concentration (μg/μL)	50	25	12.5	50	25	12.5	50	25	12.5	50	25	12.5	50	25	12.5
DDA	16	14	13	21	16	14	18	16	15	17	16	15	21	20	19
P2C	0	0	0	0	0	0	0	0	0	0	0	0	0	0	0
DDAP2C	14	13	12	15	12	9	11	11	11	10	9	8	23	21	20
Ni-DDAP2C	16	15	14	14	11	10	15	13	11	12	10	8	23	22	21
Zn-DDAP2C	12	10	9	14	10	9	17	16	14	11	10	9	24	23	22
Co-DDAP2C	17	16	13	21	19	16	20	18	16	20	18	16	24	22	21
Cu-DDAP2C	20	18	15	22	20	18	21	19	17	22	19	17	25	23	22
Amik. (30 μg/disc)	14			24			23			20			21		
DMSO	0	0	0	0	0	0	0	0	0	0	0	0	0	0	0

Table 34: Minimum inhibitory concentration data of DDAP2C Schiff base ligand and metal complexes

Compounds	Minimum inhibitory concentration (MIC) in (µg/µL)				
	E. coli	*K. pneumoniae*	*P. aeruginosa*	*Entercocci*	*S. aureus*
DDA	0.7812	0.0488	0.0976	0.3906	0.1953
DDAP2C	0.0976	0.1953	0.1953	0.3906	0.0976
Ni-DDAP2C	0.0122	0.0122	0.0488	0.0122	0.0488
Zn-DDAP2C	0.0122	0.0488	0.0122	0.0976	0.0976
Co-DDAP2C	0.0244	0.0488	0.0488	0.0976	0.0488
Cu-DDAP2C	0.0122	0.0244	0.0122	0.0488	0.0244
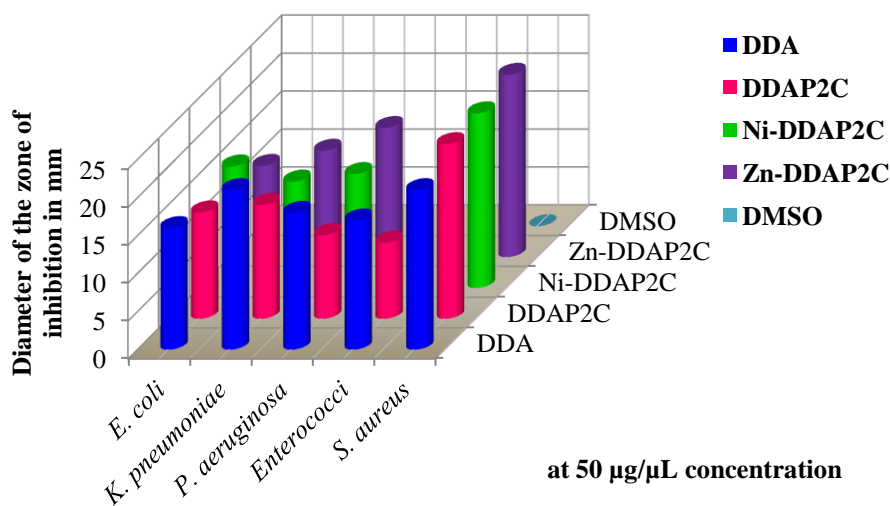
Figure 103: Bar graph showing antimicrobial activity of DDA, DDAP2C, Ni-DDAP2C, and Zn-DDAP2C at 50 µg/µL concentration
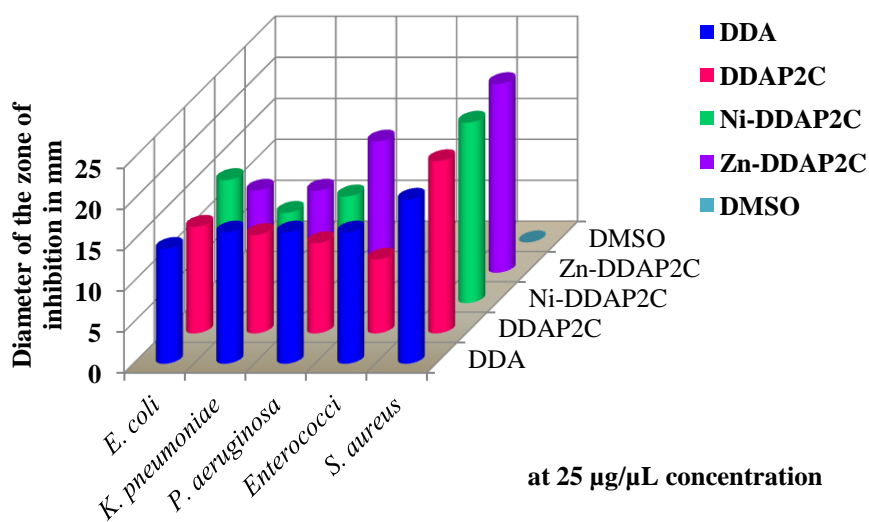
Figure 104: Bar graph showing antimicrobial activity of DDA, DDAP2C, Ni-DDAP2C, and Zn-DDAP2C at 25 µg/µL concentration
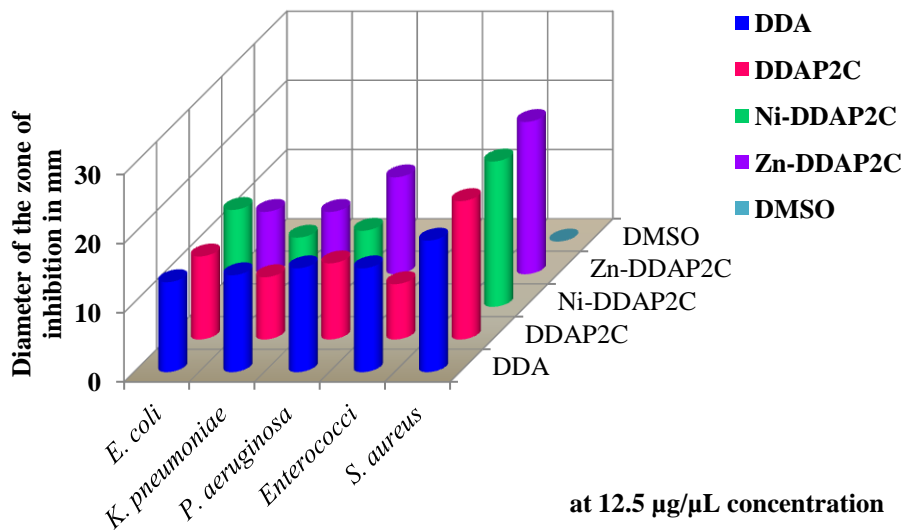
Figure 105: Bar graph showing antimicrobial activity of DDA, DDAP2C, Ni-DDAP2C, and Zn-DDAP2C at 12.5 µg/µL concentration
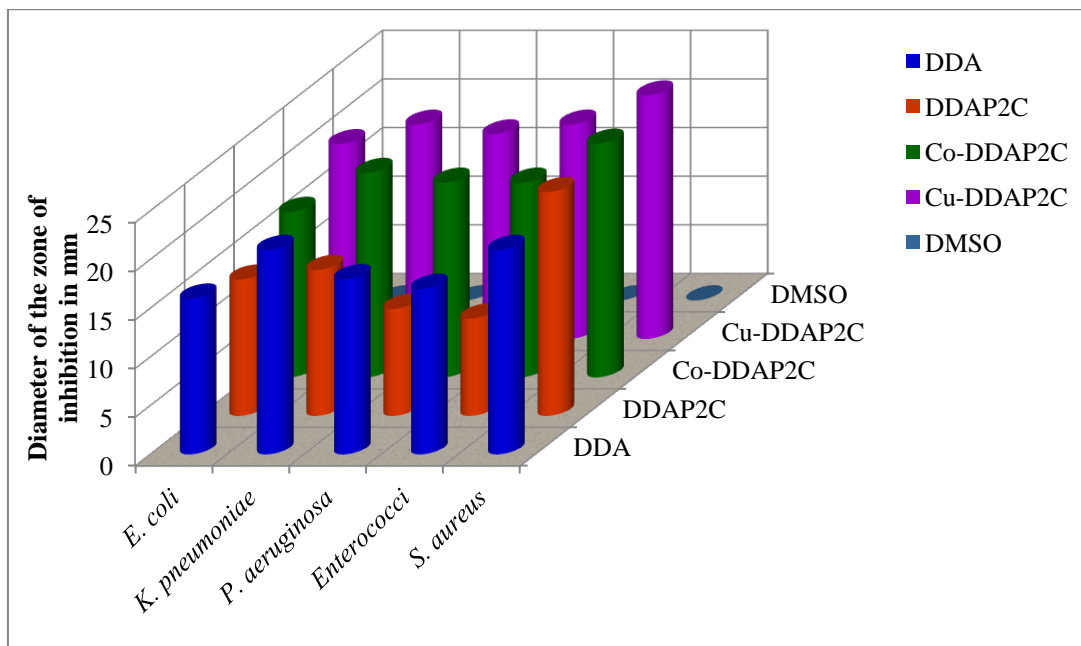
Figure 106: Bar graph showing antimicrobial activity of DDA, DDAP2C, Co-DDAP2C, and Cu-DDAP2C at 50 µg/µL concentration
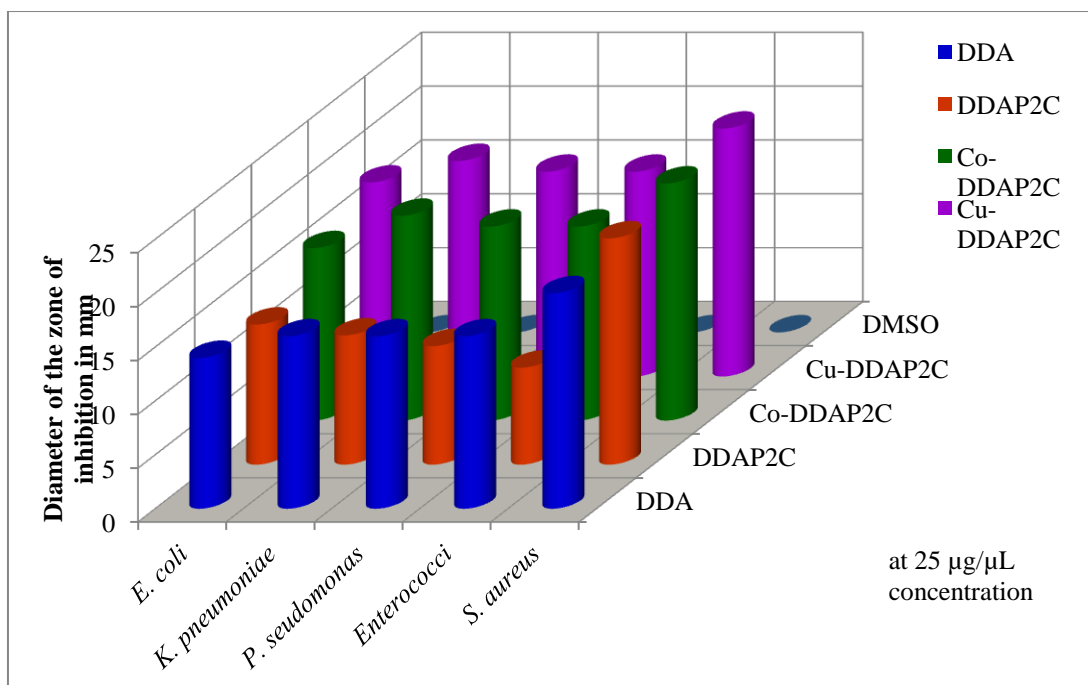
Figure 107: Bar graph showing antimicrobial activity of DDA, DDAP2C, Co-DDAP2C, and Cu-DDAP2C at 25 µg/µL concentration
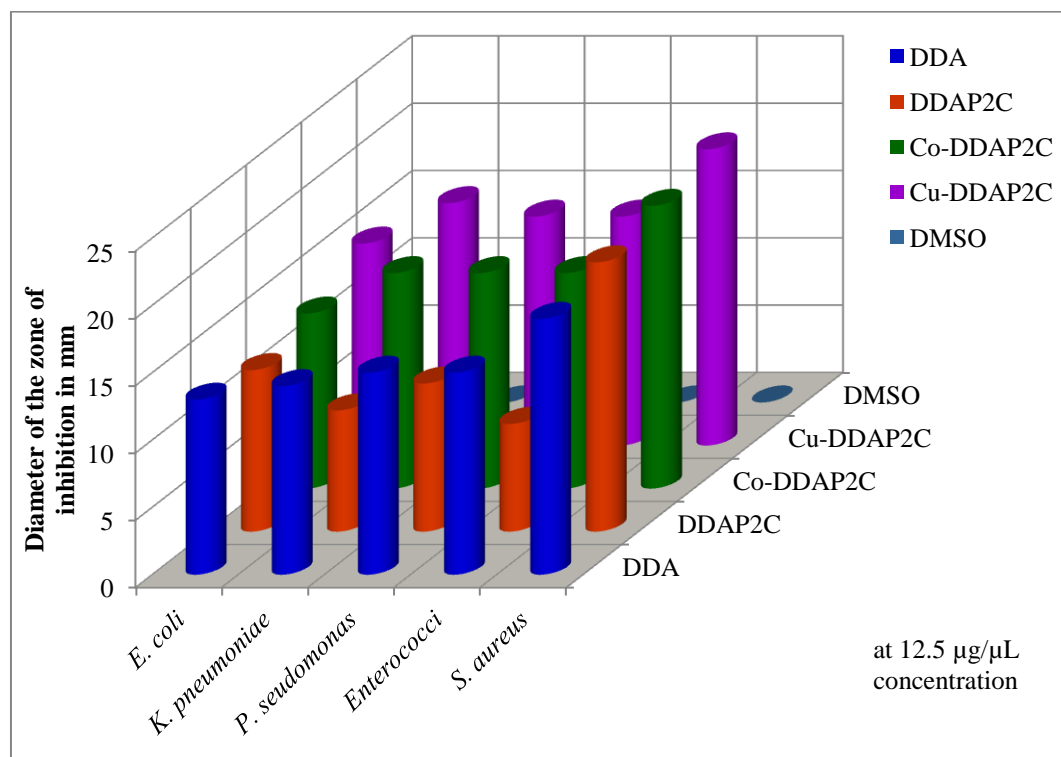
Figure 108: Bar graph showing antimicrobial activity of DDA, DDAP2C, Co-DDAP2C, and Cu-DDAP2C at 12.5 µg/µL concentration

4.10.2 Antibacterial Activity Study of DDAP3C and Metal Complexes

The modified Kirby-Bauer disc diffusion technique was utilized to test the *in vitro* antimicrobial efficacy for ligand HL and metal complexes 1, 2, 3, and 4 against five pathogenic bacteria, including *Staphylococcus aureus* (*S. aureus*), *Pseudomonas aeruginosa* (*P. aeruginosa*), *Enterococcus*, *Klebsiella pneumoniae* (*K. pneumoniae)* and *Escherichia coli* (*E. coli*). The test solutions of the proper concentrations (50, 25, and 12.5 µg/µL) were prepared by dissolving compounds in DMSO. The thoroughly sterilized, 5 mm-diameter filter paper discs were gently stuck to the swabbed medium after being soaked in the test solution. As a positive control, 30 µg/disc of amikacin was employed, while DMSO was applied to a blank disc as a negative control. The bar graphs in Figures 109–114 display the results graphically, and Table 35 lists the antibacterial potential measured as the diameter of the inhibition zones in millimeters (mm). Amikacin showed better antibacterial activity than other studied chemicals against all pathogens except *S. aureus* and *E. coli.* Compared to HL, complexes **1**, **2**, **3**, and amikacin, Complex **4** had a special antibacterial effect at all concentrations. The significant growth inhibition was caused by the ligand (HL) and all complexes, against *S. aureus*, *E. coli*, and *K. pneumoniae*, but not as much against *Enterococci* and *P. aeruginosa*.

The MIC of the test compounds was determined to evaluate their biological activities quantitatively, and the results are presented in Table 36. Although all tested compounds exhibited significant MIC against every pathogen, a comparatively lower MIC was found against *E. coli, P. aeruginosa*, and *K. pneumoniae*. The most potent antibacterial activity was demonstrated by complex **2** and **4**, with the lowest MIC (0.0244 µg/µL) for *S. aureus*. Overall, the antibacterial properties of the tested compounds were excellent and comparable based on MIC data. Tweedy's chelation theory and Overtone's approach help to explain why metal complexes exhibit more potent antibacterial activity than HL. When used on gram-positive bacteria, a metallosurfactant interacts electrostatically and hydrophobically with the cell wall and cell membrane of gram-positive bacteria, respectively.

In contrast, gram-negative bacteria, however, have a lipopolysaccharide coating on their outer membranes that may prevent the entry of amphiphilic metal-based

146

surfactants and diminish their antibacterial effects (Kargar *et al.*, 2021b). According to our research, gram-positive bacteria had stronger antibacterial properties than gram-negative bacteria. Gram-positive bacteria can absorb drugs more efficiently due to a thick layer of peptidoglycan (Keypour *et al.*, 2019; Zamani *et al.*, 2015). According to reports, more hydrophobic surfactants have more effective antibacterial properties. The pace of entering of molecules into the cells is governed by lipophilicity, which is influenced by the coordination of different metal ions.

Table 35: Antibacterial activity data of DDAP3C Schiff base ligand and metal complexes

Compounds	Diameter of the zone of inhibition in mm														
	E. coli			*K. pneumoniae*			*P. aeruginosa*			*Enterococci*			*S. aureus*		
Concentration (µg/µL)	50	25	12.5	50	25	12.5	50	25	12.5	50	25	12.5	50	25	12.5
LA(**DDA**)	16	14	13	21	16	14	18	16	15	17	16	15	21	20	19
P3C	0	0	0	0	0	0	0	0	0	0	0	0	0	0	0
HL (DDAP3C)	15	15	13	15	15	14	12	12	12	12	11	10	22	21	20
Complex **1**	16	15	14	15	14	13	12	11	10	12	12	12	23	22	21
Complex **2**	17	16	15	18	17	16	16	16	16	15	14	14	24	23	22
Complex **3**	18	17	16	22	18	16	18	17	16	17	17	16	23	22	21
Complex **4**	19	18	17	23	19	17	19	18	17	18	18	17	24	24	22
Amik. (30 µg/disc)	14			24			23			20			21		
DMSO	0	0	0	0	0	0	0	0	0	0	0	0	0	0	0

Table 36: Minimum inhibitory concentration data of DDAP3C Schiff base ligand and metal complexes

Compounds	Minimum inhibitory concentration (MIC) in (µg/µL)				
	E. coli	*K. pneumoniae*	*P. aeruginosa*	*Enterococci*	*S. aureus*
LA(**DDA**)	0.7812	0.7812	0.3906	0.3906	0.1953
HL (DDAP3C)	0.3906	0.3906	0.3906	0.1953	0.0976
Complex **1**	0.1953	0.3906	0.1953	0.0976	0.0488
Complex **2**	0.0976	0.0976	0.0976	0.0488	0.0244
Complex **3**	0.0976	0.1953	0.1953	0.0976	0.0488
Complex **4**	0.0488	0.0488	0.0976	0.0488	0.0244
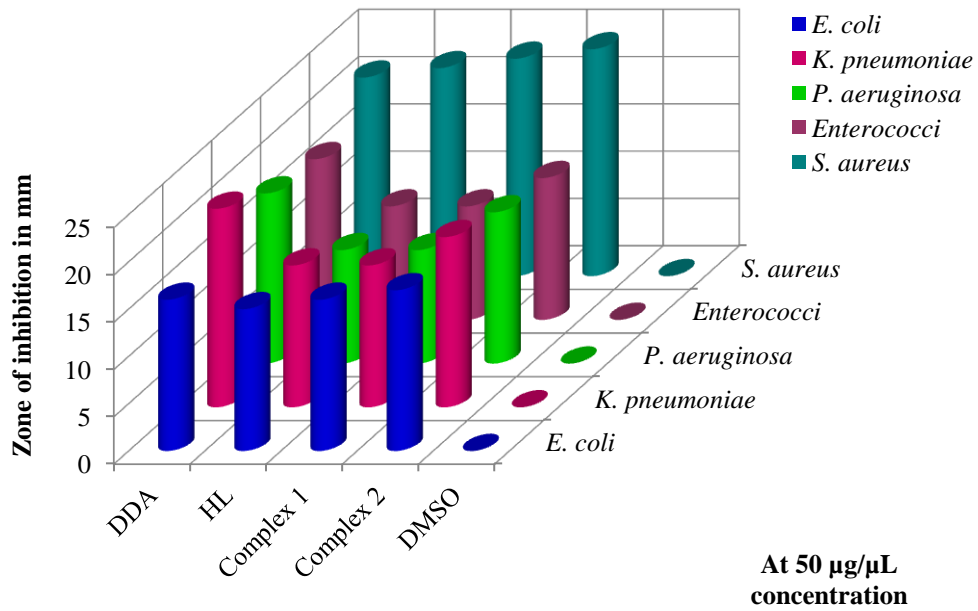
Figure 109: Bar graph showing antimicrobial activity of DDA, HL, Complex 1, and Complex 2 at 50 µg/µL concentration
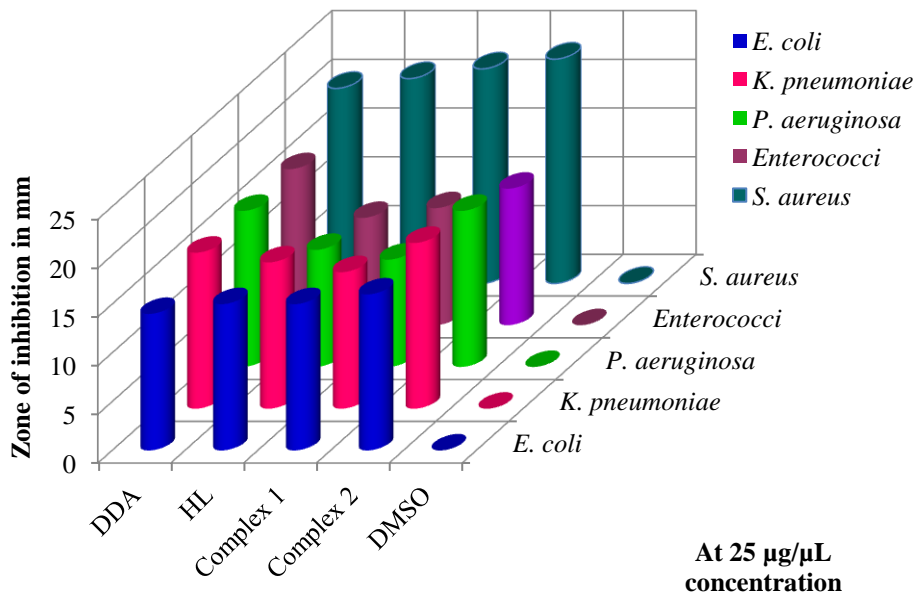
Figure 110: Bar graph showing antimicrobial activity of DDA, HL, Complex 1, and Complex 2 at 25 µg/µL concentration
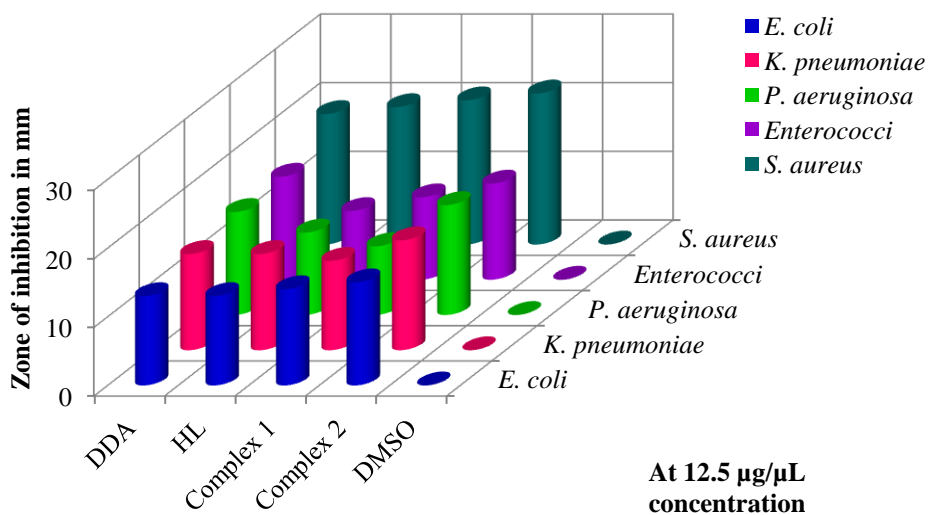
Figure 111: Bar graph showing antimicrobial activity of DDA, HL, Complex 1, and Complex 2 at 12.5 µg/µL concentration
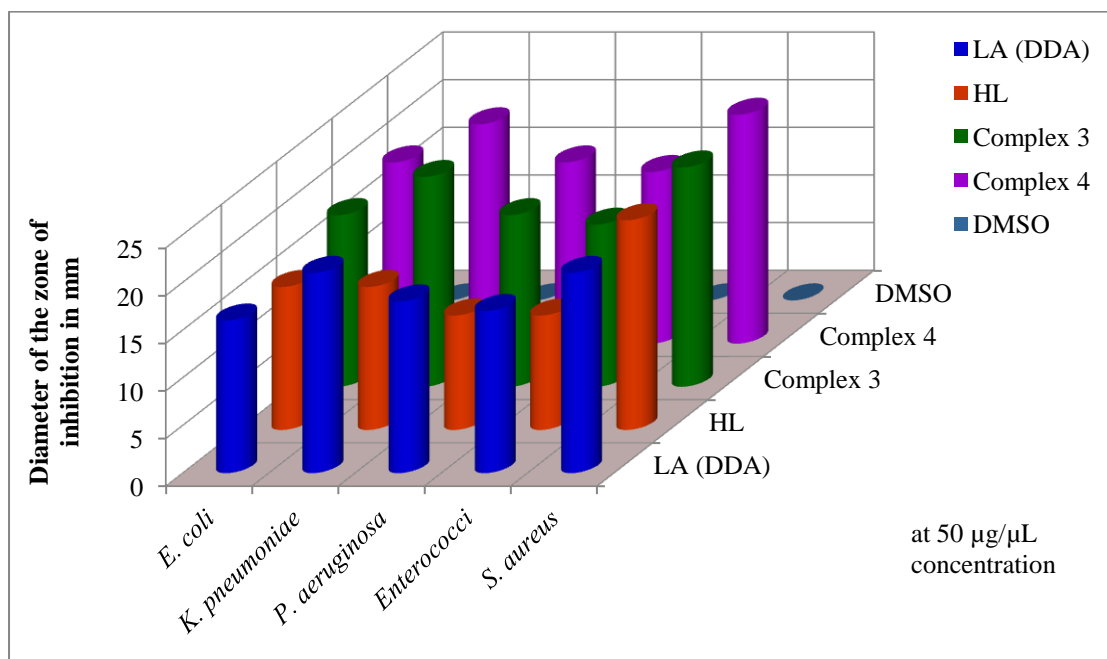
Figure 112: Bar graph showing antimicrobial activity of DDA, HL, Complex 3, and Complex 4 at 50 µg/µL concentration
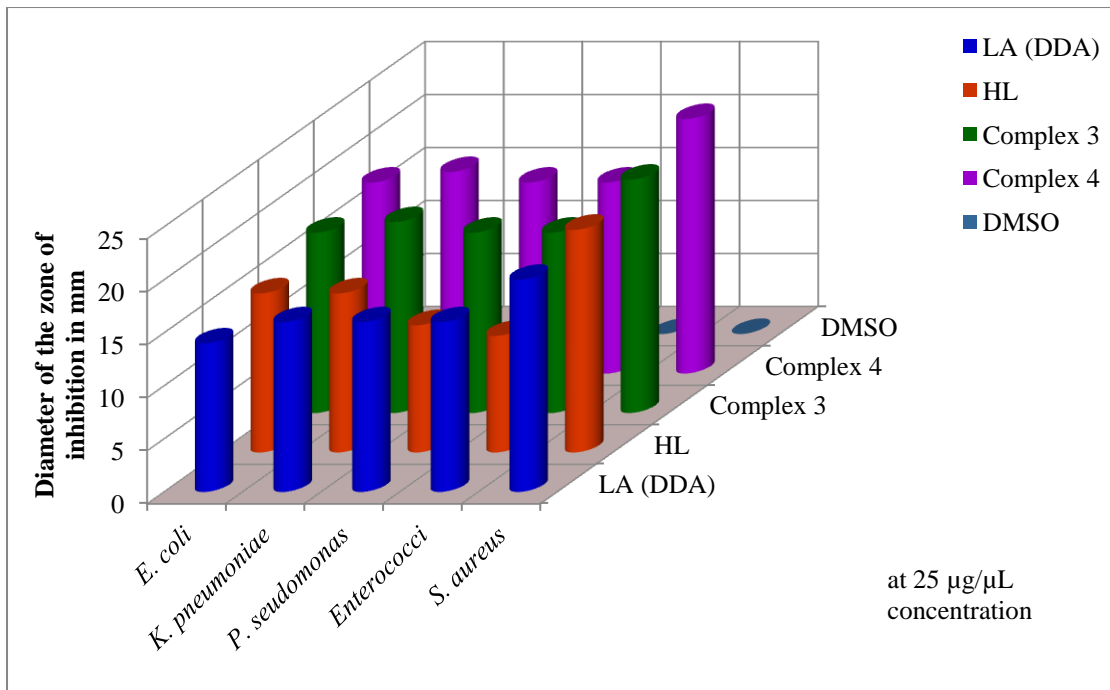
Figure 113: Bar graph showing antimicrobial activity of DDA, HL, Complex 3, and Complex 4 at 25 µg/µL concentration
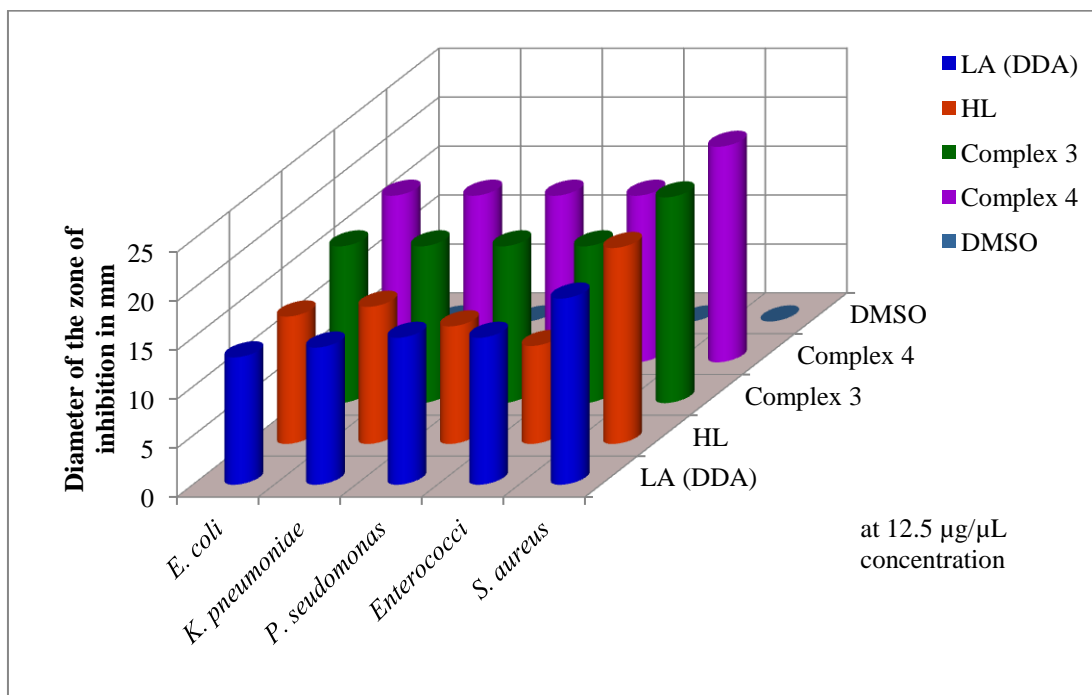
Figure 114: Bar graph showing antimicrobial activity of DDA, HL, Complex 3, and Complex 4 at 12.5 µg/µL concentration

CHAPTER 5

5. CONCLUSION AND RECOMMENDATIONS

The Schiff bases are especially interesting ligands in coordination chemistry. The distinguishing characteristics of the compounds are their straightforward synthesis processes and ease of coordination with metals for complex formation. Their multiple applications in medicine, catalysis, electronics, industry, and material science have drawn more and more attention in recent years. Our research has concentrated on the metal complexes of Schiff bases of dodecylamine and pyrrole carboxaldehyde derivatives to assess their pharmacological effectiveness through *in vitro* antibacterial evaluation tests. This thesis includes details of the investigation on the synthesis, spectral characterization, thermal, powder XRD study, and surface morphological investigation by SEM analysis, and disc diffusion technique for antibacterial assessment of the Schiff bases and metal complexes.

5.1   Conclusion

The fundamental element of Schiff base research is the growing interest in the efficacy of metal-based medications as chemotherapeutic agents. The promising compounds for medicinal chemistry can be the Schiff bases and their metal complexes because most of them have biological activity. Apart from the biological interest, this study's motivation comes from applying these molecules in other areas, such as the electronic field, material science, and extensive areas of chemistry. This research aims to synthesize two types of Schiff base ligands, DDAP2C and HL. Their metal complexes were generated through interactions with the ions of Co(II), Ni(II), Cu(II), and Zn(II). Their effective coordination with metal ions is due to the availability of donor atoms in the Schiff base ligands. One essential part of the nitrogen atom in the azomethine bond of the Schiff base ligand modifies the physicochemical profile of the molecules. When Schiff base ligands are bonded with metal ions, their many properties will change.

The synthesis of various Schiff base ligands and their related metal complexes has been documented in the appropriate sections of the thesis manuscript. Their physical

and spectral characteristics have been determined using various physical and spectral techniques, including CHN analysis, conductivity measurement, FT-IR, ^{1}H & ^{13}C NMR, MALDI-TOF-MS, ESI-MS, and electronic absorption studies. By using XRPD, TGA/DTA, and molecular modeling studies, their structure has also been further characterized and confirmed. The surface morphology has been verified by an SEM analysis, which provides information on the crystalline and surface structures. Further, the EDX analysis associated with the SEM has obtained the chemical composition of the compounds. The disc diffusion technique was used to study the antibacterial activity, which is a vital aspect of the work.

The nitrogen atom of the azomethine group participates in the legation process with metal ions, as shown by the structural study of all Schiff base ligands and metal complexes using spectroscopic methods. Both ^{1}H NMR data and FT-IR absorption data support this conclusion. Most of the compounds have molar conductivity values less between 50 to 100 (Ω^{-1} mol^{-1}cm^2) ranges, which suggest that the complexes are 1:1 electrolytic in nature. However, some of them demonstrated non-electrolytic and Co-DDAP3C has a 1:2 electrolytic characteristics. The magnetic moment and electronic absorption measurements provide convincing proof for the actual geometry of the complexes. The molecular modeling study has further supported this fact. The nanocrystalline nature of the complexes was identified by analyzing the powder XRD data and computing the particle sizes using Scherrer's formula.

According to our study, all of the synthesized ligands and complexes exhibit incredible growth inhibition when screened against clinical strains of bacterial pathogens. The metal complexes of the DDAP2C Schiff base ligand demonstrate higher levels of bacterial growth inhibition as compared to the free Schiff base ligand. Moreover, the ligand DDAP2C and its metal complexes delivered strong antibacterial sensitivity against *P. aeruginosa* and *S. aureus* bacterial pathogens. This work using the HL Schiff base ligand and metal complexes showed that all bacterial pathogens had considerable antibacterial activity at higher concentrations. Antibacterial studies had been carried out on this group of compounds with concentrations of 12.5, 25, and 50 μg/μL. Furthermore, complex **2, 3** and **4** demonstrated superior antibacterial activities than HL, complex **1**, and positive control amikacin at all concentrations.

5.2   Recommendations

The following goals are planned for future work to set continuity in research activity.

- To investigate their antifungal, anticancer, and antioxidant activities.
- To obtain a single crystal for each Schiff base ligand and metal complex and to investigate the structures of those crystals.
- To investigate the *in vivo* antibacterial study of the synthesized compounds.
- To investigate the drug carrier potential of synthesized Schiff base ligands and metal complexes.
- To investigate the catalytic and electrochemical studies of the compounds.
- To investigate the surfactant properties of the compounds by measuring conductivity at a higher temperature other than standard.
- To investigate the surfactant properties of the compounds by measuring viscosity at different temperatures.

CHAPTER 6

6. SUMMARY

There are six chapters in the thesis. The following is a summary of them:

Chapter 1 provides a general introduction and chemistry about the Schiff bases and their related complexes with nickel(II), cobalt(II), zinc(II), and copper(II), metals. The presentation discusses the synthetic design and several biological uses of Schiff bases and metal complexes. Dodecylamine, a surfactant, and derivatives of pyrrole carboxaldehyde are the precursor compounds, and information is given about their structures and chemical composition. A trace amount of biometals is essential for regulating metabolism in living. This chapter briefly describes the chemistry and biology of these metallo-elements. The concluding section of the chapter highlights the objectives and scope of the current study.

In Chapter 2, a thorough review of the relevant literature is covered. This review is crucial for validating the findings. The literature has been reviewed here based on the numerous prospective applications of the Schiff base and metal complexes.

Chapter 3 provides information on the materials employed in the current investigation and several characterization techniques used to analyze the synthesized ligands and metal complexes. This chapter describes detailed techniques for synthesizing and characterizing Schiff bases and metal complexes. Here is a brief description of the method used to conduct antibacterial analysis and the information on the organisms. The details of the findings and a discussion of the experimental work are included in

Chapter 4. This section is regarded as the skeleton of the thesis. This chapter illustrates the suggested molecular structure of the metal complexes and Schiff base ligands. This section has computed and discussed the data analysis findings related to molecular modeling, thermal decomposition, powder XRD, scanning electron microscopy, and spectrum characterizations. The text of this chapter places the tables and figures that depict the analyzed data in the appropriate places. In the end, the

antibacterial investigation data of the synthesized Schiff bases and metal complexes are summarized.

Chapter 5 contains documentation of the conclusion of the current research work. The prospects for the future and suggestions for continuing the current research endeavor are underlined.

All the chapters of the thesis are summarized in Chapter 6.

REFERENCES

Aazam, E. S., & Zaki, M. (2020). Synthesis and Characterization of Ni(II)/Zn(II) Metal Complexes Derived from Schiff Base and Orthophenylenediamine: In Vitro DNA Binding, Molecular Modeling and RBC Hemolysis. *ChemistrySelect*, **5**(2): 610–618. https://doi.org/10.1002/slct.201903583

Abdel-Rahman, L. H., Abu-Dief, A. M., Ismael, M., A.A., M. M., & Hashem, N. A. (2016). Synthesis, Structure Elucidation, Biological Screening, Molecular Modeling and DNA Binding of Some Cu(II) Chelates Incorporating Imines Derived from Amino Acids. *Journal of Molecular Structure*, **1103**: 232–244. https://doi.org/10.1016/j.molstruc.2015.09.039

Abdulghani, A. J., & Hussain, R. K. (2015). Synthesis and Characterization of Schiff Base Metal Complexes Derived from Cefotaxime with 1H-Indole-2,3-Dione (Isatin) And 4-N,N-Dimethyl-Aminobenzaldehyde. *Open Journal of Inorganic Chemistry*, 0**5**(04): 83–101. https://doi.org/10.4236/ojic.2015.54010

Aboafia, S. A., Elsayed, S. A., El-Sayed, A. K. A., & El-Hendawy, A. M. (2018). New Transition Metal Complexes of 2,4-Dihydroxybenzaldehyde Benzoylhydrazone Schiff Base (H2dhbh): Synthesis, Spectroscopic Characterization, DNA Binding/Cleavage and Antioxidant Activity. *Journal of Molecular Structure,* **1158**: 39-50. https://doi.org/10.1016/j.molstruc. 2018.01.008

Abou Melha, K. S., Al-Hazmi, G. A., Althagafi, I., Alharbi, A., Keshk, A. A., Shaaban, F., & El-Metwaly, N. (2021). Spectral, Molecular Modeling, and Biological Activity Studies on New Schiff's Base of Acenaphthaquinone Transition Metal Complexes. *Bioinorganic Chemistry and Applications,* **2021**: 1-17. https://doi.org/10.1155/2021/6674394

Abouzayed, F. I., Emam, S. M., & Abouel-Enein, S. A. (2020). Synthesis, Characterization and Biological Activity of Nano-Sized Co(II), Ni(II), Cu(II), Pd(II) and Ru(III) Complexes of Tetradentate Hydrazone Ligand. *Journal of Molecular Structure*, **1216**: 128314. https://doi.org/10.1016/j.molstruc.2020. 128314

Abu-Dief, A. M., & Mohamed, I. M. A. (2015). A Review on Versatile Applications

of Transition Metal Complexes Incorporating Schiff Bases. *Beni-Suef University Journal of Basic and Applied Sciences*, **4**(2): 119–133. https://doi.org/10.1016/j.bjbas.2015.05.004

Abu-khadra, A. S., Farag, R. S., & Abdel-hady, A. E. M. (2016). Synthesis, Characterization and Antimicrobial Activity of Schiff Base *(E)-N*-(4-(2-Hydroxybenzylideneamino) Phenylsulfonyl Acetamide Metal Complexes. *American Journal of Analytical Chemistry*, 0**7**(03): 233–245. https://doi.org/10.4236/ajac.2016.73020

Acet, Ö., Baran, T., Erdönmez, D., Aksoy, N. H., Alacabey, İ., Menteş, A., & Odabaşi, M. (2018). O-Carboxymethyl Chitosan Schiff Base Complexes as Affinity Ligands for Immobilized Metal-Ion Affinity Chromatography of Lysozyme. *Journal of Chromatography A*, **1550**: 21–27. https://doi.org/10.1016/j.chroma.2018.03.022

Addison, A. W., Rao, T. N., Reedijk, J., van Rijn, J., & Verschoor, G. C., (1984). Synthesis, Structure, and Spectroscopic Properties of Copper(II) Compounds Containing Nitrogen-Sulphur Donor Ligands; The Crystal and Molecular Structure of Aqua[L,7-bis(N-methylbenzimidazol-2'-yl)- 2,6-Dithiaheptane] Copper(II) Perchlorate. *Journal of the Chemical Society, Dalton Transactions*, (7): 1349–1356. https://doi.org/10.1039/DT9840001349

Adhikari, J., Bhattarai, A., & Chaudhary, N. K. (2022). Synthesis, Characterization, Physicochemical Studies, and Antibacterial Evaluation of Surfactant-Based Schiff Base Transition Metal Complexes. *Chemical Papers*, **76**(4): 2549–2566. https://doi.org/10.1007/s11696-022-02062-x

Adhikari, J., Bhattarai, A., & Chaudhary, N. K. (2023). Bioinorganic Interest on Co(II) and Zn(II) Complexes of Pyrrole-Based Surfactant Ligand: Synthesis, Characterization, and In Silico-ADME Study. *Journal of Molecular Structure*, **1274**: 134434. https://doi.org/10.1016/j.molstruc.2022.134434

Aggoun, D., Messasma, Z., Bouzerafa, B., Berenguer, R., Morallon, E., Ouennoughi, Y., & Ourari, A. (2021). Synthesis, Characterization and DFT Investigation of New Metal Complexes of Ni(II), Mn(II) and VO(IV) Containing N,O-Donor Schiff Base Ligand. *Journal of Molecular Structure*, **1231**: 129923. https://doi.org/10.1016/j.molstruc.2021.129923

Aghaei, M., Kianfar, A. H., & Dinari, M. (2020). Catalytic Reduction of 4-Nitrophenol by Means of Nanostructured Polymeric Schiff Base Complexes. *Applied Organometallic Chemistry,* **34**(5). https://doi.org/10.1002/aoc.5617

Ahmad, N., Alam, M., Wahab, R., Ahmed, M., & Ahmad, A. (2020). Synthesis, Spectral and Thermo-Kinetics Explorations of Schiff-Base Derived Metal Complexes. *Open Chemistry*, **18**(1): 1304–1315. https://doi.org/10.1515/chem-2020-0168

Ahmed, Y. M., Mahmoud, W. H., Omar, M. M., & Mohamed, G. G. (2021). Synthesis, Characterization and Biological Activity of Transition Metals Schiff Base Complexes Derived from 4,6-Diacetylresorcinol and 1,8-Naphthalenediamine. *Journal of Inorganic and Organometallic Polymers and Materials*, **31**(6): 2339–2359. https://doi.org/10.1007/s10904-020-01867-1

Aijuka, M., Santiago, A. E., Girón, J. A., Nataro, J. P., & Buys, E. M. (2018). Enteroaggregative Escherichia Coli is the Predominant Diarrheagenic E. Coli Pathotype Among Irrigation Water and Food Sources in South Africa. *International Journal of Food Microbiology,* **278**: 44-51. https://doi.org/10.1016/j.ijfoodmicro.2018.04.018

Al-Humaidi, J. Y. (2019). In Situ Alkaline Media: Synthesis, Spectroscopic, Morphology and Anticancer Assignments of Some Transition Metal Ion Complexes of 1-((2-Aminophenylimino) Methyl) Naphthalen-2-ol Schiff Base. *Journal of Molecular Structure*, **1183**: 190–201. https://doi.org/10.1016/j.molstruc.2019.01.083

Al-Mohaimeed, A. M., Al-Farraj, E. S., Al-Onazi, W. A., Alothman, A. A., & Almarhoon, Z. M. (2020). Synthesis, Characterization, Density Functional Theory, Thermal, Antimicrobial Efficacy, and DNA Binding/Cleavage Studies of Cu(II), Cr(III), Fe(III), Ni(II), Co(II), Zn(II), and Pt(IV) Complexes with A Derivative of 2-Hydroxyphenoxymethylfuran-5-Carbalde. *Journal of the Chinese Chemical Society,* **67**(11): 2100-2117. https://doi.org/10.1002/jccs.202000042

Alaghaz, A.-N. M. A., Zayed, M. E., & Alharbi, S. A. (2015). Synthesis, Spectral Characterization, Molecular Modeling and Antimicrobial Studies of Tridentate Azo-Dye Schiff Base Metal Complexes. *Journal of Molecular Structure*, **1084**:

36–45. https://doi.org/10.1016/j.molstruc.2014.12.013

Alharbi, A., Alzahrani, S., Alkhatib, F., Abu Al-Ola, K., Abdulaziz Alfi, A., Zaky, R., & El-Metwaly, N. M. (2021). Studies on New Schiff Base Complexes Synthesized from d^{10} Metal Ions: Spectral, Conductometric Measurements, DFT and Docking Simulation. *Journal of Molecular Liquids*, **334**: 116148. https://doi.org/10.1016/j.molliq.2021.116148

Ali, I., Wani, W. A., & Saleem, K. (2013). Empirical Formulae to Molecular Structures of Metal Complexes by Molar Conductance. *Synthesis and Reactivity in Inorganic, Metal-Organic and Nano-Metal Chemistry*, **43**(9): 1162–1170. https://doi.org/10.1080/15533174.2012.756898

Ali, O. A. M., El-Medani, S. M., Abu Serea, M. R., & Sayed, A. S. S. (2015). Unsymmetrical Schiff Base (ON) Ligand on Complexation with Some Transition Metal Ions: Synthesis, Spectral Characterization, Antibacterial, Fluorescence and Thermal Studies. *Spectrochimica Acta - Part A: Molecular and Biomolecular Spectroscopy*, **136**: 651–660. https://doi.org/10.1016/j.saa.2014.09.079

Aljahdali, M. S., Abedelkarim, A. T., El-Sherif, A. A., & Ahmed, M. M. (2014). Synthesis, Characterization, Equilibrium Studies, and Biological Activity of Complexes Involving Copper(II), 2-Aminomethylthiophenyl-4-Bromosalicylaldehyde Schiff Base, and Selected Amino Acids. *Journal of Coordination Chemistry*, **67**(5): 870–890. https://doi.org/10.1080/00958972.2014.900549

Alkıs, M. E., Kelestemür, Ü., Alan, Y., Turan, N., & Buldurun, K. (2021). Cobalt and Ruthenium Complexes with Pyrimidine Based Schiff Base: Synthesis, Characterization, Anticancer Activities and Electrochemotherapy Efficiency. *Journal of Molecular Structure*, **1226**: 129402. https://doi.org/10.1016/j.molstruc.2020.129402

Almasi, M., Vilková, M., & Bednarčík, J. (2021). Synthesis, Characterization and Spectral Properties of Novel Azo-Azomethinetetracarboxylic Schiff Base Ligand and Its Co(II), Ni(II), Cu(II) and Pd(II) Complexes. *Inorganica Chimica Acta,* **515**: 120064. https://doi.org/10.1016/j.ica.2020.120064

Alothman, A. A., Al-Farraj, E. S., Al-Onazi, W. A., Almarhoon, Z. M., & Al-Mohaimeed, A. M. (2020). Spectral Characterization, Electrochemical,

Antimicrobial and Cytotoxic Studies on New Metal(II) Complexes Containing N_2O_4 Donor Hexadentate Schiff Base Ligand. *Arabian Journal of Chemistry,* **13**(2): 3889-3902. https://doi.org/10.1016/j.arabjc.2019.02.003

Alshaheri, A. A., Tahir, M. I. M., Rahman, M. B. A., Begum, T., & Saleh, T. A. (2017). Synthesis, Characterisation and Catalytic Activity of Dithiocarbazate Schiff Base Complexes in Oxidation of Cyclohexane. *Journal of Molecular Liquids,* **240**: 486-496. https://doi.org/10.1016/j.molliq.2017.05.081

Alshater, H., El-Boraey, H. A., Homoda, A. M. A., & EL-Gammal, O. A. (2021). Improving the Surface Morphology and Crystallite Size of Isonicotinohydrazide Based Binuclear Cr(III), Zn(II) and Sn(IV) Complexes after Irradiation with γ-Rays. *Journal of Molecular Structure*, **1232**: 129985. https://doi.org/10.1016/ j.molstruc.2021.129985

Alturiqi, A. S., Al-Farraj, E. S., Anazy, M. M., & Ammar, R. A. (2020). Synthesis, Structural Identification, DNA Interaction and Biological Studies of Divalent Metal(II) Chelates of 1,2- Ethenediamine Schiff Base Ligand. *Journal of Molecular Structure*, **1219**: 128542. https://doi.org/10.1016/j.molstruc.2020.128542

Ammar, Y. A., El-Hafez, S. M. A. A., Hessein, S. A., Ali, A. M., Askar, A. A., & Ragab, A. (2021). One-Pot Strategy for Thiazole Tethered 7-Ethoxy Quinoline Hybrids: Synthesis and Potential Antimicrobial Agents as Dihydrofolate Reductase (DHFR) Inhibitors with Molecular Docking Study. *Journal of Molecular Structure*, **1242**: 130748. https://doi.org/10.1016/j.molstruc. 2021.130748

Anacona, J. R., Mago, K., & Camus, J. (2018). Antibacterial Activity of Transition Metal Complexes with a Tridentate NNO Amoxicillin Derived Schiff Base. Synthesis and Characterization. *Applied Organometallic Chemistry*, **32**(7): e4374. https://doi.org/10.1002/aoc.4374

Anacona, J. R., Noriega, N., & Camus, J. (2015). Synthesis, Characterization and Antibacterial Activity of a Tridentate Schiff Base Derived from Cephalothin and Sulfadiazine, and Its Transition Metal Complexes. *Spectrochimica Acta - Part A: Molecular and Biomolecular Spectroscopy,* **137**:16-22. https://doi.org/10.1016/ j.saa.2014.07.091

Anacona, J. R., Santaella, J., Al-shemary, R. K. R., Amenta, J., Otero, A., Ramos, C., & Celis, F. (2021). Ceftriaxone-Based Schiff Base Transition Metal(II) Complexes. Synthesis, Characterization, Bacterial Toxicity, and DFT Calculations. Enhanced Antibacterial Activity of a Novel Zn(II) Complex against S. Aureus and E. Coli. *Journal of Inorganic Biochemistry*, **223**: 111519. https://doi.org/10.1016/j.jinorgbio.2021.111519

Andiappan, K., Sanmugam, A., Deivanayagam, E., Karuppasamy, K., Kim, H. S., & Vikraman, D. (2019). Schiff Base Rare Earth Metal Complexes: Studies on Functional, Optical and Thermal Properties and Assessment of Antibacterial Activity. *International Journal of Biological Macromolecules*, **124**: 403–410. https://doi.org/10.1016/j.ijbiomac.2018.11.251

Arunadevi, A., Porkodi, J., Ramgeetha, L., & Raman, N. (2019). Biological Evaluation, Molecular Docking and DNA Interaction Studies of Coordination Compounds Gleaned from a Pyrazolone Incorporated Ligand. *Nucleosides, Nucleotides and Nucleic Acids*, **38**(9): 5656–5679. https://doi.org/10.1080/15257770.2019.1597975

Arunadevi, A., & Raman, N. (2020). Biological Response of Schiff Base Metal Complexes Incorporating Amino Acids–A Short Review. *Journal of Coordination Chemistry,* **73**(15): 2095-2116. https://doi.org/10.1080/00958972.2020.1824293

Ashok, U. P., Kollur, S. P., Arun, B. P., Sanjay, C., Suresh, K. S., Anil, N., Vasant Baburao, H., Markad, D., Ortega Castro, J., Flores-Holguin, N., & Glossman-Mitnik, D. (2020). In Vitro Anticancer Activity of 4(3H)-Quinazolinone Derived Schiff Base and Its Cu(II), Zn(II) and Cd(II) Complexes: Preparation, X-Ray Structural, Spectral Characterization and Theoretical Investigations. *Inorganica Chimica Acta,* **511**: 119846. https://doi.org/10.1016/j.ica.2020.119846

Bahron, H., Khaidir, S. S., Tajuddin, A. M., Ramasamy, K., & Yamin, B. M. (2019). Synthesis, Characterization and Anticancer Activity of Mono- and Dinuclear Ni(II) and Co(II) Complexes of a Schiff Base Derived from O-Vanillin. *Polyhedron*, **161**: 84–92. https://doi.org/10.1016/j.poly.2018.12.055

Bar, N., Chowdhury, P., Roy, D., Adhikari, S., Mondal, S., Das, G. K., & Chandra, S. K. (2021). Photochromism of Dye Containing Schiff Base-Metal Complex: A

Revisit through Spectro-Kinetic, Thermodynamic and Theoretical Analyses for the Design of a Molecular Logic Gate. *Journal of Photochemistry and Photobiology A: Chemistry*, **420**: 113505. https://doi.org/10.1016/j.jphotochem.2021.113505

Bargujar, S., Chandra, S., Chauhan, R., Rajor, H. K., & Bhardwaj, J. (2017). Synthesis, Spectroscopic Evaluation, Molecular Modelling, Thermal Study and Biological Evaluation of Manganese(II) Complexes Derived from Bidentate N,O and N,S Donor Schiff Base Ligands. *Applied Organometallic Chemistry*, **32**(3): e4149. https://doi.org/10.1002/aoc.4149

Bayeh, Y., Mohammed, F., Gebrezgiabher, M., Elemo, F., Getachew, M., & Thomas, M. (2020). Synthesis, Characterization and Antibacterial Activities of Polydentate Schiff Bases, Based on Salicylaldehyde. *Advances in Biological Chemistry*, **10**: 127–139. https://doi.org/10.4236/abc.2020.105010

Bedair, M. A., Soliman, S. A., Bakr, M. F., Gad, E. S., Lgaz, H., Chung, I. -Min., Salama, M., & Alqahtany, F. Z. (2020). Benzidine-Based Schiff Base Compounds for Employing as Corrosion Inhibitors for Carbon Steel in 1.0 M HCl Aqueous Media by Chemical, Electrochemical and Computational Methods. *Journal of Molecular Liquids*, **317**: 114015. https://doi.org/10.1016/j.molliq.2020.114015

Bedir, A. G., Abd El-Raouf, M., Abdel-Mawgoud, S., Negm, N. A., & El Basiony, N. M. (2021). Corrosion Inhibition of Carbon Steel in Hydrochloric Acid Solution Using Ethoxylated Nonionic Surfactants Based on Schiff Base: Electrochemical and Computational Investigations. *ACS Omega*, **6**(6): 4300–4312. https://doi.org/10.1021/acsomega.0c05476

Belal, A. A. M., El-Deen, I. M., Farid, N. Y., Zakaria, R., & Refat, M. S. (2015). Synthesis, Spectroscopic, Coordination and Biological Activities of Some Transition Metal Complexes Containing ONO Tridentate Schiff Base Ligand. *Spectrochimica Acta Part A: Molecular and Biomolecular Spectroscopy*, **149**: 771–787. https://doi.org/10.1016/j.saa.2015.05.005

Bhaskar, R. S., Ladole, C. A., Salunkhe, N. G., Barabde, J. M., & Aswar, A. S. (2020). Synthesis, Characterization and Antimicrobial Studies of Novel ONO Donor Hydrazone Schiff Base Complexes with Some Divalent Metal (II) Ions.

Arabian Journal of Chemistry, **13**(8): 6559-6567. https://doi.org/10.1016/j.arabjc.2020.06.012

Bhattarai, A. (2015). Studies of the Micellization of Cationic–Anionic Surfactant Systems in Water and Methanol–Water. *Journal of Solution Chemistry*, **44**(10): 2090–2105. https://doi.org/10.1007/s10953-015-0391-4

Bouzerafa, B., Aggoun, D., Ouennoughi, Y., Ourari, A., Ruiz-Rosas, R., Morallon, E., & Mubarak, M. S. (2017). Synthesis, Spectral Characterization and Study of Thermal Behavior Kinetics by Thermogravimetric Analysis of Metal Complexes Derived from Salicylaldehyde and Alkylamine. *Journal of Molecular Structure*, **1142**: 48–57. https://doi.org/10.1016/j.molstruc.2017.04.029

Bruch, M. D. (1996). *NMR Spectroscopy Techniques*. CRC Press. https://doi.org/10.1201/9781482273311

Buldurun, K. (2019). Synthesis,Characterization, Thermal Study and Optical Property Evaluation of Co(II), Pd(II) Complexes Containing Schiff Bases of Thiophene-3-Carboxylate Ligand. *Journal of Electronic Materials*, **49**(3): 1935–1943. https://doi.org/10.1007/s11664-019-07876-2

Buldurun, K., & Özdemir, M. (2020). Ruthenium(II) Complexes with Pyridine-Based Schiff Base Ligands: Synthesis, Structural Characterization and Catalytic Hydrogenation of Ketones. *Journal of Molecular Structure,* **1202**: 127266. https://doi.org/10.1016/j.molstruc.2019.127266

Buldurun, K., Turan, N., Bursal, E., Aras, A., Mantarcı, A., Çolak, N., Turkan, F., & Gülçin, İ. (2020). Synthesis, Characterization, Powder X-Ray Diffraction Analysis, Thermal Stability, Antioxidant Properties and Enzyme Inhibitions of M(II)-Schiff Base Ligand Complexes. *Journal of Biomolecular Structure and Dynamics*, **39**(17): 6480-6487. https://doi.org/10.1080/07391102.2020.1802340

Caleb Noble Chandar, S., Sangeetha, D., & Arumugham, M. N. (2013). Octadecylamine Cobalt(III) Dimethyl Glyoximato Complexes: Synthesis, Thermodynamics of Micellization, Steady-State Photolysis and Biological Activities. *Transition Metal Chemistry*, **39**(2), 159–165. https://doi.org/10.1007/s11243-013-9785-6

Calu, L., Badea, M., Chifiriuc, M. C., Bleotu, C., David, G. I., Ioniţa, G., Marutescu, L., Lazar, V., Stanica, N., Soponaru, I., Marinescu, D., & Olar, R. (2014). Synthesis, Spectral, Thermal, Magnetic and Biological Characterization of Co(II), Ni(II), Cu(II) And Zn(II) Complexes with a Schiff Base Bearing a 1,2,4-Triazole Pharmacophore. *Journal of Thermal Analysis and Calorimetry*, **120**(1): 375–386. https://doi.org/10.1007/s10973-014-3970-5

Canpolat, E., & Kaya, M. (2005). Studies on Mononuclear Chelates Derived from Substituted Schiff Base Ligands: Synthesis and Characterization of a New 5-Methoxysalicyliden-P-Aminoacetophenoneoxime and Its Complexes with Co(II), Ni(II), Cu(II), And Zn(II). *Russian Journal of Coordination Chemistry*, **31**(11): 790–794.

Cen, B., Duan, Y. X., Deng, L. Q., Wang, Y. L., Tao, X., & Shen, Y. -Z. (2018). Synthesis and Structure Characterization of Homoleptic Lanthanide Complexes Stabilized by Schiff-Base Ligands and their Application in the Polymerization of ε-Caprolactone. *Journal of Organometallic Chemistry,* **857**: 191-199. https://doi.org/10.1016/j.jorganchem.2017.12.002

Chafiq, M., Chaouiki, A., Lgaz, H., Salghi, R., Gaonkar, S. L., Bhat, K. S., Marzouki, R., Ali, I. H., Khan, M. I., Shimizu, H., & Chung, I. -M. (2019). Synthesis and Corrosion Inhibition Evaluation of a New Schiff Base Hydrazone for Mild Steel Corrosion in HCl Medium: Electrochemical, DFT, and Molecular Dynamics Simulations Studies. *Journal of Adhesion Science and Technology*, **34**(12): 1283–1314. https://doi.org/10.1080/01694243.2019.1707561

Chai, J., Wu, Y., Yang, B., & Liu, B. (2018). The Photochromism, Light Harvesting and Self-Assembly Activity of a Multi-Function Schiff-Base Compound Based on the AIE Effect. *Journal of Materials Chemistry C*, **6**(15): 4057–4064. https://doi.org/10.1039/c8tc00509e

Chandar, S. C. N., Santhakumar, K., & Arumugham, M. N. (2009). Metallosurfactant Schiff Base Cobalt(III) Coordination Complexes. Synthesis, Characterization, Determination of CMC Values and Biological Activities. *Transition Metal Chemistry*, **34**(8): 841–848. https://doi.org/10.1007/s11243-009-9272-2

Chandrasekar, T., Arunadevi, A., & Raman, N. (2021). Synthesis, Spectral Characterization, DNA-Binding and Antimicrobial Profile of Biological Active

164

Mixed Ligand Schiff Base Metal(II) Complexes Incorporating 1,8-Diaminonaphthalene. *Journal of Coordination Chemistry*, **74**(4–6): 804–822. https://doi.org/10.1080/00958972.2020.1870967

Chasapis, C. T., Ntoupa, P. S. A., Spiliopoulou, C. A., & Stefanidou, M. E. (2020). Recent Aspects of the Effects of Zinc on Human Health. *Archives of Toxicology*, **94**(5): 1443–1460. https://doi.org/10.1007/s00204-020-02702-9

Chaudhary, N. K., Guragain, B., Chaudhary, A., & Chaudhary, S. K. (2021). Heteroleptic Cadmium Complex of Glimepiride–Metformin Mixed Ligand: Synthesis, Characterization, and Antibacterial Study. *Chemical Papers*, **75**(7): 3215–3226. https://doi.org/10.1007/s11696-021-01535-9

Chauhan, D. S., Mazumder, M. A. J., Quraishi, M. A., & Ansari, K. R. (2020). Chitosan-Cinnamaldehyde Schiff Base : A Bioinspired Macromolecule as Corrosion Inhibitor for Oil and Gas Industry. *International Journal of Biological Macromolecules*, **158**: 127–138. https://doi.org/10.1016/j.ijbiomac.2020.04.200

Chaurasia, M., Tomar, D., & Chandra, S. (2019). Synthesis, Spectral Characterization, and DNA Binding Studies of Co(II), Ni(II), Cu(II) and Zn(II) Complexes of Schiff Base 2-((1H-1,2,4-Triazol-3-ylimino)methyl)-5-Methoxyphenol. *Journal of Molecular Structure,* **1179**: 431-442. https://doi.org/10.1016/j.molstruc.2018.11.027

Chowdhury, S., Rakshit, A., Acharjee, A., & Saha, B. (2019). Novel Amphiphiles and Their Applications for Different Purposes with Special Emphasis on Polymeric Surfactants. *Chemistry Select*, **4**(23): 6978–6995. https://doi.org/10.1002/slct.201901160

Coats, A., & Redfern, J. P. (1963). Thermogravimetric Analysis. *The Analyst*, **88**(1053): 906. https://doi.org/10.1039/AN9638800906

Croitor, L., Cocu, M., Bulhac, I., Bourosh, P. N., Ch. Kravtsov, V., Petuhov, O., & Danilescu, O. (2021). Evolution from Discrete Mononuclear Complexes to Trinuclear Linear Cluster and 2D Coordination Polymers of Mn(II) with Dihydrazone Schiff Bases: Preparation, Structure and Thermal Behavior. *Polyhedron*, **206**: 115329. https://doi.org/10.1016/j.poly.2021.115329

Cui, Y., Qiao, L., Li, Y., Jing, H., Li, Y., & Wang, Q. (2016). Synthesis, Solid-State

Structures, and Urease Inhibition Activities of New Copper(II) Complexes Based on O,N,O-Tridentate Schiff Bases. *Journal of Coordination Chemistry*, **69**(15): 2318–2328. https://doi.org/10.1080/00958972.2016.1206199

De Blasio, C. (2019). Experimental Methods in Chemical Engineering: Thermogravimetric Analysis—TGA. *Fundamentals of Biofuels Engineering and Technology.* 91–102. https://doi.org/10.1007/978-3-030-11599-9_7

Deboucha, W., Leklou, N., Khelidj, A., & Oudjit, M. N. (2017). Thermogravimetric Analysis (TGA). *Construction and Building Materials*, **146**: 687–701. https://doi.org/10.1016/j.conbuildmat.2017.04.132

Devi, J., Yadav, M., Kumar, D., Naik, L. S., & Jindal, D. K. (2019). Some Divalent Metal(II) Complexes of Salicylaldehyde-Derived Schiff Bases: Synthesis, Spectroscopic Characterization, Antimicrobial and In Vitro Anticancer Studies. *Applied Organometallic Chemistry*, **33**(2): 1–22. https://doi.org/10.1002/aoc.4693

Dhanaraj, C. J., & Jebapriya, M. (2020). Metal Schiff Base Complexes of Tridentate Antipyrine Based Ligand: Synthesis, Spectral Characterisation, Image Analysis and Biological Studies. *Journal of Molecular Structure*, **1220**: 128596. https://doi.org/10.1016/j.molstruc.2020.128596

Dhanaraj, C. J., & Johnson, J. (2015). Spectral, Thermal, Electrochemical, Biological and DFT Studies on Nanocrystalline Co(II), Ni(II), Cu(II) and Zn(II) Complexes with a Tridentate ONO Donor Schiff Base Ligand. *Journal of Coordination Chemistry*, **68**(14): 2449–2469. https://doi.org/10.1080/00958972.2015.1051475

Dhanaraj, C. J., & Raj, S. S., S. (2021). Co(II), Ni(II), Cu(II) and Zn(II) Complexes of 4-Aminoantipyrine Derived Schiff Base. Synthesis, Structural Elucidation, Thermal, Biological Studies. Photo Catalytic Activity. *Journal of Heterocyclic Chemistry,* **58**(4): 928-941. https://doi.org/10.1002/jhet.4209

Diab, M. A., Mohamed, G. G., Mahmoud, W. H., El-Sonbati, A. Z., Morgan, S. M., & Abbas, S. Y. (2019). Inner Metal Complexes of Tetradentate Schiff Base: Synthesis, Characterization, Biological Activity and Molecular Docking Studies. *Applied Organometallic Chemistry,* **33**(7). https://doi.org/10.1002/aoc.4945

Dineshkumar, S., & Muthusamy, A. (2015). Synthesis and Spectral Characterization

of Cross Linked Rigid Structured Schiff Base Polymers : Effect of Substituent Position Changes on Optical , Electrical and Thermal Properties. *Polymer-Plastics Technology and Engineering,* **55**(4): 368-378. https://doi.org/10.1080/03602559.2015.1098680

El-Boraey, H. A., & El-Salamony, M. A. (2018). Transition Metal Complexes with Polydentate Ligand: Synthesis, Characterization, 3D Molecular Modelling, Anticancer, Antioxidant and Antibacterial Evaluation. *Journal of Inorganic and Organometallic Polymers and Materials*, **29**(3): 684–700. https://doi.org/10.1007/s10904-018-1042-1

El-Gammal, O. A., Mohamed, F. S., Rezk, G. N., & El-Bindary, A. A. (2021). Structural Characterization and Biological Activity of a New Metal Complexes Based of Schiff Base. *Journal of Molecular Liquids*, **330**: 115522. https://doi.org/10.1016/j.molliq.2021.115522

El-Megharbel, S. M., Megahed, A. S., & Refat, M. S. (2016). Preparation, Physical and Chemical Studies on Metal Complexes of Schiff Bases as a Nucleus Key to Prepare Nanometer Oxides have Catalytic Applications: Nickel (II) Complexes Derived from 4-Aminoantipyrine Derivatives. *Journal of Molecular Liquids*, **216**: 608–614. https://doi.org/10.1016/j.molliq.2016.01.097

El-Razek, S. E. A., El-Gamasy, S. M., Hassan, M., Abdel-Aziz, M. S., & Nasr, S. M. (2019). Transition Metal Complexes of a Multidentate Schiff Base Ligand Containing Guanidine Moiety: Synthesis, Characterization, Anti-Cancer Effect, and Anti-Microbial Activity. *Journal of Molecular Structure,* **1203**:127381. https://doi.org/10.1016/j.molstruc.2019.127381

El-Shwiniy, W. H., Ibrahim, A. G., Sadeek, S. A., & Zordok, W. A. (2021). Synthesis, Structural Elucidation, Molecular Modeling and Antimicrobial Studies of 6-(2-Hydroxyphenylimine)- 2-Thioxotetrahydropyrimidin-4(1H)-one (L) Schiff Base Metal Complexes. *Applied Organometallic Chemistry*, **35**(5). https://doi.org/10.1002/aoc.6174

El-Hamid, S. M. A., Sadeek, S. A., & El-Lattif, N. S. A. (2019). Study of The Chemical Structure and Their Nematicidal Activity of N_2O_2 Tetradentate Schiff Base Metal Complexes. *Applied Organometallic Chemistry*,**33**(8). https://doi.org/10.1002/aoc.5010

El-Sonbati, A.Z., Mahmoud, W.H., Mohamed, G., G., Diab, M. A., Morgan, Sh. M., & Abbas, S. Y. (2019). Synthesis, Characterization of Schiff Base Metal Complexes and Their Biological Investigation. *Applied Organometallic Chemistry*. e5048. https://doi.org/10.1002/aoc.5048

Elsayed, S. A., El-Gharabawy, H. M., Butler, I. S., & Atlam, F. M. (2020). Novel Metal Complexes of 3-Acetylcoumarin-2-Hydrazinobenzothiazole Schiff Base: Design, Structural Characterizations, DNA Binding, DFT Calculations, Molecular Docking and Biological Studies. *Applied Organometallic Chemistry*, **34**(6). https://doi.org/10.1002/aoc.5643

Elsayed, S. A., Saad, E. M., Butler, I. S., & Mostafa, S. I. (2018). 2-Hydroxynaphthaldehyde Chitosan Schiff-Base; New Complexes, Biosorbent to Remove Cadmium(II) Ions from Aqueous Media and Aquatic Ecotoxicity Against Green Alga Pseudokirchneriella Subcapitata. *Journal of Environmental Chemical engineering*, **6**(2): 3451–3468. https://doi.org/10.1016/j.jece.2017.12.051

Elsenety, M. M., Elsayed, B. A., Ibrahem, I. A., & Bedair, M. A. (2020). Photophysical, DFT and Molecular Docking Studies of Sm(III) and Eu(III) Complexes of Newly Synthesized Coumarin Ligand. *Inorganic Chemistry Communications*, **121**: 108213. https://doi.org/10.1016/j.inoche.2020.108213

Emam, S. M., AbouEl-Enein, S. A., & Emara, E. M. (2017). Spectroscopic Studies and Thermal Decomposition for (Bis-((E)-2-(4-Ethylphenylimino)-1,2-Diphenylethanone) Schiff Base and Its Co(II), Ni(II), Cu(II), Zn(II) and Cd(II) Complexes Prepared by Direct and Template Reactions. *Journal of Thermal Analysis and Calorimetry*, **127**(2): 1611–1630. https://doi.org/10.1007/s10973-016-5835-6

Fabbrizzi, L. (2020). Beauty in Chemistry: Making Artistic Molecules with Schiff Bases. *The Journal of Organic Chemistry*, **85**(19): 12212–12226. https://doi.org/10.1021/acs.joc.0c01420

Fan, Z., Huang, J., Huang, H., & Banerjee, S. (2021). Metal-Based Catalytic Drug Development for Next-Generation Cancer Therapy. *ChemMedChem*, **16**(16): 2480–2486. https://doi.org/10.1002/cmdc.202100297

Fathi, A. M., Mandour, H. S., & HassaneAnouar, E. (2021). Characteristics of Multidentate Schiff Base Ligand and Its Complexes Using Cyclic Voltammetry, Fluorescence, Antimicrobial Behavior and DFT-Calculations. *Journal of Molecular Structure*, **1224**: 129263. https://doi.org/10.1016/j.molstruc. 2020.129263

Fathima, S. S. A., Meeran, M. M. S., & Nagarajan, E. R. (2020). Synthesis, Characterization and Biological Evaluation of Novel 2,2′-((1,2-Diphenylethane-1,2-Diylidene)bis(Azanylylidene))bis(Pyridin-3-ol)and Metal Complexes: Molecular Docking and In Silico ADMET Profile. *Structural Chemistry*, **31**(2), 521–539. https://doi.org/10.1007/s11224-019-01425-7

Fekri, R., Salehi, M., Asadi, A., & Kubicki, M. (2017). DNA/BSA Interaction, Bio-Activity, Molecular Docking Simulation Study and Electrochemical Properties of Hydrazone Schiff Base Derived Cu(II)/Ni(II) Metal Complexes: Influence of the Nuclearity and Metal Ions. *Polyhedron*, **128**: 175–187. https://doi.org/ 10.1016/j.poly.2017.02.047

Fekri, R., Salehi, M., Asadi, A., & Kubicki, M. (2019). Synthesis, Characterization, Anticancer and Antibacterial Evaluation of Schiff Base Ligands Derived from Hydrazone and Their Transition Metal Complexes. *Inorganica Chimica Acta,* **484**: 245-254. https://doi.org/10.1016/j.ica.2018.09.022

Festus, C., Okafor, S. N., & Ekennia, A. C. (2019). Heteroleptic Metal Complexes of a Pyrimidinyl Based Schiff Base Ligand Incorporating 2,2′-Bipyridine Moiety: Synthesis, Characterization, and Biological Studies. *Frontiers in Chemistry*, **7**. 1-12. https://doi.org/10.3389/fchem.2019.00862

Fetoh, A., Asla, K. A., El-Sherif, A. A., El-Didamony, H., & Abu El-Reash, G. M. (2019). Synthesis, Structural Characterization, Thermogravimetric, Molecular Modelling and Biological Studies of Co(II) and Ni(II) Schiff Bases Complexes. *Journal of Molecular Structure,* **1178**: 524-537. https://doi.org/10.1016/ j.molstruc.2018.10.066

Frei, A., Zuegg, J., Elliott, A. G., Baker, M., Braese, S., Brown, C., Chen, F., G. Dowson, C., Dujardin, G., Jung, N., King, A. P., Mansour, A. M., Massi, M., Moat, J., Mohamed, H. A., Renfrew, A. K., Rutledge, P. J., Todd, M. H.,Willans, C. E., Wilson, J. J., Cooper, M. A., & Blaskovich, M. A. T. (2020). Metal

Complexes as a Promising Source for New Antibiotics. *Chemical Science*, **11**(10): 2627-2639. https://doi.org/10.1039/C9SC06460E

Gaber, M., El-Ghamry, H. A., Fathalla, S. K., & Mansour, M. A. (2018). Synthesis, Spectroscopic, Thermal and Molecular Modeling Studies of Zn^{2+}, Cd^{2+} and UO_2^{2+} Complexes of Schiff Bases Containing Triazole Moiety. Antimicrobial, Anticancer, Antioxidant and DNA Binding Studies. *Materials Science and Engineering C*, **83**: 78–89. https://doi.org/10.1016/j.msec.2017.11.004

Gawali, I. T., & Usmani, G. A. (2019). Synthesis, Surface Active Properties and Applications of Cationic Gemini Surfactants from Triethylenetetramine. *Journal of Dispersion Science and Technology*, **41**(3): 450–460. https://doi.org/10.1080/01932691.2019.1584112

Ghanghas, P., Choudhary, A., Kumar, D., & Poonia, K. (2021). Coordination Metal Complexes with Schiff Bases: Useful Pharmacophores with Comprehensive Biological Applications. *Inorganic Chemistry Communications*, **130**: 108710. https://doi.org/10.1016/j.inoche.2021.108710

Ghosh, S. (2019). Cisplatin: The First Metal Based Anticancer Drug. *Bioorganic Chemistry*, **88**: 102925. https://doi.org/10.1016/j.bioorg.2019.102925

Gondia, N. K., & Sharma, S. K. (2018). Spectroscopic Characterization and Photophysical Properties of Schiff Base Metal Complex. *Journal of Molecular Structure,* **1171**: 619-625. https://doi.org/10.1016/j.molstruc.2018.06.010

Hameed, A., Al-Rashida, M., Uroos, M., Abid Ali, S., & Khan, K. M. (2017). Schiff Bases in Medicinal Chemistry: A Patent Review (2010-2015). *Expert Opinion on Therapeutic Patents*, **27**(1): 63–79. https://doi.org/10.1080/13543776.2017.1252752

Hasan, M., Ahsan, H., Saha, P., Naime, J., Kumar Das, A., Asraf, Md. A., & Nazmul Islam, A. B. M. (2021). Antioxidant , Antibacterial and Electrochemical Activity of (E)-N-(4 (dimethylamino) benzylidene)-4H-1,2,4-triazol-4-amine Ligand and Its Transition Metal Complexes. *Results in Chemistry*, **3**: 100115. https://doi.org/10.1016/j.rechem.2021.100115

Hashem, H. E., Mohamed, E. A., Farag, A. A., Negm, N. A., & Azmy, E. A. M. (2021). New Heterocyclic Schiff Base-Metal Complex: Synthesis,

Characterization, Density Functional Theory Study, and Antimicrobial Evaluation. *Applied Organometallic Chemistry,* **35**(9). https://doi.org/10.1002/aoc.6322

Hegazy, M. A., El-Etre, A. Y., El-Shafaie, M., & Berry, K. M. (2015). Novel Cationic Surfactants for Corrosion Inhibition of Carbon Steel Pipelines in Oil and Gas Wells Applications. *Journal of Molecular Liquids*, **214**: 347–356. https://doi.org/10.1016/j.molliq.2015.11.047

Hoskins, B. F., & Whillans, F. D. (1973). The Geometry of Pentacoordinate Complexes. *Coordination Chemistry Reviews*, **9**(3–4): 365–388. https://doi.org/10.1016/S0010-8545(00)82083-4

Hossain, M. S., Roy, P. K., Zakaria, C., & Kudrat-E-Zahan, M. (2018). Selected Schiff Base Coordination Complexes and Their Microbial Application: A Review. *International Journal of Chemical Studies*, **6**(1): 19–31.

Howsaui, H. B., Sharfalddin, A. A., Abdellattif, M. H., Basaleh, A. S., & Hussien, M. A. (2021). Synthesis, Spectroscopic Characterization and Biological Studies of Mn(II), Cu(II), Ni(II), Co(II) and Zn(II) Complexes with New Schiff Base of 2-((Pyrazine-2-Ylimino)Methyl)Phenol. *Applied Sciences,* **11**(19): 9067. https://doi.org/10.3390/app11199067

Hutchings, M., Truman, A., & Wilkinson, B. (2019). Antibiotics: Past, Present and Future. *Current Opinion in Microbiology,* **51**: 72-80. https://doi.org/10.1016/j.mib.2019.10.008

Iftikhar, B., Javed, K., Khan, M. S. U., Akhter, Z., Mirza, B., & Mckee, V. (2018). Synthesis, Characterization and Biological Assay of Salicylaldehyde Schiff Base Cu(II) Complexes and Their Precursors. *Journal of Molecular Structure*, **1155**: 337–348. https://doi.org/10.1016/j.molstruc.2017.11.022

Ikram, M., Rehman, S., Khan, A., Baker, R. J., Hofer, T. S., Subhan, F., Qayum, M., Faridoon, & Schulzke, C. (2015). Synthesis, Characterization, Antioxidant and Selective Xanthine Oxidase Inhibitory Studies of Transition Metal Complexes of Novel Amino Acid Bearing Schiff Base Ligand. *Inorganica Chimica Acta*, **428**: 117–126. https://doi.org/10.1016/j.ica.2015.01.021

Inkson, B. J. (2016). Scanning Electron Microscopy (SEM) and Transmission

Electron Microscopy (TEM) for Materials Characterization. *Materials Characterization Using Nondestructive Evaluation (NDE) Methods*. 17-43. https://doi.org/10.1016/B978-0-08-100040-3.00002-X

Ismail, B. A., Nassar, D. A., Abd El–Wahab, Z. H., & Ali, O. A. M. (2021). Synthesis, Characterization, Thermal, DFT Computational Studies and Anticancer Activity of Furfural-type Schiff Base Complexes. *Journal of Molecular Structure*, **1227**: 129393. https://doi.org/10.1016/j.molstruc. 2020.129393

Jiang, G. Q., Wang, R., Long, L. L., Sun, T., Yang, Z. C., Zhang, Y. Q., & Zhang, Q. -J. (2016). Versatile Coordination Behaviors of a Tetrapodal Schiff Base Ligand Scaffold: Formation of The Dinuclear and Trinuclear Complexes and Their Antimicrobial Activity. *Journal of Coordination Chemistry,* **69**(4): 678-686. https://doi.org/10.1080/00958972.2015.1129057

John, L., Dasan, A., Joseyphus, R. S., & Joe, I. H. (2019). Molecular Docking, Structural Characterization, DFT and Cytotoxicity Studies of Metal(II) Schiff Base Complexes Derived from Thiophene-2-Carboxaldehyde and L-Histidine. *Journal of Molecular Structure*, **1198**: 126934. https://doi.org/10.1016/ j.molstruc.2019.126934

Joshi, R., Kumari, A., Singh, K., Mishra, H., & Pokharia, S. (2020). Triorganotin(IV) Complexes of Schiff Base Derived from 1,2,4-Triazole Moiety: Synthesis, Spectroscopic Investigation, DFT Studies, Antifungal Activity and Molecular Docking Studies. *Journal of Molecular Structure*, **1206**: 127639. https://doi.org/10.1016/j.molstruc.2019.127639

Kaban, S., & Fidaner, Z. (1990). Synthesis of Schiff Bases by Condensation of Hetarylearboxaldehydes with P-phenetidine. *Monatshefte Fur Chemie Chemical Monthly*, **121**(6-7): 525–528. https://doi.org/10.1007/BF00810861

Kang, M., Oderinde, O., Han, X., Fu, G., & Zhang, Z. (2021). Development of Oxidized Hydroxyethyl Cellulose-Based Hydrogel Enabling Unique Mechanical, Transparent and Photochromic Properties for Contact Lenses. *International Journal of Biological Macromolecules*, **183**: 1162–1173. https://doi.org/10.1016/ j.ijbiomac.2021.05.029

Kareem, A., Laxmi, Arshad, M., Nami, S. A. A., & Nishat, N. (2016). Herbo-Mineral

Based Schiff Base Ligand and Its Metal Complexes: Synthesis, Characterization, Catalytic Potential and Biological Applications. *Journal of Photochemistry and Photobiology B: Biology*, **160**: 163–171. https://doi.org/10.1016/j.jphotobiol.2016.03.030

Kareem, M. J., Al-Hamdani, A. A. S., Jirjees, V. Y., Khan, M. E., Allaf, A. W., & Al Zoubi, W. (2020). Preparation, Spectroscopic Study of Schiff Base Derived from Dopamine and Metal Ni(II), Pd(II), And Pt(IV) Complexes, and Activity Determination as Antioxidants. *Journal of Physical Organic Chemistry*, **34**(3). https://doi.org/10.1002/poc.4156

Kargar, H., Ardakani, A. A., Tahir, M. N., Ashfaq, M., & Munawar, K. S. (2021a). Synthesis, Spectral Characterization, Crystal Structure and Antibacterial Activity of Nickel(II), Copper(II) and Zinc(II) Complexes Containing ONNO Donor Schiff Base Ligands. *Journal of Molecular Structure*, **1233**: 130112. https://doi.org/10.1016/j.molstruc.2021.130112

Kargar, H., Ardakani, A. A., Tahir, M. N., Ashfaq, M., & Munawar, K. S. (2021b). Synthesis, Spectral Characterization, Crystal Structure Determination and Antimicrobial Activity of Ni(II), Cu(II) and Zn(II) Complexes with the Schiff Base Ligand Derived from 3,5-Dibromosalicylaldehyde. *Journal of Molecular Structure*, **1229**: 129842. https://doi.org/10.1016/j.molstruc.2020.129842

Kargar, H., Bazrafshan, M., Fallah-Mehrjardi, M., Behjatmanesh-Ardakani, R., Rudbari, H. A., Munawar, K. S., Ashfaq, M., & Tahir, M. N. (2021). Synthesis, Characterization, Crystal Structures, Hirshfeld Surface Analysis, DFT Computational Studies and Catalytic Activity of Novel Oxovanadium and Dioxomolybdenum Complexes with ONO Tridentate Schiff Base Ligand. *Polyhedron*, **202**: 115194. https://doi.org/10.1016/j.poly.2021.115194

Kargar, H., & Fallah-Mehrjardi, M. (2021). Novel Dioxomolybdenum Complexes Containing ONO-Tridentate Schiff Base Ligands Derived from 4-Aminobenzohydrazide: Synthesis, Spectral Characterization, and Application as Efficient Homogeneous Catalysts for Selective Sulfoxidation. *Journal of the Iranian Chemical Society*, **18**(12): 3443–3456. https://doi.org/10.1007/s13738-021-02282-0

Kargar, H., Fallah-Mehrjardi, M., Behjatmanesh-Ardakani, R., Munawar, K. S.,

Ashfaq, M., & Tahir, M. N. (2021). Synthesis, Spectral Characterization, SC-XRD, HSA, DFT and Catalytic Activity of Novel Dioxovanadium(V) Complex with Aminobenzohydrazone Schiff Base Ligand: An Experimental and Theoretical Approach. *Inorganica Chimica Acta*, **526**: 120535. https://doi.org/10.1016/j.ica.2021.120535

Kashyap, S., Kumar, S., Ramasamy, K., Lim, S. M., Shah, S. A. A., Om, H., & Narasimhan, B. (2018). Synthesis, Biological Evaluation and Corrosion Inhibition Studies of Transition Metal Complexes of Schiff Base. *Chemistry Central Journal*, **12**(1). https://doi.org/10.1186/s13065-018-0487-1

Kasselouri, S., Garoufis, A., Kalkanis, G., Perlepes, S. P., & Hadjiliadis, N. (1993). Complexes of Divalent Transition Metal Chlorides with the Tetradentate Schiff Base Ligand 1,2-Bis(2′-Pyridylmethyleneimino)-benzene. *Transition Metal Chemistry*, **18** (5): 531–536. https://doi.org/10.1007/BF00136621

Kaur, G., Garg, P., & Chaudhary, G. R. (2016). Role of Manganese Based Surfactant Towards Solubilization and Photo-Physical Properties of Fluorescein. *RSC Advances*, **6**(9): 7066–7077. https://doi.org/10.1039/C5RA24938D

Kaur, G., Garg, P., Kaur, B., Chaudhary, G. R., Kumar, S., Dilbaghi, N., Hassan, P. A., & Gawali, S. L. (2018). Cationic Double Chained Metallosurfactants: Synthesis, Aggregation, Cytotoxicity, Antimicrobial Activity and Their Impact on the Structure of Bovine Serum Albumin. *Soft Matter*, **14**(25): 5306–5318. https://doi.org/10.1039/C8SM00535D

Kavitha, A., Easwaramoorthy, D., Thangeeswari, T., Parthipan, G., Shanmugan, S., & Ansari, T. (2018). Synthesis and Characterization of Tritendate Schiff Base Rare Earth Nano Metal Complexes. *Materials Today: Proceedings,* **34**: 453-459. https://doi.org/10.1016/j.matpr.2020.02.663

Kavitha, B., Sravanthi, M., & Reddy, P. S. (2019). DNA Interaction , Docking , Molecular Modelling and Biological Studies of O-Vanillin Derived Schiff Base Metal Complexes. *Journal of Molecular Structure*, **1185**: 153–167. https://doi.org/10.1016/j.molstruc.2019.02.093

Keypour, H., Forouzandeh, F., Salehzadeh, S., Hajibabaei, F., Feizi, S., Karamian, R., Ghiasi, N., & Gable, R. W. (2019). DNA Binding Studies and Antibacterial Properties of a New Schiff Base Ligand Containing Homopiperazine and

Products of Its Reaction with Zn(II), Cu(II) and Co(II) Metal Ions: X-Ray Crystal Structure of Cu(II) and Zn(II) Complexes. *Polyhedron*, **170**: 584–592. https://doi.org/10.1016/j.poly.2019.06.023

Keypour, H., Mahmoudabadi, M., Shooshtari, A., Bayat, M., Ghassemzadeh, M., Hosseinzadeh, L., Mohsenzadeh, F., & Harms, K. (2017). Synthesis and Characterization of Two New N_4O_2 Macroacyclic Schiff-Base Ligands Containing Piperazine Moiety and Mononuclear Co(III) and Cu(II) Complexes, Spectral, X-Ray Crystal Structural, Theoretical Studies, Cytotoxic and Antibacterial Properties. *Polyhedron,* **129**: 189-198. https://doi.org/10.1016/j.poly.2017.03.035

Kheirkhahi, M., Shaabani, B., & Samadi Kafil, H. (2021). Calix[4]Arene-Based Thiosemicarbazide Schiff-Base Ligand and Its Transition Metal Complexes: Synthesis and Biological Assessment. *Journal of the Iranian Chemical Society*, **18**(12): 3429–3441. https://doi.org/10.1007/s13738-021-02281-1

Kuate, M., Conde, M. A., Mainsah, E. N., Paboudam, A. G., Tchieno, F. M. M., Ketchemen, K. I. Y., Tonle Kenfack, I., & Ndifon, P. T. (2020). Synthesis, Characterization, Cyclic Voltammetry, and Biological Studies of Co (II), Ni (II), and Cu (II) Complexes of a Tridentate Schiff Base, 1- ((E) - (2- Mercaptophenylimino) Methyl) Naphthalen-2-ol (H2 L1). *Journal of Chemistry*, **2020**: 1–21. https://doi.org/10.1155/2020/5238501

Kumar, M., Sodhi, K. K., Singh, P., Agrawal, P. K., & Singh, D. K. (2019). Synthesis and Characterization of Antibiotic-Metal Complexes [FeCl$_3$(L1)2H$_2$O and Ni(NO3)$_2$(L2)2H$_2$O] and Enhanced Antibacterial Activity. *Environmental Nanotechnology, Monitoring & Management*, **11**: 100209. https://doi.org/10.1016/j.enmm.2019.100209

Kumar, R., Paul, T., Jana, O., & Mani, G. (2016). Regioselective Mannich Bases of Pyrrole-2-Carbaldehyde and Binuclear Copper(II) Complexes of Bis(iminopyrrolyl) Ligand Containing the Piperazine Ring. *Inorganica Chimica Acta*, **445**: 70–78. https://doi.org/10.1016/j.ica.2016.02.023

Kumar, L. V., & Nath, G. R. (2019). Synthesis, Characterization and Biological Studies of Cobalt(II), Nickel(II), Copper(II) and Zinc(II) Complexes of Vanillin-4-Methyl-4-Phenyl-3-Thiosemicarbazone. *Journal of Chemical Sciences*, **131**(8).

https://doi.org/10.1007/s12039-019-1658-x

Kumaravel, G., Ponya Utthra, P., & Raman, N. (2018). Exploiting the Biological Efficacy of Benzimidazole Based Schiff Base Complexes with L-Histidine as a Co-Ligand: Combined Molecular Docking, DNA Interaction, Antimicrobial and Cytotoxic Studies. *Bioorganic Chemistry*, **77**: 269–279. https://doi.org/10.1016/j.bioorg.2018.01.024

Kurt, B., Temel, H., Atlan, M., & Kaya, S. (2020). Synthesis, Characterization, DNA Interaction and Docking Studies of Novel Schiff Base Ligand Derived from 2,6-Diaminopyridine and Its Complexes. *Journal of Molecular Structure*, **1209**: 127928. https://doi.org/10.1016/j.molstruc.2020.127928

Kushnazarova, R. A., Mirgorodskaya, A. B., Kuznetsov, D. M., Tyryshkina, A. A., Voloshina, A. D., Gumerova, S. K., Lenina, O. A., Nikitin E. N., & Zakharova, L. Ya., (2021). Modulation of Aggregation Behavior, Antimicrobial Properties and Catalytic Activity of Piperidinium Surfactants by Modifying Their Head Group with a Polar Fragment. *Journal of Molecular Liquids*, **336**: 116318. https://doi.org/10.1016/j.molliq.2021.116318

Lapasam, A., Banothu, V., Addepally, U., & Kollipara, M. R. (2019). Synthesis, Structural and Antimicrobial Studies of Half-Sandwich Ruthenium, Rhodium and Iridium Complexes Containing Nitrogen Donor Schiff-Base Ligands. *Journal of Molecular Structure*, **1191**: 314–322. https://doi.org/10.1016/j.molstruc.2019.04.116

Latif, M. A., Tofaz, T., Chaki, B. M., Tariqul Islam, H. M., Hossain, M. S., & Kudrat-E-Zahan, M. (2019). Synthesis, Characterization, and Biological Activity of the Schiff Base and Its Ni(II), Cu(II), and Zn(II) Complexes Derived from 4-(Dimethylamino)benzaldehyde and S-Benzyldithiocarbazate. *Russian Journal of General Chemistry*, **89**(6): 1197–1201. https://doi.org/10.1134/S1070363219060015X

Latorre, M., Troncoso, R., & Uauy, R. (2019). Biological Aspects of Copper. *Clinical and Translational Perspectives on WILSON DISEASE*. 25-31 https://doi.org/10.1016/B978-0-12-810532-0.00004-5

Lee, S. R. (2018). Critical Role of Zinc as Either an Antioxidant or a Prooxidant in Cellular Systems. *Oxidative Medicine and Cellular Longevity*, **2018**: 1–11.

https://doi.org/10.1155/2018/9156285

Li, B., & Webster, T. J. (2017). Bacteria Antibiotic Resistance: New Challenges and Opportunities for Implant-Associated Orthopedic Infections. *Journal of Orthopaedic Research*. https://doi.org/10.1002/jor.23656

Luca, A. De, Barile, A., Arciello, M., & Rossi, L. (2019). Copper Homeostasis as Target of Both Consolidated and Innovative Strategies of Anti-Tumor Therapy. *Journal of Trace Elements in Medicine and Biology*, **55**: 204–213. https://doi.org/10.1016/j.jtemb.2019.06.008

Luepke, K. H., Suda, K. J., Boucher, H., Russo, R. L., Bonney, M. W., Hunt, T. D., & Mohr, J. F. III (2016). Past, Present, and Future of Antibacterial Economics: Increasing Bacterial Resistance, Limited Antibiotic Pipeline, and Societal Implications. *Pharmacotherapy*: *The Journal of Human Pharmacology and Drug Therapy*, **37**(1): 71–84. https://doi.org/10.1002/phar.1868

MacLachlan, M. J., Park, M. K., & Thompson, L. K. (1996). Coordination Compounds of Schiff-Base Ligands Derived from Diaminomaleonitrile (DMN): Mononuclear, Dinuclear, and Macrocyclic Derivatives. *Inorganic Chemistry*, **35**: 5492–5499. https://doi.org/10.1021/ic960237p

Magyari, J., Holló, B. B., Ješić, V.-L. S., Radanović, M. M., Armaković, S., J., Molnar, J., Kincses, A., Gajdacs, M., Spengler, G., & Mészáros Szecsenyi, K. (2018). Interactions of Schiff Base Compounds and Their Coordination Complexes with the Drug Cisplatin. *New Journal of Chemistry,* **42**(8): 5834-5843. https://doi.org/10.1039/C8NJ00357B

Mahato, S., Meheta, N., Kotakonda, M., Joshi, M., Shit, M., Choudhury, A. R., & Biswas, B. (2020). Synthesis, Structure, Polyphenol Oxidase Mimicking and Bactericidal Activity of a Zinc-Schiff Base Complex. *Polyhedron*, **194**: 114933. https://doi.org/10.1016/j.poly.2020.114933

Mahdy, A. R. E., Alfaifi, M. Y., El-Gareb, M. S., Farouk, N., & Elshaarawy, R. F. M. (2021). Design, Synthesis, and Physicochemical Characterization of New Aminothiohydantoin Schiff Base Complexes for Cancer Chemotherapy. *Inorganica Chimica Acta*, **526**: 120504. https://doi.org/10.1016/j.ica.2021.120504

Mahmoud, M. A., & Abou-elmagd, M. G. (2019). Template Synthesis, Spectral and Thermal Properties of Nd(III) Metformin Schiff-Base Complexes as Potential Hypoglycemic Agents. *Egyptian Journal of Chemistry*, **0**(0): 0–0. https://doi.org/10.21608/ejchem.2019.13640.1858

Mahmoud, M. A., Zaitone, S. A., Ammar, A. M., & Sallam, S. A. (2016). Synthesis, Spectral, Thermal and Insulin-Enhancing Properties of Oxovanadium(IV) Complexes of Metformin Schiff-Bases. *Journal of Thermal Analysis and Calorimetry*, **128**(2): 957–969. https://doi.org/10.1007/s10973-016-6018-1

Mahmoud, N. F., Abbas, A. A., & Mohamed, G. G. (2021). Synthesis, Characterization, Antimicrobial, and MOE Evaluation of Nano 1,2,4-Triazole-Based Schiff Base Ligand with Some d-Block Metal Ions. *Applied Organometallic Chemistry,* **35**(6). https://doi.org/10.1002/aoc.6219

Mahmoud, W. H., Deghadi, R. G., & Mohamed, G. G. (2016). Novel Schiff Base Ligand and Its Metal Complexes with Some Transition Elements. Synthesis, Spectroscopic, Thermal Analysis, Antimicrobial and In Vitro Anticancer Activity. *Applied Organometallic Chemistry*, **30**(4): 221–230. https://doi.org/10.1002/aoc.3420

Mahmoud, W. H., Omar, M. M., Ahmed, Y. M., & Mohamed, G. G. (2020). Transition Metal Complexes of Schiff Base Ligand Based on 4,6-Diacetyl Resorcinol. *Applied Organometallic Chemistry*, **34**(4). https://doi.org/10.1002/aoc.5528

Maiti, S. K., Kalita, M., Singh, A., Deka, J., & Barman, P. (2020). Investigation of DNA Binding and Bioactivities of Thioether Containing Schiff Base Copper(II), Cobalt(II) and Palladium(II) Complexes: Synthesis, Characterization, Spectrochemical Study, Viscosity Measurement. *Polyhedron*, **184**: 114559. https://doi.org/10.1016/j.poly.2020.114559

Majumdar, D., Das, D., Nag, S., Bhattacharyya, M., Singh, D. K., Parai, D., Bankura, K., & Mishra, D. (2020). A Rare Hetero-Bimetallic Zn(II)/Ca(II) Schiff Base Complex: Synthesis, Crystal Structure, DFT, Molecular Docking and Unveiling Antimicrobial Activity. *Journal of Molecular Structure*, **1222**: 128951. https://doi.org/10.1016/j.molstruc.2020.128951

Makovec, T. (2019). Cisplatin and Beyond: Molecular Mechanisms of Action and

Drug Resistance Development in Cancer Chemotherapy. *Radiology and Oncology*, **53**(2): 148–158. https://doi.org/10.2478/raon-2019-0018

Malik, M. A., Dar, O. A., Gull, P., Wani, M. Y., & Hashmi, A. A. (2018). Heterocyclic Schiff Base Transition Metal Complexes in Antimicrobial and Anticancer Chemotherapy. *MedChemComm*, **9**(3): 409-436. https://doi.org/: 10.1039/C7MD00526A

Manna, S. C., Mistri, S., Patra, A., Mahish, M. K., Saren, D., Manne, R. K., Santra, M. K., Zangrando, E., & Puschmann, H. (2019). Synthesis, Structure, DNA/Protein Binding, Molecular Docking and In Vitro Anticancer Activity of Two Schiff Base Coordinated Copper(II) Complexes. *Polyhedron*, **171**: 77–85. https://doi.org/10.1016/j.poly.2019.06.049

Mehta, S. K., & Kaur, R. (2013). Self-Aggregation and Solution Behavior of Synthesized Organo Transitionmetal (Co, Fe, Zn) Amphiphilic Complexes. *Journal of Colloid and Interface Science*, **393**: 219–227. https://doi.org/10.1016/j.jcis.2012.11.001

Mehta, S. K., Kaur, R., & Chaudhary, G. R. (2012). Self Aggregation and Solution Behavior of Copper and Nickel Based Surfactants. *Colloids and Surfaces A: Physicochemical and Engineering Aspects*, **403**: 103–109. https://doi.org/10.1016/j.colsurfa.2012.03.062

Mendu, P., Kumari, C. G., & Ragi, R. (2015). Synthesis, Characterization, DNA Binding, DNA Cleavage and Antimicrobial Studies of Schiff Base Ligand and Its Metal Complexes. *Journal of Fluorescence*, **25**(2): 369–378. https://doi.org/10.1007/s10895-015-1520-6

Miroslaw, B. (2020). Homo- and Hetero-Oligonuclear Complexes of Platinum Group Metals (PGM) Coordinated by Imine Schiff Base Ligands. *International Journal of Molecular Sciences*, **21**(10): 3493. https://doi.org/10.3390/ijms21103493

Mohamed, G. G., Zayed, E. M., & Hindy, A. M. M. (2015). Coordination Behavior of New Bis Schiff Base Ligand Derived from 2-Furan Carboxaldehyde and Propane-1,3-Diamine. Spectroscopic, Thermal, Anticancer and Antibacterial Activity Studies. *Spectrochimica Acta - Part A: Molecular and Biomolecular Spectroscopy*, **145**: 76-84. https://doi.org/10.1016/j.saa.2015.01.129

Mohapatra, R. K., Das, P. K., Pradhan, M. K., Maihub, A. A., & El‑ajaily, M. M. (2018). Biological Aspects of Schiff Base–Metal Complexes Derived from Benzaldehydes: An Overview. *Journal of the Iranian Chemical Society*, **15**(10): 2193-2227. https://doi.org/10.1007/s13738-018-1411-2

Mondal, S., Mandal, S. M., Mondal, T. K., & Sinha, C. (2017). Spectroscopic Characterization, Antimicrobial Activity, DFT Computation and Docking Studies of Sulfonamide Schiff Bases. *Journal of Molecular Structure*, **1127**: 557-567. https://doi.org/10.1016/j.molstruc.2016.08.011

More, G., Raut, D., Aruna, K., & Bootwala, S. (2017). Synthesis, Spectroscopic Characterization and Antimicrobial Activity Evaluation of New Tridentate Schiff Bases and Their Co(II) Complexes. *Journal of Saudi Chemical Society*, **21**(8): 954–964. https://doi.org/10.1016/j.jscs.2017.05.002

Morgan, S. M., El-Sonbati, A. Z., & Eissa, H. R. (2017). Geometrical Structures, Thermal Properties and Spectroscopic Studies of Schiff Base Complexes: Correlation Between Ionic Radius of Metal Complexes and DNA Binding. *Journal of Molecular Liquids*, **240**: 752–776. https://doi.org/10.1016/j.molliq.2017.05.114

Mukherjee, P. K., Bahadur, S., Chaudhary, S. K., Kar, A., & Mukherjee, K. (2015). Quality Related Safety Issue-Evidence-Based Validation of Herbal Medicine Farm to Pharma. *Evidence-Based Validation of Herbal Medicine*. 1–28. https://doi.org/10.1016/B978-0-12-800874-4.00001-5

Murtaza, S., Akhtar, M. S., Kanwal, F., Abbas, A., Ashiq, S., & Shamim, S. (2017). Synthesis and Biological Evaluation of Schiff Bases of 4-Aminophenazone as Antiinflammatory, Analgesic and Antipyretic Agent. *Journal of Saudi Chemical Society*, **21**: S359-S372. https://doi.org/10.1016/j.jscs.2014.04.003

Murugaiyan, M., Mani, S. P., & Sithique, M. A. (2019). Zinc(II) Centered Biologically Active Novel N,N,O Donor Tridentate Water-Soluble Hydrazide-Based O-Carboxymethyl Chitosan Schiff Base Metal Complexes: Synthesis and Characterisation. *New Journal of Chemistry*, **43**(24): 9540–9554. https://doi.org/10.1039/c9nj00670b

Nagaraj, K., Senthil Murugan, K., Thangamuniyandi, P., & Sakthinathan, S. (2015).

Electron-Transfer Reactions of Cobalt(III) Complexes. 1. The Kinetic Investigation of the Reduction of Various Surfactant Cobalt(III) Complexes by Iron(II) in Surface Active Ionic Liquids. *Spectrochimica Acta - Part A: Molecular and Biomolecular Spectroscopy*, **143**: 101–106. https://doi.org/10.1016/j.saa.2015.02.007

Nagaveni, V. B., Mahadevan, K. M., Nagabhushana, H., Naveen, S., & Lokanath, N. K. (2018). Synthesis, Crystal Structure and Excellent Photoluminescence Properties of Copper (II) and Cobalt (II) Complexes with Bis (1[(4-butylphenyl)imino]methyl naphthalen-2-ol) Schiff Base. *Journal of Science: Advanced Materials and Devices*, **3**(1): 51–58. https://doi.org/10.1016/j.jsamd.2018.01.001

Nami, S. A. A., Ullah, I., Alam, M., Lee, D. U., & Sarikavakli, N. (2016). Synthesis, Characterization, Molecular Docking and Biological Studies of Self Assembled Transition Metal Dithiocarbamates of Substituted Pyrrole-2-Carboxaldehyde. *Journal of Photochemistry and Photobiology B: Biology,* **160**: 392-399. https://doi.org/10.1016/j.jphotobiol.2016.05.010

Naureen, B., Miana, G. A., Shahid, K., Asghar, M., Tanveer, S., & Sarwar, A. (2021). Iron (III) And Zinc (II) Monodentate Schiff Base Metal Complexes: Synthesis, Characterisation and Biological Activities. *Journal of Molecular Structure*, **1231**: 129946. https://doi.org/10.1016/j.molstruc.2021.129946

Nazir, U., Akhter, Z., Janjua, N. K., Adeel Asghar, M., Kanwal, S., Butt, T. M., Sani, A., Liaqat, F., Hussain, R., & Shah, F. U. (2020). Biferrocenyl Schiff Bases as Efficient Corrosion Inhibitors for an Aluminium Alloy in HCl Solution: A Combined Experimental and Theoretical Study. *RSC Advances*, **10**(13): 7585–7599. https://doi.org/10.1039/c9ra10692h

Nazirkar, B., Mandewale, M., & Yamgar, R. (2019). Synthesis, Characterization and Antibacterial Activity of Cu (II) and Zn (II) Complexes of 5-Aminobenzofuran-2-Carboxylate Schiff Base Ligands. *Journal of Taibah University for Science*, **13**(1): 440–449. https://doi.org/10.1080/16583655.2019.1592316

Nitschke, P., Jarząbek, B., Damaceanu, M.-D., Bejan, A.-E., & Chaber, P. (2021). Spectroscopic and Electrochemical Properties of Thiophene-Phenylene Based Shiff-Bases with Alkoxy Side Groups, Towards Photovoltaic Applications.

Spectrochimica Acta - Part A: Molecular and Biomolecular Spectroscopy, **248**: 119242. https://doi.org/10.1016/j.saa.2020.119242

Noorussabah, N., Choudhary, M., Das, N., Mohan, B., Singh, K., Singh, R. K., Ahmad, K., Muhammad, S., & Kumar, S. (2020). Copper(II) and Nickel(II) Complexes of Tridentate Hydrazide and Schiff Base Ligands Containing Phenyl and Naphthalyl Groups: Synthesis, Structural, Molecular Docking and Density Functional Study. *Journal of Inorganic and Organometallic Polymers and Materials*, **30**(11): 4426–4440. https://doi.org/10.1007/s10904-020-01610-w

Nozha, S. G., Morgan, S. M., Ahmed, S. E. A., El-Mogazy, M. A., Diab, M. A., El-Sonbati, A. Z., & Abou-Dobara, M. I. (2021). Polymer Complexes. LXXIV. Synthesis, Characterizationand Antimicrobial Activity Studies of Polymer Complexes of Some Transition Metals with Bis-bidentate Schiff Base. *Journal of Molecular Structure*, **1227**: 129525. https://doi.org/10.1016/j.molstruc.2020.129525

Nyawade, E. A., Onani, M. O., Meyer, S., & Dube, P. (2020). Synthesis, Characterization and Antimicrobial Activity Studies of New 2‑Pyrral‑L‑Amino Acid Schiff Base Palladium (II) Complexes. *Chemical Papers*, **74**(11): 3705–3715. https://doi.org/10.1007/s11696-019-00986-5

Ommenya, F. K., Nyawade, E. A., Andala, D. M., & Kinyua, J. (2020). Synthesis, Characterization and Antibacterial Activity of Schiff Base, 4-Chloro-2-{(E)-[(4-fluorophenyl)imino]methyl}Phenol Metal (II) Complexes. *Journal of Chemistry*, **2020**: 1–8. https://doi.org/10.1155/2020/1745236

Osypiuk, D., Cristóvão, B., & Bartyzel, A. (2020). New Coordination Compounds of CuII with Schiff Base Ligands—Crystal Structure, Thermal, and Spectral Investigations. *Crystals*, **10**(11): 1004. https://doi.org/10.3390/cryst10111004

Özdemir, Ö. (2020). Bis-azo-linkage Schiff Bases—Part(II): Synthesis, Characterization, Photoluminescence and DPPH Radical Scavenging Properties of Their Novel Luminescent Mononuclear Zn(II) Complexes. *Journal of Photochemistry and Photobiology A: Chemistry*, **392**: 112356. https://doi.org/10.1016/j.jphotochem.2020.112356

Öztürk, S., Okay, S., & Yıldırım, A. (2020). Synthesis, Anticorrosion, Antibacterial,

and Antifungal Activity of New Amphiphilic Compounds Possessing Quinazolin-4(3H)-one Scaffold. *Russian Chemical Bulletin*, **69**(11): 2205–2214. https://doi.org/10.1007/s11172-020-3023-0

Palanimurugan, A., Dhanalakshmi, A., Selvapandian, P., & Kulandaisamy, A. (2019). Electrochemical Behavior, Structural, Morphological, Calf Thymus-DNA Interaction and In-Vitro Antimicrobial Studies of Synthesized Schiff Base Transition Metal Complexes. *Heliyon*, **5**(7): e02039. https://doi.org/10.1016/j.heliyon.2019.e02039

Palanimurugan, A., & Kulandaisamy, A. (2018). DNA, In Vitro Antimicrobial/Anticancer Activities and Biocidal Based Statistical Analysis of Schiff Base Metal Complexes Derived From Salicylalidene-4-Imino-2,3-Dimethyl-1-Phenyl-3-Pyrazolin-5-one and 2-Aminothiazole. *Journal of Organometallic Chemistry,* **861**: 263-274. https://doi.org/10.1016/j.jorganchem.2018.02.051

Palmer, L. D., & Skaar, E. P. (2016). Transition Metals and Virulence in Bacteria. *Annual Review of Genetics*, **50**(1): 67-91. https://doi.org/10.1146/annurev-genet-120215-035146

Parsaee, Z., Bahaderani, E. J., & Afandak, A. (2018). Sonochemical Synthesis, In Vitro Evaluation and DFT Study of Novel Phenothiazine Base Schiff Bases and Their Nano Copper Complexes as the Precursors for New Shaped CuO-NPs. *Ultrasonics Sonochemistry*, **40**: 629–643. https://doi.org/10.1016/j.ultsonch.2017.08.010

Patil, S. A., Prabhakara, C. T., Halasangi, B. M., Toragalmath, S. S., & Badami, P. S. (2015). DNA Cleavage, Antibacterial, Antifungal and Anthelmintic Studies of Co(II), Ni(II) and Cu(II) Complexes of Coumarin Schiff Bases: Synthesis and Spectral Approach. *Spectrochimica Acta - Part A: Molecular and Biomolecular Spectroscopy*, **137**: 641–651. https://doi.org/10.1016/j.saa.2014.08.028

Pervaiz, M., Sadiq, S., Sadiq, A., Younas, U., Ashraf, A., Saeed, Z., Zuber, M., & Adnan, A. (2021). Azo-Schiff Base Derivatives of Transition Metal Complexes as Antimicrobial Agents. *Coordination Chemistry Reviews*, **447**: 214128. https://doi.org/10.1016/j.ccr.2021.214128

Pervaiz, M., Yousaf, M., Ahmad, I., Munawar, A., Saeed, Z., Adnan, A., Gulzar, T.,

Kirn, S., Kamal, T., & Ahmad, A. (2018). Synthesis, Spectral and Antimicrobial Studies of Amino Acid Derivative Schiff Base Metal (Co, Mn, Cu, and Cd) Complexes. *Spectrochimica Acta Part A: Molecular and Biomolecular Spectroscopy,* **206**: 642-649. https://doi.org/10.1016/j.saa.2018.05.057

Prabhakara, C. T., Patil, S. A., Toragalmath, S. S., Kinnal, S. M., & Badami, P. S. (2016). Synthesis, Characterization and Biological Approach of Metal Chelates of Some First Row Transition Metal Ions with Halogenated Bidentate Coumarin Schiff Bases Containing N and O Donor Atoms. *Photochemistry and Photobiology B: Biology,* **157**: 1-14. https://doi.org/10.1016/j.jphotobiol. 2016.02.004

Praveen, B. M., Prasanna, B. M., Mallikarjuna, N. M., Jagadeesh, M. R., Hebbar, N., & Rashmi, D. (2021). Investigation of Anticorrosive Behaviour of Novel Tert-butyl 4-[(4-methyl phenyl) carbonyl] Piperazine-1-Carboxylate for Carbon Steel in 1M HCl. *Heliyon*, **7**(2): e06090. https://doi.org/10.1016/j.heliyon.2021.e06090

Radha, V. P., Chitra, S., Jonekirubavathi, S., Chung, I. M., Kim, S. -H., & Prabakaran, M. (2020). Transition Metal Complexes of Novel Binuclear Schiff Base Derived from 3,3′-Diaminobenzidine: Synthesis, Characterization, Thermal Behavior, DFT, Antimicrobial and Molecular Docking Studies. *Journal of Coordination Chemistry,* **73**(6): 1009-1027. https://doi.org/10.1080/00958972. 2020.1752372

Raj, P., Singh, A., Singh, A., & Singh, N. (2017). Syntheses and Photophysical Properties of Schiff Base Ni(II) Complexes: Application for Sustainable Antibacterial Activity and Cytotoxicity. *ACS Sustainable Chemistry and Engineering*, **5**(7): 6070−6080. https://doi.org/10.1021/acssuschemeng.7b00963

Ramesh, G., Daravath, S., Ganji, N., Rambabu, A., Venkateswarlu, K., & Shivaraj. (2020). Facile Synthesis, Structural Characterization, DNA Binding, Incision Evaluation, Antioxidant and Antimicrobial Activity Studies of Cobalt(II), Nickle(II) and Copper(II) Complexes of 3-Amino-5-(4-fluorophenyl)isoxazole Derivatives. *Journal of Molecular Structure*, **1202**: 127338. https://doi.org/10.1016/j.molstruc.2019.127338

Rao, N. N., Kishan, E., Gopichand, K., Nagaraju, R., Ganai, A. M., & Rao, P. V. (2020). Design, Synthesis, Spectral Characterization, DNA Binding, Photo

Cleavage and Antibacterial Studies of Transition Metal Complexes of Benzothiazole Schiff Base. *Chemical Data Collections*, **27**: 100368. https://doi.org/10.1016/j.cdc.2020.100368

Rawat, P., Singh, R. N., Ranjan, A., Ahmad, S., & Saxena, R. (2017). Antimycobacterial, Antimicrobial Activity, Experimental (FT-IR, FT-Raman, NMR, UV–Vis, DSC) and DFT (Transition State, Chemical Reactivity, NBO, NLO) Studies on Pyrrole-isonicotinyl Hydrazone. *Spectrochimica Acta - Part A: Molecular and Biomolecular Spectroscopy,* **179**: 1-10. https://doi.org/10.1016/j.saa.2017.02.021

Saadatkhah, N., Garcia, A. C., Ackermann, S., Leclerc, P., Latifi, M., Samih, S., Patience, G. S., & Chaouki, J. (2019). Experimental Methods in Chemical Engineering: Thermogravimetric Analysis—TGA. *The Canadian Journal of Chemical Engineering*, **98**(1): 34–43. https://doi.org/10.1002/cjce.23673

Saif, M., El-Shafiy, H. F., Mashaly, M. M., Eid, M. F., Nabeel, A. I., & Fouad, R. (2016). Synthesis, Characterization, and Antioxidant/Cytotoxic Activity of New Chromone Schiff Base Nano-Complexes of Zn(II), Cu(II), Ni(II) and Co(II). *Journal of Molecular Structure,* **1118**: 75-82. https://doi.org/10.1016/j.molstruc.2016.03.060

Sakthivel, A., Jeyasubramanian, K., Thangagiri, B., & Raja, J. D. (2020). Recent Advances in Schiff Base Metal Complexes Derived from 4-Aminoantipyrine Derivatives and Their Potential Applications. *Journal of Molecular Structure*, **1222**: 128885. https://doi.org/10.1016/j.molstruc.2020.128885

Saraf, A., Sharma, S., & Sachar, S. (2018). Insights into the Interactions of Sulfamethoxazole with Organized Assemblies of Ionic and Nonionic Surfactants. *Langmuir*, **34**(48): 14624–14632. https://doi.org/10.1021/acs.langmuir.8b02814

Satheesh, C. E., Raghavendra Kumar, P., Sharma, P., Lingaraju, K., Palakshamurthy, B. S., & Rajanaika, H. (2016). Synthesis, Characterisation and Antimicrobial Activity of New Palladium and Nickel Complexes Containing Schiff Bases. *Inorganica Chimica Acta,* **442**: 1-9. https://doi.org/10.1016/j.ica.2015.11.017

Savić, A., Gligorijević, N., Aranđelović, S., Dojčinović, B., Kaczmarek, A. M., Radulović, S., Van Deun, R., & Van Hecke, K. (2020). Antitumor Activity of Organoruthenium Complexes with Chelate Aromatic Ligands, Derived from

1,10-Phenantroline: Synthesis and Biological Activity. *Journal of Inorganic Biochemistry*, **202**: 110869. https://doi.org/10.1016/j.jinorgbio.2019.110869

Schattschneider, C., Doniz Kettenmann, S., Hinojosa, S., Heinrich, J., & Kulak, N. (2019). Biological Activity of Amphiphilic Metal Complexes. *Coordination Chemistry Reviews*, **385**: 191–207. https://doi.org/10.1016/j.ccr.2018.12.007

Seewan, A. N., Kadhim, Z. Y., & Hadi, A. A. (2018). Theoretical Treatment, Microwave Synthesis and Spectroscopic Analysis of New Schiff Bases Derived from 4- Aminoantipyrene. *Journal of Physics: Conference series*, **1003**: 012011. https://doi.org/10.1088/1742-6596/1003/1/012011

Sen, S., & Chakraborty, R. (2016). Revival, Modernization and Integration of Indian Traditional Herbal Medicine in Clinical Practice: Importance, Challenges and Future. *Journal of Traditional and Complementary Medicine*, **7**(2): 234–244. https://doi.org/10.1016/j.jtcme.2016.05.006

Sevgi, F., Bagkesici, U., Kursunlu, A. N., & Guler, E. (2017). Fe (III), Co(II), Ni(II), Cu(II) and Zn(II) Complexes of Schiff Bases Based-on Glycine and Phenylalanine: Synthesis, Magnetic/Thermal Properties and Antimicrobial Activity. *Journal of Molecular Structure*, **1154**: 256–260. https://doi.org/10.1016/j.molstruc.2017.10.052

Shabbir, M., Akhter, Z., Ahmad, I., Ahmed, S., Ismail, H., Mirza, B., McKee, V., & Bolte, M. (2016). Synthesis, Characterization, Biological and Electrochemical Evaluation of Novel Ether Based on Donor Bidentate Schiff Bases. *Journal of Molecular Structure*, **1116**: 84–92. https://doi.org/10.1016/j.molstruc.2016.03.008

Shah, R., Katouah, H., Sedayo, A. A., Abualnaja, M., Aljohani, M. M., Saad, F., Zaky, R., & El-Metwaly, N. M. (2020). Practical and Computational Studies on Novel Schiff Base Complexes Derived from Green Synthesis Approach: Conductometry as well as In-Vitro Screening Supported by In-Silico Study. *Journal of Molecular Liquids*, **319**: 114116. https://doi.org/10.1016/j.molliq.2020.114116

Shahabi, S., Hamidi, S., Ghasemi, J. B., Norouzi, P., & Shakeri, A. (2019). Synthesis, Experimental, Quantum Chemical and Molecular Dynamics Study of Carbon Steel Corrosion Inhibition Effect of Two Schiff Bases in HCl Solution. *Journal*

of Molecular Liquids, **285**: 626–639. https://doi.org/10.1016/j.molliq.2019.04.137

Shaygan, S., Pasdar, H., Foroughifar, N., Davallo, M., & Motiee, F. (2018). Cobalt (II) Complexes with Schiff Base Ligands Derived from Terephthalaldehyde and Ortho-Substituted Anilines: Synthesis, Characterization and Antibacterial Activity. *Applied Sciences*, **8**(3): 385. https://doi.org/10.3390/app8030385

Shebl, M., Adly, O. M. I., Abdelrhman, E. M., & El-Shetary, B. A. (2017). Binary and Ternary Copper(II) Complexes of a New Schiff Base Ligand Derived from 4-Acetyl-5,6-diphenyl-3(2H)-pyridazinone: Synthesis, Spectral, Thermal, Antimicrobial and Antitumor Studies. *Journal of Molecular Structure*, **1145**: 329–338. https://doi.org/10.1016/j.molstruc.2017.05.064

Shehata, M. M., Adam, M. S. S., Abdelhady, K., & Makhlouf, M. M. (2019). Facile Synthesis, Characterizations, and Impedance Spectroscopic Features of Zn(II)-bis Schiff Base Complex Films Towards Photoelectronic Applications. *Journal of Solid State Electrochemistry*, **23**(8): 2519–2531. https://doi.org/10.1007/s10008-019-04329-y

Sherif, O. E., & Abdel-Kader, N. S. (2015). DFT Calculations, Spectroscopic Studies, Thermal Analysis and Biological Activity of Supra Molecular Schiff Base Complexes. *Arabian Journal of Chemistry*, **11**(5): 700–713. https://doi.org/10.1016/j.arabjc.2015.07.008

Shu, J., Ni, T., Liu, X., Xu, B., Liu, L., Chu, W., Zhang, K., & Jiang, W. (2021). Mechanochromism, Thermochromism, Protonation Effect and Discrimination of $CHCl_3$ from Organic Solvents in a Et_2N-Substituted Salicylaldehyde Schiff Base. *Dyes and Pigments*, **195**: 109708. https://doi.org/10.1016/j.dyepig.2021.109708

Siangwata, S., Chulu, S., Oliver, C. L., & Smith, G. S. (2016). Rhodium-Catalysed Hydroformylation of 1-Octene Using Aryl and Ferrocenyl Schiff Base-Derived Ligands. *Applied Organometallic Chemistry,* **31**(4): e3593. https://doi.org/10.1002/aoc.3593

Siddappa, K., Mane, S. B., & Manikprabhu, D. (2014). Spectral Characterization and 3D Molecular Modeling Studies of Metal Complexes Involving the O, N-Donor Environment of Quinazoline-4(3H)-one Schiff Base and Their Biological Studies. *The Scientific World Journal,* **2014**: 1-13. https://doi.org/10.1155/

2014/817365

Singh, K., Kumar, Y., Puri, P., Sharma, C., & Aneja, K. R. (2017). Antimicrobial, Spectral and Thermal Studies of Divalent Cobalt, Nickel, Copper and Zinc Complexes with Triazole Schiff Bases. *Arabian Journal of Chemistry*, **10**: S978–S987. https://doi.org/10.1016/j.arabjc.2012.12.038

Sipahi, O. R., Uysal, S., Aydemir, S. S., Pullukcu, H., Tasbakan, M., Tunger, A., Calli, F. F., Yamazhan, T., Arda, B., Sipahi, H., & Ulusoy, S. (2017). Antibacterial Resistance Patterns and Incidence of Hospital-Acquired Staphylococcus Aureus Bacteremia in a Tertiary Care Educational Hospital in Turkey: A Perspective from 2001 to 2013. *Turkish Journal of Medical Sciences*, **47**: 1210–1215. https://doi.org/10.3906/sag-1607-63

Skocibusic, M., Odzak, R., Stefanic, Z., Krizic, I., Kristo, L., Jovic, O., Hrenar, T., Primozic, I., & Jurasin, D. (2016). Structure-Property Relationship of Quinuclidinium Surfactants – Towards Multifunctional Biologically Active Molecules. *Colloids and Surfaces B: Biointerfaces,* **140**: 548-559. https://doi.org/10.1016/j.colsurfb.2015.11.023

Solanki, N. G., Lam, K., Tahsin, M., Gumaste, S. G., Shah, A. V., & Serajuddin, A. T. M. (2019). Effects of Surfactants on Itraconazole-HPMCAS Solid Dispersion Prepared by Hot-Melt Extrusion I: Miscibility and Drug Release. *Journal of Pharmaceutical Sciences*, **108**(4): 1453–1465. https://doi.org/10.1016/ j.xphs.2018.10.058

Srivastava, A. K., Yadav, P., Srivastava, K., & Prasad, J. (2021). Synthesis , Characterization , Biological and Electrochemical Investigation of Copper (II) Complexes Containing 4-Chloro-2-[2,6-diisopropypphenylimino) methyl] Phenol Schiff Base Ligand and Aromatic Diinines. *Chemical Data Collections*, **32**: 100659. https://doi.org/10.1016/j.cdc.2021.100659

Suleman, V. T., Al-Hamdani, A. A. S., Ahmed, S. D., Jirjees, V. Y., Khan, M. E., Dib, A., Al Zoubi, W., & Ko, Y. G. (2020). Phosphorus Schiff Base Ligand and Its Complexes: Experimental and Theoretical Investigations. *Applied Organometallic Chemistry*, **34**(4). https://doi.org/10.1002/aoc.5546

Sumrra, S. H., Sahrish, I., Raza, M. A., Ahmad, Z., Zafar, M. N., Chohan, Z. H., Khalid, M., & Ahmed, S. (2020). Efficient Synthesis, Characterization, and In

Vitro Bactericidal Studies of Unsymmetrically Substituted Triazole-Derived Schiff Base Ligand and Its Transition Metal Complexes. *Monatshefte Für Chemie - Chemical Monthly*, **151**(4): 549–557. https://doi.org/10.1007/s00706-020-02571-z

Sumrra, S. H., Zafa, W., Asghar, M. L., Mushtaq, F., Raza, M. A., Nazar, M. F., Nadeem, M. A., Imran, M., & Mumtaz, S. (2021). Computational Investigation of Molecular Structures, Spectroscopic Properties, Cholinesterase Inhibition and Antibacterial Activities of Triazole Schiff Bases Endowed Metal Chelates. *Journal of Molecular Structure*, **1238**. 130382. https://doi.org/10.1016/j.molstruc.2021.130382

Tadavi, S. K., Yadav, A. A., & Bendre, R. S. (2018). Synthesis and Characterization of a Novel Schiff Base of 1,2-Diaminopropane with Substituted Salicyaldehyde and Its Transition Metal Complexes: Single Crystal Structures and Biological Activities. *Journal of Molecular Structure,* **1152**: 223-231. https://doi.org/10.1016/j.molstruc.2017.09.112

Tampieri, A., Szabó, M., Medina, F., & Gulyás, H. (2020). A Brief Introduction to the Basics of NMR Spectroscopy and Selected Examples of Its Applications to Materials Characterization. *Physical Sciences Reviews*, **6**(1). https://doi.org/10.1515/psr-2019-0086

Tawfik, S. M., & Zaky, M. F. (2015). Corrosion Inhibition Performance of Some Schiff Base Anionic Surfactant Complexes of Cobalt(II), Copper(II), and Zinc(II) on Carbon Steel in 1.0 M HCl. *Research on Chemical Intermediates*, **41**(11): 8747–8772. https://doi.org/10.1007/s11164-015-1926-4

Toth, A., Schnedl, S., Painer, D., Siebenhofer, M., & Lux, S. (2019). Interfacial Catalysis in Biphasic Carboxylic Acid Esterification with a Nickel-Based Metallosurfactant. *ACS Sustainable Chemistry and Engineering*, **7**(22): 18547–18553. https://doi.org/10.1021/acssuschemeng.9b04667

Turan, N., Buldurun, K., Alan, Y., Savci, A., Çolak, N., & Mantarcı, A. (2019). Synthesis, Characterization, Antioxidant, Antimicrobial and DNA Binding Properties of Ruthenium(II), Cobalt(II) and Nickel(II) Complexes of Schiff Base Containing O-Vanillin. *Research on Chemical Intermediates*. https://doi.org/10.1007/s11164-019-03806-3

Turtoi, M., Anghelache, M., Patrascu, A. A., Maxim, C., Manduteanu, I., Calin, M., & Popescu, D. -L. (2021). Synthesis, Characterization, and In Vitro Insulin-Mimetic Activity Evaluation of Valine Schiff Base Coordination Compounds of Oxidovanadium(V). *Biomedicines*, **9**(5): 562. https://doi.org/10.3390/biomedicines9050562

Tyagi, P., Chandra, S., Saraswat, B. S., & Sharma, D. (2015). Design, Spectral Characterization, DFT and Biological Studies of Transition Metal Complexes of Schiff Base Derived from 2-Aminobenzamide, Pyrrole and Furan Aldehyde. *Spectrochimica Acta - Part A: Molecular and Biomolecular Spectroscopy*, **143**: 1–11. https://doi.org/10.1016/j.saa.2015.02.027

Tyers, M., & Wright, G. D. (2019). Drug Combinations: A Strategy to Extend the Life of Antibiotics in the 21st Century. *Nature Reviews Microbiology*, **17**(3): 141–155. https://doi.org/10.1038/s41579-018-0141-x

Uddin, M. N., Ahmed, S. S., & Alam, S. M. R. (2020). REVIEW: Biomedical Applications of Schiff Base Metal Complexes. *Journal of Coordination Chemistry*, **73**(23): 3109–3149. https://doi.org/10.1080/00958972.2020.1854745

Vamsikrishna, N., Daravath, S., Ganji, N., Pasha, N., & Shivaraj. (2020). Synthesis, Structural Characterization, DNA Interaction, Antibacterial and Cytotoxicity Studies of Bivalent Transition Metal Complexes of 6-Aminobenzothiazole Schiff Base. *Inorganic Chemistry Communications*, **113**: 107767. https://doi.org/10.1016/j.inoche.2020.107767

Veeralakshmi, S., Nehru, S., Arunachalam, S., Kumar, P., & Govindaraju, M. (2014). Study of Single and Double Chain Surfactant-Cobalt(III) Complexes and their Hydrophobicity, Micelle Formation, Interaction with Serum Albumins and Antibacterial Activities. *Inorganic Chemistry Frontiers*, **1**(5): 393–404. https://doi.org/10.1039/c4qi00018h

Venkateswarlu, K., Ganji, N., Daravath, S., Kanneboina, K., Rangan, K., & Shivaraj. (2019). Crystal Structure, DNA Interactions, Antioxidant and Antitumor Activity of Thermally Stable Cu(II), Ni(II) And Co(III) Complexes of an N,O Donor Schiff Base Ligand. *Polyhedron*, **171**: 86–97. https://doi.org/10.1016/j.poly.2019.06.048

Verma, R., Mishra, A., & Mitchell-Koch, K. R. (2015). Molecular Modeling of

Cetylpyridinium Bromide, a Cationic Surfactant, in Solutions and Micelle. *Journal of Chemical Theory and Computation*, **11**(11): 5415–5425. https://doi.org/10.1021/acs.jctc.5b00475

Vinusha, H. M., Kollur, S. P., Revanasiddappa, H. D., Ramu, R., Shirahatti, P. S., Nagendra Prasad, M. N., Chandrashekar, S., & Begum, M. (2019). Preparation, Spectral Characterization and Biological Applications of Schiff Base Ligand and Its Transition Metal Complexes. *Results in Chemistry*, **1**: 100012. https://doi.org/10.1016/j.rechem.2019.100012

Vlasenko, V. G., Garnovskii, D. A., Aleksandrov, G. G., Makarova, N. I., Levchenkov, S. I., Trigub, A. L., Zubavichus, Ya. V., Uraev, A. I., Koshchienko, Yu. V., & Burlov, A. S. (2019). Electrochemical Synthesis, Structural, Spectral Studies and DFT Calculations of Heteroleptic Metal-Chelates Bearing N, N, S Tridentate Tosylamino Functionalized Pyrazole Containing Schiff Base and 1,10-Phenanthroline. *Polyhedron,* **157**: 6-17. https://doi.org/10.1016/j.poly.2018.09.065

Wagay, T. A., Askari, H., & Ismail, K. (2020). Synthesis, Aggregation and Adsorption Behavior of Benzyldimethylhexadecylammonium Based Double-Chained Metallosurfactants. *Journal of Molecular Liquids,* **299**: 112234. https://doi.org/10.1016/j.molliq.2019.112234

Wagay, T. A., Dey, J., Kumar, S., Aswal, V. K., & Ismail, K. (2016). Aggregation and Surface Behavior of Aqueous Solutions of: Cis -bis(1,3-diaminopropane)bis(dodecylamine)cobalt(III) nitrate. A Double-Chained Metallosurfactant. *RSC Advances*, **6**(71): 66900–66910. https://doi.org/10.1039/c6ra04199j

Weng, T., Zhang, K., Wu, B., Chen, X., Zou, Q., Zeng, T., & Zhu, L. (2019). Orthogonally Incorporating Dual-Fluorescence Control into Gated Photochromism for Multifunctional Molecular Switching. *Chemistry - A European Journal,* **25**(67): 1581-1587. https://doi.org/10.1002/chem.201903759

Wright, G. D. (2017). Opportunities for Natural Products in 21st Century Antibiotic Discovery. *Natural Product Reports*, **34**(7): 694–701. https://doi.org/10.1039/c7np00019g

Yaşar, Ü., Gönül, İ., Türkeş, C., Demir, Y., & Beydemir, Ş. (2021). Transition-Metal

Complexes of Bidentate Schiff-Base Ligands: In Vitro and In Silico Evaluation as Non-Classical Carbonic Anhydrase and Potential Acetylcholinesterase Inhibitors. *ChemistrySelect*, **6**(29): 7278–7284. https://doi.org/10.1002/slct.202102082

Yeğiner, G., Gülcan, M., Işık, S., Ürüt, G. Ö., Özdemir, S., & Kurtoğlu, M. (2017). Transition Metal (II) Complexes with a Novel Azo-Azomethine Schiff Base Ligand: Synthesis, Structural and Spectroscopic Characterization, Thermal Properties and Biological Applications. *Journal of Fluorescence*, **27**(6): 2239–2251. https://doi.org/10.1007/s10895-017-2166-3

Yusuf, T. L., Oladipo, S. D., Zamisa, S., Kumalo, H. M., Lawal, I. A., Lawal, M. M., & Mabuba, N. (2021). Design of New Schiff-Base Copper(II) Complexes: Synthesis, Crystal Structures, DFT Study, and Binding Potency Toward Cytochrome P450 3A4. *ACS Omega*, **6**(21): 13704–13718. https://doi.org/10.1021/acsomega.1c00906

Zafar, W., Sumrra, S. H., & Chohan, Z. H. (2021). A Review: Pharmacological Aspects of Metal Based 1,2,4-Triazole Derived Schiff Bases. *European Journal of Medicinal Chemistry*, **222**: 113602. https://doi.org/10.1016/j.ejmech.2021.113602

Zamani, F., Zendehdel, M., Mobinikhaledi, A., & Azarkish, M. (2015). Complexes of N,N-bis (salicylidene)4,5-dimethyl-1,2-phenylenediamine Immobilized on Porous Nanomaterials: Synthesis, Characterization and Study of Their Antimicrobial Activity. *Microporous and Mesoporous Materials*, **212**: 18–27. https://doi.org/10.1016/j.micromeso.2015.02.052

Zayed, E. M., Mohamed, G. G., & Hindy, A. M. M. (2014). Transition Metal Complexes of Novel Schiff Base: Synthesis, Spectroscopic Characterization, and In Vitro Antimicrobial Activity of Complexes. *Journal of Thermal Analysis and Calorimetry,* **120**(1): 893-903. https://doi.org/10.1007/s10973-014-4061-3

Zhou, M., Zhang, Z., Xu, D., Hou, L., Zhao, W., Nie, X., Zhou, L., & Zhao, J. (2017). Synthesis of Three Gemini Betaine Surfactants and their Surface Active Properties. *Journal of the Taiwan Institute of Chemical Engineers,* **74**: 7-13. https://doi.org/10.1016/j.jtice.2016.10.012

Ziklo, N., Bibi, M., & Salama, P. (2021). The Antimicrobial Mode of Action of

Maltol and its Synergistic Efficacy with Selected Cationic Surfactants. *Cosmetics*, **8**(3): 86. https://doi.org/10.3390/cosmetics8030086

Zoubi, W. Al, Al-Hamdani, A. A. S., Ahmed, S. D., & Ko, Y. G. (2017). Synthesis, Characterization, and Biological Activity of Schiff Bases Metal Complexes. *Journal of Physical Organic Chemistry*, **31**(2): e3752. https://doi.org/ 10.1002/poc.3752

APPENDIX

Table A1: List of chemicals and reagents

S.N.	Chemicals and reagents	Source
1	Dodecylamine	Spectrochem Pvt. Ltd. Mumbai, India
2	Pyrrole-2-carboxaldehyde	Sigma Aldrich
3	Pyrrole-3-carboxaldehyde	Alfa-Aesar
6	Methanol	Merck
7	Ethanol	Qualigens, Merck
8	$CoCl_2. 6H_2O$	Merck
9	$NiCl_2. 6H_2O$	Merck
10	$CuCl_2. 2H_2O$	Merck
11	$ZnCl_2$	Merck
12	Acetone	Merck
13	Dimethylsulphoxide (DMSO)	Qualigens
14	Sodium hydroxide	Himedia co.
15	Nutrient agar	Himedia co.
16	MHN agar	Himedia co.
17	pH buffer capsule	Merck
18	Hydrochloric acid	Merck
19	Tryptone soya broth	Himedia co.
20	Peptone water	Himedia co.

Table A2: List of instruments and glass apparatus

S.N.	Instruments and glass apparatus	Source
1	Magnetic stirrer	Vitco co. India
2	Heating mantle	Local company
3	Digital balance (4 digits)	Sartorius QUINTIX 224-1S analytical balance
4	Conical flask (100 mL)	Borosil
5	Beaker (100 mL)	Borosil
6	Magnetic beads	Local
7	Condenser	Borosil
8	Pipette	Borosil
9	Measuring cylinder	Borosil
10	Pipette pump	Polylab
11	Glass adaptors	Borosil

Table A3: Solubility data of Schiff base ligands and metal complexes

S.N.	Compounds	Methanol	Water	Ethanol	DMSO	DMF
1	DDAP2C	S	IS	S	S	S
2	HL (DDAP3C)	S	IS	S	S	S
3	Co-DDAP2C	S	IS	S	S	S
4	Ni-DDAP2C	S	IS	S	S	S
5	Cu-DDAP2C	S	IS	S	S	S
6	Zn-DDAP2C	S	IS	S	S	S
7	Co-DDAP3C	PS	IS	PS	S	S
8	Ni-DDAP3C	PS	IS	PS	S	S
9	Cu-DDAP3C	PS	IS	PS	S	S
10	Zn-DDAP3C	PS	IS	PS	S	S

IS = Insoluble

S = Soluble

PS = Partial soluble
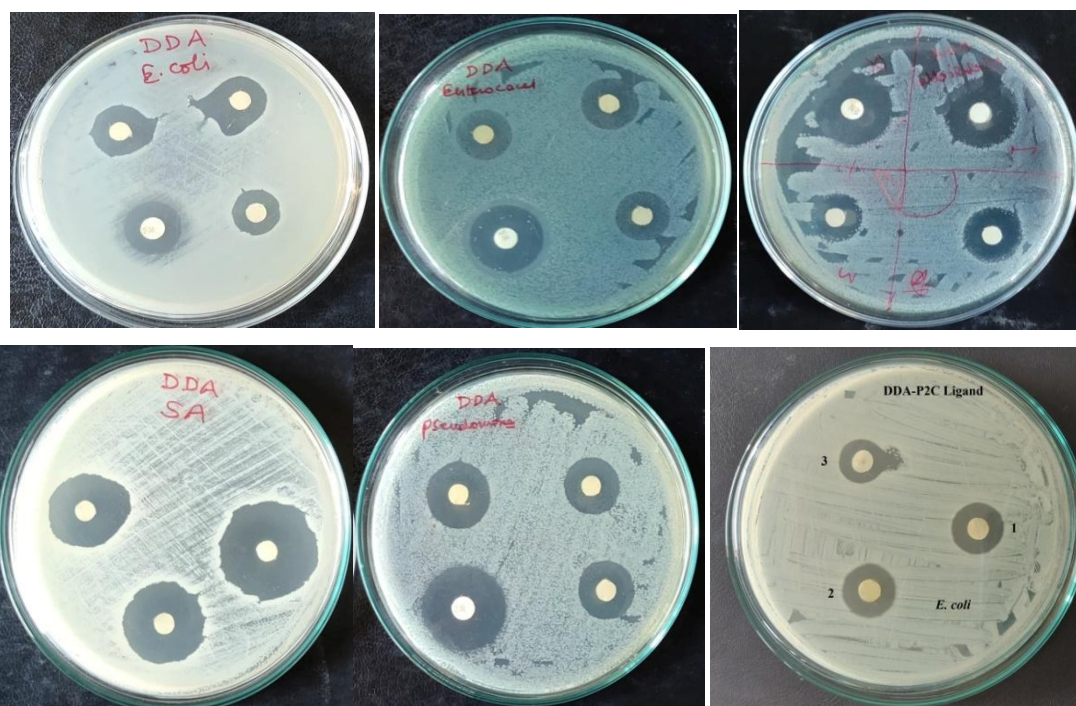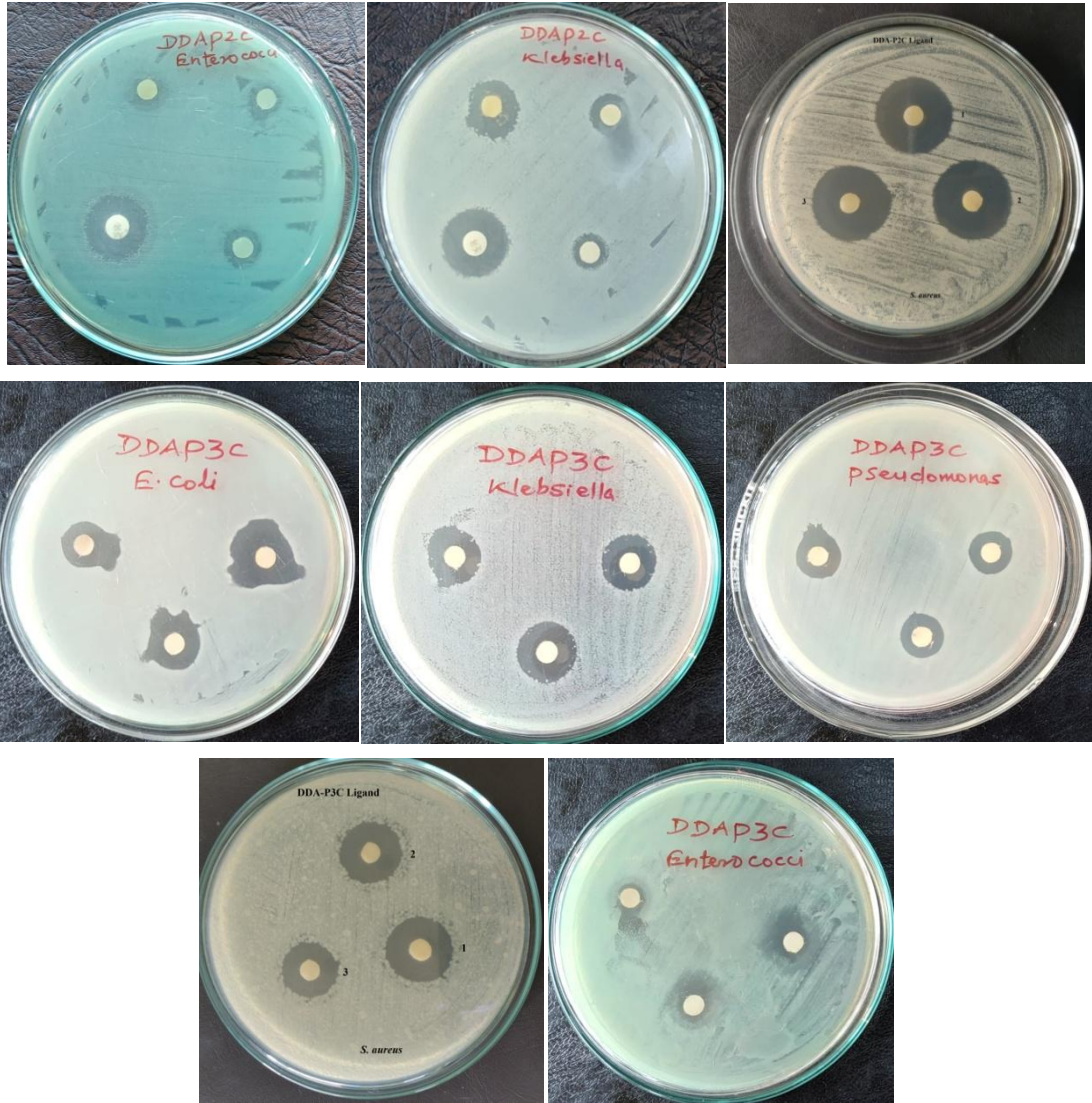
Figure A1: Antibacterial activity against pathogenic bacteria with DDA, DDAP2C and DDAP3C Schiff base ligands
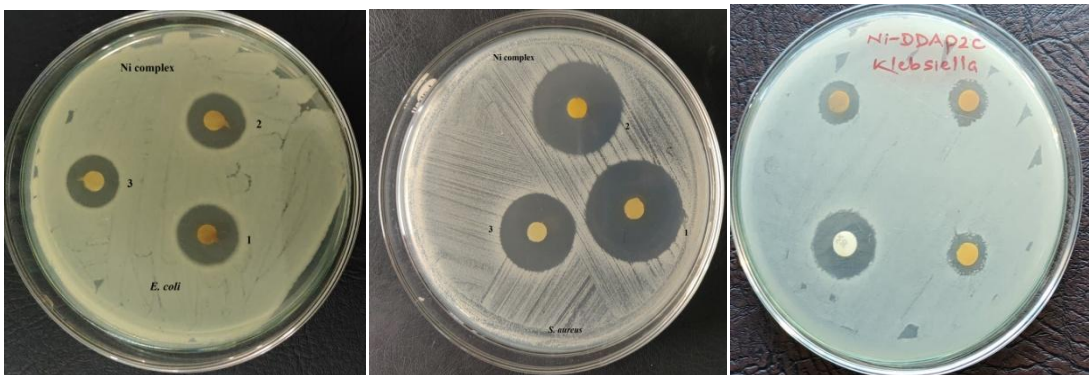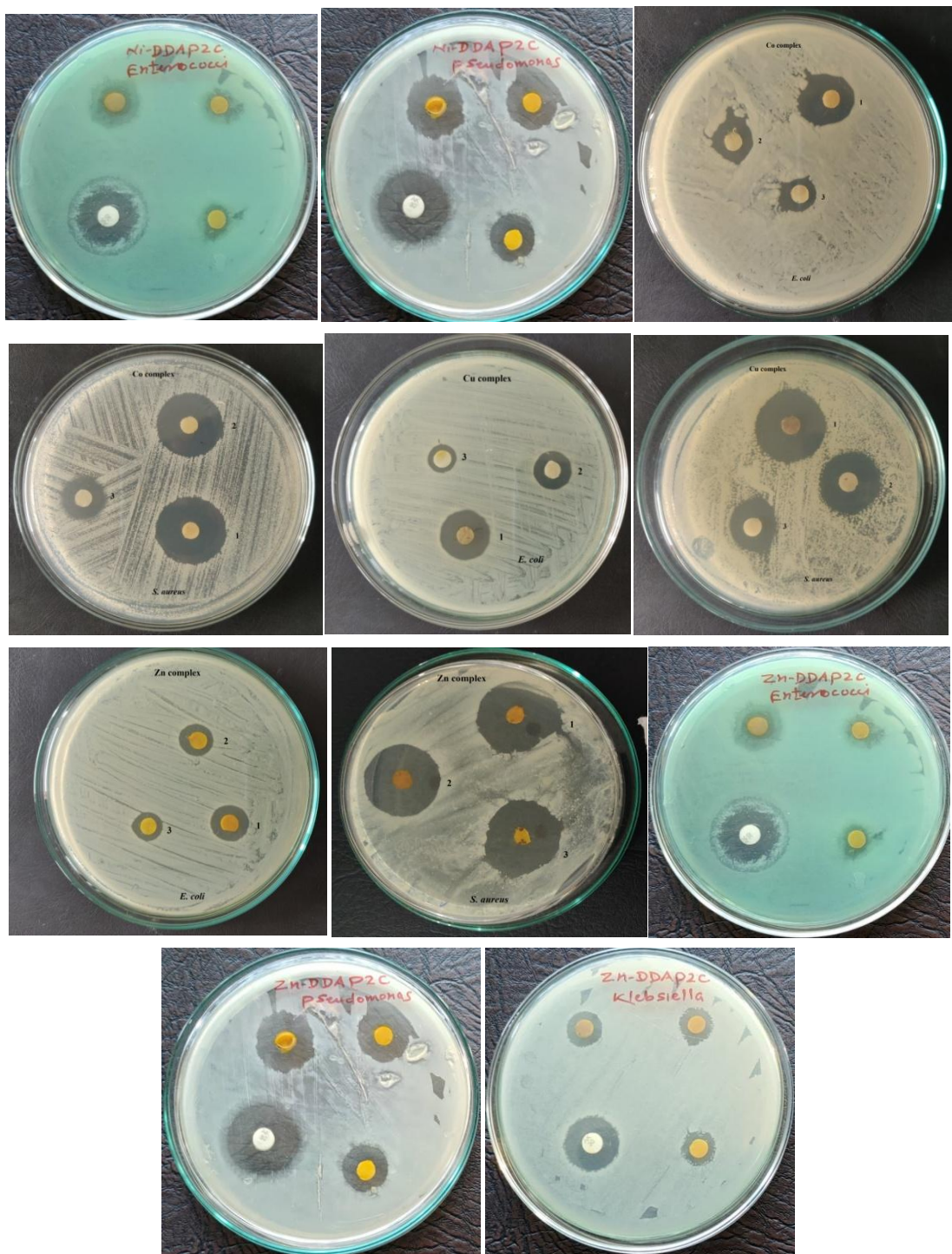
Figure A2: Antibacterial activity against pathogenic bacteria with metal complexes of DDAP2C Schiff base ligand
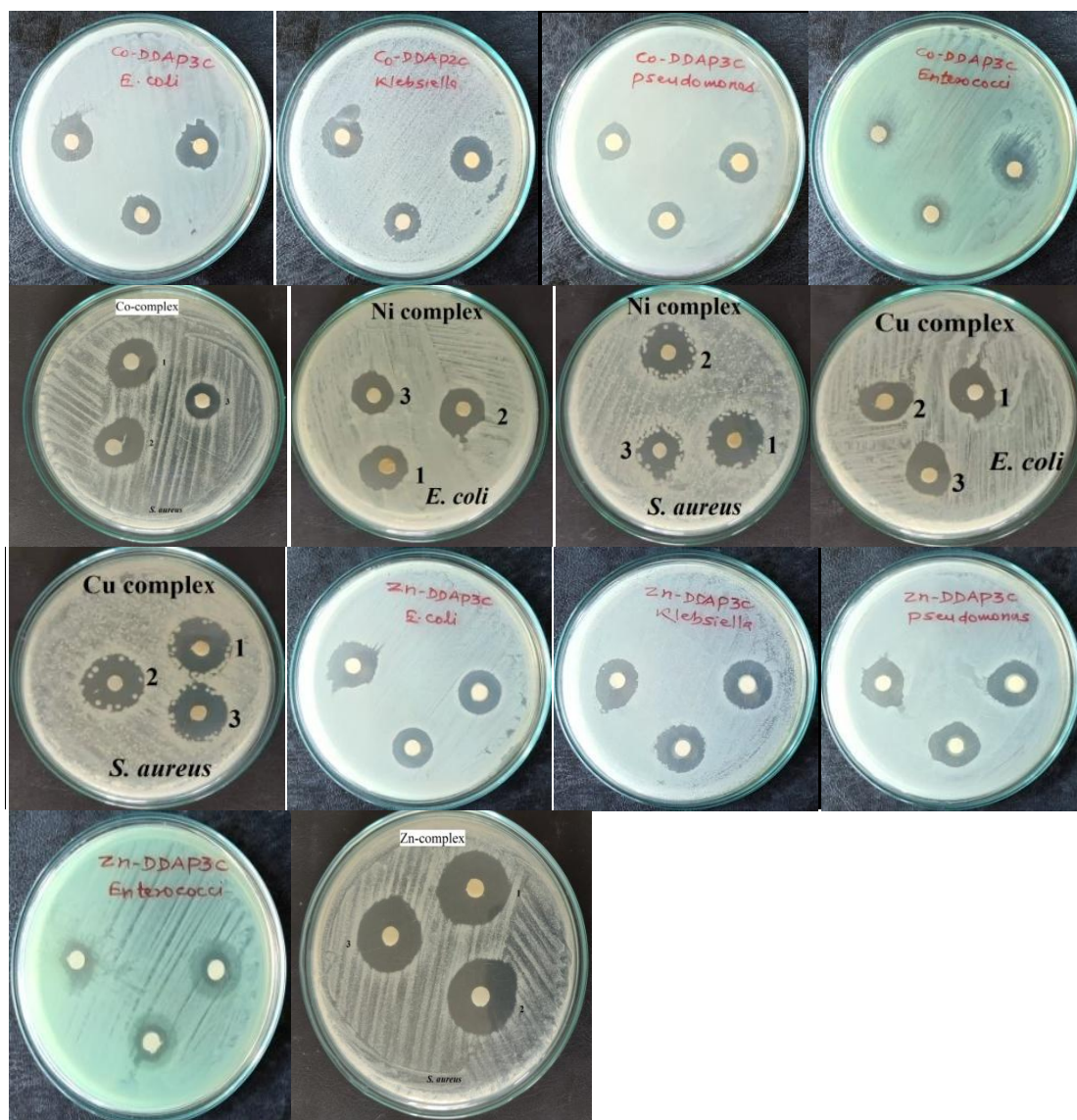
Figure A3: Antibacterial activity against pathogenic bacteria with metal complexes of DDAP3C Schiff base ligand

Figure A4: Sample picture of DDAP2C ligand and metal complexes

Figure A5: Sample picture of DDAP3C ligand and metal complexes

List of Publications and Scientific Paper Presentations

List of Publications

1. **Adhikari, J.,** Bhattarai, A., & Chaudhary, N. K. (2023). Data analysis for SEM-EDX , thermokinetics , surfactant , and corrosion inhibition activity of Co (II) and Zn (II) complexes of pyrrole-based surfactant ligand. *Data in Brief*, *48*: 109124. https://doi.org/10.1016/j.dib.2023.109124

2. **Adhikari, J.,** Bhattarai, A., & Chaudhary, N. K. (2023). Bioinorganic interest on Co(II) and Zn(II) complexes of pyrrole-based surfactant ligand: synthesis, characterization, and in silico-ADME study. *Journal of Molecular Structure*, *1274*: 134434. https://doi.org/10.1016/j.molstruc.2022.134434

3. **Adhikari, J.,** Bhattarai, A., & Chaudhary, N. K. (2022). Synthesis, characterization, physicochemical studies, and antibacterial evaluation of surfactant-based Schiff base transition metal complexes. *Chemical Papers*, *76*(4): 2549–2566. https://doi.org/10.1007/s11696-022-02062-x

Scientific Paper Presentations

1. Scientific paper presentation entitled **"Synthesis, characterization, physicochemical studies, and antibacterial evaluation of surfactant-based Schiff base transition metal complexes"** in the **"International Chemical Congress (ICC-2023): Chemistry for sustainable Development"**, May 25 - 27, 2023, in Park Village Resort, Kathmandu, Nepal, organized by Nepal Chemical Society in association with the School of Materials Science and Engineering, Liaocheng University, China, and Central Department of Chemistry at Tribhuvan University, Kathmandu, Nepal.

2. Scientific paper presentation entitled **"Bioinorganic interest on Co(II) and Zn(II) complexes of pyrrole-based surfactant ligand: Synthesis, characterization, and *in silico*-ADME study"** in the **"International Scientific Research Conference"** dated 28 - 29 November, 2022 at Jaipur, India, jointly organized by International Scientific Research Association, Apex University, Jaipur, India, Research Culture Society & Institute of science and Technology, Eurasian University.

3. Scientific poster presentation entitled **"Physiochemical studies on the surfactant-based Schiff base transition metal complexes"** in **"The 8ᵗʰ Asian Conference on Colloid & Interface Science (ACCIS 2019)",** Sept. 24-27, Kathmandu, Nepal, organized by the **Asian Society for Colloid and Surface Science (ASCASS)** held in Pulchowk Campus, Institute of Engineering, Tribhuvan University, Lalitpur, Kathmandu, Nepal.

4. Participation in the **"Workshop on Carbon Dots (CDs): An amazing multi functional nano particle"** organized by Department of Chemistry, Mahendra Morang Adarsh Multiple Campus, Tribhuvan University and Nepal Chemical Society, Biratnagar, Province 1, Nepal on 2 August, 2022.

5. Participation in the **International Seminar on "Frontiers in Tea Research-2020"**, date: March 6, 2020, organized by **DEPARTMENT OF TEA SCIENCE, UNIVERSITY OF NORTH BENGAL, INDIA.**

6. Participation in the **"Workshop on Research Writting & Publishing"** organized by Research Management cell, Mahendra Morang Adarsh Multiple Campus, Biratnagar & supported by University Grants Commission, Nepal held at Biratnagar from 8th-11th May, 2019.

ELSEVIER

Data Article

Data analysis for SEM-EDX, thermokinetics, surfactant, and corrosion inhibition activity of Co(II) and Zn(II) complexes of pyrrole-based surfactant ligand

Check for updates

Janak Adhikari, Ajaya Bhattarai, Narendra Kumar Chaudhary*

Department of Chemistry, Mahendra Morang Adarsh Multiple Campus, Biratnagar, (Tribhuvan University) Nepal

ARTICLE INFO

ABSTRACT

This manuscript reports a dataset for the scanning electron microscopy with energy dispersive X-ray analysis (SEM-EDX), surfactant properties, thermokinetics, and corrosion inhibition activity of $[[Co(HL)_2.2H_2O] \ Cl_2.H_2O]]$ (**1**) and $[[Zn(HL)_2.Cl] \ Cl.3H_2O]]$ (**2**) complexes with surfactant-based Schiff base ligand (**HL**). It contains analyzed data related to thermokinetics, such as the activation energy (E^*), entropy change (ΔS^*), enthalpy change (ΔH^*), and free energy change (ΔG^*) of **HL** and metal complexes. It also contains the SEM micrographs and EDX images of the studied ligand and metal complexes. A detailed analysis of the critical micelle concentration (CMC) data and figures illustrating the surfactant behavior of the synthesized complexes are presented in this article. The data for the corrosion inhibition activity of all synthesized compounds are also included. The dataset is related to the research article entitled "Bioinorganic interest on Co(II) and Zn(II) complexes of pyrrole-based surfactant ligand: Synthesis, characterization, and in silico-ADME study".

Specifications Table

Subject	Materials science
Specific subject area	Analytical Chemistry, Corrosion, and surface science
Type of data	Tables, Images, and Figures
How the data were acquired	Thermogravimetric analysis: Perkin Elmer STA6000 thermal analyzer under the N_2 atmosphere. The slopes and intercepts of thermogravimetric analysis and differential thermal analysis (TGA/DTA) plots were analyzed to obtain thermokinetics data. A JEOL 6390 LA scanning electron microscope was used to generate SEM micrographs of the ligand and complexes and EDX images of complexes. Conductivity: An Auto Ranging digital conductivity TDS meter TCM 15+ was used to record conductivity data at 308 and 318 K temperatures. Corrosion inhibition: The weight loss method was used to evaluate corrosion inhibition on carbon steel coupons using a four-digit digital balance (Sartorius QUINTIX 224-1S analytical balance).
Data format	Raw and analyzed data
Description of data collection	Using Origin software, thermokinetic parameters were generated from TGA/DTA data. The conductivity data were processed in easy plot software to calculate CMC and Gibb's free energy of micellization. The SEM-EDX imaging was performed to analyze surface morphology and elemental composition. Corrosion inhibition data on carbon steel coupons were used to measure anticorrosion efficacy.
Data source location	Department of Chemistry, Mahendra Morang Adarsh Multiple Campus, Biratnagar, (Tribhuvan University), Nepal. SAIF, STIC Cochin, India.
Data accessibility	*Analyzed data and images are included with the article, and the raw data is deposited in the repository.* *Repository name: Mendeley Data* DOI:10.17632/99f4dxttm8.*2* https://data.mendeley.com/datasets/99f4dxttm8
Related research article	*J. Adhikari, A. Bhattarai, N. K. Chaudhary, Bioinorganic interest on Co(II) and Zn(II) complexes of pyrrole-based surfactant ligand: Synthesis, characterization, and in silico-ADME study, J. Mol. Struct., 1274 (2023), 134434.* https://doi.org/10.1016/j.molstruc.2022.134434

Value of the Data

- Researchers in the area of material science may find the present data useful in investigating kinetic behavior and surfactant properties of compounds used in drug delivery systems.
- The SEM-EDX images are helpful in identifying morphological changes that occur during complexation of the ligand for the formation of metal complexes.
- Corrosion inhibition efficiency data collected for carbon steel (CS) coupons can be used to evaluate the efficacy of the inhibitor in other corrosive solutions (media).
- This result can be used to compare the thermal stability and decomposition rates of other surfactant-fabricated metal complexes.

1. Objective

The surface properties of the metal complexes make them particularly suitable for pharmaceutical applications. Several factors influence biochemical interactions with pathogens, includ-
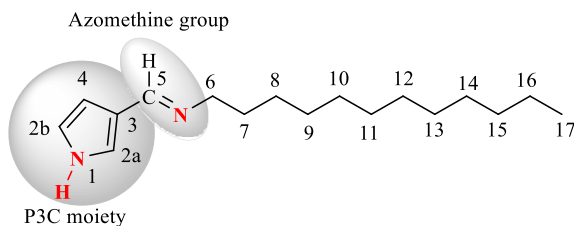
Fig. 1. Structure of Schiff base ligand (HL).

Table 1
Elemental composition of complexes detected from EDX analysis.

Element	Complex **1**		Complex **2**	
	Weight (%)	Atomic (%)	Weight (%)	Atomic (%)
C	79.81	91.51	55.18	79.59
O	3.09	2.66	3.73	4.05
Cl	11.86	4.61	19.47	9.51
Co	5.2	1.21	-	-
Zn	-	-	19.19	5.08

ing adsorption ability, thermokinetic stability, and surface morphology. The main goal of this study is to explore the data on how they selectively bind to specific regions of the pathogens by forming micellar aggregates at different temperatures based on degrees of micellization and free energy of micellization. The surface morphology and grain size of the complexes determine drug delivery effectiveness. Their anti-corrosion properties also make them ideal for a wide range of metal-based components as well as pharmaceutical applications. The datasets included in this manuscript are additional quantitative parameters that will add significant value to the complexes and support our previous publications [1,2].

2. Data Description

In this study, we share SEM-EDX, thermokinetics, CMC, free energy of micellization, and anticorrosion activity data for $[[Co(HL)_2.2H_2O] Cl_2.H_2O]]$ (**1**) and $[[Zn(HL)_2.Cl] Cl.3H_2O]]$ (**2**) complexes with surfactant-based Schiff base ligand (**HL**) (Fig 1). The ligand was prepared by refluxing of a mixture of an ethanolic solution of pyrrole-3-carbaldehyde (**P3C**) and laurylamine (**LA**) in a 1:1 stoichiometric ratio.

The SEM micrographs of ligand and complexes are presented in Fig. 2. The micrographs illustrate the variation in surface morphology for metal complexation of ligands with metal ions. The somewhat rod-shaped crystalline structure of the micrograph of **HL** has changed to the unevenly distributed morphological mass of the complexes after complexation.

Table 1 reports the elemental composition of the complexes detected from EDX analysis. It revealed the presence of various non-metal atoms, such as N, O, and Cl, and the respective metals. The EDX data indicated the expected elemental composition of the complexes as well, and the EDX images are shown in Mendeley Research data file [3].

The Coats-Redfern equation was used to calculate the thermodynamic and kinetic parameters of each decomposition step for the synthesized complexes. The results are presented in Table 2. A consecutive increase in the E^* value in each decomposition step was observed. Table 2 showed negative ΔS^*, positive ΔH^*, and positive ΔG^* values for all complexes [4–6]. Details regarding these parameters can be found in Section 3.2.

The conductivity versus concentration plots of **LA**, complex **1** and complex **2** are shown in Figs. 3-5. The specific conductivity values varied before and after CMC. Owing to the formation
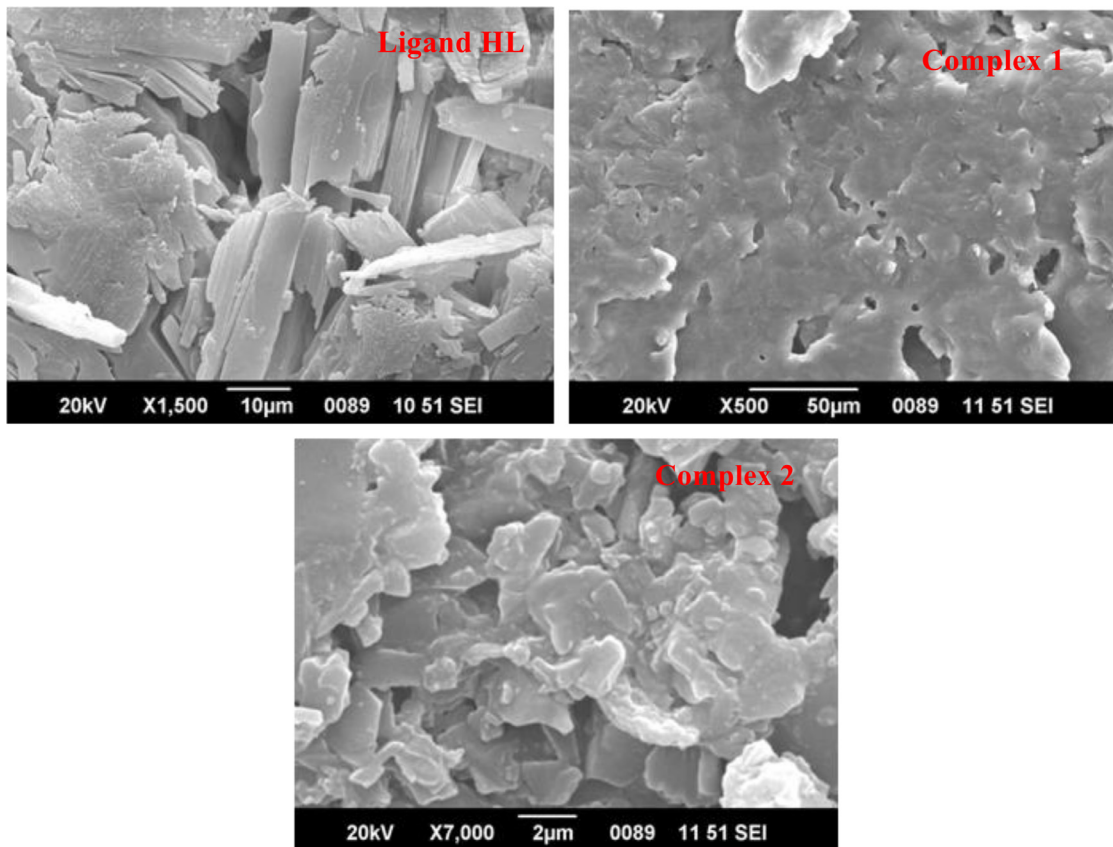
Fig. 2. SEM micrograph of (a) Ligand (HL), (b) Complex 1, (c) Complex 2.

Table 2
Thermodynamic and kinetic parameters.

Complexes	Step	r	A (s^{-1})	T_{max} (K)	E^* (kJ/mol)	ΔS^* (J/K.mol)	ΔH^* (kJ/mol)	ΔG^* (kJ/mol)
Complex 1	1	-0.99	6.32×10^{10}	391.28	86.13	-40.40	82.88	98.68
	2	-0.98	8.09×10^{10}	471.69	108.39	-39.89	104.46	123.28
	3	-0.98	3.85×10^{10}	685.83	153.15	-49.19	147.45	181.19
Complex 2	1	-0.99	3.75×10^{10}	374.06	82.89	- 44.35	79.78	96.36
	2	-0.99	9.78×10^9	482.24	100.59	-57.65	96.59	124.39
	3	-0.99	4.29×10^8	702.57	126.27	- 86.77	120.43	181.39
	4	-0.99	1.72×10^{12}	907.61	226.83	-19.94	219.28	240.08

Here, r is Pearson's correlation coefficient, and A is Arrhenius pre-exponential factor.

Table 3
Physicochemical parameters.

Compounds	T (K)	CMC (mol L^{-1})	ΔG_m^o (kJ/mol)	$\alpha = S_2/S_1$	Std. Dev. in Linear Fit (SD)
LA	308	4.02×10^{-2}	-12.50	0.48	0.1200
	318	4.68×10^{-2}	-12.21	0.49	0.1703
Complex 1	308	3.59×10^{-4}	-32.09	0.42	0.1738
	318	4.33×10^{-4}	-31.33	0.47	0.7464
Complex 2	308	2.64×10^{-4}	-34.16	0.38	0.2744
	318	3.76×10^{-4}	-32.94	0.42	0.0561

Here S1 and S2 represent premicellar and postmicellar slopes.

Table 4
Corrosion parameters.

Compound	Concentration (ppm)	Corrosion rate (mm per year)	Inhibition efficiency (η) (%)	Surface coverage (θ)
HL	200	8.88	80.19	0.8041
	400	7.42	82.84	0.8204
	600	6.06	86.42	0.8596
	800	5.24	88.29	0.8821
	1000	4.05	90.94	0.9100
Complex **1**	200	5.31	88.07	0.8759
	400	4.58	89.72	0.8930
	600	3.79	91.51	0.9158
	800	3.45	92.28	0.9271
	1000	1.95	95.62	0.9550
Complex **2**	200	7.27	81.28	0.8259
	400	6.22	83.72	0.8425
	600	5.41	87.28	0.8763
	800	3.93	91.18	0.9155
	1000	2.90	93.51	0.9325
Control (1N HCl)	44.68			

of micelles with lower ionic mobility, the conductivity decreases after the CMC point [7]. Table 3 presents physicochemical data calculated from conductivity vs concentration plots. A higher CMC was reported for **LA** and complexes **1** and **2** at 318 K than at 308 K. A larger CMC value for **LA** (1.5×10^{-2} M) compared to complex **1** (3.21×10^{-4} M) and complex **2** (1.98×10^{-4} M) was also reported previously [1]. The Gibbs free energy of micellization (ΔG_m^o) was negative for all (Table 3) and became more negative from **LA** to complex **1** and then to complex **2** at a particular temperature, indicating spontaneity.

The anticorrosion activity was investigated using the weight-loss method, and the corrosion parameters are listed in Table 4. Table 5 presents the mass loss data for the carbon steel coupons during the experiments. Graphs showing the corrosion rate, inhibition efficiency, and surface coverage are shown in Figs. 6-8.
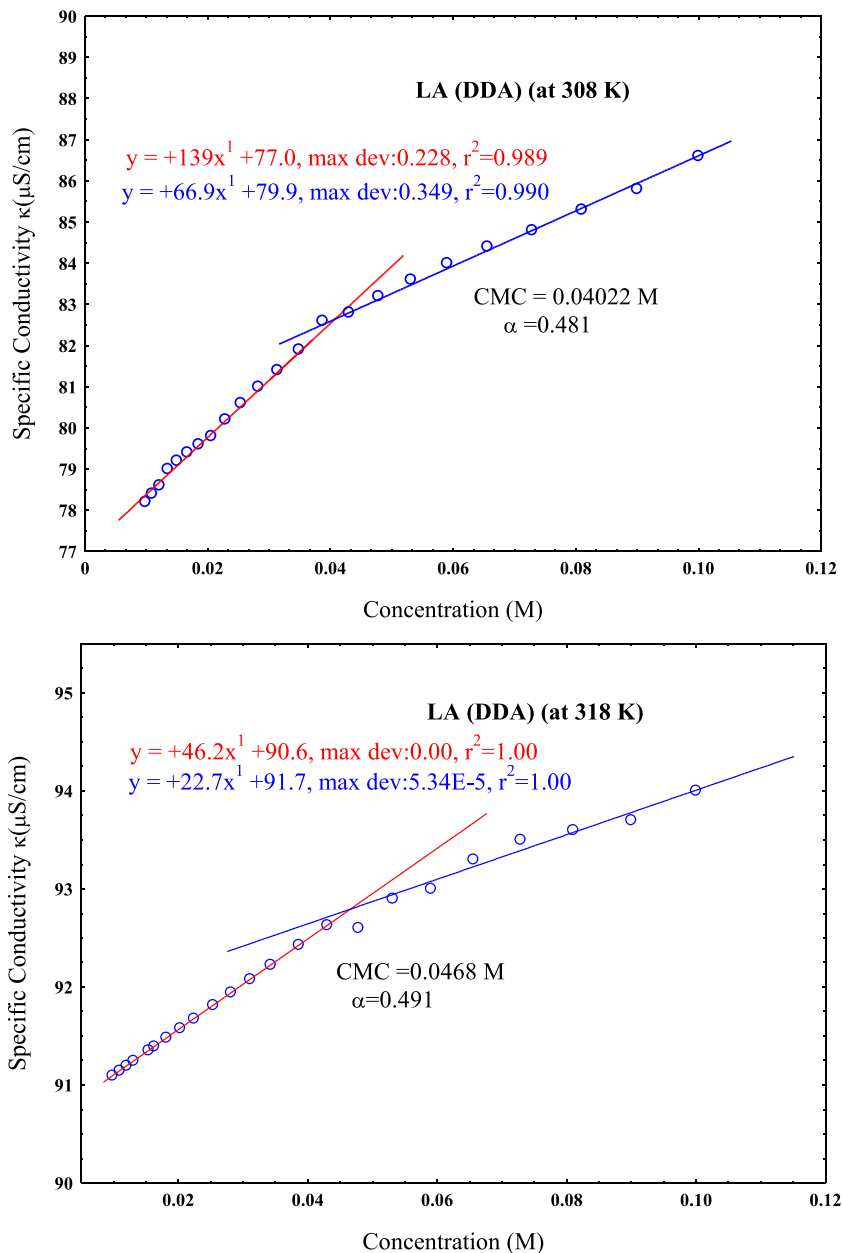
Fig. 3. Plot of conductivity versus concentration of LA (DDA) at 308 K, and 318 K.

3. Experimental Design, Materials and Methods

3.1. SEM-EDX Analysis

SEM-EDX analysis was performed in JEOL 6390 LA scanning electron microscope with 3,00,000 X magnification, and accelerating voltage of 0.5-30 kV. EDX resolution was 136 eV under the detection area 30 mm^2.
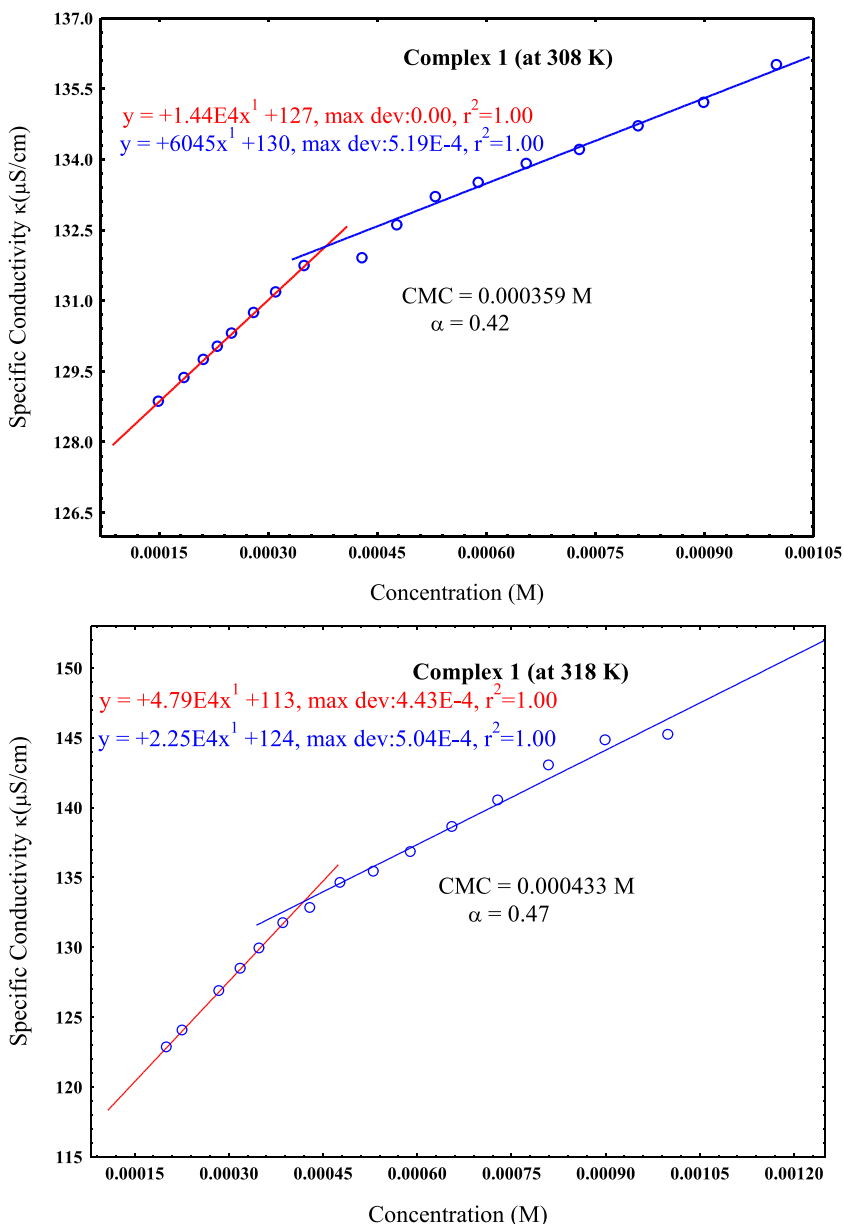
Fig. 4. Plot of conductivity versus concentration of Complex 1 at 308 K, and 318 K.

3.2. Thermogravimetric Analysis

TGA/DTA analysis was performed in Perkin Elmer STA6000 thermal analyzer with vertical type furnace under N_2 atmosphere. The heating scan of the sample was done from 40 to 750°C at a linear heating rate of 10°C/min. The data were processed in Origin software to extract thermokinetics parameters. The parameters such as $E*$, $\Delta H*$, $\Delta S*$, and $\Delta G*$ of each decomposi-
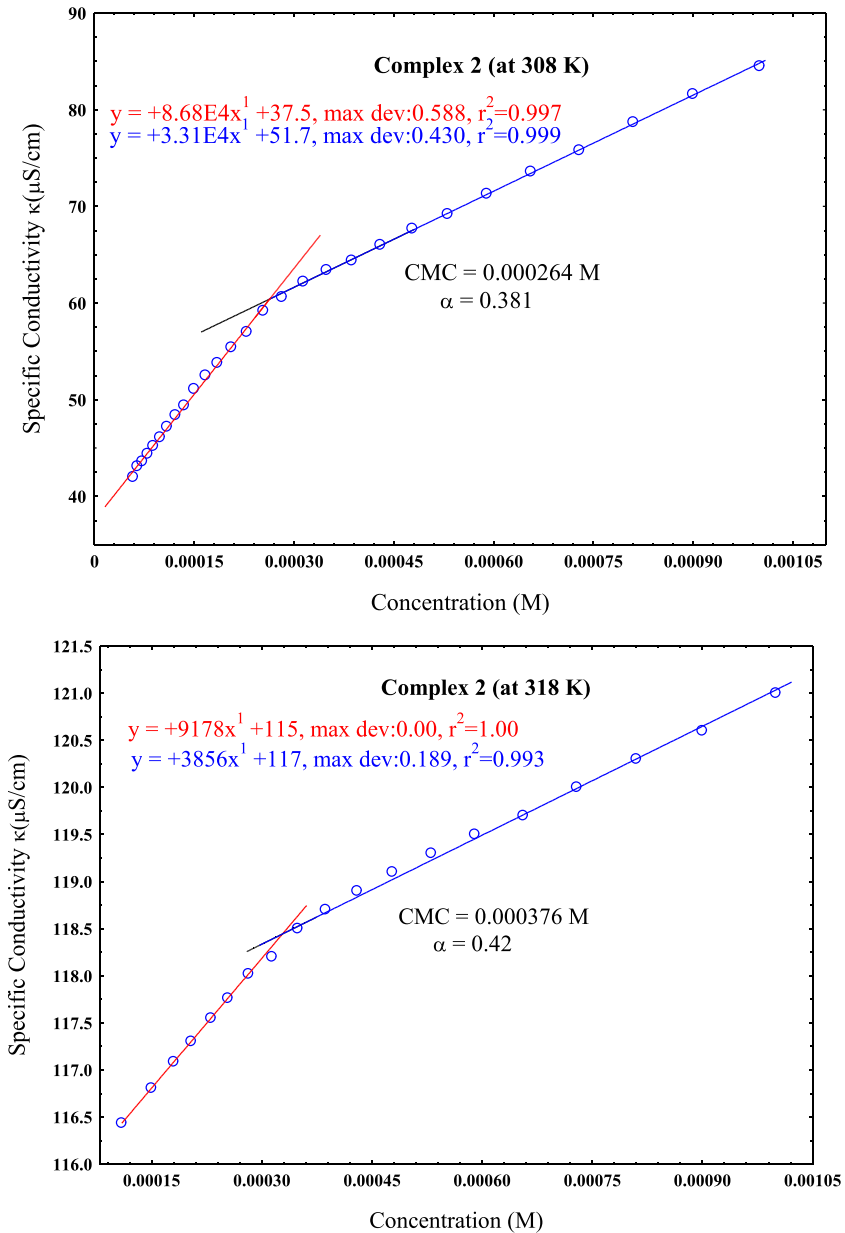
Fig. 5. Plot of conductivity versus concentration of Complex 2 at 308 K, and 318 K.

tion step were evaluated using the Coast-Redfern equation (1) [8].

$$\ln\left[-\frac{\ln(1-\alpha)}{T^2}\right] = \ln\left[\frac{AR}{\beta E^*}\right] - \frac{E^*}{RT} \tag{1}$$

Where α is the fraction decomposed at time t, β denotes the linear heating rate, A denotes the Arrhenius pre-exponential factor, and R represents the general gas constant. A plot of the
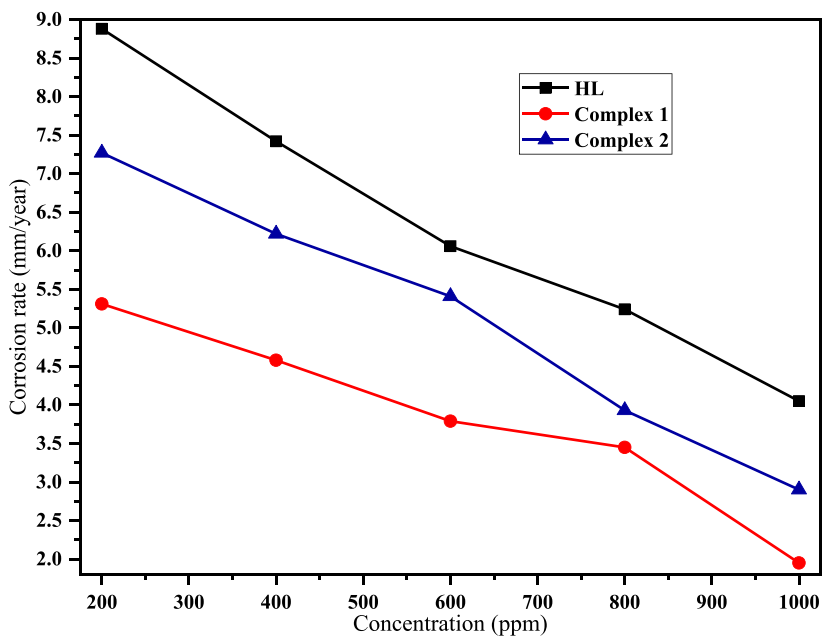
Fig. 6. Variation of corrosion rate with concentration.
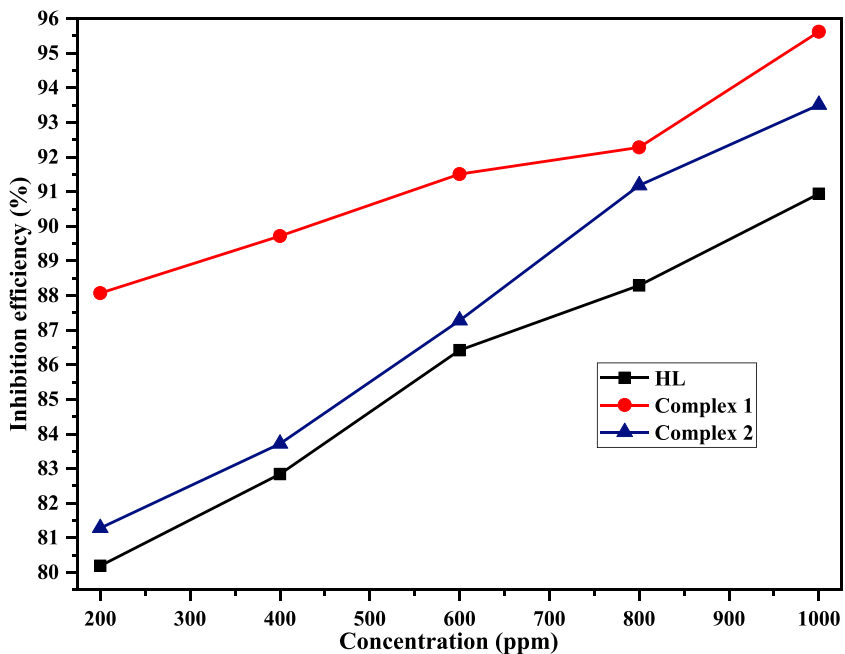
Fig. 7. Variation of inhibition efficiency with concentration.

Table 5

Mass loss of carbon steel coupons.

Compounds				
1N HCl (Control)	Concentration (ppm)	HL	Complex 1	Complex 2
Mass loss (gm)		Mass loss (gm)	Mass loss (gm)	Mass loss (gm)
0.089	200	0.0175	0.0110	0.0135
	400	0.0150	0.0095	0.012
	600	0.0125	0.0075	0.011
	800	0.0105	0.0065	0.0075
	1000	0.0080	0.0040	0.006
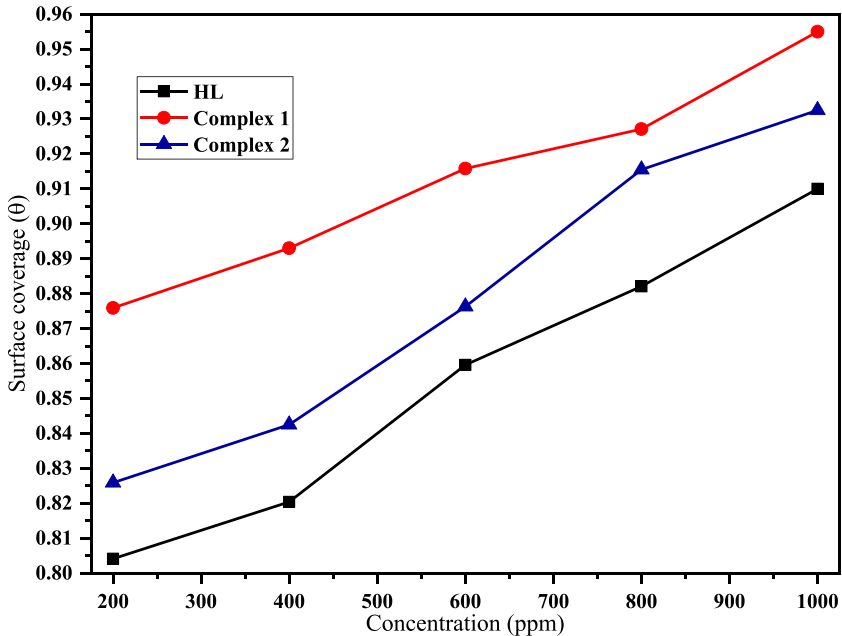
Fig. 8. Surface coverage with concentration.

left-hand side against 1000/T of equation (1) gives a straight line whose slope ($-E^*/R$) determines the activation energy (kJmol^{-1}), and the intercept indicates the value of A in the s^{-1} unit. Using equations (2, 3, and 4), other thermodynamic parameters such as the ΔG^*, ΔH^*, and ΔS^* were determined [6]. In equation (2), k_B is Boltzmann constant and h is Plank's constant.

$$\Delta S^* = Rln\left[\frac{Ah}{k_B T}\right] \tag{2}$$

$$\Delta H^* = E^* - RT \tag{3}$$

$$\Delta G^* = \Delta H^* - T\Delta S^* \tag{4}$$

3.3. Surfactant Activity Study

Conductivity measurements were performed to investigate the surfactant properties of the synthesized complexes. The study was conducted at temperatures of 308, and 318 K. The CMC

was determined by plotting the specific conductivity (κ) against the concentration of the surfactant solution. The intersection of the two lines defines the CMC point, from which the degree of micellization (α) was calculated using the formula:

$$\alpha = S_2/S_1 \tag{5}$$

Similarly, Gibb's free energy of micellization was calculated from the formula:

$$\Delta G_{\mathrm{m}}^o = RT(2 - \alpha) \ln CMC \tag{6}$$

3.4. Corrosion Inhibition Activity Study

Carbon steel (CS) coupons cut to sizes of 2 cm × 2 cm × 0.07 cm were abraded with 80, 320, 600, 800, 1000, and 1200 grade emery (silicon carbide) papers. Stock solutions (1000 ppm) of **HL**, complex **1**, and complex **2** inhibitors were prepared in 100 mL of a 1.0 N HCl solution. The stock solution was diluted to obtain solutions with the desired concentrations of 800, 600, 400, and 200 ppm. Distilled water-washed, acetone-dried, and moisture-free abraded coupons were weighed and immersed in 25 mL of diluted solutions in crucibles with and without inhibitors. After 6 h of exposure, the coupons were removed and weighed as described above. Measurements were performed in triplicate to reduce errors. The size of each coupon was measured by using a digital screw gauge. The corrosion rate (CR) (mm/yr), inhibition efficiency (IE) percent (η), and surface coverage (θ) were calculated using the following equations (7-9) [9].

$$\text{Corrosion rate, } CR = \frac{87600 \times \Delta w}{d \times A \times t} \tag{7}$$

Where Δw represents the weight loss in grams, d is the density of the CS in grams per cc, A is the area of the CS coupons, and t represents immersion time in hours.

$$\text{Inhibition efficiency \%, } \eta = \frac{CR - CR'}{CR} \times 100\% \tag{8}$$

Here, CR and CR' denote the corrosion rates in the absence and presence of the inhibitors, respectively.

$$\text{Surface coverage, } \theta = \frac{W_1 - W_2}{W_1} \tag{9}$$

Where, w_1 and w_2 represent the weight reduction in the absence and presence of the inhibitor, respectively.

Declaration of Competing Interest

The authors declare no competing financial interests or personal relationships that could influence the study reported in this article.

Data Availability

SEM-EDX, thermokinetics, surfactant and corrosion inhibition activity of Co(II) and Zn(II) complexes of (E)-N-((1Hpyrrol-3yl)methylene)dodecan-1-amine Schiff base (Original data) (Mendeley Data).

CRediT Author Statement

Janak Adhikari: Methodology, Investigation, Data curation, Writing – original draft; **Ajaya Bhattarai:** Writing – review & editing; **Narendra Kumar Chaudhary:** Supervision, Conceptualization, Data curation, Software, Formal analysis, Writing – review & editing.

Ethics Statements

This study did not involve human or animal subjects or social media platforms for analysis. Therefore, data ethics statements were not required based on the journal policy.

Acknowledgments

References

[1] J. Adhikari, A. Bhattarai, N.K. Chaudhary, Bioinorganic interest on Co(II) and Zn(II) complexes of pyrrole-based surfactant ligand: synthesis, characterization, and in silico-ADME study, J. Mol. Struct. 1274 (2023) 134434, doi:10.1016/J.MOLSTRUC.2022.134434.

[2] J. Adhikari, A. Bhattarai, N.K. Chaudhary, Synthesis, characterization, physicochemical studies, and antibacterial evaluation of surfactant-based Schiff base transition metal complexes, Chem. Pap. 76 (2022) 2549–2566, doi:10.1007/s11696-022-02062-x.

[3] N.K. Chaudhary, J. Adhikari, A. Bhattarai, SEM-EDX, thermokinetics, surfactant and corrosion inhibition activity of Co(II) and Zn(II) complexes of (E)-N-((1Hpyrrol-3yl)methylene)dodecan-1-amine Schiff base, Mendeley Data, 2023, doi:10.17632/99f4dxttm8.2.

[4] M.S. Refat, H.A. Saad, A.A. Gobouri, M. Alsawat, A.M.A. Adam, S.M. El-Megharbel, Charge transfer complexation between some transition metal ions with azo Schiff base donor as a smart precursor for synthesis of nano oxides: an adsorption efficiency for treatment of Congo red dye in wastewater, J. Mol. Liq. 345 (2022) 117140, doi:10.1016/j.molliq.2021.117140.

[5] A. Fetoh, K.A. Asla, A.A. El-Sherif, H. El-Didamony, G.M. Abu El-Reash, Synthesis, structural characterization, thermogravimetric, molecular modelling and biological studies of Co(II) and Ni(II) Schiff bases complexes, J. Mol. Struct. 1178 (2019) 524–537, doi:10.1016/j.molstruc.2018.10.066.

[6] O.A. El-Gammal, F.S. Mohamed, G.N. Rezk, A.A. El-Bindary, Structural characterization and biological activity of a new metal complexes based of Schiff base, J. Mol. Liq. 330 (2021) 115522, doi:10.1016/j.molliq.2021.115522.

[7] A. Bhattarai, Studies of the micellization of cationic-anionic surfactant systems in water and methanol-water mixed solvents, J. Solution Chem. 44 (2015) 2090–2105, doi:10.1007/s10953-015-0391-4.

[8] A.W. Coats, J.P. Redfern, Thermogravimetric analysis, Analyst 88 (1963), doi:10.1039/AN9638800906.

[9] M. Messali, M. Larouj, H. Lgaz, N. Rezki, F.F. Al-Blewi, M.R. Aouad, A. Chaouiki, R. Salghi, I.M. Chung, A new schiff base derivative as an effective corrosion inhibitor for mild steel in acidic media: experimental and computer simulations studies, J. Mol. Struct. 1168 (2018) 39–48, doi:10.1016/j.molstruc.2018.05.018.
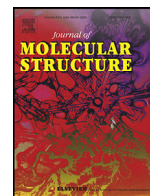
Bioinorganic interest on Co(II) and Zn(II) complexes of pyrrole-based surfactant ligand: Synthesis, characterization, and *in silico*-ADME study

Janak Adhikari, Ajaya Bhattarai, Narendra Kumar Chaudhary*

Department of Chemistry, Mahendra Morang Adarsh Multiple Campus, Tribhuvan University, Biratnagar, Nepal

ARTICLE INFO

ABSTRACT

This study aimed to design and develop surfactant-incorporated drugs to address the issues related to their antibacterial properties and drug delivery systems. Herein, a Schiff base ligand (HL), (E)-N-((1H-pyrrol-3yl)methylene)dodecan-1-amine, and its two metal complexes $[[Co(HL)_2.2H_2O]\ Cl_2.H_2O]]$ (1) and $[[Zn(HL)_2.Cl]\ Cl.3H_2O]]$ (2) was synthesized from the seed compounds laurylamine (LA) and pyrrole-3-carboxaldehyde (P3C) by a wet chemical method. They were fully characterized by elemental microanalysis, FT-IR, ^{1}H, ^{13}C NMR, ESI-MS, MALDI-TOF-MS, and UV-visible spectroscopy. Characterization was further accomplished by magnetic moment measurements, powder X-ray diffraction (PXRD), and thermo gravimetric (TGA/DTA) analyses. Based on the executed data, an octahedral geometry was proposed for complex 1 and distorted trigonal bipyramidal geometry for complex 2. This was further authenticated by running the MM2 function in the CsChemOffice Ultra 16 programs to achieve minimum energy. The electrolytic nature of the prepared compounds was evaluated using conductivity measurements. The critical micelle concentration (CMC) values of the complexes were obtained from a graphical plot of concentration versus specific conductivity. The Kirby-Bauer paper disk diffusion technique was used to explore the antibacterial activity of the synthesized compounds. Moreover, the metal complexes exhibited remarkable antibacterial activities. These were further quantified using minimum inhibitory concentration (MIC) tests. An *in silico* ADME study was conducted to predict the drug-likeliness properties of all synthesized compounds.

© 2022 Elsevier B.V. All rights reserved.

1. Introduction

Currently, chemical engineers and pharmacists are developing new inorganic chemistry strategies to enhance the biomedical properties of drugs. Pharmacists have recently focused their efforts on metal-based chemotherapy in response to the serendipitous discovery of cisplatin as an anticancer drug [1]. Metals are crucial components of several commercial drugs because they form coordination complexes vital in pharmacology [2]. Many metal-based drugs exhibit various biological properties, including antibacterial [3], antiviral [4], antifungal [5], anticancer [3,6], antitubercular [7], herbicidal, and antitumor effects. Metal complexes interact effectively with intercellular components and target biomolecules *in vivo* owing to their attractive redox chemistry and thermodynamic stability. Biologically relevant metals, even those from the same group and period, behave differently in different environments and provide distinct insights into the biological processes associated with cell inhibition [8]. Therefore, we aimed to modulate the bio-

chemical activity of these metal complexes by altering their coordination spheres using surfactants.

Surfactants in pharmaceutical science have emerged as invaluable alternatives for improving the potency of conventional drugs. Simultaneously, they renovated the drug delivery system to improve the efficiency of drugs with poor aqueous solubilities [9]. Surfactants are amphiphilic organic compounds used as emulsifiers, wetting agents, solubilizers, corrosion inhibitors, fabric softeners, mineral concentrators, petroleum processing, cleaning detergents, health and personal care products, foods, and crop protection, etc. [10]. The pharmaceutical industry uses surfactants to enhance drug activity owing to their antifungal, antibacterial, and antiviral properties [11]. The amphiphilic nature of surfactants dramatically alters the biological activities of many medicinal substances. Surfactant-added drug molecules can exert several effects either by increasing the solubilization behavior of solid drugs or by increasing membrane permeability in the lipid layer [12]. The hydrophobic nature of the surfactant facilitated the self-aggregation and micellization of the molecules. These properties can lead to various geometric structures, such as monolayers, bilayers, and micelles, which affect the physicochemical profile of the aggregates [13].

Metallosurfactants prepared from Schiff bases comprise metal ions as hydrophilic head groups and hydrocarbons as hydrophobic tail groups. Typically, drugs are administered in the complex form *in vivo* to achieve the desired effect. Metallosurfactants can function as drugs by interacting with various organic bioactive molecules, DNA, and proteins to facilitate drug metabolism [14]. The characteristics of surfactant-based drugs were examined in this study to relate the current treatment to drug delivery. Another consequence of this new pharmacology is antibiotic resistance, which has become a significant problem in medical science, resulting in mortality and morbidity. Recently emerged bacteria have developed antibacterial resistance through various mechanisms of enzymatic action on host cells, which require improvements in the pharmacological value of traditional medicines by complexing them or adding surfactants as prodrugs or synthesizing surfactant-based modified complexes.

In recent years, the synthesis of Schiff bases and their transition-metal complexes has received substantial attention for the development of chelating agents as viable alternatives to coordination compounds. In addition to their biological activities, they have good coordinating properties. Coordination interactions greatly influence the biochemistry of ligands and metal moieties [15]. The azomethine linkage within the Schiff base is responsible for exhibiting bioactivities such as its anticancer, antiviral, and antibacterial activity. Because of their numerous biological activities, five-membered heterocyclic compounds such as pyrrole and its derivatives are of great interest to chemists. Many natural products contain the essential core units of bioactive and pharmacologically active compounds.

Herein, we report the synthesis of an asymmetrical Schiff base ligand (HL) from laurylamine (LA) and pyrrole-3-carboxaldehyde (P3C) and their two metal complexes 1 and 2 with divalent 3d-metals (Co^{+2} and Zn^{+2}). They were characterized using ^1H and ^{13}C NMR, UV-visible spectroscopy, ESI-MS, MALDI-TOF-MS, FT-IR, TGA/DTA, and powder X-ray diffraction. The geometry of the synthesized compounds was optimized using the MM2 function of CsChemOffice molecular modeling software. The standard Kirby-Bauer paper disk diffusion technique was used to explore antibacterial potency against gram-positive and gram-negative bacteria. Furthermore, their potency against the target pathogens was quantitatively assessed by measuring the minimum inhibitory concentration (MIC) values.

2. Experimental

2.1. Materials and reagents

The chemicals Laurylamine (LA) and pyrrole-3-carboxaldehyde (P3C) were procured from Spectrochem, Mumbai, India, and Alfa Aesar, respectively, and were used as received. Mueller Hinton Agar (MHA) was purchased from HiMedia, India. Ethanol, which was used as the solvent, was procured from Qualigen. Zn and Co chloride salts were purchased from Merck. Analytical reagent (AR-) grade chemicals and solvents were used in all the experiments.

2.2. Instruments

Conductivity measurements of LA, HL, and complexes 1 and 2 were recorded using an auto-ranging digital conductivity/TDS meter TCM 15+. A Thermo Finnigan Flash EA1112 Series CHN analyzer was used to determine the CHN % of the compounds. Their melting points were recorded using a VEEGO ASD-10013 programmable melting-point apparatus. A Thermo Nicolet Avatar 370 FT-IR spectrophotometer was used to analyze the FT-IR spectra in the 4000–400 cm^{-1} range using a KBr matrix. A Bruker Avance III 400 MHz NMR spectrometer was used to record the ^1H and ^{13}C NMR spectra, using DMSO–$d6$ as the working solvent and TMS as the internal reference standard. An Agilent Cary 5000 UV.-visible spectrophotometer with a quartz cuvette was used to record the electronic absorption spectra of the synthesized compounds using DMSO as a solvent in the 200–800 nm wavelength region. Autoflex MALDI-TOF and Agilent Q-TOF mass spectrometers were used to record positive-mode ESI-mass spectra of the synthesized compounds. Powder X-ray diffraction (XRD) patterns were recorded on a Bruker AXS D8 Advance X-ray diffractometer using a monochromatized Cu-K_α line with a 1.5406 Å wavelength of the radiation source. TGA/DTA measurements were performed using a Perkin-Elmer thermal analyzer with a linear heating rate of 10 °C min^{-1} in the temperature range of 40–750 °C. Molecular modeling parameters were obtained using the energy optimization task via MM2 calculations supported by the CsChemOffice software program.

2.3. Preparation of HL

Initially, a solution of P3C (4 mmol, 0.3804 g) in 15 ml ethanol was prepared, followed by a solution of LA (4 mmol, 0.7414 g) in another 15 ml ethanol. Both solutions were mixed and magnetically stirred in a 100 ml round bottom flask. The mixture was refluxed for 7 h at 30 °C and cooled to room temperature. A light-orange solid was obtained. It was then filtered, re-crystallized from absolute ethanol, and dried over anhydrous $CaCl_2$. The product was stored in an airtight vial in the refrigerator. Scheme 1 illustrates the preparation route of HL, complexes 1 and 2.

2.4. Preparation of complexes 1 and 2

In two separate experiments, a solution of 0.25 mmol metal chloride salts ($CoCl_2.6H_2O$ (0.0599 g) and $ZnCl_2$ (0.0341 g)) prepared in 10 ml ethanol was added drop-wise to a hot solution of HL (0.5 mmol, 0.1312 g) in ethanol and refluxed for several hours. Stable solid products of the metal complexes 1 and 2 were obtained by cooling the solution under normal atmospheric conditions. They were washed several times with absolute ethanol, re-crystallized, and dried over anhydrous $CaCl_2$ in a desiccator. The products were stored in airtight vials in a refrigerator until further use.

2.5. Antibacterial activity study

2.5.1. Disc diffusion study

The *in vitro* antimicrobial screening of HL and complexes 1 and 2 was tested against five human pathogenic bacteria, including *Staphylococcus aureus* (*S. aureus*), *Enterococcus, Klebsiella pneumoniae* (*K. pneumoniae*), *Escherichia coli* (*E. coli*), and *Pseudomonas aeruginosa* (*P. aeruginosa*) using the modified Kirby-Bauer paper disk diffusion technique. The desired concentration of pathogens (comparable to 0.5 McFarland turbidity standards) was obtained from a fresh bacterial culture revived by inoculation in 5 ml of nutrient broth and incubated for 3 h at 35 °C [16]. Agar plates were prepared according to standard procedures. Test organisms were spread uniformly on agar plates using sterile stick swabs. Appropriate concentrations of the test compounds were obtained by dissolving them in DMSO. Well-sterilized filter paper disks of 5 mm diameter size soaked in the test solution were carefully stuck to the swabbed medium. Amikacin, 30 µg/disk, was used as a positive control, and a blank disk soaked in DMSO was used as a negative control. The loaded plates were incubated for 24 h at 37 °C, and the diameters of the zones of inhibition in millimeters (mm) around each disk were measured to compare their antibacterial efficacy [17]. This study was repeated in triplicate to reduce measurement errors.
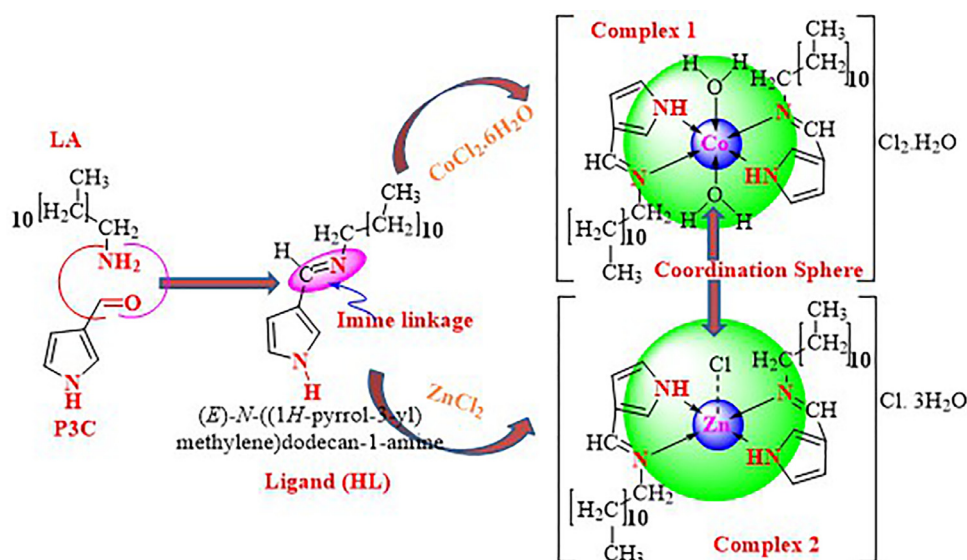
Scheme 1. Synthetic route for ligand (HL) and metal complexes.

2.5.2. Minimum inhibitory concentration (MIC) study

MIC represents the lowest concentration of test compounds that did not show any visible growth of organisms in the broth mixed with the test compounds. Stock solutions of test compounds (50 μg/μL) were prepared in DMSO. A two-fold serial dilution technique was used to obtain lower concentration gradients [18]. The bacterial suspensions (100 μL) were added to each diluted solution and incubated for 24 h at 37 °C. Each measurement was repeated three times to reduce measurement errors. Broth containing the bacterial suspension was used as the negative control, and broth containing no bacteria was used as the positive control.

2.6. In silico ADME properties study

Drug discovery and development require time, materials, and facilities. The development of a theoretical investigation is crucial to reduce these factors and predict potential drug applications. A chemical compound must meet the pharmacokinetics of ADME and have excellent biological activity in vitro. Physicochemical criteria were computed in silico using the Swiss ADME online predictor for validating the parameters.

3. Results and discussion

3.1. Physicochemical study

The Metal complexes were soluble in DMSO and sparingly soluble in methanol/ethanol, whereas HL was soluble in both. Elemental microanalysis strongly supports ML_2-type stoichiometry with 1:2 metal-ligand ratios. Metal coordination to HL occurs through the N, N donor atoms, suggesting the bidentate nature of the ligand. Further confirmation of the geometry of the complexes was provided by the $(M^{\bullet+})$ ion peak in the mass spectra, resonance signals in the ^{1}H and ^{13}C NMR spectra, UV absorption bands, and characteristic bands in the FT-IR spectra. These complexes are stable in the air; therefore, they can be maintained in desiccators for a long time without decomposition. To prevent the loss of biological potency, they were stored in a refrigerator at a temperature of <10 °C. The molar conductance values in 10^{-3} (M) DMSO solution were within the ranges of 1:2 and 1:1 electrolytes for complexes 1 and 2, respectively, indicating that they are electrolytes [19]. Based on these findings, it was concluded that two ions and one ion outside the coordination sphere of complexes 1 and 2 served as the counter ions. All efforts to grow single crystals for crystallographic structure determination failed, and we preferred PXRD to investigate the crystal parameters. The micro-analytical and physical data of HL and its complexes are presented in Table 1.

3.2. Conductivity study

The specific conductivities of LA and its complexes 1 and 2 were measured at 298 K at varying concentrations to estimate the critical micelle concentration (CMC) and degree of micellization (α). The plot of conductivity versus concentration shows two straight lines, one representing the pre-micellar region and the other representing the post-micellar region. The inflection point of the two straight lines in the plot gives the CMC, and the slope ratio between the post-micellar and pre-micellar regions determines the degree of micellization (α). Fig. 1 illustrates the conductivity-concentration plot, and Table 2 presents the calculated values of CMC and (α). We previously reported the CMC value for LA (1.5×10^{-2} M) at 298 K in the literature [20], and this value is higher than the CMC of the complexes reported here. The calculated CMC values of complexes 1 and 2 were 3.21×10^{-4} M and 1.98×10^{-4} M, respectively. This variation in the CMC of the complexes can be explained by their electrolytic nature as well as variations in the electronegativity and size of the metal ions. The increase in the CMC of the complexes is generally due to an increase in the electronegativity of the metals and a decrease in their ionic radii. Zn is less electronegative than Co, and Zn^{+2} has a greater ionic radius than Co^{+2}. Therefore, the CMC trend in this study is consistent with our prediction. A greater ionic strength around micelles reduces repulsion among polar head groups, makes micellization easier, and lowers the CMC with respect to the increased ionic size [21,22]. Gibbs free energy of micellization $(\Delta G°_m)$ was calculated using the following equation:

$$\Delta G°_m = (2 - \alpha) \, RT \, ln(CMC)$$

This value was negative, indicating that micellization occurred spontaneously. Metallosurfactants with large metal ions have higher head polarity, so their negative $(\Delta G°_m)$ values increase. In our study, complex 2 had a higher negative $(\Delta G°_m)$ because of easier micellization. These results indicated that metal-based surfactants are more likely to micellize [23].

Table 1
Micro-analytical and physical data of the ligand (HL) and its complexes.

Compounds	Empirical Formula	Formula Wt.	Yield%	Color	M.Pt. (°C)	Calculated (Found) (%)		
						C	H	N
HL	$C_{17}H_{30}N_2$	262	80	Light Orange	67–69	77.80 (77.91)	11.52 (11.31)	10.67 (10.48)
Complex 1	$C_{34}H_{66}Cl_2CoN_4O_3$	708	75	Green	70–76	57.78 (58.02)	9.13 (9.25)	7.93 (7.81)
Complex 2	$C_{34}H_{66}Cl_2N_4O_3Zn$	714	68	Reddish Brown	68–70	57.26 (57.34)	9.05 (8.95)	7.86 (7.80)

Fig. 1. Plot of conductivity versus concentration of (a) complex 1, (b) complex 2.

Table 2
Values of premicellar slope (S_1), postmicellar slope (S_2), degree of micellization (α), critical micelle concentration (CMC), and Gibbs free energy of micellization ($\Delta G^o{}_m$) of DDA, Complex 1 and Complex 2 in DMSO at 298 K.

Compounds	S_1 ($\mu S\ cm^{-1}\ L \cdot mole^{-1}$)	S_2 ($\mu S\ cm^{-1}\ L \cdot mole^{-1}$)	α	CMC (mole L^{-1})	$\Delta G^o{}_m$ (kJmol^{-1})
DDA	633	240	0.379	1.53×10^{-2}	−16.79
Complex 1	3.98×10^4	1.34×10^4	0.337	3.21×10^{-4}	−33.14
Complex 2	6.42×10^4	1.02×10^4	0.159	1.98×10^{-4}	−38.89

Table 3
Selected FT-IR data of HL and its metal complexes.

Compounds	ν(NH)	ν(C=N) (imine)	ν (C-H)	ν (C=C)	ν (C-N)	ν(M-N)	ν(M-O)	ν (H$_2$O)/δ(H$_2$O) Coordinated
HL	3131	1644	2916, 2847	1470, 1511	1375	-		-
Complex 1	3134	1653	2910, 2848	1470, 1513	1376	416	549	3551, 961
Complex 2	3222	1664	2922, 2851	1466, 1519	1380	418	-	-

3.3. FT-IR spectral analysis

The most significant IR bands (4000–400 cm^{-1}) were identified in the spectra to establish the bonding sites of the ligand when coordinated with metal ions. The reported FT-IR data are presented in Table 3. Comparative analysis of the band positions in the IR spectra of HL and its complexes suggested that HL behaves as a neutral bidentate N, N donor ligand with azomethine-N and pyrrole-N as coordination sites. The FT-IR spectra are shown in Figs. S1–S3. The ν(HC=N) stretching vibration band of the azomethine group shifted to higher wavenumbers upon complexation, indicating the bonding of this nitrogen with metal ions. It appeared at 1644 cm^{-1} in the HL spectrum and shifted to 1653 and 1664 cm^{-1} in the spectra of complexes 1 and 2, respectively. This may be due to the +I effect caused by the long-chain alkyl group

of the surfactant moiety [24,25]. The pyrrole ring ν(N-H) stretching vibration band for HL at 3131 cm^{-1} and metal complexes at 3134 and 3222 cm^{-1} indicated the participation of this nitrogen in the complexation. The greater shift of the ν(N-H) stretching vibration in complex 2 might be due to hydrogen bonding, whereas a slight shift in complex 1 implies no loss of H atoms even after complexation. A new band was observed at higher wavenumbers (3551 cm^{-1}) in the IR spectrum of complex 1, which correlates with the overlap of coordinated water and Co^{+2} ions [26,27]. Another sharp peak at 961 cm^{-1} corresponds to the bending vibration of the coordinated H$_2$O. The most exciting and obvious fact for M-N and M-O coordination in the complexes was confirmed by the absorption bands observed in the lower wavenumber region of the spectra. The absorption bands due to the ν(M–N) stretch for complex 1 were observed at 416 and 448 cm^{-1}, corresponding to

Table 4
^{1}H and ^{13}C NMR spectral data of HL and complex 2.

	Ligand (HL)	Complex 2		Ligand (HL)	
H	δ (ppm)	δ (ppm)		C	δ (ppm)
H-1	7.11 (s, J = 1.01 Hz, 1H)	7.77 (s, J = 1.01 Hz, 1H)		C-2a	122.51
H-(2a/2b)	6.75 (s, J = 1.00 Hz, 1H)	7.05 (s, J = 1.00 Hz, 1H)		C-2b	119.04
H-4	6.34 (s, J = 1.02 Hz, 1H)	6.77 (s, J = 1.05 Hz, 1H)		C-3	121.3
H-5	8.11 (s, J = 1.03 Hz, 1H)	8.56 (s, J = 0.96 Hz, 1H)		C-4	108.2
(H-6 & 7)	1.51/1.53 (m, J = 2.01 Hz, 2H)	1.64 (m, J = 2.07 Hz)		C-5	155
	–	–		C-6	60.69
(H-8) – (H-15)	1.23–1.26 (m, J = 14.02 Hz)	1.24–1.29 (m, J = 14.61 Hz)		C-7	30.74
H-16	1.52	–		C-8	26.71
H-17	0.83–0.86 (t, J = 3.1 Hz, 3H)	0.83–0.87 (t, J = 4.11 Hz)		(C-9) – (C-14)	28.59–28.93
H$_{(H2O)}$	3.33–3.39	3.58–3.61 (broad, J = 2.31 Hz)		C-15	31.18
				C-16	21.98
				C-17	13.84

coordination with azomethine nitrogen and pyrrole ring nitrogen, respectively. Another band at 549 cm^{-1} confirmed ν(M–O) stretching. The ν(M–N) stretching vibration band of complex 2 was observed at 418 cm^{-1}. These major diagnostic bands and their positional shifts from free ligands to metal complexes strongly support the proposed structure of these complexes [28,29].

3.4. ^{1}H and ^{13}C NMR spectral analysis

A better understanding of the formation of the HL was also supported by ^{1}H and ^{13}C NMR spectral analyses. A comparison of the ^{1}H NMR signals of the HL and complex 2 clarified the coordination mode of the ligand. The NMR spectral data are presented in Table 4. The spectrum of HL (Fig. S4) showed a singlet at δ 8.1 ppm due to azomethine proton (-N=CH-), indicating that Schiff base was formed [30,31]. This peak for complex 2 has undergone a downfield shift from δ 8.1 ppm to δ 8.5 ppm, which might be due to the share of lone pair electrons to the central metal ion, indicating the formation of (Zn←N) linkage [32]. The pyrrole N-H proton resonated as a singlet at δ 7.11 ppm for HL, which after complexation, has undergone a downfield shift at δ 7.77 ppm. The other significant ^{1}H NMR signals for HL are 6.75 (s, H-(2a/2b)), 6.34 (s, H-4), and 3.33–3.39 (H$_{H2O}$). These peaks in the spectrum of complex 2 (Fig. S5) appeared almost in a similar position with only minor variation, supporting the legation of HL to Zn^{+2} via the azomethine group. ^{13}C NMR spectral analysis is another clear indicator of ligand formation. A signal at 155 ppm in the ^{13}C NMR spectrum of HL is attributed to azomethine carbon (C-5). The pyrrole ring carbons displayed signals at 122.51 ppm (C-2a), 119.04 ppm (C-2b), 121.3 ppm (C-3), and 108.2 ppm (C-4). The methyl and methylene carbons of the long chain of surfactant portion of the molecule exhibited signals ranging from 13.84 ppm to 60.69 ppm. ^{13}C NMR spectrum of HL is shown in Fig. S6. All these NMR spectral values support the formation of the free ligand as well as the chelation of ligand with metal for complex formation.

3.5. UV-visible spectral study

UV-visible spectral data are presented in Table 5, and spectra are illustrated in Fig. 2. The spectrum of HL exhibited two distinct absorption bands in the ultraviolet region of the spectrum. The first band appeared at 275 nm due to the $\pi \rightarrow \pi^*$ electronic

transition of the pyrrole ring. This high energy band appeared at 268 and 286 nm in the spectra of complexes 1 and 2, respectively. The second absorption band at 373 nm for HL is attributed to the $\pi \rightarrow \pi^*$ and $n \rightarrow \pi^*$ transition of the azomethine group [33]. These bands are also seen in the spectra of complexes with peak values of 350 nm and 392 nm, respective for complexes 1 and 2 [34]. The UV-visible spectral data of complex 1 coupled with magnetic moment data (4.2 BM) illustrated its octahedral geometry [35]. There were three absorption bands reported in the spectrum of complex 1 in the visible range. These absorption bands at 661 nm, 552 nm, and 444 nm are assigned as $\nu_1 4T_{1g}(F) \rightarrow 4T_{2g}(F)$, $\nu_2 4T_{1g}(F) \rightarrow 4A_{2g}(F)$, $\nu_3 4T_{1g}(F) \rightarrow 4T_{1g}(P)$ electronic transitions respectively and agree with octahedral geometry. The UV-visible spectrum of complex 2 displayed two absorption bands at 286m and 392 nm, illustrating $\pi \rightarrow \pi^*$ and $n \rightarrow \pi^*$ transitions. Broadening of the band at 392 nm may result from the interaction of the ligand to metal charge transfer (LMCT) band with the $n \rightarrow \pi^*$ transition. The spectrum did not show d-d transition due to the complete d^{10} electronic configuration of zinc. Additionally, FT-IR, ^{1}H NMR, and the thermal study revealed 3H$_2$O molecules as the structural unit of this complex. All this evidence, UV-visible, and molar conductivity data suggested distorted trigonal bipyramidal geometry for complex 2 [36].

3.6. Mass spectral study

The mass spectra of the studied compounds are shown in Figs. (S7 - S9). The spectrum of HL exhibited a high-intensity peak at 263 m/z, which was assigned to the [M^{+}+H] peak. Accordingly, HL must have a molecular mass of 262 m/z, according to the nitrogen rule. Fragment peaks were observed at m/z 235, 187, and 186. MALDI-TOF mass spectrum of complex 1 showed a base peak at 610.56 m/z with a relative intensity of 6454 (a.u.) and a molecular ion peak though small at 707.65 m/z with a relative intensity of 165 (a.u.). Accordingly, its molecular mass was assigned as 708 m/z, which is in agreement with its theoretical value. In addition, fragment peaks with variable intensities were detected at m/z 593, 582, 523, 453, and 446. The mass spectrum of complex 2 showed a [M^{+}−2H] peak at 711.466 m/z. As a result, its molecular mass was assigned as 714 m/z, which is consistent with its theoretical molecular mass. Several other peaks were detected at m/z 655, 487, 469, and 449, all of which were fragment peaks. Therefore, the

Table 5
UV/visible, magnetic moments, and molar conductivity data of HL and its metal complexes.

Compounds	Peak positions nm	Assignment	Magnetic moment (BM)	Λc (Ω^{-1} cm^2 mol^{-1})
HL	275	$\pi \rightarrow \pi^*$,	0	5.6
	373	$n \rightarrow \pi^*$		
Complex 1	268	$\pi \rightarrow \pi^*$	4.2	108.8
	350	$n \rightarrow \pi^*$		
	444	$^4T_{1g}$ (F) $\rightarrow ^4T_{1g}$ (P)		
	552	$^4T_{1g}$ (F) $\rightarrow ^4A_{2g}$ (F)		
	661	$^4T_{1g}$ (F) $\rightarrow ^4T_{2g}$ (F)		
Complex 2	286	$\pi \rightarrow \pi^*$	0	83.6
	392	$n \rightarrow \pi^*$		
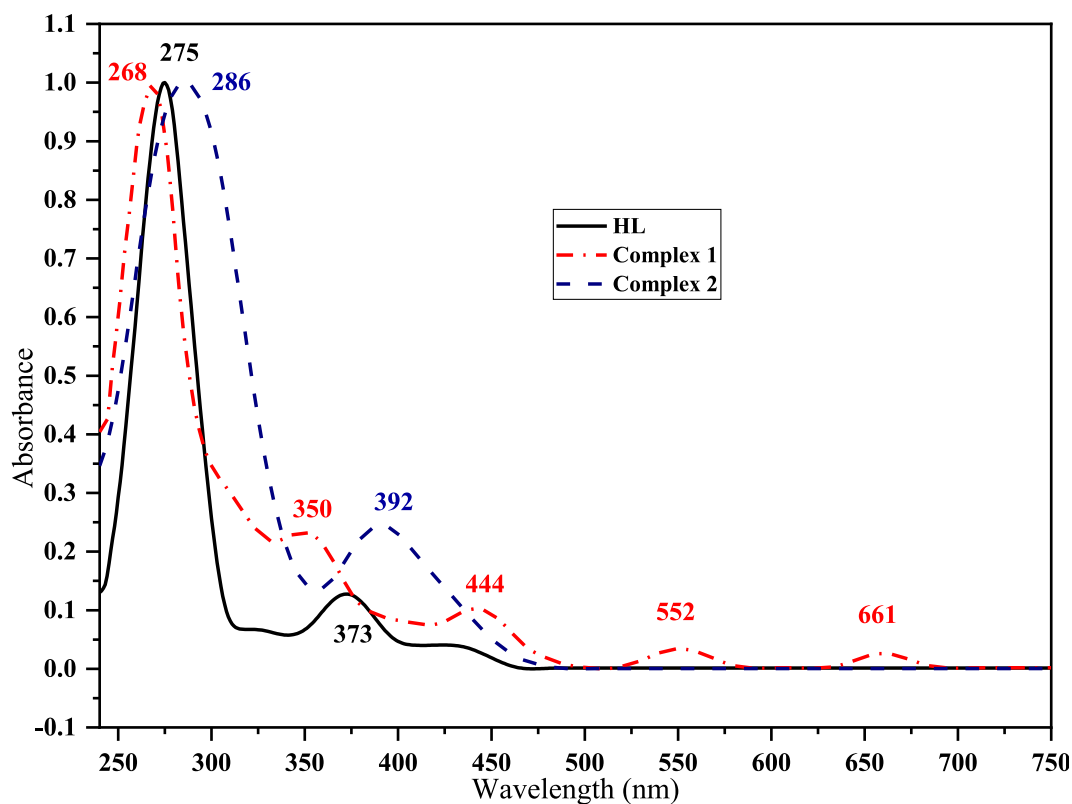
Fig. 2. UV-visible spectra of ligand (HL), and its complexes.

Table 6
Thermal decomposition data of complexes.

Complexes	Steps	TG range (°C)	DTA				
		Δm % found (Cal.)	T_i	T_f	T_{DTG}	Mass loss	T_{DTA}
Complex 1	1	3.86	73.57	147.35	118.13	0.17	-
	2	26.05	152.31	250.62	198.54	1.14	
	3	17.74	378.05	476.31	412.68	0.40	422.89
Complex 2	1	1.55	67.77	132.65	100.91	0.10	-
	2	13.21	156.64	250.43	209.09	0.90	195.27
	3	33.13	342.07	474.57	429.42	1.69	445.36
	4	92.11	551.07	700.11	634.46	2.72	637.19

proposed molecular formula for all compounds was strongly supported by the mass spectral values [37,38].

3.7. TGA/DTA study

Thermogravimetric analysis (TGA) was conducted in an N_2 atmosphere at a linear heating rate of 10 °C/min in the temperature range of 40−750 °C [39]. The TGA/DTA data are presented in Table 6, and thermograms showing various decomposition steps

are presented in Figs. 3 and 4. Complex 1 decomposed in three stages, the first of which occurred at 73.6–147.4 °C with a T_{DTG} peak at 118.1 °C. This may be due to the loss of the outer sphere H_2O and 2Cl atoms. A part of the ligand moiety and coordinated H_2O was lost in the second stage of decompositionat 152.3–250.6 °C with a corresponding mass loss of 1.1364 mg (26.05%) and a T_{DTG} peak at 198.5 °C. The entire ligand moiety was eliminated in the third stage at 378.1–476.3 °C, with a T_{DTG} peak at 412.7 °C and a mass loss of 0.4098 mg (17.74%), leaving a solid residue of
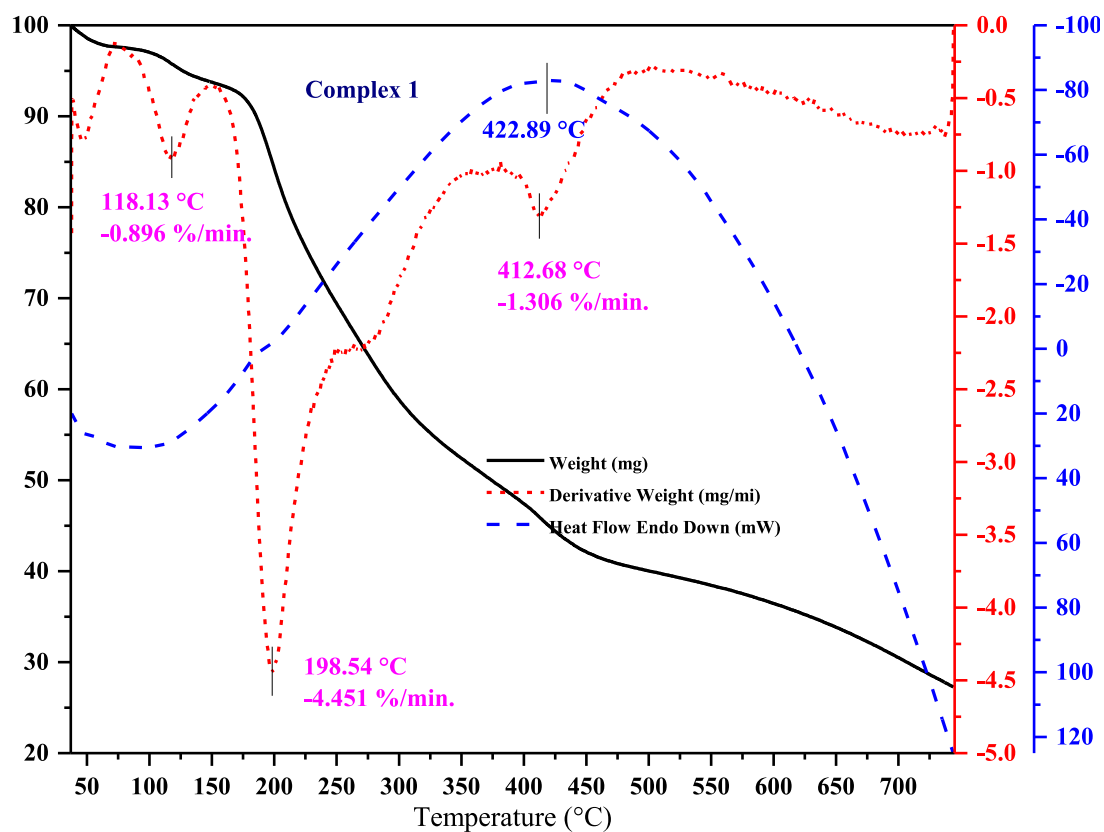
Fig. 3. Thermogram of complex 1.
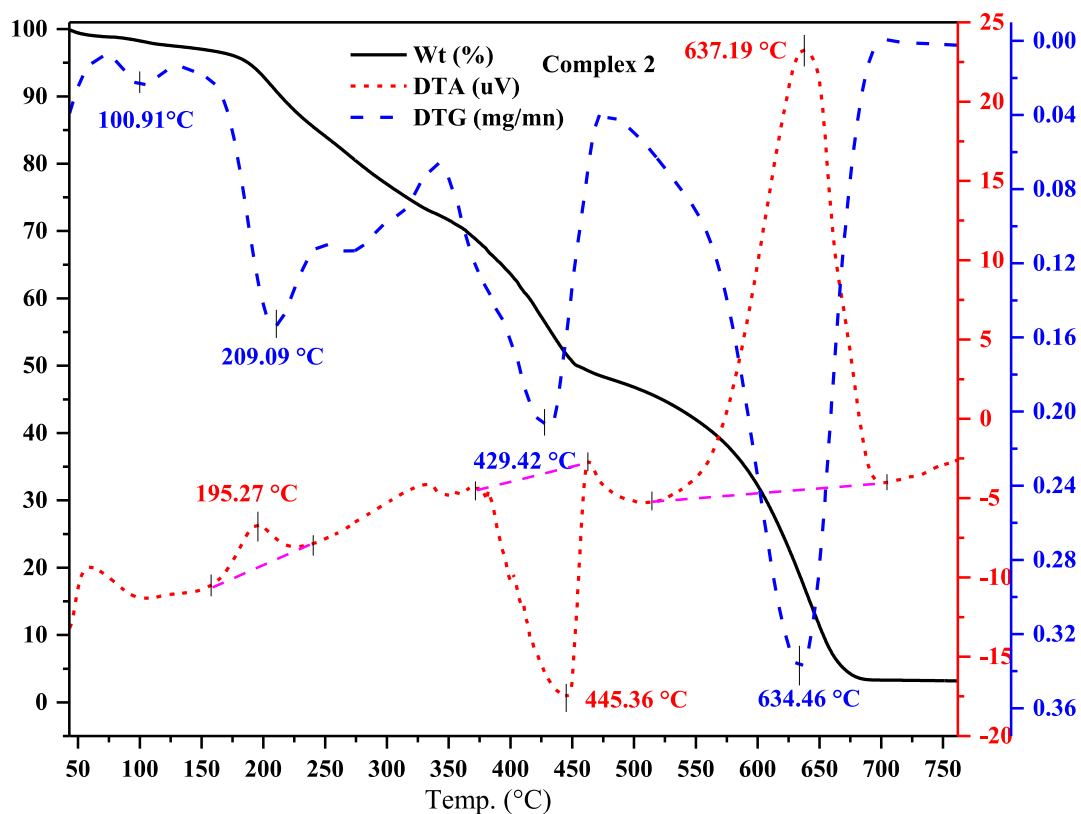
Fig. 4. Thermogram of complex 2.
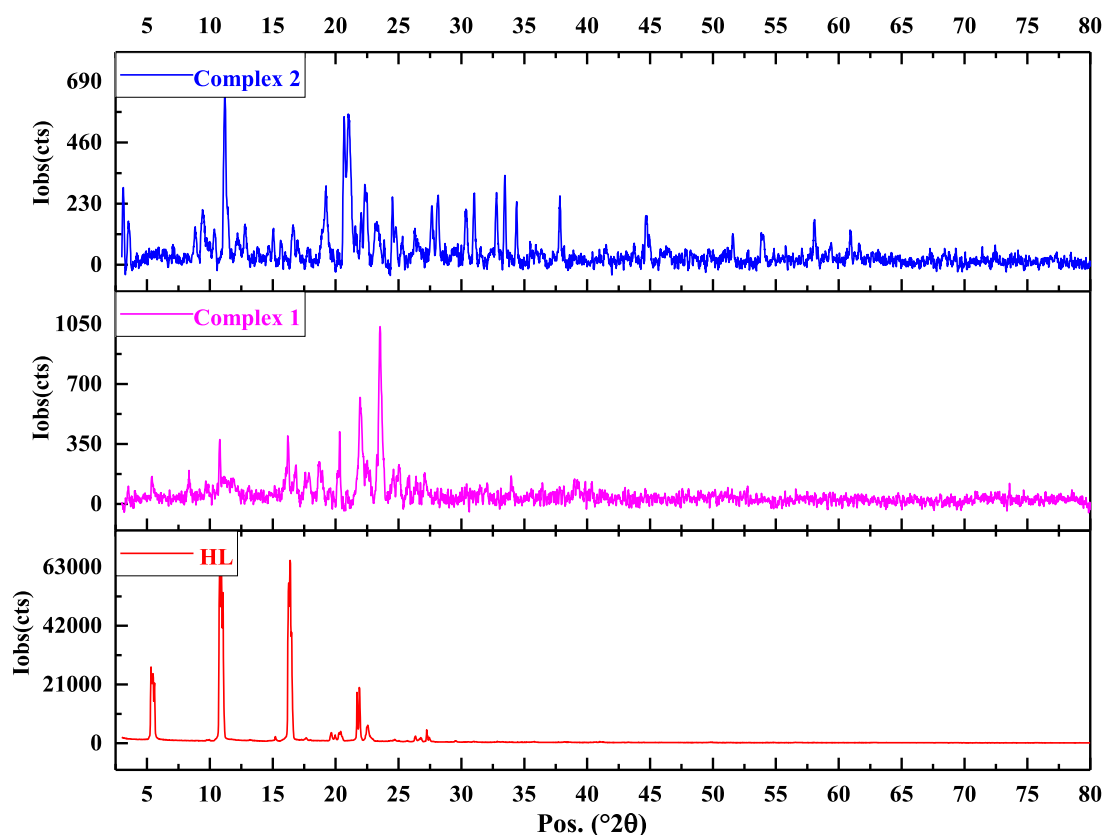
Fig. 5. Powder X-ray diffractogram of HL and its complexes.

cobalt oxide. Complex 2 decomposed in four stages, the first of which occurred at a temperature of 67.77 - 132.65 °C with a T_{DTG} peak at 100.91 °C. This implies the loss of outer sphere H_2O and a Cl atom with a mass loss of 0.108 mg (1.55%). The second stage of decomposition in the temperature range of 156.64 - 250.43 °C with T_{DTG} peak at 209.09 °C is associated with a less intense shoulder peak, and this might be due to the loss of a part of ligand moiety and coordinated Cl-atom. The third decomposition step at 342.07–474.57 °C with a T_{DTG} peak at 429.42 °C correlates elimination of the ligand moiety with a mass loss of 1.69 mg (33.13%). The fourth and final decomposition step at 551.07–700.11 °C with a T_{DTG} peak at 634.46 °C correlates elimination of the total ligand moiety with a mass loss of 2.718 mg (92.11%), leaving a solid residue of ZnO [40]. The horizontal portion of the thermogram seen after 700.11 °C represents a stable solid ZnO residue.

3.8. Powder X-ray diffraction (PXRD) study

Although single-crystal X-ray crystallography (SC-XRD) is the most credible way to study the structure of complexes, we used PXRD to determine the crystal parameters because single-crystal growth attempts were unsuccessful. The diffractogram of HL and its complexes are presented in Figs. 5 and S10–S12. The diffractogram of HL showed 13 reflection peaks in the 2θ range of 0–27° with the highest intensity peak at 10.75° and a corresponding d-spacing value of 0.072 Å. Likewise, the diffractograms of complexes 1 and 2 displayed 13 and 25 reflection peaks in the entire X-ray scan range, with their respective highest intensity peaks at 23.54° ($d = 0.157$ Å) and 11.21° ($d = 0.075$ Å). Their average crystallite size was calculated using Debye-Scherrer's equation [41]. The respective crystallite sizes of HL and complexes 1 and 2 were 119.88, 17.35, and 27.44 nm, illustrating the nano-sized crystalline nature of the complexes [42]. The difference in the XRD patterns suggested co-

ordination of the ligand to the metal for complex formation, and a decrease in crystallite size was observed. This decreased crystallite size explains the better antibacterial potency of the metal complexes than that of the Schiff base [43]. The crystallinity refers to the percentage of crystalline peaks over the entire XRD scan range. These values for HL, complexes 1 and 2 were calculated to be 85.8, 28.7, and 58.2%, respectively (Table 7). The peak-wise data for the dislocation density (δ) and microstrain (ε) are presented in Tables S1-S3. Dislocation density refers to the number of dislocation lines per unit area (nm^{-2}) of the crystal, which causes a crystallographic defect, and microstrain (ε) refers to the variation in lattice parameters [44].

3.9. Molecular modeling study

Geometry optimization revealed a structural transformation following ligand-induced complex formation. Figs. (S13, 6, and 7) illustrate the optimized 3D structures of HL and the complexes. Through several rounds of energy optimization, the minimum optimized energies of HL, complex 1, and 2 were reported to be 19.34, 815.28, and 312.85 kcal/mole, respectively. The specific structural parameters, such as the bond lengths and bond angles, are listed in Table 8. In complexes 1 and 2, the azomethine bond (-HC=N) (1.26 Å) of HL was elongated to 1.29 and 1.27 Å, respectively. Because complex 2 has relatively low energy, it might be more stable than complex 1 [18]. Bond length and bond angle values are also consistent with the octahedral geometry of complex 1 and the distorted trigonal bipyramidal geometry of complex 2. The data in the table indicate that complexation results in an increase in the bond lengths due to a decrease in the electron density in the coordinated atoms of the ligand (HL) [45]. Furthermore, the geometry index (τ_5) value of complex 2 was calculated to be 1.1, slightly deviating from its ideal value of 1 for perfectly trigonal bipyramidal

Table 7

Crystal parameters of HL and complexes.

Compounds	No. of crystalline peaks	Av. crystallite size (nm)	Crystallinity(%)	Dislocation density x 10⁻³ range	Microstrain x 10⁻³ range
HL	13	119.87	85.82	0.03–0.99	1.37–6.22
Complex 1	13	17.34	28.71	1.23–169.35	4.75–73.04
Complex 2	25	27.43	58.27	0.47–62.66	1.99–44.31

Table 8

Selected bond lengths and bond angles of HL and its complexes.

Compounds	Bonded Atoms	Bond length (Å)	Bonded Atoms	Bond angle (°)	Final geom.energy
HL	C(4)-N(5)	1.26			19.34 kcal/mol
	N(5)-C(1)	1.26			
	C(7)-N(9)	1.26			
	N(9)-C(10)	1.48			
Complex 1	Co(16)-N(13)	1.88	O(41)-Co(16)-O(40)	91.75	815.28 kcal/mol
	Co(16)-N(12)	1.88	N(12)-Co(16)-N(13)	161.35	
	Co(16)-O(41)	1.17	N(15)-Co(16)-N(9)	107.59	
	O(40)-Co(16)	1.17	N(13)-Co(16)-O(40)	94.93	
	Co(16)-N(9)	1.88	N(12)-Co(16)-O(41)	94.47	
	Co(16)-N(15)	1.88	N(15)-Co(16)-N(12)	85.36	
	C(11)-N(13)	1.29	O(40)-Co(16)-N(9)	80.03	
	C(10)-N(12)	1.29	N(12)-Co(16)-N(9)	83.84	
Complex 2	Zn(16)-N(9)	1.94	N(15)-Zn(16)-N(9)	97.29	312.85 kcal/mol
	Zn(16)-N(13)	1.94	N(15)-Zn(16)-N(13)	96.82	
	Zn(16)-N(12)	1.94	N(12)-Zn(16)-N(15)	90.70	
	Zn(16)-Cl(40)	2.25	N(9)-Zn(16)-N(12)	163.81	
	N(15)-Zn(16)	1.94	N(13)-Zn(16)-N(9)	90.92	
	N(12)-C(10)	1.27	N(12)-Zn(16)-N(13)	102.1	
	N(13)-C(11)	1.27	N(13)-Zn(16)-Cl(40)	154.99	
			N(12)-Zn(16)-Cl(40)	83.36	
			N(15)-Zn(16)-Cl(40)	107.56	
			Cl(40)-Zn(16)-N(9)	80.82	

Fig. 6. 3D-optimized geometrical structure of complex 1.

geometry [46,47]. This validates pentacoordinate around the zinc atom with distorted trigonal bipyramidal geometry (Figs. 6 and 7).

3.10. Antibacterial activity study

The structural components of chemicals have a profound effect on their biological activity. Furthermore, the amphiphilic nature of molecules also influences their biological activities [48,49]. In complexes, metals link organic ligands to cellular components of microorganisms and enhance their biological activities [50]. Test solutions of HL and complexes 1 and 2 were prepared in DMSO at concentrations of 50, 25, and 12.5 µg/µL. A standard reference drug, amikacin (30 µg/disk), was used to compare the potencies of the synthesized compounds. The diameters of the zones of inhibition in millimeters (mm) are listed in Table 9, and the results are graphically shown in the bar graph Figs. 8–10. With all pathogens except *S. aureus* and *E. coli,* amikacin exhibited higher antibacterial activity than any other tested compounds. Complex 2 exhib-
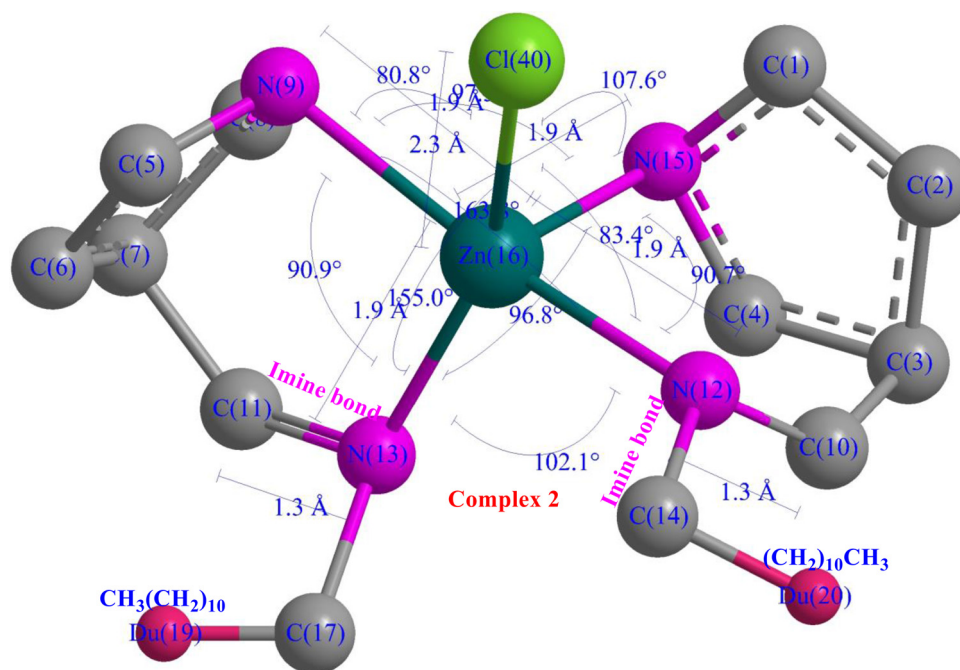
Fig. 7. 3D-optimized geometrical structure of complex 2.

Table 9
Antibacterial activity data of HL and its metal complexes.

Compounds	Diameter of the zone of inhibition in mm														
	E. coli			K. pneumoniae			P. aeruginosa			Enterococci			S. aureus		
Concentration (µg/µL)	50	25	12.5	50	25	12.5	50	25	12.5	50	25	12.5	50	25	12.5
LA	16	14	13	21	16	14	18	16	15	17	16	15	21	20	19
P3C	0	0	0	0	0	0	0	0	0	0	0	0	0	0	0
HL	15	15	13	15	15	14	12	12	12	12	11	10	22	21	20
Complex 1	16	15	14	15	14	13	12	11	10	12	12	12	23	22	21
Complex 2	17	16	15	18	17	16	16	16	16	15	14	14	24	23	22
Amik. (30 µg/disk)	14			24			23			20			21		
DMSO	0	0	0	0	0	0	0	0	0	0	0	0	0	0	0
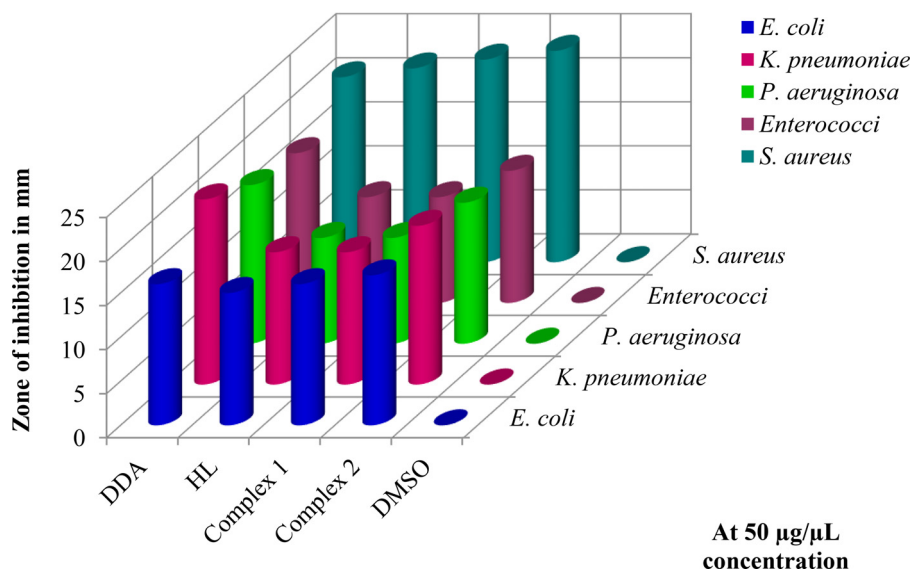
Fig. 8. Bar graph showing antimicrobial activity at 50 µg/µL concentration.
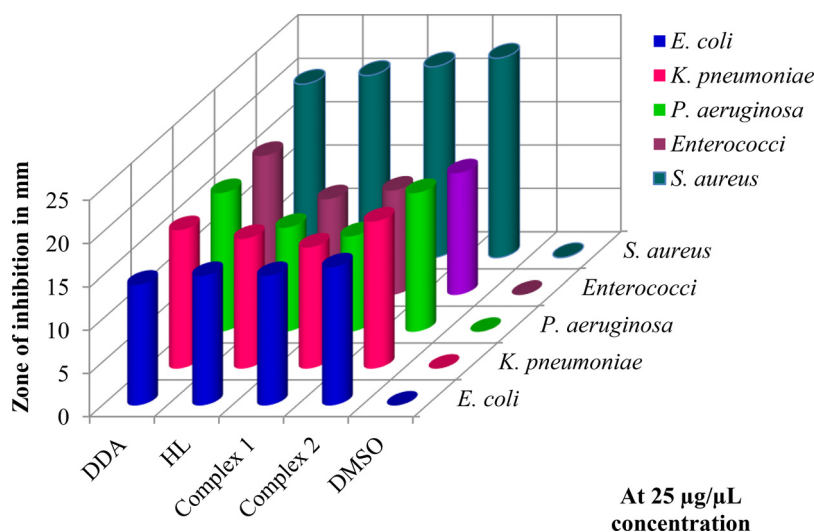
Fig. 9. Bar graph showing antimicrobial activity at 25 µg/µL concentration.
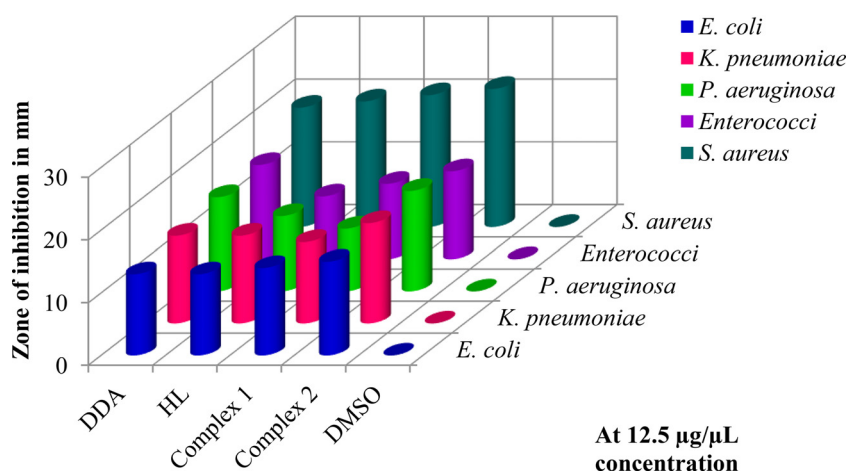
Fig. 10. Bar graph showing antimicrobial activity at 12.5 µg/µL concentration.

Table 10
Minimum inhibitory concentration data.

Compounds	Minimum inhibitory concentration (MIC) in (µg/µL)				
	E. coli	*K. pneumoniae*	*P. aeruginosa*	*Enterococci*	*S. aureus*
LA	0.7812	0.7812	0.3906	0.3906	0.1953
HL	0.3906	0.3906	0.3906	0.1953	0.0976
Complex 1	0.1953	0.3906	0.1953	0.0976	0.0488
Complex 2	0.0976	0.0976	0.0976	0.0488	0.0244

ited better antibacterial activity at all concentrations compared to HL, complex 1, and amikacin. There was significant growth inhibition by HL and complexes 1 and 2 against *E. coli, K. pneumoniae*, and *S. aureus* but comparatively less inhibition against *P. aeruginosa* and *Enterococci*.

A quantitative assessment of their biological activities was performed by determining the MIC of the compounds. The MIC (µg/µL) of the studied compounds is listed in Table 10. All of them showed remarkable MIC values against all the pathogens. Relatively lower MIC values were observed for the tested compounds against *S. aureus, Enterococci*, and *K. pneumoniae*. The lowest MIC value (0.0244 μg/μL) of complex 2 against *S. aureus* showed higher antibacterial activity. The MIC data showed remarkable and compa-

rable antibacterial activities for the synthesized compounds. Overtone's concept and chelation theory explain the better antibacterial activity of metal complexes than that of HL. A metallosurfactant interacts hydrophobically with the bacterial cell membrane and electrostatically with its cell wall when applied to gram-positive bacteria. However, gram-negative bacteria have a lipopolysaccharide layer on their outer membranes, which may block amphiphilic metallo-surfactants from entering and reducing their antibacterial properties [51]. In our investigation, gram-positive bacteria had relatively higher antibacterial potency than gram-negative bacteria. A thick coating of peptidoglycan allows gram-positive bacteria to absorb drugs more effectively [52,53]. More hydrophobic surfactants have been reported to exhibit more potent antibacterial properties.

Table 11

In silico physicochemical properties and drug-likeness predictions of synthesized compounds.

Compound	Fraction Csp3	nRotB	HBA	HBD	iLogP	Molar refractivity (MR)	ESOLlog S	TPSA (Å²)	Lipinski violations
HL	0.71	12	1	1	3.97	87.13	−4.57 MS	28.15	-
Complex 1	0.71	24	5	5	0.00	195.10	−10.33 IS	83.99	1 MW>500
Complex 2	0.71	24	5	5	0.00	195.10	−10.37 IS	83.99	1 MW>500

Fraction Csp3 = Ratio of sp3 hybridized carbons to the total carbon count of the molecule.

nRotB = Number of rotatable bonds, HBA = Number of hydrogen bond acceptor,.

HBD = Number of hydrogen bond donors, iLogP = lipophilicity, log S = water solubility, ESOL = estimated solubility with moderately soluble (MS) and IS = insoluble, TPSA = Topological polar surface area.

Table 12

Pharmacokinetic/ADME properties of HL and its complexes.

Pharmacokinetic/ADME properties									
Compound	GI Abs	BBB Permeant	P-gp Subtrate	CYP1A2 Inhibitor	CYP2C19 Inhibitor	CYP2C9 Inhibitor	CYP2D6 Inhibitor	CYP3A4 Inhibitor	logKp (cm/s)
HL	High	Yes	No	Yes	Yes	No	Yes	No	−3.73
Complex 1	High	No	Yes	No	No	No	No	No	−2.16
Complex 2	Low	No	Yes	No	No	No	No	No	−2.20

GI = gastrointestinal, BBB = blood brain barrier, P-gp = protoglycoprotein.

CYPs = cytochrome family enzymes, logKp = skin permeation.

The coordination of various metal ions also influences lipophilicity, which determines the pace at which molecules enter the cells.

3.11. In silico *ADME study*

An *in silico* drug-likeness and pharmacokinetic study was conducted to better understand the *in vitro* antibacterial activities of the synthesized compounds. Table 11 shows the predicted data for drug likeness obtained using the Swiss ADME online predictor. Drug-likeness prediction is based on Lipinski's rule of five, which considers molecular weight ($\leq$500), hydrogen bond acceptor ($\leq$10), hydrogen bond donor ($\leq$5), and lipophilicity (ilogP $\leq$5) to qualify a drug molecule [54]. The predicted logP values for both metal complexes were 0.00, which indicates their amphipathic nature, whereas HL had 3.97 logP values, indicating a lipophilic nature. The predicted TPSA values for HL and complexes ranged from 28.15 to 83.99 Å², suggesting their excellent intestinal absorption [55]. Because their estimated human skin permeability coefficient (log Kp) values ranged from 2.16 to 3.37 cm/s, the synthesized compounds were predicted to have low skin permeability. The skin permeation of HL was predicted to be relatively low. The pharmacokinetics descriptor data for HL and metal complexes 1 and 2 are presented in Table 12. High GI absorption of HL and complex 1, as well as HL permeation through the blood-brain barrier (BBB), have been reported. Complexes 1 and 2 were predicted as P-gp substrates. Overall, Swiss ADME data analysis revealed a more incredible opportunity for HL to be a drug candidate. CYP450 inhibition prediction showed that ligand HL inhibited CYP1A2, CYP2C19, and CYP2D6 isoforms but not CYP2C9 and CYP3A4. The synthesized complexes were unable to inhibit CYP450 isoforms. The bioavailability scores for HL and metal complexes ranged from 0.55 - 0.56. The predicted synthetic accessibility for HL was 2.94, whereas that for complexes 1 and 2 was 5.46 and 5.53.

Bioavailability radar plots of the compounds are shown in Figs. S14–S16. Size, solubility, saturation, polarity, lipophilicity, and flexibility are the six physicochemical characteristics of the pink area of the radar plot that ideally describe oral bioavailability [56]. HL has all parameters within the pink region of the radar plot except for the number of rotatable bonds, which is >9 [57]. There is a lack of oral bioavailability of metal complexes based on radar plots because their physicochemical properties are primarily outside the pink room.

4. Conclusion

In this study, we prepared a neutral surfactant-based N, N donor Schiff base ligand (HL) and its two metal complexes 1 and 2. Based on UV-visible and magnetic moment data, octahedral and distorted trigonal bipyramidal geometry have been assigned to complexes 1 and 2, respectively. Both complexes exhibited ionic surfactant behavior based on molar conductivity measurements. Thermal analysis, FT-IR, and ^{1}H NMR spectral studies revealed the involvement of hydrated and coordinated H_2O in complex formation. PXRD analysis indicated their crystalline nature with average crystallite sizes of 119.88, 17.35, and 27.44 nm for HL, complex 1, and complex 2. Complexes possess lower CMC values than the pure surfactant (LA), indicating their greater micellization capacity. A very low ($\triangle G^{\circ}_m$) value for the complexes indicates the easy formation of micelles relative to LA. The TGA/DTA study revealed the thermal stability of the complexes. In the Swiss ADME study, HL met several physicochemical criteria for the ADME profile and was predicted to possess drug-like properties according to Lipinski's rule of five. The tested compounds showed excellent antibacterial activity against the studied pathogens at all concentrations, as demonstrated by their diameter of the zone of inhibition and minimum inhibitory concentrations (MICs). Overall, metal complexes were more effective than ligands in killing bacteria.

Funding

This study has no funding.

Data availability

All the data are included in the manuscript and are available for the readers.

Supplementary description

The supplementary file contains Figures and Tables as a supporting part of this study. The FT-IR spectra of HL and complexes

1and 2 are shown in Figs. S1and S2. In Figs. S4 and S5, the ^{1}H NMR spectra of HL and complex 2 are shown. The ^{13}C NMR spectrum of HL is presented in Fig. S6. Figs. S7–S9, the mass spectra of HL and complexes1 and 2 are presented. The individual diffractogram of the ligands and complexes are shown in Figs. S10–S12. The 3D-optimized geometrical structure of the HL is shown in Fig. S13. Figs. S14–S16 show the Swiss ADME bioavailability radar, which explains the pharmacokinetic properties of the HL and complexes. Tables S1–S3 report crystallographic data of HL and complexes.

Declaration of Competing Interest

There are no known conflicts of interest to declare.

CRediT authorship contribution statement

Janak Adhikari: Investigation, Methodology, Formal analysis, Writing – original draft. **Ajaya Bhattarai:** Writing – review & editing. **Narendra Kumar Chaudhary:** Supervision, Conceptualization, Formal analysis, Writing – review & editing.

Data availability

Data will be made available on request.

Acknowledgments

Supplementary materials

Supplementary material associated with this article can be found, in the online version, at doi:10.1016/j.molstruc.2022.134434.

References

[1] M. Zhang, C. Saint-Germain, G. He, R.W.Y. Sun, Drug delivery systems for anti-cancer active complexes of some coinage metals, Curr. Med. Chem. 25 (2018) 493–505, doi:10.2174/0929867324666170511152441.

[2] R.K. Sodhi, S. Paul, Metal complexes in medicine: an overview and update from drug design perspective, Cancer Ther. Oncol. Int. J. (2019) 14, doi:10.19080/ctoij.2019.14.555883.

[3] S. Sen, M. Won, M.S. Levine, Y. Noh, A.C. Sedgwick, J.S. Kim, J.L. Sessler, J.F. Arambula, Metal-based anticancer agents as immunogenic cell death inducers: the past, present, and future, Chem. Soc. Rev. (2022), doi:10.1039/d1cs00417d.

[4] D. Cirri, A. Pratesi, T. Marzo, L. Messori, Metallo therapeutics for COVID-19. Exploiting metal-based compounds for the discovery of new antiviral drugs, Expert Opin. Drug Discov. 16 (2021) 39–46, doi:10.1080/17460441.2020.1819236.

[5] Y.A. Gur'eva, O.A. Zalevskaya, O.G. Shevchenko, P.A. Slepukhin, V.A. Makarov, A.V. Kuchin, Copper(ii) complexes with terpene derivatives of ethylenediamine: synthesis, and antibacterial, antifungal and antioxidant activity, RSC Adv. (2022), doi:10.1039/d2ra00223j.

[6] M. Ghalkhani, S.I. Kaya, N.K. Bakirhan, Y. Ozkan, S.A. Ozkan, Application of nanomaterials in development of electrochemical sensors and drug delivery systems for anticancer drugs and cancer biomarkers, Crit. Rev. Anal. Chem. (2020) 1–23 0, doi:10.1080/10408347.2020.1808442.

[7] V. Baliram, T.P. Sanjay, K.P.M. Arvind, Synthesis, spectral characterization and antitubercular study of novel quinoline Schiff base and its metal complexes, Anal. Chem. Lett. 11 (2021) 523–538, doi:10.1080/22297928.2021.1921616.

[8] H.Y. Khan, S. Parveen, I. Yousuf, S. Tabassum, F. Arjmand, Metal complexes of NSAIDs as potent antitumor chemotherapeutics: mechanistic insights into cytotoxic activity via multiple pathways primarily by inhibition of COX–1 and COX–2 enzymes, Coord. Chem. Rev. 453 (2022) 214316, doi:10.1016/J.CCR.2021.214316.

[9] Y.B.G. JM da Silva Leite, M.F. Patriota, J.L. de La Roca, Soares-Sobrinho, New perspectives in drug delivery systems for the treatment of tuberculosis, Curr. Med. Chem. (2021), doi:10.2174/0929867328666210629154908.

[10] Q. Xu, Y. Bai, X. Zhao, M. Ren, S. Wang, F. Kong, Synthesis and characterization of an amphiphilic lignin-based cationic surfactant, Ind. Crops Prod. 164 (2021) 113376, doi:10.1016/j.indcrop.2021.113376.

[11] K. Barrantes, J.J. Araya, L. Chacón, R. Procupez-Schtirbu, F. Lugo, G. Ibarra, V.H. Soto, Antiviral, antimicrobial, and antibiofilm properties of biosurfactants, in: Biosurfactants for a Sustainable Future, John Wiley & Sons Ltd., 2021, pp. 245–268.

[12] M. Masjedi, T. Montahaei, An illustrated review on nonionic surfactant vesicles (niosomes) as an approach in modern drug delivery: fabrication, characterization, pharmaceutical, and cosmetic applications, J. Drug Deliv. Sci. Technol. (2021), doi:10.1016/j.jddst.2020.102234.

[13] D. Neubauer, M. Jaśkiewicz, M. Bauer, A. Olejniczak-Kęder, E. Sikorska, K. Sikora, W. Kamysz, Biological and physico-chemical characteristics of arginine-rich peptide gemini surfactants with lysine and cystine spacers, Int. J. Mol. Sci. (2021) 22, doi:10.3390/ijms22073299.

[14] R. Migliore, T. Biver, G. Barone, C. Sgarlata, Quantitative analysis of the interactions of metal complexes and amphiphilic systems: calorimetric, spectroscopic and theoretical aspects, Biomolecules (2022), doi:10.3390/biom12030408.

[15] M. Conkova, V. Montes-García, M. Konopka, A. Ciesielski, P. Samorì, A.R. Stefankiewicz, Schiff base caped gold nanoparticles for efficient transition metal cations sensing in organic media, Chem. Commun. (2022) 5773–5776, doi:10.1039/d2cc00497f.

[16] E. Laiq, N. Shahid, Antimicrobial activities of Schiff base metal complexes of first transition series, Biosci. Biotechnol. Res. Asia 18 (2021) 575–583.

[17] M. Pervaiz, M. Yousaf, I. Ahmad, M. Munawar, Z. Saeed, A. Adnan, T. Gulzar, S. Kirn, T. Kamal, A. Ahmad, Synthesis, spectral and antimicrobial studies of amino acid derivative Schiff base metal (Co, Mn, Cu, and Cd) complexes, Spectrochim. Acta Part A Mol. Biomol. Spectrosc. 206 (2019) 642–649, doi:10.1016/j.saa.2018.05.057.

[18] N.K. Chaudhary, B. Guragain, A. Chaudhary, S.K. Chaudhary, Heteroleptic cadmium complex of glimepiride–metformin mixed ligand: synthesis, characterization, and antibacterial study, Chem. Pap. 75 (2021) 3215–3226, doi:10.1007/s11696-021-01535-9.

[19] I. Ali, W.A. Wani, K. Saleem, Empirical formulae to molecular structures of metal complexes by molar conductance, Synth. React. Inorg. Met. Nano Met. Chem. 43 (2013) 1162–1170, doi:10.1080/15533174.2012.756898.

[20] J. Adhikari, A. Bhattarai, N.K. Chaudhary, synthesis, characterization, physicochemical studies, and antibacterial evaluation of surfactant-based Schiff base transition metal complexes, Chem. Pap. 76 (2022) 2549–2566, doi:10.1007/s11696-022-02062-x.

[21] K. Nagaraj, S. Sakthinathan, S. Arunachalam, Synthesis, CMC determination and nucleic acid-binding interaction of a surfactant copper(II) complex containing amino acid-Schiff base ligand:[Cu(sal-ala)(bpy)(DA)], J. Iran. Chem. Soc. 12 (2015) 267–275, doi:10.1007/s13738-014-0481-z.

[22] S.C.N. Chandar, K. Santhakumar, M.N. Arumugham, Metallosurfactant Schiff base cobalt(III) coordination complexes. synthesis, characterization, determination of CMC values and biological activities, Transit. Met. Chem. 34 (2009) 841–848, doi:10.1007/s11243-009-9272-2.

[23] S.K. Mehta, R. Kaur, G.R. Chaudhary, Self aggregation and solution behavior of copper and nickel based surfactants, Colloids Surf. A Physicochem. Eng. Asp. 403 (2012) 103–109, doi:10.1016/j.colsurfa.2012.03.062.

[24] K. Buldurun, N. Turan, E. Bursal, A. Mantarcı, F. Turkan, P. Taslimi, İ. Gülçin, Synthesis, spectroscopic properties, crystal structures, antioxidant activities and enzyme inhibition determination of Co(II) and Fe(II) complexes of Schiff base, Res. Chem. Intermed. 46 (2019) 283–297, doi:10.1007/s11164-019-03949-3.

[25] B. Naureen, G.A. Miana, K. Shahid, M. Asghar, S. Tanveer, A. Sarwar, Iron(III) and zinc(II) monodentate Schiff base metal complexes: synthesis, characterization and biological activities, J. Mol. Struct. 1231 (2021) 129946, doi:10.1016/j.molstruc.2021.129946.

[26] X. Ran, L. Wang, D. Cao, Y. Lin, J. Hao, Synthesis, characterization and in vitro biological activity of cobalt(II), copper(II) and zinc(II) Schiff base complexes derived from salicylaldehyde and D,L-selenomethionine, Appl. Organomet. Chem. 25 (2011) 9–15, doi:10.1002/aoc.1680.

[27] M.A. Diab, G.G. Mohamed, W.H. Mahmoud, A.Z. El-Sonbati, S.M. Morgan, S.Y. Abbas, Inner metal complexes of tetradentate Schiff base: synthesis, characterization, biological activity and molecular docking studies, Appl. Organomet. Chem. 33 (2019) 1–13, doi:10.1002/aoc.4945.

[28] A.A.M. Belal, I.M. El-Deen, N.Y. Farid, R. Zakaria, M.S. Refat, Synthesis, spectroscopic, coordination and biological activities of some transition metal complexes containing ONO tridentate Schiff base ligand, Spectrochim. Acta Part A Mol. Biomol. Spectrosc. 149 (2015) 771–787, doi:10.1016/j.saa.2015.05.005.

[29] S.S. Jawoor, S.A. Patil, S.S. Toragalmath, Synthesis and characterization of heteroleptic Schiff base transition metal complexes: a study of anticancer, antimicrobial, DNA cleavage and anti-TB activity, J. Coord. Chem. 71 (2018) 271–283, doi:10.1080/00958972.2017.1421951.

[30] S.A. Güngör, M. Köse, F. Tümer, M. Tümer, Photoluminescence, electrochemical, SOD activity and selective chemosensor properties of novel asymmetric porphyrin-Schiff base compounds, Dye Pigment 130 (2016) 37–53, doi:10.1016/j.dyepig.2016.03.007.

[31] F.K. Ommenya, E.A. Nyawade, D.M. Andala, J. Kinyua, Synthesis, characterization and antibacterial activity of Schiff base, 4-chloro-2-{(E)-[(4-Fluorophenyl)imino]methyl}phenol metal(II) complexes, J. Chem. (2020) 2020, doi:10.1155/2020/1745236.

[32] H. Kargar, A.A. Ardakani, M.N. Tahir, M. Ashfaq, K.S. Munawar, Synthesis, spectral characterization, crystal structure and antibacterial activity of nickel(II), copper(II) and zinc(II) complexes containing ONNO donor Schiff base ligands, J. Mol. Struct. 1233 (2021) 130112, doi:10.1016/j.molstruc.2021.130112.

[33] A.A. Mohamed, S.A. Sadeek, Ligational and biological studies of Fe(III), Co(II),

Ni(II), Cu(II), and Zr(IV) complexes with carbamazepine as antiepileptic drug, Appl. Organomet. Chem. 35 (2021) 1–16, doi:10.1002/aoc.6178.

[34] S.K. Maiti, M. Kalita, A. Singh, J. Deka, P. Barman, Investigation of DNA binding and bioactivities of thioether containing Schiff base copper(II), cobalt(II) and palladium(II) complexes: synthesis, characterization, spectrochemical study, viscosity measurement, Polyhedron 184 (2020) 114559, doi:10.1016/j.poly.2020.114559.

[35] G. More, D. Raut, K. Aruna, S. Bootwala, Synthesis, spectroscopic characterization and antimicrobial activity evaluation of new tridentate Schiff bases and their Co(II) complexes, J. Saudi Chem. Soc. 21 (2017) 954–964, doi:10.1016/j.jscs.2017.05.002.

[36] R. Kalarani, M. Sankarganesh, G.G.V. Kumar, M. Kalanithi, Synthesis, spectral, DFT calculation, sensor, antimicrobial and DNA binding studies of Co(II), Cu(II) and Zn(II) metal complexes with 2-amino benzimidazole Schiff base, J. Mol. Struct. 1206 (2020) 127725, doi:10.1016/j.molstruc.2020.127725.

[37] M.A. Hussien, N. Nawar, F.M. Radwan, N.M. Hosny, Spectral characterization, optical band gap calculations and DNA binding of some binuclear Schiff-base metal complexes derived from 2-amino-ethanoic acid and acetylacetone, J. Mol. Struct. 1080 (2015) 162–168, doi:10.1016/j.molstruc.2014.09.071.

[38] M. Sakthi, A. Ramu, Synthesis, structure, DNA/BSA binding and antibacterial studies of NNO tridentate Schiff base metal complexes, J. Mol. Struct. 1149 (2017) 727–735, doi:10.1016/j.molstruc.2017.08.040.

[39] N. Beyazit, D. Çakmak, C. Demetgül, Chromone-based Schiff base metal complexes as catalysts for catechol oxidation: synthesis, kinetics and electrochemical studies, Tetrahedron 73 (2017) 2774–2779, doi:10.1016/j.tet.2017.03.081.

[40] K. Singh, P. Turk, A. Dhanda, Synthesis, spectral characterization, and antimicrobial evaluation of new imine derived from 3-methylthiophene-2-carboxaldehyde and its Co(II), Ni(II), Cu(II), and Zn(II) metal complexes, Appl. Organomet. Chem. 35 (2021) 1–14, doi:10.1002/aoc.6088.

[41] M.S. Refat, H.A. Saad, A.A. Gobouri, M. Alsawat, A.M.A. Adam, S.M. El-Megharbel, Charge transfer complexation between some transition metal ions with azo Schiff base donor as a smart precursor for synthesis of nano oxides: an adsorption efficiency for treatment of Congo red dye in wastewater, J. Mol. Liq. 345 (2022) 117140, doi:10.1016/j.molliq.2021.117140.

[42] E. Bursal, F. Turkan, K. Buldurun, N. Turan, A. Aras, N. Çolak, M. Murahari, M.C. Yergeri, Transition metal complexes of a multidentate Schiff base ligand containing pyridine: synthesis, characterization, enzyme inhibitions, antioxidant properties, and molecular docking studies, BioMetals 34 (2021) 393–406, doi:10.1007/s10534-021-00287-z.

[43] A. Palanimurugan, A. Dhanalakshmi, P. Selvapandian, A. Kulandaisamy, Electrochemical behavior, structural, morphological, Calf Thymus-DNA interaction and in-vitro antimicrobial studies of synthesized Schiff base transition metal complexes, Heliyon 5 (2019) e02039, doi:10.1016/j.heliyon.2019.e02039.

[44] S.G. Nozha, S.M. Morgan, S.E.A. Ahmed, M.A. El-Mogazy, M.A. Diab, A.Z. El-Sonbati, M.I. Abou-Dobara, Polymer complexes. LXXIV. Synthesis, characterization and antimicrobial activity studies of polymer complexes of some transition metals with bis-bidentate Schiff base, J. Mol. Struct. 1227 (2021) 129525, doi:10.1016/j.molstruc.2020.129525.

[45] H.A. El-Boraey, M.A. El-Salamony, Transition metal complexes with polydentate ligand: synthesis, characterization, 3D molecular modelling, anticancer, antioxidant and antibacterial evaluation, J. Inorg. Organomet. Polym. Mater. 29 (2019) 684–700, doi:10.1007/s10904-018-1042-1.

[46] A.W. Addison, T.N. Rao, Synthesis, structure, and spectroscopic properties of copper(II) compounds containing nitrogen-sulphur donor ligands; the crystal and molecular structure of aqua[l,7-bis(N-methylbenzimidazol-2'-yl)-2,6-dithiaheptane]copper(II) perchlorate, J. Chem. Soc. Dalton Trans. (1984) 1349–1356.

[47] B.F. Hoskins, F.D. Whillans, The geometry of pentacoordinate complexes, Coord. Chem. Rev. 9 (1973) 365–388, doi:10.1016/S0010-8545(00)82083-4.

[48] S. Caleb Noble Chandar, D. Sangeetha, M.N. Arumugham, Octadecylamine cobalt(III) dimethyl glyoximato complexes: synthesis, thermodynamics of micellization, steady-state photolysis and biological activities, Transit. Met. Chem. 39 (2014) 159–165, doi:10.1007/s11243-013-9785-6.

[49] K. Sasikala, S. Arunachalam, Antimicrobial activity, spectral studies and micellar properties of some surfactant-cobalt(III) complexes, Chem. Sci. Trans. 2 (2013) 157–166, doi:10.7598/cst2013.38.

[50] K. Venkateswarlu, S. Daravath, G. Ramesh, P.V.A. Lakshmi, Shivaraj, Investigation of DNA binding and bioactivities of furan cored Schiff base Cu(II), Ni(II), and Co(III) complexes: synthesis, characterization and spectroscopic properties, Appl. Organomet. Chem 35 (2021) 1–20, doi:10.1002/aoc.6326.

[51] H. Kargar, A.A. Ardakani, M.N. Tahir, M. Ashfaq, K.S. Munawar, Synthesis, spectral characterization, crystal structure determination and antimicrobial activity of Ni(II), Cu(II) and Zn(II) complexes with the Schiff base ligand derived from 3,5-dibromosalicylaldehyde, J. Mol. Struct. 1229 (2021) 129842, doi:10.1016/j.molstruc.2020.129842.

[52] A. Arunadevi, N. Raman, Biological response of Schiff base metal complexes incorporating amino acids–a short review, J. Coord. Chem. 73 (2020) 2095–2116, doi:10.1080/00958972.2020.1824293.

[53] H. Kargar, F. Aghaei-Meybodi, R. Behjatmanesh-Ardakani, M.R. Elahifard, V. Torabi, M. Fallah-Mehrjardi, M.N. Tahir, M. Ashfaq, K.S. Munawar, Synthesis, crystal structure, theoretical calculation, spectroscopic and antibacterial activity studies of copper(II) complexes bearing bidentate schiff base ligands derived from 4-aminoantipyrine: influence of substitutions on antibacterial activity, J. Mol. Struct. 1230 (2021) 129908, doi:10.1016/j.molstruc.2021.129908.

[54] C.A. Lipinski, F. Lombardo, B.W. Dominy, P.J. Feeney, Experimental and computational approaches to estimate solubility and permeability in drug discovery and development settings, Adv. Drug Deliv. Rev. 64 (2012) 4–17, doi:10.1016/j.addr.2012.09.019.

[55] H.D.S. Souza, R.P.F. De Sousa, B.F. Lira, R.F. Vilela, N.H.P.B. Borges, E.O. Lima, J.U.G. Jardim, Synthesis, in silico study and antimicrobial evaluation of new Selenoglycolicamides, J. Braz. Chem. Soc. (2018) 1–10, doi:10.21577/0103-5053.20180148.

[56] A. Daina, O. Michielin, V. Zoete, SwissADME: a free web tool to evaluate pharmacokinetics, drug-likeness and medicinal chemistry friendliness of small molecules, Sci. Rep. 7 (2017) 1–13, doi:10.1038/srep42717.

[57] S. Parveen, Biophysical and theoretical investigation of benzo[c]coumarin functionalized Schiff base with human serum albumin, Chem. Pap. 75 (2021) 2339–2351, doi:10.1007/s11696-020-01496-5.

ORIGINAL PAPER

Synthesis, characterization, physicochemical studies, and antibacterial evaluation of surfactant-based Schiff base transition metal complexes

Janak Adhikari[1] · Ajaya Bhattarai[1] · Narendra Kumar Chaudhary[1]

Abstract

The use of surfactants to enhance the efficacy of most conventional drugs is the recent progress of pharmacology. The rationale of this research is to design and develop surfactant incorporated drugs to overcome the challenges of antibiotic resistance. Herein, we report the synthesis of a novel surfactant-based Schiff base ligand (DDAP2C) from dodecylamine (DDA) and pyrrole-2-carboxaldehyde (P2C) and its two metal complexes, Ni-DDAP2C and Zn-DDAP2C. Characterization was performed by spectroscopic techniques such as ^{1}H and ^{13}CNMR, electronic absorption spectral study, FT-IR, and ESI-mass spectrometry. They were further characterized by elemental microanalysis, powder X-ray diffraction, SEM-EDAX, and TGA/DTA analyses to obtain significant structural information. The conductance study revealed non-electrolytic nature. The critical micelle concentration (CMC) of the synthesized compounds was calculated using conductivity data. We extended our study to derive various surface properties and thermodynamic parameters from the CMC calculations. The popular Coats–Redfern equation was used to compute the kinetic and thermodynamic properties. Powder X-ray diffraction was performed to determine the crystallinity, crystallite size, microstrain, and dislocation density of the crystals. Geometry optimization was performed by running the MM2 job in CsChemOffice Ultra 16 programs and ArgusLab 4.0.1 version software. The antibacterial potency of the ligand and metal complexes was demonstrated by the standard Kirby–Bauer paper disk diffusion technique for *E. coli*, *K. pneumoniae*, *P. aeruginosa*, *Enterococci*, and *S. aureus* bacteria. Their actual potency against all pathogens was further assessed quantitatively by evaluating the minimum inhibitory concentration (MIC) tests and revealed a significant bacterial growth inhibition.

Keywords Schiff base · Thermodynamic parameters · Surface properties · Antibacterial activities · Spectroscopic characterization

Introduction

Biomedical approaches to inorganic chemistry have expanded the interest of pharmacists in the design and formulation of new chemotherapeutics. The use of metals in medicine cannot be ignored as most of the recent drugs are coordination compounds that have made significant contributions to pharmacology. Most of the important drugs in pharmacology are metal complexes that have a diverse range of applications such as antibacterial, antiviral, analgesics, anti-inflammatory, anticancer, and antitubercular (Danish et al. 2020; Baecker et al. 2021; Naureen et al. 2021; Prasad

et al. 2021). Our interest is to modify the biological profile of such metal complexes by changing ligand behavior with a particular focus on surfactant activity. Surfactants are surface-active agents that are used as emulsifiers, solubilizers, wetting agents, and suspension stabilizers (Alwadani and Fatehi 2018). The amphiphilic nature of surfactants has a significant impact on the biological activity of many pharmaceuticals (Abdul Rub 2019). One of the major issues in the biological activity of conventional drugs is their solubility in vivo in an aqueous medium in the human body, which can affect the biological profile of drugs. Surfactant-added drug formulations can exert various effects, either by deaggregation and dissolution of solid drugs or by increasing membrane permeability in the lipid layer of the cell wall (Attwood 1983). Chemically, surfactant molecules possess an ionic/nonionic polar head group and a long hydrophobic carbon chain. This nature of the surfactant can organize

✉ Narendra Kumar Chaudhary
  chem_narendra@yahoo.com

[1] Department of Chemistry, Tribhuvan University, Mahendra Morang Adarsh Multiple Campus, Biratnagar, Nepal

molecules in different shapes, such as micelles, bilayers, monolayers, and other geometrical shapes. Therefore, the physicochemical profiles of the aggregates can respond in another way (Anestopoulos et al. 2020). Surfactants are the foundation components of many physical, chemical, and biological systems. They are widely used as antiseptics in cosmetics (Kumar and Tyagi 2014), as surface-active agents in detergents (Lutfullina et al. 2013), germicides (Tatsumi et al. 2014), and pharmaceutical industries. Surfactant-based Schiff base metal complexes (metallo-surfactant) have peculiar properties of surfactants consisting of a head group with metal ions and a hydrocarbon chain as a tail group (Wagay and Ismail 2017). Generally, drugs are administered in complex forms in vivo to achieve the desired effect. Complex interactions occur between surfactant-based drugs and proteins that may affect the mechanism of drug metabolism in association with enzymes (Stephansen et al. 2015). The amphiphilic nature of metal complexes is important because of their potential applications in magnetic, catalytic, and biological activities (Brown et al. 2013; Kaur et al. 2018; Donner et al. 2019). Considering all these aspects of surfactant-based drugs, this research will add to the desire for current therapeutics for drug delivery. Another consequence of the need to develop new chemotherapeutics, especially antibiotics, is antibiotic resistance, which has become a major issue in modern pharmacology. Newly emerged bacterial strains with different modes of enzymatic action on host cells are gaining antibacterial resistance, and we have left no options for improving drug activities of conventional drugs either by complexation or by adding prodrugs in the form of surfactants or surfactant-based modified molecules (Ambika et al. 2019).

The primary amines condense with carbonyl compounds to produce an important class of compounds called Schiff bases, which are important ligands that interact with metal ions via azomethine nitrogen (Tsantis et al. 2020). This class of compounds contains active donor atoms to chelate metals for the formation of a metal complex. Owing to their facile synthesis, easy availability, and excellent solubility in various common solvents, Schiff bases have been considered for complex formation in modern coordination chemistry (Kajal et al. 2013). They have wide applications in various fields of chemical science, pharmaceutical science as a powerful drug, electronic field, various biological systems, polymers, dyes, and other fields (Mangamamba et al. 2014). The complexation behavior of Schiff bases is important because of the changes in their physical, chemical, and biological profiles. Therefore, Schiff base compounds deserve special attention from chemists and pharmacists to increase their potential applications and have also shown promising guidelines for the design of more effective antimicrobials (Teran et al. 2019). Due to the chelation behavior of Schiff bases, they can be used as pharmaceutical substances to ameliorate various health problems caused by metal poisoning in the human body. In this study, we selected some heterocyclic compounds for the generation of the Schiff base. Heteroaromatic compounds are also drug substances that are present in many natural drugs. Compounds containing donor atoms such as oxygen, sulfur, and nitrogen constitute a special group of compounds that exhibit significant biological activities (Almarhoon et al. 2019). A five-membered simple heterocyclic compound called pyrrole and its derivatives have attracted the attention of chemists because of their various biological activities (Khashi et al. 2015; Halawa et al. 2017). Pyrrole-2-carboxaldehyde is a pyrrole-based aromatic aldehyde that can be used to synthesize many modified drug candidates (Nami et al. 2016).

The current literature search revealed fewer reports on surfactant-based Schiff base metal complexes, their synthesis, and characterization (Negm et al. 2010; Lakshmipraba et al. 2015; Garg et al. 2016), especially for the complexation behavior with 3d transition metal ions. The present study has aimed to describe the synthesis of a novel Schiff base ligand from dodecylamine (a surfactant) and pyrrole-2-carboxaldehyde and its two metal complexes with divalent 3d metal ions (Ni^{2+} and Zn^{2+}). Characterization of the synthesized complexes was performed by ^1H and ^{13}CNMR, UV–Vis, ESI-mass, FT-IR, SEM-EDAX, thermal analyses, and crystal characterization by powder X-ray diffraction. In addition, we implemented the CMC approach to obtain important information about the surface properties of molecules that may affect their biological activity. The geometry of the synthesized compounds was optimized using the MM2 function in the CsChemOffice molecular modeling software program. This study was further pursued to explore the antibacterial potency of the synthesized compounds against some gram-negative and gram-positive bacterial strains using the standard Kirby–Bauer paper disk diffusion technique (Chaudhary and Mishra 2018). The antibacterial activity was further confirmed by minimum inhibitory concentration (MIC) tests.

Experimental

Materials and reagents

The chemicals, dodecylamine (DDA), and pyrrole-2-carboxaldehyde (P2C) in a pure form were obtained from Spectrochem, Mumbai, India, and Sigma-Aldrich, Germany, respectively, and used without further purification. Mueller–Hinton agar (MHA) was purchased from Himedia, India. Ethanol used as a solvent was procured from Qualigen. Nickel and zinc chloride salts were procured from Merck. Analytical reagent (AR) grade chemicals and solvents were used in the synthesis.

Instruments

The melting point was recorded on VEEGO ASD-10013 programmable melting point equipment. Conductivity measurement was taken on an Auto-ranging digital conductivity/TDS meter TCM 15+ at 25 °C. A Thermo Finnigan FLASH EA 1112 Series CHN analyzer was used to record the patterns of CHN % of the synthesized compounds. FT-IR spectral analysis was performed on a Thermo Nicolet Avtar 370 FT-IR spectrophotometer in a KBr matrix over the spectral range 400–4000 cm^{-1}. A Bruker Avance III 400 MHz NMR spectrometer was used to record the ^{1}H and ^{13}CNMR spectra of the ligand and Zn-DDAP2C in DMSO-d6 solvent. An Agilent Cary 5000, UV–Vis spectrophotometer, with a quartz cuvette, was used to register the electronic absorption spectra of the synthesized compounds in DMSO in the 200–800 nm wavelength range. An Agilent Q-TOF mass spectrometer was used to record the ESI-mass spectrum of the DDAP2C ligand. The mass spectra of the complexes were recorded on MALDI-TOF: Bruker Autoflex max LRF instrument. The X-ray powder diffraction patterns of the synthesized compounds were recorded on a Bruker AXS D8 Advance X-ray diffractometer with a monochromatized Cu-Kα line at a wavelength of 1.5406 Å radiation source. Thermogravimetric analysis was performed on a PerkinElmer thermal analyzer in the temperature range of 40–750 °C. The instrument was operated at a linear heating rate of 20 °C min^{-1}. A JEOL 6390LA/ OXFORD XMX N scanning electron microscope with EDAX functionality (SEM-EDAX) was used to record the micrograph of the compounds and to quantify the elements of the studied compounds. The energy optimization job was performed using the MM2 supported CsChemOffice software program to record the modeling parameters.

Synthesis of Schiff base ligand (DDAP2C)

A well-stirred solution of DDA (10 mmol, 1.8535 g) in 20 ml ethanol was mixed with a warm and homogenously stirred solution of P2C (10 mmol, 0.951 g) dissolved in ethanol (20 ml). The resulting solution was refluxed at 30 °C for 6 h and cooled by a slow diffusion process (Maurya et al. 2003). A reddish-brown solid (yield 75%) was obtained at room temperature by volume reduction. The solid ligand was recrystallized in absolute ethanol and dried over anhydrous CaCl$_2$. The product was kept in an airtight vial and stored in a refrigerator for the next steps of work. The detailed scheme for the synthesis of ligand and metal complexes is shown in Fig. 1.

Synthesis of metal complexes

To the hot and homogenously stirred solution of DDAP2C (1 mmol, 0.2624 gm) in ethanol, 10 ml ethanolic solution of 1 mmol metal chloride salts, NiCl$_2$.6H$_2$O (0.2376 gm), and ZnCl$_2$ (0.1362 gm) was added dropwise in two separate experiments and stirred for several hours under hot condition. Solid metal complexes (yield 68% for Ni-DDAP2C and 70% for Zn-DDAP2C) were obtained by slow diffusion of the solution under normal atmospheric conditions. They were washed several times with absolute ethanol and recrystallized to obtain solid crystals. They were further dried over anhydrous CaCl$_2$ and stored in a refrigerator in an airtight vial for future use.

Antibacterial activity study

Disk diffusion study

The in vitro antibacterial evaluation of the synthesized compounds was carried out against five human pathogenic bacteria like *E. coli, K. pneumoniae, P. aeruginosa, Enterococci*, and *S. aureus*. This was performed using the modified Kirby–Bauer paper disk diffusion technique. A fresh bacterial culture was revived by inoculating in 5 ml nutrient broth and incubated for 3 h at 35 °C to obtain the desired concentration of bacteria ready for use. Agar plates were prepared according to the standard procedures. The organism was swabbed uniformly onto agar media using a sterile stick swab. The desired concentrations of the solution of test compounds were prepared in DMSO. The well-sterilized paper disks of 5 mm diameter size loaded with the test solution were carefully stuck on the swabbed media. For positive control, amikacin, 30 µg/disk, was used. After incubation of the loaded media at 37 °C for 24 h, the diameter of the zone of inhibition around each disk was measured to compare
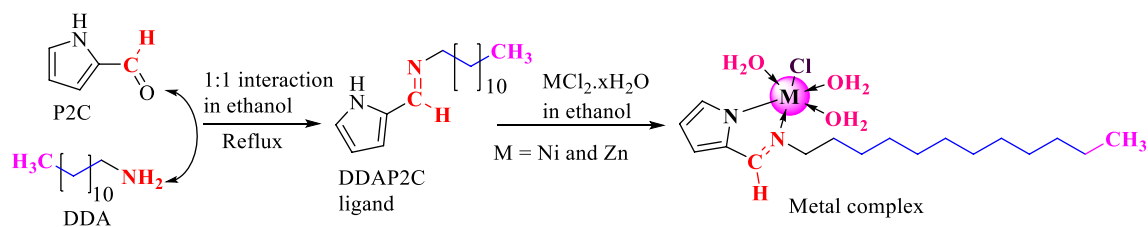

Fig. 1 Schematic presentation of the synthesis of DDAP2C and metal complexes

their antibacterial potency. This study was conducted in triplicate to reduce the error of measurement.

Minimum inhibitory concentration (MIC) study

The MIC is the lowest concentration of the test compounds which does not show any visible growth of organisms in a broth mixed with test compounds. The stock solution of 50 μg/μL concentration of the compounds was prepared in DMSO, and a twofold serial dilution technique was applied to get lower concentration gradients for the exact study (Patel and Khan 2011; Chaudhary et al. 2021). To each of the diluted solutions, 0.1 mL bacterial suspension was added and incubated for 24 h at 37 °C. Each measurement was repeated three times to reduce the measurement error. The broth containing bacterial suspension was considered as the negative control, and the other containing no bacteria was considered the positive control.

Results and discussion

Physical data measurement

The elemental microanalysis, conductivity, m. pt., and other physical data of DDAP2C and its metal complexes are reported in Table 1. The analysis revealed ML-type geometry with a 1:1 metal–ligand ratio. They were soluble in ethanol and less polar solvents such as DMSO and DMF but insoluble in water. The reported m. pt. of compounds was 59 ± 1, 172 ± 2, and 106 ± 1 °C respective of DDAP2C, Ni-DDAP2C, and Zn-DDAP2C. We reported light green solid for Ni-DDAP2C and leaf brown solid for Zn-DDAP2C complex. The proposed molecular structure of the complexes was determined and confirmed by careful study of physical data, which are in good support of their artifact structures.

Critical micelle concentration (CMC) study

The conductivity of the solutions was recorded after proper mixing of the components at a constant temperature. The variation in the conductivity with concentrations

of the surfactant and its complexes is shown in Fig. 2a–c. The specific conductivity increased with an increase in concentration, and the slope changed after a particular concentration. The point of intersection of the two linear variations of the plot gives the CMC. The conductivity measurement was taken in triplicates at 298.15 K, and the accuracy of the CMC value was found to be within ± 2–3% error. The calculated CMC of surfactant and metal complexes is shown in Table 2. The metal complexes possess much lower CMC values than the surfactant, dodecylamine (1.53×10^{-2} M); which resembles the CMC of dodecylammonium chloride. There are two reasons for the decrease in CMC of metal complexes compared to surfactants. The first reason for this decrease may be due to an increase in hydrophobicity of hydrocarbon chains, which promotes the tendency of micellization. As a result, the CMC of metal complexes decreases (Mehta et al. 2012). The second reason is that when the metallo-surfactants dissolve, they often dissociate into surface-active molecules and ions. Generally, the trends of increase in CMC values of metal complexes in a period may be due to the increase in electronegativity and decrease in ionic radius of metal atoms. But, zinc does not follow the trend and gives a lower CMC than nickel. The electronegativity of zinc ion (1.65) is lower than nickel (1.91), and the ionic radius of zinc (74 pm) is larger than those of nickel (70 pm). It can be assumed quite correctly that the ionic character also changes with the change in electronegativity. This increases the ionic strength around the micelles, resulting in a sort of screening effect (Mehta and Kaur 2013). The reduced repulsion among polar head groups facilitates micellization and lowers CMC values. Metals penetrate more deeply into the micelle, reduce the electrostatic repulsion, and thus lower CMC value. Finally, it has been concluded that the 3d metal complexes of the surfactants have higher micellization capacity than common synthetic organic surfactants. This behavior of surfactant-based metal complexes is due to the interaction of metal ions with the long hydrophobic chain of the surfactant (Mehta and Kaur 2013). The free energies of the micelle formation of complexes were calculated using the pseudo-phase separation model (Bhattarai et al. 2017).

Table 1 Microanalytical and physical data of the DDAP2C and its complexes

Complex	Empirical Formula	Formula Wt	Color	M.Pt. (°C)	Calculated (Found) (%)		
					C	H	N
DDAP2C	$C_{17}H_{30}N_2$	262	Reddish Brown	58–59	77.80 (77.329)	11.52 (11.360)	10.67 (10.465)
Ni-DDAP2C	$C_{17}H_{35}ClN_2NiO_3$	410	Light Green	170–175	49.85 (49.57)	8.65 (8. 35)	6.84 (6. 89)
Zn-DDAP2C	$C_{17}H_{35}ClN_2O_3Zn$	416	Leaf Brown	105–107	49.05 (48.772	8.47 (8. 96)	6.73 (6. 40)
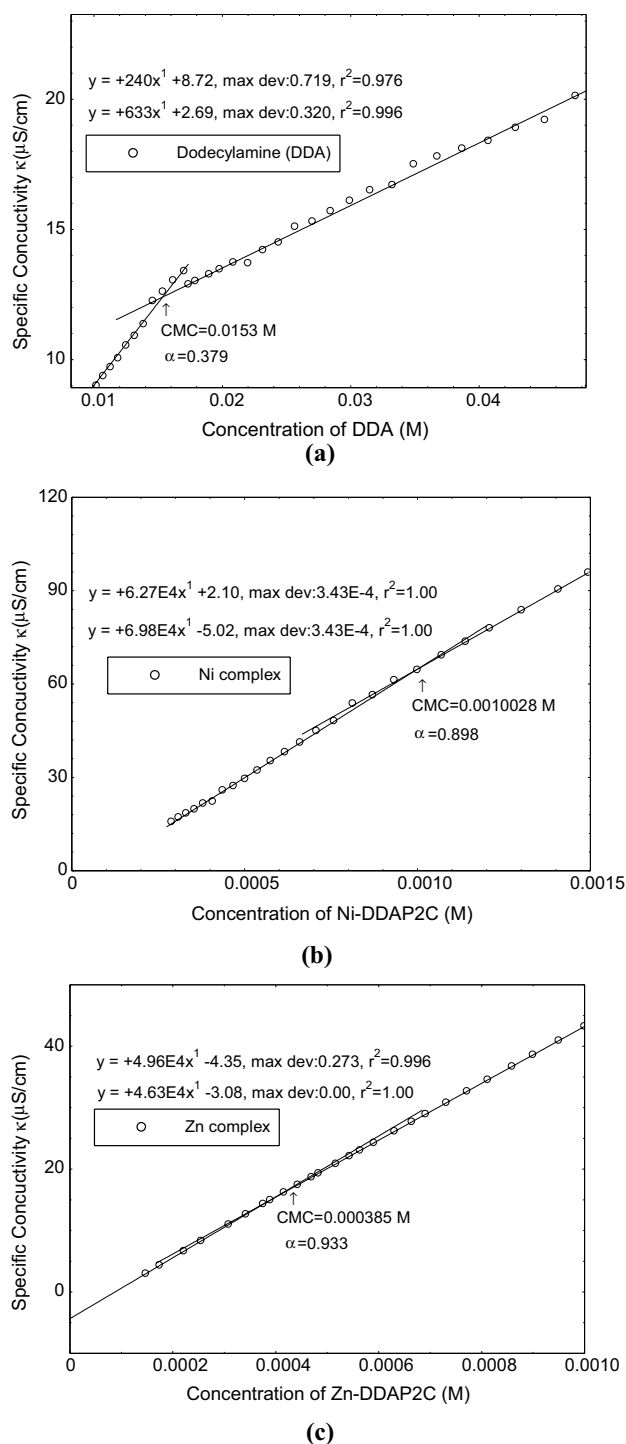
Fig. 2 Plot of conductivity versus concentration of **a** DDA, **b** Ni-DDAP2C, **c** Zn-DDAP2C

$$\Delta G^{\circ}_m = (2 - \alpha)RTlnCMC$$

where R, T, and α are the gas constant, absolute temperature, and degree of micellar ionization, respectively. ΔG°_m was negative for all complexes and became less negative

in the descending order of Zn-DDAP2C, Ni-DDAP2C, and DDA. High negative $\Delta G^{\circ}m$ indicates the spontaneous micellization process and follows the order Zn-DDAP2C > Ni-DDAP2C > DDA. Surfactants containing large metal ions have increased head polarity. As the polarity of the head increases, the negative Gibbs free energy of micellization also increases. This result is more favorable for the micellization of metal-based surfactants (Chandar et al. 2009).

Spectroscopic characterization

FT-IR spectroscopy

The FT-IR data of the ligand (DDAP2C) and its complexes are summarized in Table 3 and the spectra of the complexes are presented in Figs. S1S and S2S. The IR absorption peaks provide useful structural information of the newly synthesized compounds. The spectrum of DDAP2C (Fig. 3) showed a broad absorption band at 3163 cm^{-1} assigned for the ν(NH) stretch, and two intense absorption bands at 2848 and 2927 cm^{-1} due to –CH$_3$, ν(CH) stretch. The absence of pyrrole N–H stretching vibration band at 3163 cm^{-1} in the IR spectra of metal complexes provides strong evidence for deprotonation of N–H moiety during complexation (Han et al. 2003; Tyagi et al. 2015; Gherras et al. 2018). The metal complexes delivered broad absorption bands positioned at 3440 and 3447 cm^{-1} for Ni-DDAP2C and Zn-DDAP2C complexes, respectively, which are assigned for the ν(OH) stretch of associated water molecules. A high-intensity band at 1648 cm^{-1} for DDAP2C is assigned to azomethine ν(C=N) stretch, which has shifted 19 to 26 cm^{-1} downward in complexes (Mohamed et al. 2011; Upadhyay et al. 2013; Mbugua et al. 2020). The corresponding ν(C=N) stretching bands for Ni-DDAP2C and Zn-DDAP2C complexes are observed at 1629 and 1622 cm^{-1}. The ν(Ar–C=C) stretching vibration bands for DDAP2C were observed at 1421, 1470, and 1553 cm^{-1}, and little variation was observed in these bands after complexation. The absorption band assigned for ν(C-N) stretch at 1366 cm^{-1} for DDAP2C has shifted to 1385 and 1378 cm^{-1} for Ni-DDAP2C and Zn-DDAP2C complexes, respectively (Mohamed et al. 2011; Buldurun et al. 2019). Besides these characteristic absorption bands, the metal complexes showed a less intense band at 452 cm^{-1} for Ni-DDAP2C and 466 cm^{-1} for Zn-DDAP2C, assigned to ν(M–N) stretch (Anila et al. 2017). These IR absorption data provide strong evidence for the formation of the metal complex via the azomethine nitrogen of DDAP2C.

^{1}H and ^{13}CNMR spectral analysis

The comparison of the NMR spectra of the DDAP2C and its diamagnetic Zn-DDAP2C complex gives important

Table 2 Values of premicellar slope (S1), postmicellar slope (S2), degree of dissociation ( ), critical micelle concentration (CMC), and Gibbs free energy of micellization (ΔGo m) of DDA, Ni-DDAP2C and Zn-DDAP2C in ethanol medium at 298.15 K

Compounds	S_1 (μS cm^{-1} l·mole^{-1})	S_2 (μS cm^{-1} l·mole^{-1})	α	CMC (mole L^{-1})	$\Delta G^o{}_m$ (kJmol^{-1})
DDA	240	633	0.379	1.53×10^{-2}	− 16.79
Ni-DDAP2C	6.27×10^4	6.98×10^4	0.898	1.002×10^{-3}	− 18.86
Zn-DDAP2C	4.63×10^4	4.96×10^4	0.933	3.85×10^{-4}	− 20.79

Table 3 Selected IR data of DDAP2C and its complexes in cm^{-1}

Complex	ν(NH)	ν(C=N) (imine)	ν (C–H)	ν (Ar–C=C)	ν (C–N)	ν(M–N)	ρ_w H$_2$O Coordinated
DDAP2C	3163	1648	2927, 2848	1421,1470,1553	1366	–	–
Ni-DDAP2C	–	1629	2924, 2854	1469, 1511	1385	452	3440
Zn-DDAP2C	–	1622	2924, 2848	1476	1378	466	3447

Fig. 3 FT-IR spectrum of DDAP2C
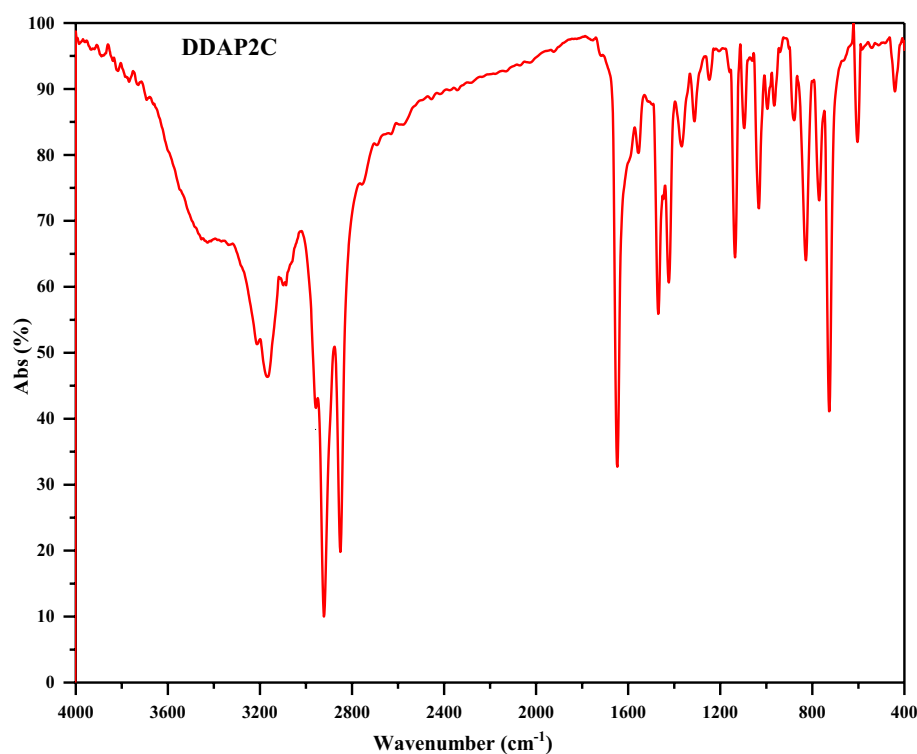
information about the proton/carbon environment and its chemical shift within the molecule. Their ^{1}HNMR spectral data are documented in Table 1S. The DDAP2C exhibited a signal at δ 8.041 ppm attributed to the azomethine (–CH=N) proton and this indicates the formation of Schiff base ligand. This signal for Zn-DDAP2C was shifted downfield to δ 8.486 ppm indicating the participation of azomethine nitrogen in complex formation (Nami et al. 2016; Tyagi et al. 2017; Kabeer et al. 2019). The pyrrole ring protons of DDAP2C resonating at 6.088–6.852 ppm were shifted downfield in the 6.455–7.664 ppm range for the Zn–DDAP2C complex (Singh et al. 2010). The pyrrole NH proton of DDAP2C displayed a singlet at 11.296 ppm, the absence of which in the ^{1}HNMR spectrum of Zn-DDAP2C confirms the complexation associated with zinc–nitrogen binding (Bhowon et al. 2004; Lobana et al. 2012; Paul and Bhattacharya 2014; Gherras et al. 2018). The ^{1}HNMR and ^{13}CNMR spectral data incorporated in the structure of the ligand and Zn-DDAP2C are presented in Figs. 4, 5 and their ^{1}HNMR spectra are given in Figs. S3S and S4S.
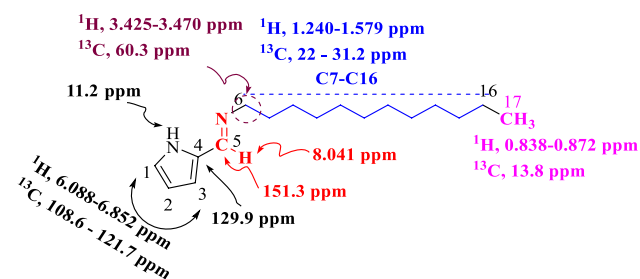
Fig. 4 ^{1}HNMR and ^{13}CNMR spectral data of DDAP2C

^{13}CNMR spectral study gives insight into the carbon atoms in the molecules and their electronic environment. The azomethine carbon (C=N) of the DDAP2C resonated at δ 151.3 ppm (Kumar et al. 2016). The carbons of the pyrrole ring delivered peaks at δ 108.6–129.9 ppm. These peaks were found in the range δ 105.9–128.3 ppm in the ^{13}CNMR spectrum of the Zn-DDAP2C complex (Vinusha et al. 2019). The methyl carbons of DDAP2C delivered signal at δ 13.8 ppm and the methylene carbons exhibited the signals in the range δ 21.9–31.2 ppm. There was no appreciable variation in chemical shifts for these carbons in the ^{13}CNMR spectrum of the Zn-DDAP2C. The ^{13}CNMR spectra of the DDAP2C and Zn-DDAP2C are presented in Figs. S5S and S6S and their data are documented in Table 2S.
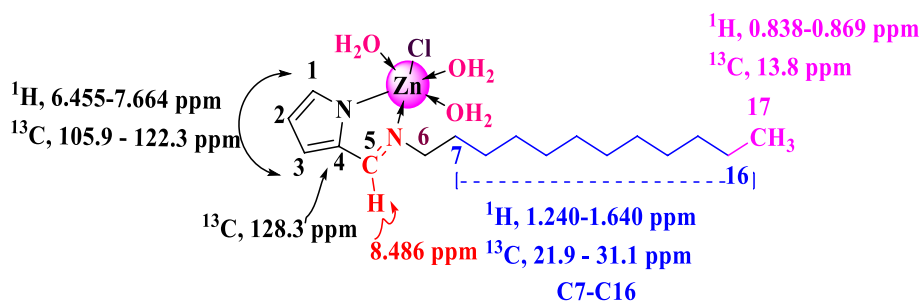
ESI-mass spectral study

Figures (S7S-S9S) report ESI-mass spectra of DDAP2C and its metal complexes. The [M$^-$+H] peak for DDAP2C was reported at m/z 263 and it represents the base peak. The other fragment peaks reported in the spectrum were at m/z 187 and 186. Therefore, based on the nitrogen rule, the molecular mass of DDAP2C was assigned to 262 amu. Similarly, the [M$^+$] peaks for Ni-DDAP2C and Zn-DDAP2C were recorded at m/z 410 and 416, respectively. All these mass spectral peak values strongly support the proposed molecular formula of the compounds (Reshma et al. 2019).

Electronic absorption spectral study

The electronic absorption spectrum (Fig. S10S) and magnetic moment data for DDAP2C and its complexes are documented in Table 4. The spectrum of DDAP2C displayed three absorption bands at 283, 325, and 346 nm assigned to the π→π* transition within the aromatic ring, n→π* transition of free electrons of the azomethine (C=N) group, and intra-ligand charge transfer (ILCT) band, resulting from the interaction of the aromatic ring and the azomethine group respectively (Canpolat and Kaya 2005).

The electronic absorption spectrum of the Ni-DDAP2C complex showed five absorption bands at 294, 322, 441, 548, and 627 nm (Canpolat and Kaya 2005; Sharaby 2005). The band at 294 nm is due to the n→π* transition, while the band at 322 nm represents the ligand metal charge transfer (LMCT) band. The n→π* transition of the ligand has undergone a bathochromic shift in the complex (Uçar et al. 2008; Manjuraj et al. 2020). The absorption bands at 441, 548, and 627 nm have been assigned respectively for $^3A_{2g}$→$^3T_{1g}$ (P), $^3A_{2g}$→$^3T_{1g}$ (F), and $^3A_{2g}$→$^3T_{2g}$ transitions. These transitions confirm the octahedral geometry of the Ni-DDAP2C complex (Jain and Mishra 2016). It is further evidenced by its magnetic moment data of 2.95 BM. The

Table 4 Electronic absorption spectra, magnetic moments and specific conductivity data of DDAP2C and its complexes

Comp	Peak positions (nm)	Assignment	Magnetic moment (BM)	Conductance (μS/cm)
DDAP2C	283	π→π*,	–	7.5
	325	n→π *,		
	346	Intra-ligand charge transfer band		
Ni-DDAP2C	294	n→π*	2.95	64.5
	322	(LMCT) band		
	441	$^3A_{2g}$→$^3T_{1g}$(P)		
	548	$^3A_{2g}$→$^3T_{1g}$(F)		
	627	$^3A_{2g}$→$^3T_{2g}$		
Zn-DDAP2C	285	π→π*	0	43.2
	321	n→π *		
	443	(LMCT) band		

Fig. 5 ^{1}HNMR and ^{13}CNMR spectral data of Zn-DDAP2C

Zn-DDAP2C complex delivered three absorption bands at 285, 321, and 443 nm, representing $\pi \rightarrow \pi^*$, $n \rightarrow \pi$ *, and LMCT bands. However, the d-d transition band was absent because of its complete d^{10} electronic configuration (Orojloo et al. 2015; Chaudhary and Mishra 2018). The thermal study also suggested the association of three molecules of water as a structural component in the Zn-DDAP2C complex and six coordination numbers have been assigned for it. Based on analytical, thermal, spectral, and conductivity data, an octahedral geometry has been proposed for the Zn-DDAP2C complex (Turan et al. 2019).

TGA/DTA study

Thermal properties

The prepared metal complexes were introduced for thermogravimetric analysis in a nitrogen atmosphere, and the thermal operation was carried out at a linear heating rate of 20 °C/min in the temperature range of 40 to 750 °C (Chaudhary and Guragain 2019). In this study, the thermal and kinetic parameters were obtained by analyzing TGA/DTA plots, and the data are shown in Table 5. The results precisely agree with the proposed chemical structures recommended by other analytical data. The TGA plot of the Ni-DDAP2C (Fig. 6a) showed the four-phase decomposition pattern between 108.15 and 602.07 °C. The first decomposition step started at 108.15 °C and ended at 204.98 °C, with a mass loss of 0.36 mg (6.18%) may be due to the loss of coordinated water molecules (Hankare and Chavan 2003; Mohamed et al. 2011). The second decomposition step represents a partial ligand loss with a mass of 1.763 mg (34.199%) in the temperature range 266.3 to 375.16 °C. The exothermal effect was reported in this step with a T_{DTG} peak at 338.17 °C and a T_{DTA} peak at 357.80 °C (Chaudhary and Mishra 2018). The loss of the ligand moiety with a mass of 0.711 mg (21.77%) and a T_{DTG} peak at 413.60 °C was observed in the third decomposition step in the temperature limits of 386.01–443.05 °C. The fourth and final step

decomposition, with $T_{DTG} = 567.31$ °C within the temperature range of 493.01 to 602.07 °C, represents the total loss of the ligand moiety and leaves a solid residue of nickel oxide (Alturiqi et al. 2018). This was ensured by the formation of a horizontal plateau in the thermogram after 602.07 °C. This step showed an exothermal effect with a T_{DTA} peak at 569.96 °C.

The thermogram of Zn-DDAP2C (Fig. 6b) displayed five decomposition steps with various shoulder peaks. The first decomposition step between 158.09 and 214.42 °C represents a mass loss of 0.143 mg (2.56%) corresponding to the loss of three coordinated water molecules with $T_{DTG} = 188.82$ °C (Mahmoud et al. 2018). A mass loss of 0.906 mg (17.98%) was noticed in the second phase of decomposition within the temperature range of 319.06 to 384.83 °C which may be due to the partial loss of ligand moiety. This second phase of decomposition is associated with a shoulder peak at $T_{DTG} = 359.49$ °C with the corresponding T_{DTA} peak at 372.05 °C showing an exothermal effect. The third decomposition step occurred in the temperature range of 394.02 to 464.36 °C with a mass loss of 1.084 mg (27.01%) due to loss of the ligand part with a corresponding T_{DTG} peak at 443.48 °C (Chaudhary and Mishra 2018; Chaudhary and Guragain 2019). The fourth decomposition step observed in the temperature range of 500.73 to 575.61 °C, with $T_{DTG} = 531.95$ °C, represents the loss of a ligand fragment with an estimated mass loss of 0.824 mg (32.04%). The fifth and last decomposition step occurred in the temperature range of 607.58 to 723.32 °C with T_{DTG} at 651.69 °C. This represents the complete loss of the ligand moiety, leaving ZnO as a stable residue. This was confirmed from the horizontal segment of the TGA curve after 723.32 °C. The exothermal effect was concluded for this step with a T_{DTA} peak at 651.69 °C.

Kinetic properties study

The kinetics and thermodynamic properties of the metal complexes were calculated by analyzing the TGA/DTA

Table 5 Thermal decomposition data of Ni-DDAP2C and Zn-DDAP2C

Complex	Steps	TG range (°C) Δm % found (Cal.)	DTA T_i	T_f	T_{DTG}	Mass loss	T_{DTA}	Peak
Ni-DDAP2C	1	6.18	108.15	204.98	173.71	0.36	–	–
	2	34.199	266.3	375.16	338.97	1.763	357.80	Exo
	3	21.77	386.01	443.05	413.60	0.711	–	–
	4	57.326	493.01	602.07	567.31	1.252	569.96	Exo
Zn-DDAP2C	1	2.56	158.09	214.42	188.82	0.143	–	–
	2	17.98	319.06	384.83	359.49	0.906	372.05	Exo
	3	27.01	394.02	464.36	443.48	1.084	–	–
	4	32.04	500.73	575.61	531.95	0.824	–	–
	5	93.56	607.58	723.32	651.69	1.394	–	–

Fig. 6 TGA/DTA curve of (**a**) Ni-DDAP2C, (**b**) Zn-DDAP2C

plots and the calculated data are documented in Table 6. These properties were assessed graphically using the Coats–Redfern equations (Coats and Redfern 1963; Garg et al. 2016; Al Zoubi et al. 2017).

$$\ln\left[-\frac{\ln(1-\alpha)}{T^2}\right] = \ln\left[\frac{AR}{\beta E^*}\right] - \frac{E^*}{RT}$$

Here β denotes the linear heating rate (dT/dt), and α denotes the fraction of decomposition at T (K) temperature. E^* represents the activation energy, and A indicates Arrhenius's

Table 6 Thermodynamic and kinetic parameters of Ni-DDAP2C and Zn-DDAP2C

Comp	Step	r	A (s^{-1})	T_{max} (K)	E^* (J/mol)	S^* (J/K.mol)	H^* (kJ/mol)	G^* (kJ/mol)
Ni-DDAP2C	1	−0.99317	1316.62	446.71	877.460	−188.556	−2.836	81.393
	2	−0.99159	709.818	611.97	550.886	−196.331	−4.537	115.599
	3	−0.99082	446.783	686.60	280.348	−201.115	−5.428	132.658
	4	−0.99141	338.531	840.31	270.704	−205.101	−6.715	165.633
Zn-DDAP2C	1	−0.99078	279.439	461.82	249.836	−201.719	−3.589	89.568
	2	−0.99168	560.628	632.49	331.812	−198.546	−4.927	120.651
	3	−0.99178	477.918	716.48	342.869	−200.909	−5.614	138.333
	4	−0.99083	338.896	804.95	258.898	−204.735	−6.433	158.368
	5	−0.99178	281.035	924.69	252.247	−207.445	−7.436	184.134

pre-exponential factor. R denotes the gas constant. The graphical plot of the left-hand side against 1/T in the Coats–Redfern equation gives a straight line whose slope (-E*/R) gives the energy of activation (kJmol^{-1}) and its intercept gives the value of A in the s^{-1} unit. Other thermodynamic properties such as free energy of activation (ΔG*), enthalpy of activation (ΔH*), and entropy of activation (ΔS*) were obtained by applying the relation (Chaudhary and Mishra 2018).

$$\Delta S^* = Rln\ln\left[\frac{Ah}{K_BT}\right]$$

$$\Delta H^* = E^* - RT$$

$$\Delta G^* = \Delta H^* - T\Delta S^*$$

The following facts have materialized:

1. The activation energy (E*) of the successive steps increases step by step, indicating a decreasing rate of complex decomposition. The rate of decomposition of ligand moiety in the metal complex slowed down, indicating greater thermal stability of the complex (Abdou et al. 2013).
2. In most of the decomposition steps, the value of entropy of activation, S^*, was negative, and this indicated a slow reaction process with more ordered complexes than reactants. Furthermore, negative values in the decomposition steps indicated a non-spontaneous process of decomposition (Patel and Patel 2020).
3. A negative value of enthalpy, ΔH*, led to the conclusion that the process of decomposition is exothermic in all decomposition steps (Al-Radadi et al. 2020).
4. For all steps, the value of ΔG* was positive, proving that the decomposition is non-spontaneous (Bouzerafa et al. 2017).

Powder X-ray diffraction study

Single-crystal growth was unsuccessful, and we used powder X-ray diffraction study to explore the crystal properties of DDAP2C and its metal complexes. The crystal system and its refinement parameters are listed in Tables 3S–5S (Ahmad et al. 2020). The PXRD patterns (Fig. S11S) of the compounds were evaluated in the range of 2θ (3—80°) to understand the lattice dynamics of the compound. It provides a clear idea about the purity of a solid having a definite crystal structure. The diffractogram exhibited sharp peaks, suggesting its crystalline nature. The full width at half maximum (FWHM) of the diffraction peaks obtained from the refinement was used to evaluate the particle size (Mehta and Kaur 2013). The DDAP2C showed

7 reflection peaks in the diffractogram with 100% peak intensity at 7.54429° and a respective d-spacing value of 0.050677113 Å. Its nanocrystalline nature was verified by an average crystallite size of 8.458120653 nm. Likewise, Ni-DDAP2C displayed 8 reflection peaks in the diffractogram with the most intense peak at 24.59293° and a respective interplanar d-spacing value 0.164050872 Å. The average crystallite size (35.83735112 nm) of this complex represents its nanocrystalline nature. In the diffractogram of Zn-DDAP2C, 13 reflection peaks have been recorded, with the most intense peak at 4.09947° and a respective interplanar d-spacing value of 0.027551316 Å. The crystallite size (53.2379956 nm) revealed its nanocrystalline nature. The crystallite size (D) of the synthesized compound was evaluated from PXRD patterns by using Debye–Scherrer's equation (Justin Dhanaraj and Salin Raj 2020).

$$D = (K\lambda/\beta Cos\theta)$$

here λ represents the wavelength, and   and   (radian) denote the full width at half maxima, and the diffraction angle, respectively. K denotes a constant called the shape factor with a value of 0.9 (Sheng et al. 2012). Comparison of their X-ray diffraction patterns revealed different interplanar d-spacing values with variable peak intensities, which may suggest the formation of the complex.

The dislocation density ( ) of the complexes was calculated from the value of (D). It describes the number of dislocation lines per unit area (nm^{-2}) of the crystal (Aly and Fathalla 2020). The relationship between the dislocation density ( ) and average crystallite size (D) is given by the equation:

$$\delta = (1/D^2)$$

The calculated values of (δ) for DDAP2C, Ni-DDAP2C, and Zn-DDAP2C were found to be 13.98×10^{-3}, 0.779×10^{-3}, and 0.353×10^{-3}, respectively. The δ data differ for complexes relative to the ligand which also supports complex formation. Similarly, another important parameter that describes the variations in the lattice parameters across the sample is the microstrain (ε) which was evaluated from the value of the peak position (2θ) and its corresponding FWHM (Badawi et al. 2019).

$$\varepsilon = \beta/4tan\theta$$

Here   represents the diffraction angle in radians and β denotes the FWHM. The microstrain values obtained for DDAP2C, Ni-DDAP2C, and Zn-DDAP2C were 0.04340, 0.01353, and 0.01127, respectively. The different values of ε for the ligand and complexes assure that they are different compounds that also support the formation of the complex from the ligand. The variation of lattice parameters across

the sample is greater in the case of the ligand relative to its complexes.

SEM and EDAX study

Scanning electron microscopy study was conducted to predict the surface morphology of the synthesized compounds, and the SEM micrographs are illustrated in Fig. 7. A broken ice-like structure associated with the heterogeneous matrix was observed in the SEM micrograph of the DDAP2C. However, Ni-DDAP2C revealed a rocklike structure with a minute non-uniform matrix scattered over it. Zn-DDAP2C exhibited a broken glass-like structure, on which an uneven distribution of the matrix was observed (de Araújo et al. 2017). The energy-dispersive X-ray diffraction analysis (EDAX) technique was used to determine the chemical composition of metal complexes. The peaks of essential elements such as C, O, Cl, and metal components, which constitute the molecules of Ni-DDAP2C and Zn-DDAP2C, were identified in the EDAX profile [Figs. S12S, S13S], supporting their proposed structures. They showed predictable

elements present in the synthesized compounds (Zaky and Fekri 2017). The complexes were also examined using the SEM-EDAX system, where the presence of Ni and Zn ions as the metal was confirmed by the brighter regions on the SEM micrograph of the complexes (Barbosa et al. 2017).

Molecular modeling study

The optimization of the structure related to the theoretical calculation of molecules was studied by running an MM2 job in CsChemOffice 3D Ultra 16.0. It provides useful information about changes in molecular coordinates, changes in bond lengths, and bond angles. From this, we assure the structural change after the complexation. Appropriate stereochemistry has been established through modification and manipulation of molecular coordinates to achieve molecular geometry with a reasonably low energy state (Chaudhary and Mishra 2018). The potential energy of a molecule is considered to be the algebraic sum of the following given energy terms:

Fig. 7 SEM micrograph of (**a**) DDAP2C, (**b**) Ni-DDAP2C, (**c**) Zn-DDAP2C

(a)

(b)

(c)
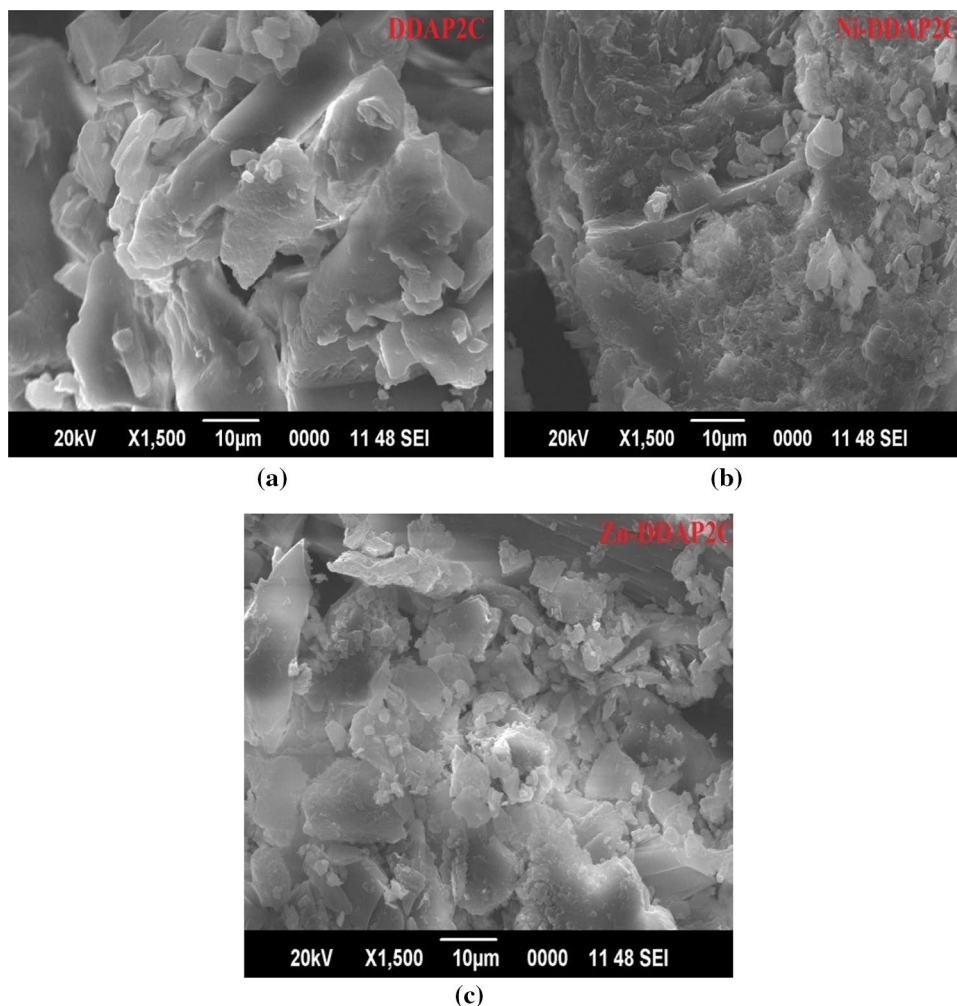
$$E = E_{str} + E_{ang} + E_{tor} + E_{vdw} + E_{oop} + E_{ele}$$

here E denotes the energy associated with the given types of interaction. The subscripts ele, oop, vdw, tor, ang, and str denote electronic interaction, out-of-plane bending, van der Waals interactions, torsion deformation, angle bending, and bond stretching, respectively (Rajiv and Rajni 2011; Siddappa et al. 2014). The analytical data and spectral studies confirmed the hexacoordination of Ni-DDAP2C and Zn-DDAP2C, which was further confirmed by molecular modeling techniques. The 3D-optimized geometrical structures of DDAP2C and the metal complexes are shown in Figs. 8, S14S, and S15S. The structure of the complexes was optimized to evaluate their structural details. Energy optimization was repeated many times to obtain average minimum energy. The bond length and bond angle parameters of DDAP2C and metal complexes are listed in Table 7. From the molecular modeling study for the selected bond lengths and bond angles of DDAP2C and its metal complexes, the following observations have been established.

1. The C(6)–N(7), N(7)–C(9), and C(4)–C(6) bond lengths change due to the coordination of DDAP2C with metal through the N atoms of azomethine (–CH=N) and pyrrole ring. As a result, M–N bonds are formed in all complexes (El-Samanody et al. 2018).
2. The O–Ni, N–Ni, Ni–Cl, and Ni–N bond lengths in Ni-DDAP2C are shorter than the corresponding O–Zn, N–Zn, Zn-Cl, and Zn-N bond lengths in Zn-DDAP2C. Similarly, in metal complexes, the M–O bond was found longer than M–N bond (Gaber et al. 2019).
3. The Ni-DDAP2C has greater energy than Zn-DDAP2C. This suggests greater stability of the Zn-DDAP2C complex than Ni-DDAP2C (Singh et al. 2017).
4. The bond angle values for Ni-DDAP2C and Zn-DDAP2C support their octahedral geometry.

Therefore, from the above observations, it was concluded that the electron density in the coordinated atoms of DDAP2C decreases after complexation, and consequently, the bond length increases (e.g., CH=N, N–H) (Gaber et al. 2017).

Antibacterial activity study

The structural components of chemicals have a profound effect on their biological activity. In addition, the amphiphilic nature of molecules also plays a significant role in determining their biological potential (Ilker et al. 2004; Negm and Zaki 2008). In regard to metal complexes, metals bridge organic ligands with cellular components of the microorganisms and improve their biological significance (Rojas et al. 2017). In this study, we have interacted the synthesized compounds with organisms for the precise evaluation of their antibacterial potency, and this study was done by disk diffusion technique (Gupta et al. 2020; Priya Dharsini et al. 2020). For this purpose, solutions of the synthesized compounds were prepared in DMSO at a concentration of 50, 25, and 12.5 µg/µL. The growth inhibition values are reported in Table 8. The relative antimicrobial efficacy of the complexes was compared with amikacin 30 µg/disk as a standard reference drug. The graphical results are shown in the bar graph Figs. 9, 10, 11. With all pathogens, the antibacterial activity of amikacin was found higher than other studied compounds, except *S. aureus,* and *E. coli* where the activity was comparable. The Zn-DDAP2C complex showed lower antibacterial activity with *E. coli*, compared to DDAP2C, Ni-DDAP2C, and the control drug amikacin at all concentrations. The antibacterial data revealed a higher growth inhibition of ligand and metal complexes against *P. aeruginosa* and *S. aureus*. All metal complexes showed greater growth inhibition at high concentrations and significantly lesser growth inhibition at low concentrations. The growth inhibition values of metal complexes are almost comparable.

Fig. 8 3D-optimized geometrical structure of Ni-DDAP2C
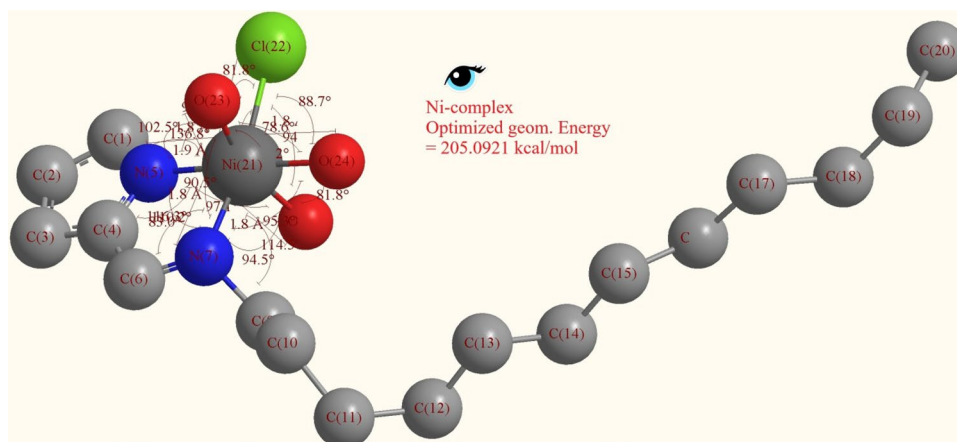
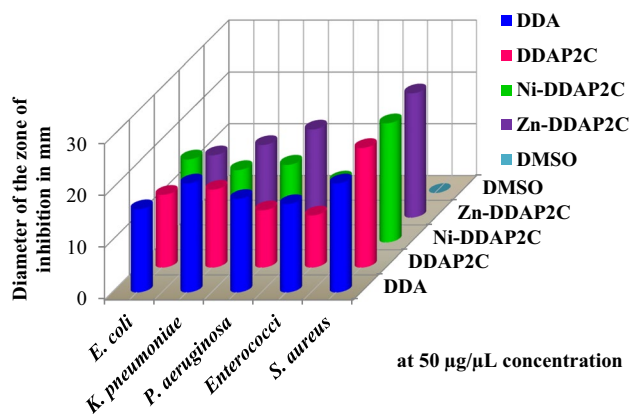**Table 7** Selected bond lengths and bond angles of DDAP2C and its complexes

Complex	Bonded Atoms	Bond length (Å)	Bonded Atoms	Bond angle (°)	Final geom energy
DDAP2C	C(1)-N(5)	1.241			18.9431 kcal/mol
	C(4)-N(5)	1.251			
	C(3)-C(4)	1.376			
	C(2)-C(3)	1.366			
	C(1)-C(2)	1.372			
	N(7)-C(9)	1.471			
	C(6)-N(7)	1.278			
	C(4)-C(6)	1.344			
Ni- DDAP2C	O(23)-Ni(21)	1.890	O(23)-Ni(21)-O(25)	160.200	205.0921 kcal/mol
	O(25)-Ni(21)	1.840	O(23)-Ni(21)-O(24)	78.639	
	O(24)-Ni(21)	1.826	O(23)-Ni(21)-N(5)	102.474	
	N(5)-Ni(21)	1.804	O(23)-Ni(21)-Cl(22)	81.841	
	Ni(21)-Cl(22)	2.180	O(23)-Ni(21)-N(7)	90.544	
	N(7)-Ni(21)	1.827	O(25)-Ni(21)-O(24)	81.824	
	N(7)-C(9)	1.494	O(25)-Ni(21)-N(5)	97.149	
	C(6)-N(7)	1.257	O(25)-Ni(21)-Cl(22)	94.589	
	C(4)-C(6)	1.346	O(25)-Ni(21)-N(7)	94.451	
			O(24)-Ni(21)-Cl(22)	88.693	
			O(24)-Ni(21)-N(7)	95.316	
			N(5)-Ni(21)-Cl(22)	93.103	
			N(5)-Ni(21)-N(7)	83.040	
			Cl(22)-Ni(21)-N(7)	170.549	
			Ni(21)-N(7)-C(9)	114.497	
			Ni(21)-N(7)-C(6)	116.263	
			Ni(21)-N(5)-C(1)	136.846	
			Ni(21)-N(5)-C(4)	110.205	
Zn-DDAP2C	O(25)-Zn(21)	1.929	O(25)-Zn(21)-O(24)	81.471	155.3826 kcal/mol
	O(24)-Zn(21)	1.892	O(25)-Zn(21)-O(23)	73.981	
	O(23)-Zn(21)	1.918	O(25)-Zn(21)-Cl(22)	83.807	
	Zn(21)-Cl(22	2.237	O(25)-Zn(21)-N(5)	87.600	
	N(5)-Zn(21)	1.921	O(25)-Zn(21)-N(7)	169.725	
	N(7)-Zn(21)	1.934	O(24)-Zn(21)-O(23)	155.388	
	N(7)-C(9)	1.567	O(24)-Zn(21)-Cl(22)	82.273	
	C(6)-N(7)	1.285	O(24)-Zn(21)-N(5)	96.101	
	C(4)-C(6)	1.330	O(24)-Zn(21)-N(7)	96.896	
			O(23)-Zn(21)-Cl(22)	96.600	
			O(23)-Zn(21)-N(5)	81.336	
			O(23)-Zn(21)-N(7)	106.939	
			Cl(22)-Zn(21)-N(5)	171.398	
			Cl(22)-Zn(21)-N(7)	106.090	
			N(5)-Zn(21)-N(7)	82.475	
			Zn(21)-N(7)-C(9)	123.434	
			Zn(21)-N(7)-C(6)	111.925	
			C(1)-N(5)-Zn(21)	140.573	
			Zn(21)-N(5)-C(4)	106.980	

The MIC data of the test compounds are listed in Table 9. Based on the data, it can be inferred that all the studied compounds possess good antibacterial potency. The results exhibited greater susceptibility of DDA, DDAP2C, and metal complexes against *S. aureus*. Similarly, *Enterococci* were also found to be susceptible to these compounds. An

Table 8 Antibacterial activity data of DDAP2C and metal complexes

Compounds	Diameter of the zone of inhibition in mm														
	E. coli			*K. pneumoniae*			*P. aeruginosa*			*Enterococci*			*S. aureus*		
Concentration (μg/μL)	50	25	12.5	50	25	12.5	50	25	12.5	50	25	12.5	50	25	12.5
DDA	16	14	13	21	16	14	18	16	15	17	16	15	21	20	19
P2C	0	0	0	0	0	0	0	0	0	0	0	0	0	0	0
DDAP2C	14	13	12	15	12	9	11	11	11	10	9	8	23	21	20
Ni-DDAP2C	16	15	14	14	11	10	15	13	11	12	10	8	23	22	21
Zn-DDAP2C	12	10	9	14	10	9	17	16	14	11	10	9	24	23	22
Amik. (30 μg/disk)	14			24			23			20			21		
DMSO	0	0	0	0	0	0	0	0	0	0	0	0	0	0	0

Fig. 9 Bar graph showing antimicrobial activity at 50 μg/μL concentration
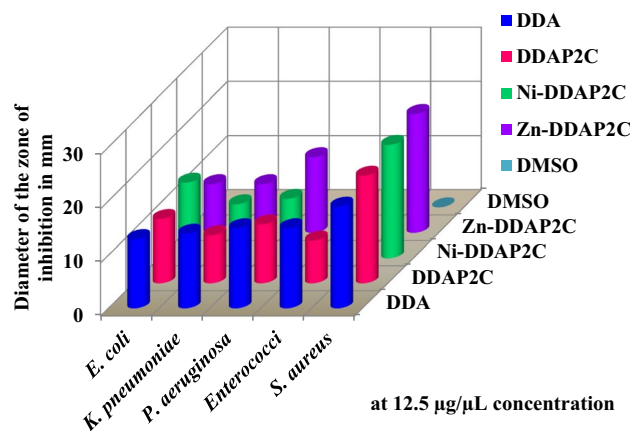
Fig. 11 Bar graph showing antimicrobial activity at 12.5 μg/μL concentration
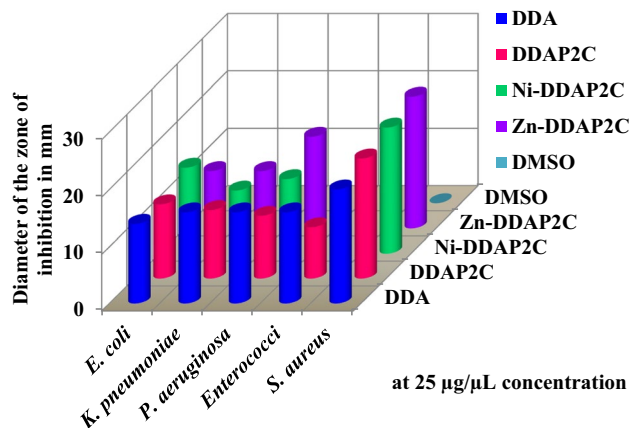
Fig. 10 Bar graph showing antimicrobial activity at 25 μg/μL concentration

improved MIC value was recorded for Ni-DDAP2C against all pathogens. The antibacterial potency against *E. coli* follows the order (Ni-DDAP2C, Zn-DDAP2C) (0.0122 μg/μL) > DDAP2C (0.0976 μg/μL) > DDA (0.7812 μg/μL). The data also revealed that Zn-DDAP2C is more active against

P. aeruginosa, with the lowest MIC value of 0.0122 μg/μL. The Ni-DDAP2C complex with a MIC value of 0.0488 μg/μL showed greater antibacterial potency against *S. aureus*. Overall the MIC results indicated that all the tested compounds possess excellent and comparable antibacterial activity against all isolates, and thus, metal complexes are suggested as the best antibacterial agent.

This increased activity of complexes is explained by two theories:

1. The overtone theory: It asserts that the antibacterial activity of the compound depends on its permeability in the cell membrane which plays an important role by allowing only lipid-soluble molecules to pass (Reiss et al. 2021).

2. Tweedy's theory: This theory explains that the polarity of the metal ion decreases significantly after chelation due to the overlap with the ligand orbital and the sharing of positive charges with donor atoms or groups. Furthermore, it improves the penetration ability of metal complexes in lipid membranes and the blockage of

Table 9 Minimum inhibitory concentration data

Coumpounds	Minimum inhibitory concentration (MIC) in (μg/μL)				
	E. coli	*K. pneumoniae*	*P. aeruginosa*	*Entercocci*	*S. aureus*
DDA	0.7812	0.0488	0.0976	0.3906	0.1953
DDAP2C	0.0976	0.1953	0.1953	0.3906	0.0976
Ni-DDAP2C	0.0122	0.0122	0.0488	0.0122	0.0488
Zn-DDAP2C	0.0122	0.0488	0.0122	0.0976	0.0976

metal-binding sites in microbial enzymes by increasing electron delocalization over the entire chelate ring (Fekri et al. 2019; Srivastava 2021). The complexes also obstruct cell respiration and block protein synthesis which restricts the growth of the organisms.

The effectiveness of metallo-surfactant complexes for different organisms is determined by their hydrophobicity and amphiphilic properties. With gram-positive bacteria, there is hydrophobic interaction of the metallo-surfactants with the cell membrane and electrostatic interaction with the bacterial cell wall. However, with gram-negative bacteria, the lipopolysaccharide layer of the outer membrane may prevent the entrance of amphiphilic metallo-surfactants and reduce antibacterial potency (Maneedaeng et al. 2018). In our study, the antibacterial potency with gram-positive bacteria was seen relatively higher than gram-negative bacteria. It has been suggested that the antibacterial potency of more hydrophobic surfactants is high. In addition, lipophilicity, which regulates the rate at which molecules enter cells, is also affected by coordination with different metal ions.

Conclusions

The correlative study of CMC with the biological efficacy of organic ligands and their metal complexes is a new trend in pharmaceutical research and several new pieces of information on the drug profile of the substances can be accounted for. The amphiphilic nature of surfactant-designed drugs has a special effect on lipid bilayer, causing easy disruption and solubilization of cell membrane and enhances drug activities. So, the recent challenges of antibacterial resistance may be ameliorated by designing either the surfactant-added drugs or synthesizing surfactant-based drugs. In the present study, we prepared a surfactant-based Schiff base ligand, DDAP2C, and its two metal complexes such as Ni-DDAP2C and Zn-DDAP2C. A lower CMC value was detected for metal complexes relative to DDA. The electronic absorption spectral study and magnetic moment data supported octahedral geometry for both complexes. The conductivity data revealed the non-electrolytic nature of the synthesized compounds. The PXRD study showed their crystalline nature with average crystallite size 8.45, 35.83, and 53.237 nm

respective for DDAP2C, Ni-DDAP2C, and Zn-DDAP2C. The TGA/DTA study showed the thermally stable nature of the complexes. The tested compounds have shown excellent and comparable antibacterial activity against the studied pathogens at all concentrations which were further ensured by minimum inhibitory concentration (MIC) values. Based on MIC data, the Ni-DDAP2C complex is found more susceptible to *E. coli, K. pneumonia*, and *Enterococci* bacteria and this may be due to its lowest CMC value. Similarly, the Zn-DDAP2C complex was found more susceptible to *E. coli* and *P. aeruginosa*. Overall, the metal complexes were found to have relatively better antibacterial potency than the ligand. Therefore; the biological results of our study can be extended to develop new and potent surfactant-based metallo-drugs for the treatment of drug-resistant pathogens.

Author contributions N.K.C. designed the study. J.A. experimented and performed analysis. J.A. and N.K.C. prepared the manuscript. A.B. and N.K.C. critically revised the manuscript. All authors have read and approved the manuscript.

Data availability All the data are included in the manuscript and are available for the readers.

Declarations

Conflict of interest There are no conflicts to declare.

References

Abdou SN, Faheim AA, Alaghaz MA, A-N, (2013) Synthesis, spectral characterization, cyclic voltammetry, molecular modeling and catalytic activity of Sulfa-drug divalent metal complexes. Curr Synth Syst Biol 02:112. https://doi.org/10.4172/2332-0737.1000112

Abdul Rub M (2019) Aggregation and interfacial phenomenon of amphiphilic drug under the influence of pharmaceutical excipients (green/biocompatible gemini surfactant). PLoS ONE 14:1. https://doi.org/10.1371/journal.pone.0211077

Ahmad N, Anouar EH, Tajuddin AM et al (2020) Synthesis, characterization, quantum chemical calculations and anticancer activity of a Schiff base NNOO chelate ligand and Pd(II) complex. PLoS ONE 1:1–17. https://doi.org/10.1371/journal.pone.023114 7

Al-Radadi NS, Zayed EM, Mohamed GG, Abd El Salam HA (2020) Synthesis, spectroscopic characterization, molecular docking, and evaluation of antibacterial potential of transition metal complexes obtained using triazole chelating ligand. J Chem 2020:1. https://doi.org/10.1155/2020/1548641

Al Zoubi W, Al-Hamdani AAS, Ahmed SD, Ko YG (2017) A new azo-Schiff base: Synthesis, characterization, biological activity and theoretical studies of its complexes. Appl Organomet Chem 1:3895. https://doi.org/10.1002/aoc.3895

Almarhoon ZM, Al-Onazi WA, Alothman AA et al (2019) Synthesis, DNA binding, and molecular docking studies of dimethylaminobenzaldehyde-based bioactive Schiff bases. J Chem 2019:1. https://doi.org/10.1155/2019/8152721

Alturiqi AS, Alaghaz ANMA, Ammar RA, Zayed ME (2018) Synthesis, spectral characterization, and thermal and cytotoxicity studies of Cr(III), Ru(III), Mn(II), Co(II), Ni(II), Cu(II), and Zn(II) complexes of Schiff base derived from 5-hydroxymethylfuran-2-carbaldehyde. J Chem 2018:1. https://doi.org/10.1155/2018/5816906

Alwadani N, Fatehi P (2018) Synthetic and lignin-based surfactants: challenges and opportunities. Carbon Resour Convers 1:126–138. https://doi.org/10.1016/j.crcon.2018.07.006

Aly SA, Fathalla SK (2020) Preparation, characterization of some transition metal complexes of hydrazone derivatives and their antibacterial and antioxidant activities. Arab J Chem 13:3735–3750. https://doi.org/10.1016/j.arabjc.2019.12.003

Ambika S, Manojkumar Y, Arunachalam S et al (2019) Biomolecular Interaction, anti-cancer and anti-angiogenic properties of cobalt(III) Schiff base complexes. Sci Rep 9:1–14. https://doi.org/10.1038/s41598-019-39179-1

Anestopoulos I, Kiousi DE, Klavaris A et al (2020) Surface active agents and their health-promoting properties: molecules of multifunctional significance. Pharmaceutics 12:1–35. https://doi.org/10.3390/pharmaceutics12070688

Anila BN, Nair MKM, Sreedharan J, Sylas VP (2017) Synthesis, characterization, molecular modeling, antimicrobial and DNA binding studies of cobalt(II) complexes of 2, 3-(Diimino-4'-antipyrinyl) butane with varying counter ions. Asian J Chem 29:1757–1760. https://doi.org/10.14233/ajchem.2017.20344

Attwood D (1983) Biological implications of surfactant presence in formulations 7.1

Badawi EA, Abdel-Rahman MA, Mostafa A, Abdel-Rahman M (2019) Determination of the crystallite size & micro-strain by novel method from XRD profile. Appl Phys 2:1–15. https://doi.org/10.31058/j.ap.2019.21001

Baecker D, Sesli Ö, Knabl L et al (2021) Investigating the antibacterial activity of salen/salophene metal complexes: Induction of ferroptosis as part of the mode of action. Eur J Med Chem 209:112907. https://doi.org/10.1016/j.ejmech.2020.112907

Barbosa HFG, Attjioui M, Paula A, et al (2017) Synthesis, characterization and biological activities of biopolymeric Schiff bases prepared with chitosan and salicylaldehydes and their Pd(II) and Pt(II) complexes. molecules 22:1. https://doi.org/10.3390/molecules22111987

Bhattarai A, Pathak K, Dev B (2017) Cationic and anionic surfactants interaction in water and methanol-water mixed solvent media. J Mol Liq 229:153–160. https://doi.org/10.1016/j.molliq.2016.12.021

Bhowon MG, Li Kam Wah H, Dosieah A et al (2004) Synthesis, characterization, and catalytic activity of metal Schiff base complexes derived from pyrrole-2-carboxaldehyde. Synth React Inorg Met Chem 34:1–16. https://doi.org/10.1081/SIM-120027314

Bouzerafa B, Aggoun D, Ouennoughi Y et al (2017) Synthesis, spectral characterization and study of thermal behavior kinetics by thermogravimetric analysis of metal complexes derived from salicylaldehyde and alkylamine. J Mol Struct 1142:48–57. https://doi.org/10.1016/j.molstruc.2017.04.029

Brown P, Bushmelev A, Butts CP et al (2013) Properties of new magnetic surfactants. Langmuir 29:3246–3251. https://doi.org/10.1021/la400113r

Buldurun K, Turan N, Savcı A, Çolak N (2019) Synthesis, structural characterization and biological activities of metal(II) complexes with Schiff bases derived from 5-bromosalicylaldehyde: Ru(II) complexes transfer hydrogenation. J Saudi Chem Soc 23:205–214. https://doi.org/10.1016/j.jscs.2018.06.002

Canpolat E, Kaya M (2005) Studies on mononuclear chelates derived from substituted Schiff-base ligands: Synthesis and characterization of a new 5-bromosalicyliden-p- aminoacetophenoneoxime and its complexes with Co(II), Ni(II), Cu(II) and Zn(II). Russ J Coord Chem 31:790–794. https://doi.org/10.1007/s11173-005-0170-7

Chandar SCN, Santhakumar K, Arumugham MN (2009) Metallosurfactant Schiff base cobalt(III) coordination complexes. Synthesis, characterization, determination of CMC values and biological activities. Transit Met Chem 34:841–848. https://doi.org/10.1007/s11243-009-9272-2

Chaudhary NK, Mishra P (2018) Bioactivity of some divalent M(II) complexes of penicillin-based Schiff base ligand: synthesis, spectroscopic characterization, and thermal study. J Saudi Chem Soc 22:601–613. https://doi.org/10.1016/j.jscs.2017.10.003

Chaudhary NK, Guragain B (2019) Synthesis, thermal characterization and in vitro antibacterial assessment of Co(II) and Cd(II) Complexes of Schiff base derived from amoxicillin and thiophene-2-carbaldehyde. Asian J Chem 31:1. https://doi.org/10.14233/ajchem.2019.21882

Chaudhary NK, Guragain B, Chaudhary A, Chaudhary SK (2021) Heteroleptic cadmium complex of glimepiride–metformin mixed ligand: synthesis, characterization, and antibacterial study. Chem Pap 75:3215–3226. https://doi.org/10.1007/s11696-021-01535-9

Coats A, Redfern JP (1963) Thermogravimetric analysis. Analyst 88:1

Danish M, Raza MA, Khalid H et al (2020) New metal complexes of sulfonamide: synthesis, characterization, in-vitro anticancer, anticholinesterase, antioxidant, and antibacterial studies. Appl Organomet Chem 35:1–13. https://doi.org/10.1002/aoc.6033

de Araújo EL, Barbosa HFG, Dockal ER, Cavalheiro ÉTG (2017) Synthesis, characterization, and biological activity of Cu(II), Ni(II), and Zn(II) complexes of biopolymeric Schiff bases of salicylaldehydes and chitosan. Int J Biol Macromol 95:168–176. https://doi.org/10.1016/j.ijbiomac.2016.10.109

Donner A, Trepka B, Theiss S et al (2019) NHC-Metallosurfactants as active polymerization catalysts. Langmuir 35:16514–16520. https://doi.org/10.1021/acs.langmuir.9b02152

El-Samanody ESA, AbouEl-Enein SA, Emara EM (2018) Molecular modeling, spectral investigation and thermal studies of the new asymmetric Schiff base ligand; (E)-N'-(1-(4-((E)-2-hydroxybenzylideneamino)phenyl)ethylidene)morpholine-4-carbothiohydrazide and its metal complexes: Evaluation of their antibacterial. Appl Organomet Chem 32:1–18. https://doi.org/10.1002/aoc.4262

Fekri R, Salehi M, Asadi A, Kubicki M (2019) Synthesis, characterization, anticancer and antibacterial evaluation of Schiff base ligands derived from hydrazone and their transition metal complexes. Inorganica Chim Acta 484:245–254. https://doi.org/10.1016/j.ica.2018.09.022

Gaber M, Khedr AM, Elsharkawy M (2017) Characterization and thermal studies of nano-synthesized Mn(II), Co(II), Ni(II), and Cu(II) complexes with adipohydrazone ligand as new promising antimicrobial and antitumor agents. Appl Organomet Chem e3885. https://doi.org/10.1002/aoc.3885

Gaber M, El-Wakiel N, El-Baradie K, Hafez S (2019) Chromone Schiff base complexes: synthesis, structural elucidation, molecular modeling, antitumor, antimicrobial, and DNA studies of Co(II), Ni(II), and Cu(II) complexes. J Iran Chem Soc 16:169–182. https://doi.org/10.1007/s13738-018-1494-9

Garg P, Kaur G, Chaudhary GR (2016) Transition metal based single chained surfactants: Synthesis, aggregation behavior and enhanced photoluminescence properties of fluorescein. RSC Adv 6:108573–108582. https://doi.org/10.1039/c6ra21811c

Gherras H, Yahiaoui A, Hachemaoui A et al (2018) Synthesis and characterization of poly (2,5-diyl pyrrole-2-pyrrolyl methine) semiconductor copolymer. J Semicond 39:1. https://doi.org/10.1088/1674-4926/39/10/102001

Gupta B, Kumari A, Belwal S et al (2020) Synthesis, characterization of platinum(II) complexes of Schiff base ligands and evaluation of cytotoxic activity of platinum nanoparticles. Inorg Nano-Metal Chem 1:1–12. https://doi.org/10.1080/24701556.2020.1728552

Halawa AH, El-Gilil SMA, Bedair AH et al (2017) Synthesis, biological activity and molecular modeling study of new Schiff bases incorporated with indole moiety. Zeitschrift Fur Naturforsch - Sect C J Biosci 72:467–475. https://doi.org/10.1515/znc-2017-0025

Han H, Ruan WJ, Zhao XJ et al (2003) Binuclear transition metal complexes of unsymmetrical tetradentate Schiff base ligands. Synth React Inorg Met Chem 33:1011–1023. https://doi.org/10.1081/SIM-120021934

Hankare PP, Chavan SS (2003) Studies on some binuclear metal complexes with tetradentate ligand derived from 5-(2′-thiazolylazo) salicylaldehyde and 2-aminophenol. Synth React Inorg Met Chem 33:423–434. https://doi.org/10.1081/SIM-120019996

Ilker MF, Nüsslein K, Tew GN, Coughlin EB (2004) Tuning the hemolytic and antibacterial activities of amphiphilic polynorbornene derivatives. J Am Chem Soc 126:15870–15875. https://doi.org/10.1021/ja045664d

Jain RK, Mishra AP (2016) Microwave synthesis, spectral, thermal, 3D molecular modeling analysis and antimicrobial activities of some transition metal complexes of Schiff bases derived from 5-bromosalicylaldehyde. J Saudi Chem Soc 20:127–137. https://doi.org/10.1016/j.jscs.2012.06.002

Justin Dhanaraj C, Salin Raj SS (2020) Synthesis, characterization and biological studies of Schiff base metal complexes derived from 4-aminoantipyrine, acetamide, and p-phenylenediamine. Inorg Chem Commun 108087:1. https://doi.org/10.1016/j.inoche.2020.108087

Kabeer H, Hanif S, Arsalan A et al (2019) Structural-dependent N, O-donor imine-appended Cu(II)/Zn(II) complexes : synthesis, spectral, and in vitro pharmacological assessment. ACS Omega. https://doi.org/10.1021/acsomega.9b03762

Kajal A, Bala S, Kamboj S et al (2013) Schiff Bases : A Versatile Pharmacophore. J Catal 2013:1. https://doi.org/10.1155/2013/893512

Kaur G, Garg P, Kaur B et al (2018) Cationic double chained metallosurfactants: Synthesis, aggregation, cytotoxicity, antimicrobial activity and their impact on structure of Bovine serum albumin. Soft Matter. https://doi.org/10.1039/C8SM00535D

Khashi M, Davoodnia A, Prasada Rao Lingam VS (2015) DMAP catalyzed synthesis of some new pyrrolo[3,2-e][1,2,4]triazolo[1,5-c] pyrimidines. Res Chem Intermed 41:5731–5742. https://doi.org/10.1007/s11164-014-1697-3

Kumar N, Tyagi R (2014) Dimeric surfactants: Promising ingredients of cosmetics and toiletries. Cosmetics 1:3–13. https://doi.org/10.3390/cosmetics1010003

Kumar R, Paul T, Jana O, Mani G (2016) Regioselective Mannich bases of pyrrole-2-carbaldehyde and binuclear copper(II) complexes of bis(iminopyrrolyl) ligand containing the piperazine ring. Inorganica Chim Acta 445:70–78. https://doi.org/10.1016/j.ica.2016.02.023

Lakshmipraba J, Arunachalam S, Solomon RV et al (2015) Surfactant-copper(II) Schiff base complexes: Synthesis, structural investigation, DNA interaction, docking studies, and cytotoxic activity. J Biomol Struct Dyn 33:877–891. https://doi.org/10.1080/07391102.2014.918523

Lobana TS, Kumari P, Bawa G et al (2012) Pyrrole-2-carbaldehyde thiosemicarbazonates of Nickel(II) and palladium(II): Synthesis, structure, and spectroscopy. Zeitschrift Fur Anorg Und Allg Chemie 638:804–810. https://doi.org/10.1002/zaac.201200012

Lutfullina GG, Abdullin IS, Bujanova AG (2013) Study of surface active characteristics of developed detergent for fur treatment. Tenside, Surfactants, Deterg 50:90–92. https://doi.org/10.3139/113.110236

Mahmoud WH, Fatma MMO, Gehad NS (2018) Synthesis, characterization, spectroscopic and theoretical studies of transition metal complexes of new nano Schiff base derived from L - histidine and 2 - acetylferrocene and evaluation of biological and anticancer activities. Appl Organomet Chem 1:1–18. https://doi.org/10.1002/aoc.4386

Maneedaeng A, Phoemboon S, Chanthasena P, Chudapongse N (2018) Synthesis, interfacial properties, and antimicrobial activity of a new cationic gemini surfactant. Korean J Chem Eng 35:2313–2320. https://doi.org/10.1007/s11814-018-0133-6

Mangamamba T, Ganorkar MC, Swarnabala G (2014) Characterization of complexes synthesized using Schiff base ligands and their screening for toxicity two fungal and one bacterial species on rice pathogens. Int J Inorg Chem 2014:22. https://doi.org/10.1155/2014/736538

Manjuraj T, Yuvaraj T, Jayanna N, et al (2020) Spectral, DFT studies, molecular docking and antibacterial activity of Schiff base derived from furan-2-carbaldehyde and their metal (II) complexes. J Turkish Chem Soc Sect A Chem 7:447–460. https://doi.org/10.18596/jotcsa.467859

Maurya RC, Patel P, Rajput S (2003) Synthesis and characterization of mixed ligand complexes of Cu(II), Ni(II), Co(II), Zn(II), Sm(III), and U(VI)O2, with a Schiff base derived from the sulfa drug sulfamerazine and 2,2′-bipyridine. Synth React Inorg Met Chem 33:801–816. https://doi.org/10.1081/SIM-120021647

Mbugua SN, Sibuyi NRS, Njenga LW et al (2020) New Palladium(II) and Platinum(II) Complexes Based on Pyrrole Schiff Bases: Synthesis, Characterization, X-ray Structure, and Anticancer Activity. ACS Omega 5:14942–14954. https://doi.org/10.1021/acsomega.0c00360

Mehta SK, Kaur R (2013) Self-aggregation and solution behavior of synthesized organo transition metal (Co, Fe, Zn) amphiphilic complexes. J Colloid Interface Sci 393:219–227. https://doi.org/10.1016/j.jcis.2012.11.001

Mehta SK, Kaur R, Chaudhary GR (2012) Self-aggregation and solution behavior of copper and nickel-based surfactants. Colloids Surface A Physicochem Eng Asp 403:103–109. https://doi.org/10.1016/j.colsurfa.2012.03.062

Mohamed GG, Omar MM, El-Ela MSA, Hindy AMM (2011) Preparation of macrocyclic Schiff-base ligand and antibacterial activities of transition metal complexes thereof. Toxicol Environ Chem 93:57–72. https://doi.org/10.1080/02772248.2010.501033

Nami SAA, Ullah I, Alam M et al (2016) Synthesis, characterization, molecular docking, and biological studies of self-assembled transition metal dithiocarbamates of substituted pyrrole-2-carboxaldehyde. J Photochem Photobiol B Biol 160:392–399. https://doi.org/10.1016/j.jphotobiol.2016.05.010

Naureen B, Miana GA, Shahid K et al (2021) Iron (III) and zinc (II) monodentate Schiff base metal complexes: Synthesis, characterisation and biological activities. J Mol Struct 1231:129946. https://doi.org/10.1016/j.molstruc.2021.129946

Negm NA, Zaki MF (2008) Structural and biological behaviors of some nonionic Schiff-base amphiphiles and their Cu(II) and Fe(III) metal

complexes. Colloids Surfaces B Biointerfaces 64:179–183. https://doi.org/10.1016/j.colsurfb.2008.01.018

Negm NA, Zaki MF, Salem MAI (2010) Cationic Schiff base amphiphiles and their metal complexes: Surface and biocidal activities against bacteria and fungi. Colloids Surfaces B Biointerfaces 77:96–103. https://doi.org/10.1016/j.colsurfb.2010.01.012

Orojloo M, Nourian F, Arabahmadi R, Amani S (2015) Ni(II), Cu(II), and Zn(II) complexes derived from a new Schiff base-2-((Z)-(3-methylpyridine-2- yleimino)methyl)phenol and synthesis of nano sized metal oxide particles from these compounds. Quim Nov 38:1187–1191. https://doi.org/10.5935/0100-4042.20150128

Patel DD, Patel KR (2020) Ni(II) and Zn(II) Schiff base complexes: Synthesis, characterization, and study of thermodynamic parameters and activation energy. Mater Today Proc. https://doi.org/10.1016/j.matpr.2020.02.079

Patel NB, Khan IH (2011) Synthesis of 1,2,4-triazole derivatives containing benzothiazoles as pharmacologically active molecule. J Enzyme Inhib Med Chem 26:527–534. https://doi.org/10.3109/14756366.2010.535794

Paul P, Bhattacharya S (2014) Palladium complexes of pyrrole-2-aldehyde thiosemicarbazone: Synthesis, structure and spectral properties. J Chem Sci 126:1547–1555. https://doi.org/10.1007/s12039-014-0699-4

Prasad HSN, Ananda AP, Najundaswamy S et al (2021) Design, synthesis and molecular docking studies of novel piperazine metal complexes as potential antibacterial candidate against MRSA. J Mol Struct 1232:130047. https://doi.org/10.1016/j.molstruc.2021.130047

Priya Dharsini GR, Thanaraj C, Velladurai R (2020) Metal chelates of tridentate (NNO) 1,2,4-triazine Schiff base: Synthesis, physicochemical investigation, and pharmacological screening. J Inorg Organomet Polym Mater 30:2315–2322. https://doi.org/10.1007/s10904-019-01413-8

Rajiv K, Rajni J (2011) Computational approach on architecture and tailoring of organic metal complexes derived from streptomycin and Zn, Cd and Pb: antimicrobial effectiveness. Appl Organomet Chem 25:791–798. https://doi.org/10.1002/aoc.1838

Reiss A, Cioater N, Dobritescu A et al (2021) Bioactive Co(II), Ni(II), and Cu(II) complexes containing a tridentate sulfathiazole-based (ONN) Schiff base. Molecules 26:1. https://doi.org/10.3390/molecules26103062

Reshma R, Joseyphus RS, Dasan A, John L (2019) Synthesis and spectral characterization of metal complexes of Schiff base derived from indole-3-carboxaldehyde and L-histidine as potent biocides. J Coord Chem 72:3326–3337. https://doi.org/10.1080/00958972.2019.1695126

Rojas S, Devic T, Horcajada P (2017) Metal organic frameworks based on bioactive components. J Mater Chem B 5:2560–2573. https://doi.org/10.1039/C6TB03217F

Sharaby CM (2005) Studies of some new cyclodiphosphazane complexes of Fe(III), Fe(II), Co(II), Ni(II), Cu(II), Zn(II), and Cd(II). Synth React Inorganic, Met Nano-Metal Chem 35:133–142. https://doi.org/10.1081/SIM-200035687

Sheng T, Fu Z, Wang X et al (2012) Solvothermal synthesis and luminescence properties of BaCeF 5, and BaCeF 5: Tb 3+, Sm 3+ nanocrystals: An approach for white light emission. J Phys Chem C 116:19597–19603. https://doi.org/10.1021/jp306935k

Siddappa K, Mane SB, Manikprabhu D (2014) Spectral characterization and 3D molecular modeling studies of metal complexes involving the O, N-donor environment of quinazoline-4(3H)-one Schiff base and their biological studies. Sci World J 2014:1. https://doi.org/10.1155/2014/817365

Singh BK, Mishra P, Prakash A, Bhojak N (2017) Spectroscopic, electrochemical and biological studies of the metal complexes of the Schiff base derived from pyrrole-2-carbaldehyde and ethylenediamine. Arab J Chem 10:S472–S483. https://doi.org/10.1016/j.arabjc.2012.10.007

Singh BK, Prakash A, Rajour HK et al (2010) Spectroscopic characterization and biological activity of Zn(II), Cd(II), Sn(II), and Pb(II) complexes with Schiff base derived from pyrrole-2-carboxaldehyde and 2-amino phenol. Spectrochim Acta - Part A Mol Biomol Spectrosc 76:376–383. https://doi.org/10.1016/j.saa.2010.03.031

Srivastava VK (2021) Synthesis, characterization, and biological studies of some biometal complexes. Futur J Pharm Sci 7:455–460. https://doi.org/10.1186/s43094-021-00191-w

Stephansen KB, García-díaz M, Jessen F et al (2015) Interactions between surfactants in solution and electrospun protein fibers-effects on release behavior and fiber properties. Mol Biol Int. https://doi.org/10.1021/acs.molpharmaceut.5b00614

Tatsumi T, Imai Y, Kawaguchi K et al (2014) Antimicrobial activity of cationic Gemini surfactant containing an oxycarbonyl group in the lipophilic portion against gram-positive and gram-negative microorganisms. J Oleo Sci 63:137–140. https://doi.org/10.5650/jos.ess13089

Teran R, Guevara R, Mora J et al (2019) Characterization of antimicrobial, antioxidant, and leishmanicidal activities of Schiff base derivatives of 4-aminoantipyrine. Molecules 24:1. https://doi.org/10.3390/molecules24152696

Tsantis ST, Tzimopoulos DI, Holynska M (2020) Oligonuclear actinoid complexes with Schiff bases as ligands — Older Achievements and Recent Progress

Turan N, Buldurun K, Çolak N, Özdemir Ä (2019) Preparation and spectroscopic studies of Fe(II), Ru(II), Pd(II), and Zn(II) complexes of Schiff base containing terephthalaldehyde and their transfer hydrogenation and Suzuki-Miyaura coupling reaction. Open Chem 17:571–580. https://doi.org/10.1515/chem-2019-0074

Tyagi P, Chandra S, Saraswat BS, Sharma D (2015) Design, spectral characterization, DFT and biological studies of transition metal complexes of Schiff base derived from 2-aminobenzamide, pyrrole and furan aldehyde. Spectrochim Acta - Part A Mol Biomol Spectrosc 143:1–11. https://doi.org/10.1016/j.saa.2015.02.027

Tyagi P, Tyagi M, Agrawal S et al (2017) Synthesis, characterization of 1,2,4-triazole Schiff base derived 3d-metal complexes: Induces cytotoxicity in HepG2, MCF-7 cell line, BSA binding fluorescence, and DFT study. Spectrochim Acta - Part A Mol Biomol Spectrosc 171:246–257. https://doi.org/10.1016/j.saa.2016.08.008

Uçar I, Bulut I, Bulut A, Büyükgüngör O (2008) Synthesis, crystal structure, spectroscopic and electrochemical properties of nickel(II) dipicolinate complex with ethylisonicotinate. J Coord Chem 61:2449–2456. https://doi.org/10.1080/00958970801927076

Upadhyay A, Vaidya S, Venkatasai VS et al (2013) Synthesis and characterization of 3d and 4f metal complexes of Schiff base ligands. Polyhedron 66:87–96. https://doi.org/10.1016/j.poly.2013.02.039

Vinusha HM, Kollur SP, Revanasiddappa HD et al (2019) Preparation, spectral characterization and biological applications of Schiff base ligand and its transition metal complexes. Results Chem 1:100012. https://doi.org/10.1016/j.rechem.2019.100012

Wagay TA, Ismail K (2017) Thermal, aggregation, counterion binding, light scattering, and adsorption behavior of cis-chlorobis (ethylenediamine) dodecylaminecobalt(III) perchlorate metallosurfactant in aqueous sodium perchlorate medium. Colloid Polym Sci. https://doi.org/10.1007/s00396-017-4145-2

Zaky R, Fekri A (2017) Solvent-free mechanochemical synthesis of Zn(II), Cd(II), and Cu(II) complexes with 1-(4-methoxyphenyl)-4-(2-(1-(pyridin-2-yl)-ethylidene)hydrazinyl)-1H-pyrrole-3-carbonitrile. Green Process Synth 7:515–523. https://doi.org/10.1515/gps-2017-0057

International Chemical Congress (ICC-2023)

Chemistry for Sustainable Development

May 25-27, 2023 | Kathmandu, Nepal

Organized by

Nepal Chemical Society

in association with

Central Department of Chemistry

Tribhuvan University

Certificate of Participation

This is to certified that

Prof./Dr./Mr./Ms. .... Janak Adhikari ....

....

has participated and delivered oral lecture in International Chemical Congress (ICC-2023) held in Park Village Hotel, Kathmandu, Nepal during May 25-27, 2023.

Dr. Surendra K. Gautam	**Dr. Mahesh K. Joshi**	**Prof. Dr. Jagadeesh Bhattrai**
Conference Convener	Conference Secretary	Conference Co-convener
(President NCS)	(General Secretary NCS)	(HoD, CDC, TU)

Date: May 27, 2023

International Scientific Research Conference

Date: 28 - 29 November, 2022   Jaipur, India

Jointly organized by
International Scientific Research Association
Apex University, Jaipur, India
Research Culture Society
&
Institute of Science and Technology, Eurasian University

Certificate of Participation and Presentation

This is to Certify that

Janak Adhikari

has participated and presented a Paper / Article / Poster / Project titled

Bioinorganic interest on Co(II) and Zn(II) complexes of pyrrole-based surfactant ligand: Synthesis, characterization, and in silico-ADME study

in the 'International Scientific Research Conference' dated 28 - 29 November, 2022.
at Jaipur, India.

Certificate Ref.No: ISRC2022/CPP/001

Jessica		*Gupta*	
Dr. Jessica C.	**Prof. (Dr) Pankaj kr. Sharma**	**Dr. K.D. Gupta**	**Dr. C. M. Patel**
ISRC - 2022 Conference Chair	ISRC - 2022 Conference Chair	ISRC - 2022 Conference Coordinator	Director, Research Culture Society.
Head, Scientific Research Association	Registrar, Apex University,	Apex University,	President, Scientific Research Organization.
Institute of Science and Technology, EU	Jaipur, India	Jaipur, India	http://www.researchculturesociety.org

The 8th Asian Conference on Colloid & Interface Science (ACCIS 2019)

Sept. 24-27, Kathmandu, Nepal

ASCASS
ASIAN SOCIETY FOR COLLOID AND SURFACE SCIENCE
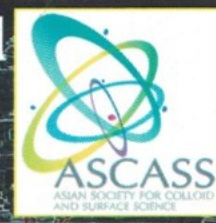
Certificate of Participation

This is to certify that

Janak Adhikari

has participated and contributed **Poster Presentation** in

The 8th Asian Conference on Colloid & Interface Science (ACCIS 2019) organized by the **Asian Society for Colloid and Surface Science (ASCASS)** held in Pulchowk Campus, Institute of Engineering, Tribhuvan University, Lalitpur, Kathmandu, Nepal.

Dr. Lok Kumar Shrestha
Chairperson (ACCIS 2019)

September 27, 2019

Prof. Dr. Toyoko Imae
President (ASCASS)

WORKSHOP ON

Carbon Dots (CDs): An amazing multi functional nano particle

2 August, 2022

Certificate Of Participation
Awarded to

Janak Adhikari. M.M.A.M. Campus. Biratnagar.

For contributing as a participant in **Carbon Dots (CDs): An amazing multi functional nano particle** one-day workshop organized by Department of Chemistry, Mahendra Morang Adarsh Multiple Campus, Tribhuvan University and Nepal Chemical Society, Biratnagar, Province 1, Nepal.

Ghanshyam Shrivastav	**Prof. Dr. Ajaya Bhattarai**	**Dr. Surendra Kumar Gautam**	**Prof. Dr. Roger M. Leblanc**
Chairman	President	President	Fulbright Specialist
Department of Chemistry,	Nepal Chemical Society,	Nepal Chemical Society,	Department of Chemistry
M.M.A.M.C., T.U.	Province 1	Kathmandu	University of Miami, FL, USA
Biratnagar-12			

UNIVERSITY OF NORTH BENGAL

Accredited by NAAC with Grade A

ENLIGHTENMENT TO PERFECTION

International Seminar on "Frontiers in Tea Research-2020"

March 6, 2020

Organized by

DEPARTMENT OF TEA SCIENCE

CERTIFICATE

This is to certify that Prof./Dr./Mr./Mrs/Miss...........**Janak Adhikari**...............

of ....**Department of Chemistry, MMAMC, Tribhuvan Univ.**...........has delivered an invited Lecture/Oral

presentation/Poster presentation/participated in the one day International Seminar on "Frontiers in Tea Research-2020" held at the University of North

Bengal on 6th March, 2020.

He/She has presented a paper titled ....

Prof. Pranab Ghosh	**Dr. Chandra Ghosh**	**Dr. M. Bhattacharya & Dr. Sonali Ray**
Chairman	Head, Department of Tea Science	**Conveners**
Organizing Committee	**Convener, Organizing Committee**	**Organizing Committee**

WORKSHOP ON RESEARCH WRITING AND PUBLISHING

8th-11th May, 2019

Certificate

This is to Certify that Mr./Mrs. **Janak Adhikari**

of **Mahendra Morang Adarsh Multiple Campus, Biratnagar** participated

in the Workshop on Research Writting & Publishing organized by Research Management cell,

Mahendra Morang Adarsh Multiple Campus, Biratnagar & supported by University Grants

Commission, Nepal held at Biratnagar from 8th–11th May, 2019.

Prof. Dr. Devendra Adhikari	**Mr. Baburam Timalsena**	**Dr. Tilak Prasad Gautam**
(Facilitator)	(Campus Chief)	(Co-ordinator)
	M.M.AM. Campus, Biratnagar	Workshop Organizing Committee,
		Reaserch Management Cell,
		M.M.A.M. Campus, Biratnagar